The thermodynamic design and rating of the heat exchangers for an Aqua-Ammonia absorption-desorption heating and refrigeration cycle

JP Botha

22745432

Dissertation submitted in fulfilment of the requirements for the
Degree Masters in Mechanical Engineering at the
Potchefstroom Campus of the North-West University

Supervisor: Prof CP Storm

November 2016

Dedicated to the love of my life

Acknowledgement

The design of the heat exchangers for an aqua-ammonia absorption-desorption cycle would not have seen the light without the help and support of many people. I would like to make use of this opportunity to thank all the people who made this oeuvre possible. I would like to express my sincere gratitude to my mentor, Prof. Chris Storm for the opportunity to complete a study on aqua-ammonia heat exchangers. Furthermore, I would like to thank Prof. Chris Storm for his guidance through the course of this design. He not only provided the necessary guidance and allowed me to develop my own ideas, but also helped improve my people skills. I feel fortunate in getting the opportunity to work with him. Finally, I would like to thank my fiancée for her love and inspiration, and my parents for motivating me and keeping my spirits up all the time.

Abstract

Title: The thermodynamic design and rating of the heat exchangers for an Aqua-Ammonia absorption-desorption heating and refrigeration cycle

Author: Jeanré P. Botha

Institution: North-West University: Potchefstroom

Student Number: 22745432

Supervisor: Prof. CP Storm

In today's day and age the search for more reliable, sustainable, energy efficient systems is a constant. Over the last three decades large emphasis has been placed on vapour compression cycles and making them as energy efficient as possible. To increase or decrease the temperature of a controlled volume requires large amounts of shaft work [kW], however by developing and conducting research into old technologies it could be possible to obtain a sustainable alternative heating/cooling system. Aqua-ammonia absorption-desorption cycles are able to operate on renewable energy, as this process removes the energy hungry compressor from the refrigeration cycle and replaces it with a generator, absorber, rectifier, and regenerative heat exchanger. Absorption-desorption cycles are the earliest form of refrigeration cycle, with the earliest dating back to 1824. Pure ammonia refrigerant is one of only few alternative refrigerants with zero ODP (Ozone Depletion Potential) and zero GWP (Global Warming Potential) accepted by all governments, ASHRAE, UNEP, International Institution of Refrigeration, and almost all Institutes of Refrigeration worldwide (ASHRAE, 1994).

In view of that, an investigation is required into alternative heating/cooling cycles, which can be adapted and optimised to suit the limitations and requirements of alternative energy sources. Contained within this dissertation are the thermodynamic and mechanical designs required for the heat exchangers of an aqua-ammonia absorption-desorption cycle. The study includes an extensive theoretical background and literature review, which led to the further investigation of the thermophysical properties of aqua-ammonia refrigerant. Furthermore, the oeuvre includes the verification and validation of the thermodynamic design and rating model for seven heat exchangers, which are required to fully optimise the coefficient of performance of the aqua-ammonia absorption-desorption cycle. The software package MS Excel was used to code the preliminary thermodynamic design model, after which the software package EES was utilised to verify that the preliminary thermodynamic design model had no mathematical errors. Validation of the thermodynamic design models came in the form of predicted overall heat transfer coefficient values versus typically expected overall heat transfer coefficient ranges. Where the typical U_c ranges have

similar or near identical heat exchanger configuration to that of the thermodynamic design models in this dissertation.

The mechanical design isn't directly related to the main focus of this study, but does form an integral part of the overall design of aqua-ammonia heat exchangers and is included in the scope of work. The mechanical design includes the necessary first principle considerations to ensure the safe operation of the heating and refrigeration package unit.

Keywords: Aqua-ammonia; absorption-desorption; thermophysical properties; heat exchanger(s); thermodynamic design; two-phase; turning point; heating and refrigeration.

Table of Contents

Chapter 1

Chapter 2

Chapter 3

Chapter 4

Chapter 5

Chapter 6

Annexure

List of Figures

Chapter 1

Chapter 2

Chapter 3

Chapter 4

Chapter 5

List of Tables

Chapter 2

Chapter 3

Chapter 4

Chapter 5

Nomenclature

A_{cs}	Bundle cross flow area	m^2
A_s	Heat transfer surface area	m^2
B	Baffle spacing	m
c	Capacity ratio	-
C	Clearance	m
C_{cr}	Heater geometry constant	-
C_p	Specific thermal capacity	J/kg.K
C_n	Heat transfer coefficient correction factor	-
C_{sf}	Surface-fluid combination constant	-
COP	Coefficient of performance	-
d	Diameter	m
D_e	Equivalent diameter	m
D_s	Inner shell diameter	m
F	Force	N
F_c	Log mean temperature difference correction factor	-
g	Gravitational acceleration	m/s^2
G_s	Mass velocity	$kg/m^2.s$
Gz	Graetz number	-
h	Heat transfer coefficient	$W/m^2.K$
k	Thermal conductivity	W/m.K
L	Length	m
L_t	Heat transfer tube length	m
M	Molar	kg/k.mol
$\dot{m}$	Mass flow rate	kg/s
N_L	Number of tube rows	-
N_p	Number of tube passes	-
N_t	Number of tubes	-
Nu	Nusselt number	-
NTU	Number of transfer units	-
P	Pressure	Pa
P_D	Design pressure	Pa
P_T	Pitch size	m
Pe	Pèclet number	-
Pr	Prandtl number	-

PR	Pitch ratio	-
Q	Quality	-
$\dot{Q}$	Heat transfer rate	W
r	Radius	m
Re	Reynolds number	-
t	Wall thickness	m
T	Temperature	°C or K
u	Velocity	m/s
U_c	Overall heat transfer coefficient	$W/m^2.K$
U_f	Fouling overall heat transfer coefficient	$W/m^2.K$
$\dot{V}$	Volume flow rate	m^3/s
x	Mass concentration	kg/kg
y	Molar concentration	k.mol/k.mol

Greek Symbols

α	Enthalpy	J/kg
δ	Film thickness	m
ε	Effectiveness	-
θ	General thermophysical property variable	-
μ	Dynamic viscosity	kg/m.s
ρ	Density	kg/m^3
σ	Stress	Pa
φ	Circumferential angle	rad
Δ	Delta or difference	-
Σ	Sum of	-

Subscripts

fg	Latent
b	Bulk
c	Cold
cb	Convective boiling
CF	Counter-flow
clnt	Coolant
crit	Critical
DSN	Average ambient design conditions
est	Estimation
h	Hot
i or in	In
l	Saturated liquid
LMTD	Log mean temperature difference
m	Mean
max	Maximum
min	Minimum
mix	Mixture
nb	Nucleate boiling
o or out	Out
PF	Parallel-flow
s or S	Shell side
sat	Saturation
sh	Shear
SMR	Summer ambient design conditions
ss	Strong aqua-ammonia solution
t or T	Tube side
TP	Turning Point
v	Saturated vapour
WRT	Winter ambient design conditions
ws	Weak aqua-ammonia solution
XF	Cross-flow

Abbreviations

ABS	Absorber
Aux	Auxiliary heat exchanger
BP	Bubble pump generator
CAD	Computer aided design
DHC	De-superheating condenser
EES	Engineering equation solver
Evap	Evaporator
HTC	Heat transfer coefficient
HTEX	Heat exchanger
H&R	Heating and refrigeration
IAWPS	International Association for the Properties of Water and Steam
LMTD	Log mean temperature difference
MTD	Mean temperature difference
PC	Pre-cool heat exchanger
Regen	Regenerative heat exchanger
S1C	Stage 1 Condenser
S2C	Stage 2 Condenser

Chapter 1

1 INTRODUCTION

Summary

In today's day and age the search for low-energy consuming and environmentally friendly systems are a constant. This could not be more relevant to a struggling energy sector of South Africa and the global need to shift energy requirements from fossil energy sources onto alternative energy sources, which would lead to positive effects on the environment and stimulate economic growth. A large consumer of electrical energy is temperature manipulation in a controlled volume, which requires large amounts of shaft work [kW] to increase or decrease the temperature. The most difficult temperature manipulation is the removal of heat, known as refrigeration. Thus, an investigation is needed into alternative heating/cooling cycles, which can be adapted and optimised to suit the limitations and requirements of alternative energy sources. South Africa is one of only a few countries blessed with high levels of solar irradiation all year round, and would be a prime candidate for investigating a solar-powered heating/cooling cycle. One such alternative heating/cooling cycle that utilises heat energy is an absorption-desorption cycle.

1.1 History of Absorption-Desorption Refrigeration Cycles

Refrigeration is well known to just about every person on earth, as “the machine keeping my food cold”. This is due to the globalisation during the early 20th century of the household refrigerator and its commercial applicant in food stores. Refrigeration can be described as the transfer of heat from the surroundings to a chamber with an absence of heat.

Thus, refrigeration’s most important application is the preservation of food. Most foods kept at room temperature will spoil rapidly, which is due to the rapid growth of bacteria. Refrigerators preserve food by maintaining the food at an optimum temperature of 4 [°C], which is low enough to halter the growth of bacteria, but high enough that there aren’t any ice crystallisations within the food (Althouse et al., 1992).

The history of refrigeration started with continuous consumption refrigeration, whereby a cooling effect is obtained by utilising elementary refrigerants, such as melting ice or sublimation of solid carbon dioxide (dry-ice) at atmospheric pressure. Today, the most common form of refrigeration is the vapour compression cycle, which utilises a continuous cycle of its working fluid, known as a refrigerant. Although vapour compression cycles are the most popular form of refrigeration cycles today, these weren’t the earliest refrigeration cycles. Absorption-desorption cycles are the earliest form of refrigeration cycle dating back to 1824 (Althouse et al., 1992). Solid absorption systems operate on the principle discovered by Michael Faraday in the early 1820’s.

Through experiments Faraday succeeded in liquefying ammonia, which scientists had believed to be a fixed gas, by exposing the ammonia vapour to silver chloride powder. After the vapour has been absorbed by the silver chloride, heat was applied and a liquid solution was the product. Edmond Carré developed the first absorption machine in 1850, by using sulphuric acid and water solution (Althouse et al., 1992). It was only his brother Ferdinand Carré who demonstrated an ammonia-water refrigeration machine in 1859; later in 1860 he received the first U.S. patent for a commercial absorption unit. ‘Serve Electrically’ was founded in 1902 as the Hercules Buggy Works and became a manufacturer of electric refrigerators, the company is known as Servel. Servel purchased the US rights to a new AB Electrolux gas heat driven absorption refrigerator invented by a couple of Swedish engineering students, Carl G. Munters and Baltzar von Platen during the 1930’s. The production of the AB Electrolux absorption refrigerator stretched from 1926 to the early 1950’s (Thevenot, 1979).

Absorption-desorption systems have experienced ups and downs over the years. The absorption-desorption cycle was the predecessor to the vapour-compression cycle in the late nineteenth century. Absorption-desorption systems were used in domestic refrigerators and as refrigeration for large chemical and process industries. Prices of natural gas, fuel availability and governmental policies caused the decline in sales of absorption-desorption refrigerators during the mid-1970’s in the USA (Forley, 2000), although Asian countries with electricity shortages have

shown an increase in sales since the mid-1970's. Absorption-desorption refrigeration hit its peak in 1981 with two absorption-desorption plants created by former USSR Borsig GmbH, which had a cooling capacity of 22.1 [MW] at -5 [°C] in the evaporator (Srikhirin et al., 2001).

However, in the late 20th century focus shifted to vapour compression cycles, and absorption-desorption cycle technology was shelved due to the assumption that the cycle has a high power consumption and low overall efficiency. Now, at the turn of the century the assumption has been re-evaluated, where it was found that both cycles waste similar amounts of energy. Where the vapour compression cycle uses electricity generated at around 35% efficiency in power plants, and absorption-desorption cycles uses heat energy. When the 35% efficiency of power stations are factored into the overall efficiency of vapour compression cycles, then, the two cycles become comparable (Srikhirin et al., 2001). Thus, it can be assumed that absorption-desorption cycle technology could be economically viable in areas with energy concerns.

Coefficient of Performance

When dealing with the coefficient of performance of an absorption-desorption cycle, a different approach is needed to that of the vapour compression cycle. Thus, for the absorption-desorption cycle the coefficient of performance as proposed by (Stoecker & Jones, 1983) can be expressed as:

$$COP_{abs} = \frac{\dot{Q}_{ref}}{\dot{Q}_{gen}}, \tag{1.1}$$

with

$\dot{Q}_{ref}$ ≡ Refrigeration capacity [kW]

$\dot{Q}_{gen}$ ≡ Heat added to the generator [kW]

The values of COP_{abs} for aqua-ammonia are commonly 0.7 compared to the commonly obtained COP of 3 to 4 for vapour compression cycle, although the coefficient of performance of the heating capacity should also be taken into account for the absorption-desorption cycle (Stoecker & Jones, 1983). The values of heating capacity COP_{abs} are commonly between 1.5 to 1.7, thus, it can be concluded that the absorption-desorption cycle fully utilises its heat source input, whether it be solar- or industrial waste heat energy.

1.2 Background of an Aqua-Ammonia Absorption-Desorption Cycle

Absorption-desorption cycles have two great advantages, namely, the cycle requires no rotating mechanical components and any heat source to power the generator component. Even low grade industrial waste heat can be utilised to power the generator in an absorption-desorption cycle. This is due to the natural circulation of the working fluid within the absorption-desorption cycle, also

known as Gibbs free energy (Stoecker & Jones, 1983). Figure 1.1 illustrates the fundamental component cycle of an absorption-desorption cycle, but more specifically that of a LiBr-water cycle. Thus for the purpose of this dissertation, focus will be kept on aqua-ammonia absorption-desorption cycles.

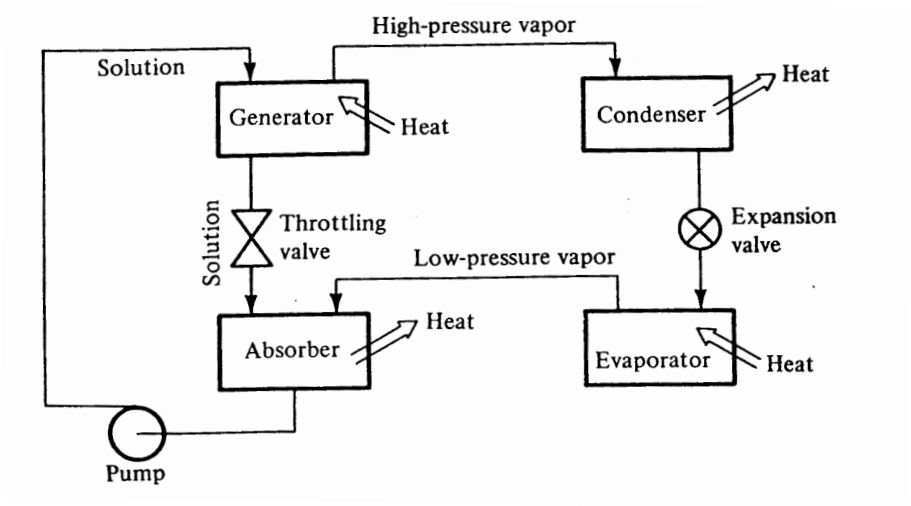

Figure 1.1: Basic schematic of an absorption-desorption system (Stoecker & Jones, 1983).

An aqua-ammonia absorption-desorption cycle requires the addition of two extra components, namely, the rectifier and the analyser. The purposes of these components are to remove the unwanted water vapour content from the refrigerant vapour, which is released by the generator. The positioning of the above mentioned components are illustrated in Fig. 1.2, along with all other fundamental components of an aqua-ammonia absorption-desorption cycle.

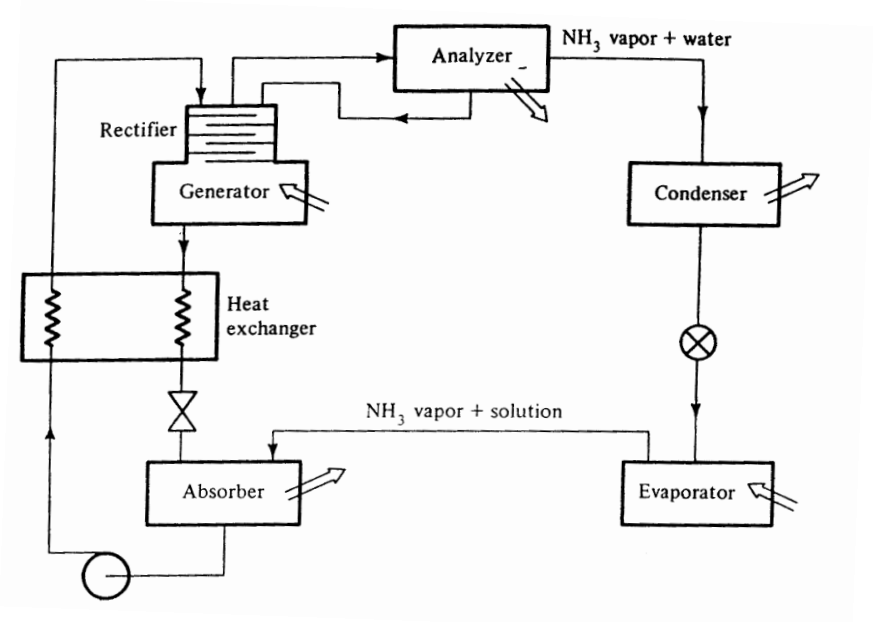

Figure 1.2: Basic component representation of an Aqua-ammonia absorption-desorption cycle (Stoecker & Jones, 1983).

The generator/bubble pump component is where the desorption process of the cycle takes place. Here the refrigerant absorbent pair is separated, though the addition of heat, which in effect boils the refrigerant off of the strong concentrated aqua-ammonia solution. This process creates a high concentrated vapour refrigerant, which next enters the rectifier.

The rectifier is a contact counter current water vapour remover. The refrigerant vapour that is driven off by the generator flows through a series of staggered stacked plates. The plates simply let weak solution aqua-ammonia dribble down collecting any water, be it liquid or vapour. The analyser is a closed water cooled heat exchanger, with the function of condensing water vapour out of the near pure ammonia solution, with the water flowing back into the rectifier.

High pressure pure ammonia vapour flows to the condenser, where the refrigerant is condensed into a high pressure liquid. Condensation is achieved by the removal of heat by the much ‘colder’ coolant fluid. The coolant temperature raises to an effective percentage of that of the refrigerant, the coolant can now be used in the means of heating purposes. The high pressure liquid refrigerant flows through an expansion valve, whereby the pressure drops slightly. The pressure doesn’t drop as dramatically as that of the vapour compression cycle, due to the absorption-desorption cycle circulating with Gibbs free energy. The dramatic drop in ‘pressure’ is caused by the addition of an auxiliary gas, i.e. Hydrogen or Helium. The presence of an auxiliary gas causes the refrigerant to have a very low partial pressure, which in turn is the same effect as that of the vapour compression cycle. The refrigerant then enters the evaporator, where heat is added to evaporate or more commonly known boil the refrigerant to a state of saturated vapour. The exchange of heat within the evaporator is simply put, where refrigeration happens.

The low partial pressure saturated vapour ammonia is sucked from the evaporator to the absorber, the suction is caused by the high affinity ammonia and water have for one another. Weak solution aqua-ammonia and high concentration saturated ammonia react exothermically to form a strong aqua-ammonia solution. The strong solution returns back to the generator, passing through a heat exchanger, known as, the regenerator. A regenerator is fundamental to the aqua-ammonia absorption desorption cycle, with the main purpose of lowering the temperature of the weak solution entering the absorber is to increase the concentration of the strong solution exiting the absorber.

The component diagram represented by Fig. 1.3 is a basic illustration of the aqua-ammonia absorption-desorption cycle used for this study, with the addition of two pre-coolers, namely, the de-superheating condenser and pre-cool heat exchanger. The component diagram also represents the layout of the heat exchangers and the path of the primary refrigerant. These components are placed at different height intervals to optimise the buoyancy forces to circulate the refrigerant.

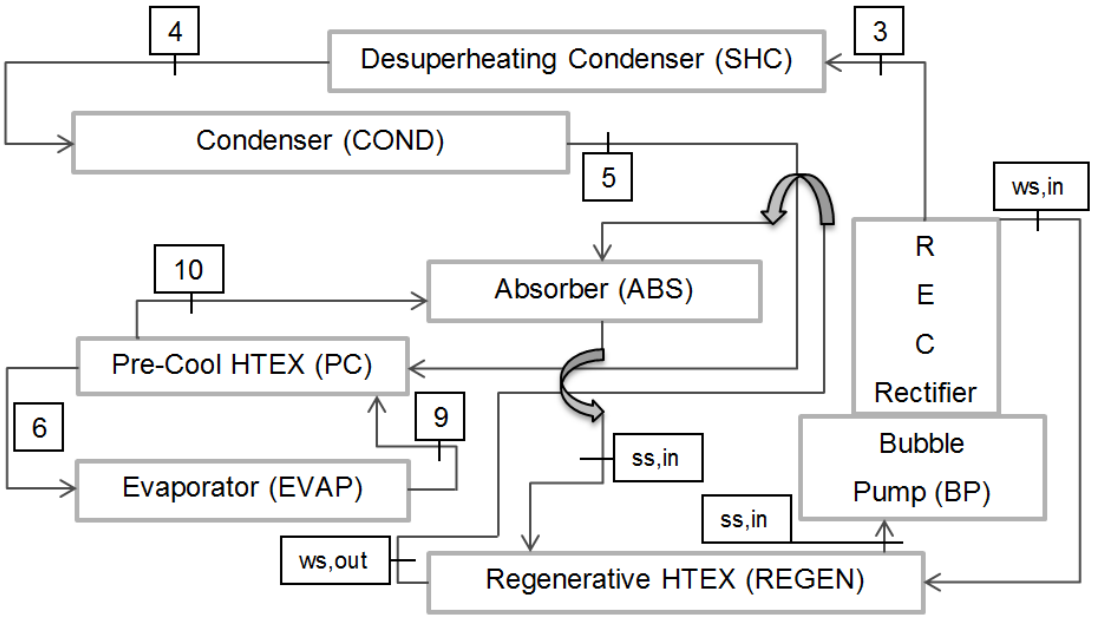

Figure 1.3: Schematic representation of the components within an aqua-ammonia absorption-desorption heating & refrigeration cycle.

1.3 Rationale for Research

This study forms part of a larger research project that seeks to experimentally test an aqua-ammonia absorption-desorption heating and refrigeration package unit that utilises solar irradiation to power the heat source required in the bubble pump generator. Multiple sources are available for the thermodynamic design and rating of heat exchangers, but very few or out-dated sources are available for the thermodynamic design and rating of aqua-ammonia heat exchangers. The out-dated sources of thermodynamic design for aqua-ammonia heat exchangers are based on the assumption that the working fluid is a pure substance and not on an aqueous ammonia solution. Research is specifically required into the thermodynamic design and rating of heat exchangers utilizing aqua-ammonia in the ambiguous two-phase and superheated vapour regions. As this study is interwoven into the larger project it's largely dependent on the progress of other studies being conducted coherently, which may halter the progress of this study.

1.4 Problem Statement

An investigation into the thermodynamic design and rating of all of the heat exchangers in an aqua-ammonia absorption-desorption cycle is required to complete the experimental setup of the heating and refrigeration package unit. This directly ties into the investigation of alternative heating/cooling cycles as the heat exchangers of an absorption-desorption cycle play a fundamental role in making the cycle function at its optimum. The heat exchangers must be designed to adapt to the limitations and requirements of alternative energy sources.

1.5 Objectives

The purpose of this study is to investigate the thermodynamic design and rating for shell and tube heat exchangers used in an experimental solar-powered aqua-ammonia absorption-desorption heating and refrigeration (H&R) package unit. The study aims to develop a software based thermodynamic design and rating model of the condenser, pre-cool heat exchanger, evaporator, and regenerative heat exchanger for the specific use in an aqua-ammonia absorption-desorption H&R package unit or refrigeration cycles with laminar flow regime mass flow rates. The development of the thermodynamic design and rating model will require verification and validation to ensure that the heat exchangers are sized accurately, and practically viable. The thermodynamic design and rating model should comply with the requirements and limitations that a solar-powered aqua-ammonia absorption-desorption heating and refrigeration package unit entails. This includes the optimal type and number of heat exchangers required to produce a heating capacity COP of 1.3 and a cooling capacity COP of 0.7, with 1.5 [kW] heating capacity and 0.8 [kW] cooling capacity.

This study aims to utilise the thermodynamic design and rating model to complete the mechanical design of the heat exchangers for an aqua-ammonia absorption-desorption cycle. The mechanical design will include first order principles to ensure the safe operation of the heat exchangers. Furthermore, the mechanical design will include a full set of manufacturing and assembly drawings of each heat exchanger and its non-standard components.

1.6 Research Methodology

In the beginning of any research project it's fundamental to gain knowledge on the subject matter. Therefore, the first step is to compile a comprehensive literature and theoretical background study on aqua-ammonia, absorption-desorption refrigeration cycles, and the thermodynamic design and rating of heat exchangers. Investigation into the behavioural characteristics of aqua-ammonia refrigeration cycles and its thermophysical properties are required to complete an accurate and satisfactory thermodynamic design model.

Convention dictates that a functional analysis is required before the design requirements and specifications, but to keep the oeuvre concise the functional analysis can be construed from the comprehensive literature review and theoretical background study, and thermophysical property investigation of aqua-ammonia absorption-desorption refrigeration cycles to form the design requirements. The design requirements will be ranked according to its level of importance and utilised in a concept design evaluation matrix.

The software package Microsoft Excel (MS Excel) will be utilised for the preliminary thermodynamic design model with the Engineering Equation Solver (EES) used to verify that there are no mathematical errors in the MS Excel thermodynamic design model. The MS Excel

thermodynamic design model must accommodate multiple design-sizing options, in other words the design model must have multiple shell and tube diameters that generate an array of heat exchanger designs to choose from. Furthermore, the MS Excel thermodynamic design model must incorporate the option of multiple design layouts, for instance single or double tube pass, 45° or 60° tube bundle layout. The preliminary design criteria will be based on the thermal heat exchanger efficiency, the tube length over shell diameter ratio ($2 < L/D_s < 7$), and the number of tubes ($2 < N_t < 100$). The thermal efficiency of each heat exchanger will be measured using the NTU-effectiveness method and standardised counter- or cross-flow NTU vs. effectiveness curves. The thermal efficiency should be as close to the theoretical maximum as possible. The NTU-effectiveness method will fulfil another important duty, which is determining whether the assumed outlet temperature of the secondary fluid is satisfactory in accordance to a real world heat exchanger scenario.

After the thermodynamic design model of each heat exchanger is verified, the validation process can commence. The validation process will prove that the correlations utilised in solving the sizing and rating problem of each heat exchanger is accurate and satisfactory. It should be noted that this study is limited to validating the predicted overall heat transfer coefficient to typically expected overall heat transfer coefficient ranges, as this study/design project is coherently completed with several other postgraduate studies to create an experimental solar-driven aqua-ammonia absorption-desorption H&R cycle. Thus, the validation can't be completed by comparing predicted vs. experimental results until the entire experimental setup is completed. Furthermore, computational fluid dynamic software was considered, but due to the complex and unpredictable nature of two-phase and superheated aqua-ammonia solutions and the large number of heat exchangers to be designed it's decided not to use CFD software packages.

With the thermodynamic design and rating models verified and validated, the mechanical design process will be completed. First order principles will be applied to the mechanical considerations such as tube sheet thickness, shell wall thickness, tube wall thickness, and number of bolts for end-cap headers. It should be noted that this oeuvre is limited to first order principles for the mechanical design as it isn't within direct focus of the title of this study, and therefore Finite Element Analysis software will not be considered. The evaluated concepts, thermodynamic design and rating models, and mechanical considerations will be utilised to complete the manufacturing and assembly drawings of the heat exchangers.

Chapter 2

2 LITERATURE REVIEW AND THEORETICAL BACKGROUND STUDY

Introduction

The aim of this chapter is to expand the briefly discussed problem and its setting in Chapter 1. Compiled within this chapter is the fundamental literature and theoretical background required to complete the thermodynamic design of a heat exchanger that uses aqua-ammonia as its refrigerant. The literature surveyed will be divided into the following categories:

- Aqua-ammonia absorption-desorption cycle components.
- Heat exchanger classification.
- Thermophysical properties of aqua-ammonia solutions.
- Thermophysical properties of ethylene glycol solutions.
- Thermodynamic design and rating of shell and tube heat exchangers.

2.1 Aqua-Ammonia Absorption-Desorption Cycle Components

In order to design components for an absorption-desorption refrigeration system it's required to know the functions of all the components of the absorption-desorption cycle. Although some of these components are out of scope for this study, it remains fundamental to understand each components function, thermodynamically and mechanically in the cycle.

- Generator (Bubble Pump)
- Rectifier (Distiller)
- Condenser
- Pre-Cool Heat Exchanger
- Venturi Nozzle
- Evaporator
- Absorber
- Regenerative Heat Exchanger

2.1.1 Generator (Bubble Pump) and Rectifier (Distiller)

The generator utilises the addition of heat to boil-off pure ammonia out of the strong aqueous ammonia solution, in other words by adding heat to the generator it's then able to boil near pure ammonia out of a high concentration ammonia water mixture. The amount of heat added to the generator is optimised for the system pressure as determined by ambient temperature conditions. The heat source is a solar collector, which has direct influences from the ambient conditions. Thus, if ambient temperatures are high the generator will have high heat input and high pressure output, with the opposite being true for low ambient temperatures.

A well-designed generator should be able to control the quantity and mass concentration of ammonia released into the working refrigerant to ensure the minimum water concentration is boiled off. The generator (bubble pump) isn't that simply put as adding heat to the aqueous ammonia solution, it is required to: break up the refrigerant from the absorbent, and raise the temperature of the strong solution to saturation temperature (Vicatos, n.d.). Generators have been powered by many sources of heat, including, steam, gas burner, solar radiation, and electricity. In the case of this project group the generator is powered by solar irradiation.

The purpose of the rectifier is to remove minute concentrations of water remaining in aqua-ammonia vapour exiting the generator. The typical rectifier is comprised of a stacked plate column, whereby rising high concentration ammonia vapour comes into contact with liquid strong solution trickling down. Thus, converting water vapour into liquid and purifying the ammonia pure to a theoretical maximum of 99 wt% ammonia.

2.1.2 Condenser

The condenser component can be viewed as a heat exchanger, where heat is removed from the refrigerant entering as superheated vapour and exiting as saturated liquid. The heat removed from the refrigerant is added to a secondary refrigerant or brine, which can be used to heat other industrial or commercial components. The secondary refrigerant could also be utilised in domestic components such as: tumble-dryer, dish-washer, washing machine, and the heated swimming pool. The heat removed from the condenser is added to the heat capacity of the cycle with which the coefficient of performance can be calculated.

2.1.3 Pre-Cool Heat Exchanger

The pre-cool heat exchanger plays the role of increasing the efficiency of the absorption-desorption cycle, where heat is removed from the saturated liquid exiting the condenser and added to the saturated vapour exiting the evaporator. By reducing the temperature of the saturated aqua-ammonia liquid it increases the refrigeration capacity and thus the coefficient of performance. However, it's slightly at the cost of the absorber's ability to absorb, this problem is rectified by the regenerative heat exchanger. The thermal efficiency of the pre-cool heat exchanger will be predominately low due to the fluids having similar mass flow rates but large differences in specific thermal capacity.

2.1.4 Venturi Nozzle

The venturi nozzle can act as an expansion valve, which reduces the pressure of liquid refrigerant, and as a flow regulator for optimal thermal siphoning of the absorption-desorption cycle. Commonly, expansion valves accelerate the refrigerant through an orifice whereby the pressure drops dramatically and the refrigerant undergoes 'flashing'. Flashing occurs when a liquid at high pressure suddenly drops to low pressure, which decreases the temperature of the fluid drastically. Expansion valves are considered have an isothermal process. A venturi has a smooth continuous reduction of inner diameter to the required orifice, where pressure is at its lowest and fluid velocity at its highest. Now, introducing a small tube to the small orifice, as shown in Fig. 2.1, a suction force is created at the opening of the small tube.

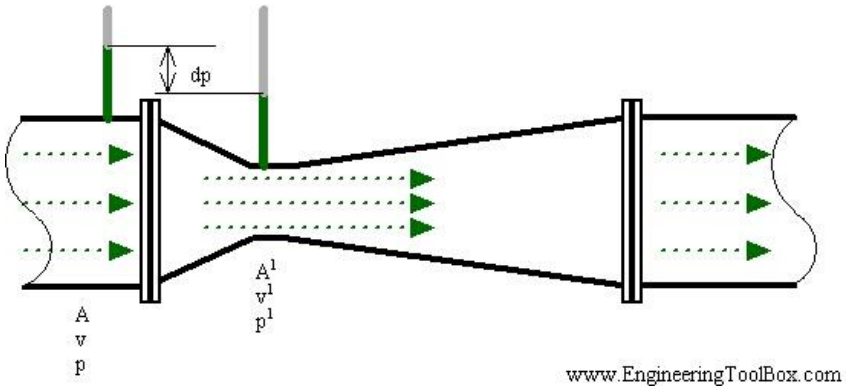

Figure 2.1: Control volume diagram of a venturi (Engineeringtoolbox, 2015).

A venturi is vital for the suction force it can generate, as it removes the auxiliary gas (helium) from the absorber and re-distributes it to the evaporator. As the venturi has a fixed diameter it can regulate the liquid column that ensures the evaporator receives its exact mass flow rate.

2.1.5 Evaporator

The evaporator is the refrigeration side of the absorption-desorption cycle, and it is where heat is added to the refrigerant from a secondary refrigerant. The addition of heat to the refrigerant lets it evaporate to a state of pure saturated ammonia vapour with the last of the water concentration not evaporating and purged to the absorber. The temperature of the secondary refrigerant is near evaporator operating temperature and can now be used to cool other industrial or commercial components. The secondary refrigerant can also be used for domestic components such as: refrigerators, deep freezes, and air-conditioning.

2.1.6 Absorber

The absorber is one of the primary components of the absorption-desorption cycle, where the working fluid of pure ammonia is absorbed by the weak solution aqueous ammonia. The absorption process has an exothermal reaction whereby heat needs to be removed to increase the concentration of ammonia absorption into the weak solution aqua-ammonia. The mass transfer of the absorption process requires a large contact area between pure ammonia superheated vapour and sub-cooled weak solution liquid. Several absorber types are listed in (Perry & Chilton, 1973), classified according to its geometry:

- Spray absorber.
- Bubble absorber.
- Packed column absorber.
- Wetted wall column absorber.
- Plate column absorber.

The performance of an absorber depends on the rate of absorption and removal of the heat generated (Perez-Blanco, 1988). The rate of absorption is determined by the diffusion of ammonia vapour through the liquid phase and the flow of coolant affects the rate of removal of heat generated by the exothermic absorption reaction (Perez-Blanco, 1988). Low coolant flow would result in decreased mass transfer due to the increased vapour pressure (Perez-Blanco, 1988). By increasing the contact area between the ammonia vapour and the weak solution absorbent through the liquid phase enhances the diffusion of the ammonia vapour. Vital to the thermal siphoning of the absorption-desorption cycle is that the pressure of the superheated pure ammonia vapour is slightly higher than the pressure of the sub-cooled weak solution liquid (Vicatos, n.d.).

2.1.7 Regenerative Heat Exchanger

The regenerative heat exchanger plays a vital role in the coefficient of performance of the absorption-desorption cycle. The regenerative heat exchanger lies between the absorption and desorption components, where heat is added to the strong solution heading to the generator and heat is removed from the weak solution heading towards the absorber. For the generator to work more effectively the strong solution's temperature must be raised to near saturation temperature, and for the absorber to work more effectively the weak solution must be cooled for better absorption. Thus, the regenerative heat exchanger must be as thermally efficient as mechanically and financially possible.

2.2 Heat Exchanger Classification

Heat exchangers are categorised into two primary categories, namely, recuperative and regenerative heat exchangers (Walker, 1990). Heat exchangers consisting of two-fluid heat transfer are called recuperative (Kakaç & Liu, 2002), where the recuperative heat exchangers are classified according to the flow direction of the hot and cold fluid streams. Consequently, heat exchangers can have the following fluid flow patterns:

- Parallel-flow, where both fluids flow in the same direction.
- Counter-flow, where the fluids flow in the opposite direction parallel of one another.
- Cross-flow, where the fluids cross each other with an angle near 90°.
- Mixed-flow, where the fluids may flow in the same and opposite directions at once.

Some examples of regenerative heat exchangers are rotary regenerators used to pre-heat the air entering a large coal-fired steam power plant, and a gas turbine rotary regenerator. Regenerative heat exchangers are classified as two types of heat exchangers, namely, disk-type and drum-type. As the absorption-desorption cycle requires the design of fluid-to-fluid heat exchangers, only recuperative heat exchangers are considered. Recuperative heat exchangers are

split into two main groups, namely, plate- and tubular heat exchangers. However, for the purpose of this study only tubular heat exchangers will be investigated.

2.2.1 Tubular Heat Exchangers

Tubular heat exchangers are constructed of circular pipes and tubes, where one of the fluids flows inside of the inner tube and the other fluid over the outside of that same tube (Kakaç & Liu, 2002). The diameters of the tubes, the number of tubes, the distance between tubes, and the tube arrangements can be altered, thus, creating a significant amount of design permutations to suit its design specifications. Tubular heat exchangers can be further classified as (Walker, 1990):

- Double-pipe heat exchangers.
- Shell and tube heat exchangers.
- Spiral tube type heat exchangers.

Double-Pipe Heat Exchangers

A common double-pipe heat exchanger is constructed of two pipes, where the smaller pipe is concentrically placed inside the larger pipe, as illustrated by Fig. 2.2.

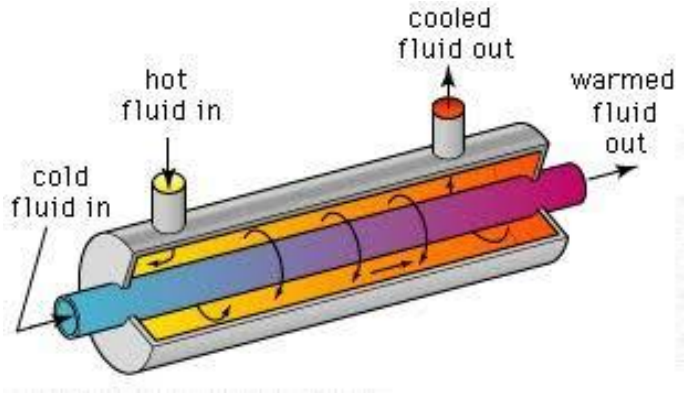

Figure 2.2: Double-pipe heat exchanger (Britannica, 2006).

This type of heat exchanger is relatively easy to manufacture, though it does have a disadvantage when it comes to heat transfer surface area, where it has the larger heat transfer area requirement to the equivalent shell and tube arrangement. Double-pipe heat exchangers are commonly used where one of its fluids is highly corrosive, has high pressure and temperature, and is channelled through the inner pipe (Martin, 1992).

Shell and Tube Heat Exchangers

Shell and tube type heat exchangers are constructed with a number of round tubes placed inside large cylindrical shells. The tubes placed in parallel to each other are known as a tube bundle.

Shell and tube heat exchangers are commonly used as pre-heaters in electricity generating power stations, condensers, oil coolers, in process applications, and in the chemical industry (Walker, 1990). In a shell and tube heat exchanger where the tube sheets are fixed, in other words the tube sheets are welded to the shell, there is then no access to the outside of the tube bundle. A fixed tube sheet, which is sealed completely, would be beneficial where a volatile refrigerant is used. A typical single tube and shell pass heat exchanger is depicted in Figure 2.3.

Figure 2.3: Shell and tube heat exchanger (HRS Heat Exchangers, 2016).

A large number of shell and tube flow arrangements are used depending on the heat duty, pressure drop specification, pressure level, fouling, cost, manufacturing techniques, and cleaning requirements (Kakaç & Liu, 2002). Transverse baffles are used on the shell side of the shell and tube heat exchanger; this is to improve the shell side heat transfer coefficient and to structurally support the tubes. Shell and tube heat exchangers can be designed for any operating condition, heat transfer capacity, and financial capital expenditure.

2.2.2 Influence of Working Fluids

According to (Walker, 1990) there are various aspects that need to be considered with regards to the working fluid. These are:

- Pressure - The pressure within the heat exchanger module has a remarkable impact on the wall-thickness that is required, therefore the fluid with the higher pressure should preferably be allocated to flow though the tubes.
- Corrosive fluids – The more corrosive fluid must flow through the tubes, it is needless to say, but otherwise both the shell and tubes will be corroded.
- Fouling – The more seriously fouling fluid should be allocated to flow through the tubes, as it is easier to maintain.
- Pressure drop – Depending on the arrangement of the tube bundle and flow arrangement, the pressure drop of tube side flow is predominately less than shell side pressure drops. Thus, the fluid that can afford a slightly larger pressure drop is allocated to shell side flow.

- Mass flow - Commonly the fluid that has a lower mass flow rate should be allocated to shell side flow, this is due to turbulent flow being achieved at a lower Reynolds number within the tube bundle rather than within the tubes itself. This increases the heat transfer coefficient of the fluid with the lower mass flow rate.

Design conflicts will arise when these requirements clash with one another and it is up to the designer to do a proper trade-off and find the most thermally and ergonomically efficient solution.

2.3 Thermophysical Properties of Aqua-Ammonia Solutions

2.3.1 Introduction to the Thermophysical Properties of Aqua-Ammonia Solution

The thermodynamic design and rating calculations of heat exchangers and more specifically heat exchangers for an absorption-desorption H&R cycles, require the access to simple and conservative mathematical methods to calculate the thermophysical (thermodynamic + transport) properties of aqua-ammonia mixtures. Despite the extended history of absorption-desorption cycles, data and methods of calculating thermophysical properties for ammonia-water mixtures are inadequate and don't cover all regions which are vital to the design sizing.

Thermophysical properties are readily found in heat transfer text books, for example (Cengel & Ghajar, 2011) & (Borgnakke & Sonntag, 2009), but these are mainly for pure substances. Then there are software programs which do deliver some thermophysical properties of mixtures, such as EES and (N.I.S.T, 2016), but do not supply a full set of thermophysical properties for all regions of the fluid mixture. Most sources only supply thermodynamic properties and one transport property, i.e. density, where properties namely, conductivity, viscosity, and Prandtl number (known as the transport properties) are required to complete the thermodynamic design. Thus, extensive research was required to find a mathematical calculation method of determining the transport properties of aqua-ammonia solutions.

Increasing interest in recent years in the re-development of absorption-desorption refrigeration has led to a significant research effort on the availability of new thermophysical properties formulation. A Swiss company specialising in the development of thermodynamic and transport properties published a research paper in 2004 entitled, "Thermophysical Properties of {NH_3 + H_2O} Solutions for the Industrial Design of Absorption Refrigeration Equipment". The research paper of (Conde-Petit, 2004) covers regions of interest for the thermodynamic design of the heat exchangers for an aqua-ammonia absorption-desorption cycle. Conde-Petit (2004) has based its formulation of unified and conceptually simple equations for thermophysical properties on Helmoltz free energies in (Tilner-Roth & Friend, 1998) or Gibbs free energies as documented in (Ibrahim & Klein, 1993) and (El-Sayed & Tribus, 1985). The mathematical calculation methods illustrated in (Conde-Petit, 2004), included the thermodynamic and transport properties of saturated liquid and saturated vapour phase of an ammonia-water solution at a specified pressure

and concentration. Therefore, the comprehensive research paper and mathematical models of Conde-Petit (2004) are illustrated in detail in Appendix A 1. These mathematical models will be used to determine the thermophysical properties of aqua-ammonia and aid the thermodynamic design and rating model of the heat exchangers in the aqua-ammonia absorption-desorption H&R cycle.

2.4 Thermophysical Properties of Ethylene Glycol-Water Solutions

Ethylene glycol and water solutions are considered to be secondary refrigerants or brines. These types of refrigerants are used in air conditioning, refrigeration, and heating plants where on every occasion indirect heat transfer processes takes place. The thermophysical properties of brines can be calculated by means of a mathematical model proposed in (Conde-Petit, 2011), which include specific thermal capacity, density, dynamic viscosity, thermal conductivity, and Prandtl number. Full review of the mathematical model used to determine the thermophysical properties of an ethylene glycol water solution are available in the extended literature review of Appendix A 1.2.

2.5 Thermodynamic Design and Rating

This section focuses on the most common problem of heat exchanger designs, the sizing and rating thereof. The sizing problem involves the calculation of the heat exchanger's dimensions, including the selection of applicable heat exchanger type. The sizes are determined to meet the requirements of the specified hot- and cold fluid inlet and outlet temperatures, mass flow rates, and allowable pressure drop. On the other hand is the rating problem, which is based on the sized heat exchanger's overall heat transfer coefficient, the inlet and outlet temperatures, prescribed mass flow rates, and heat transfer surface area. The procedure when solving the sizing problem of a heat exchanger's design can be found in (Kakaç & Liu, 2002) as:

- Select the type of heat exchanger suitable for the application.
- Calculate or assume any unknown in- or outlet temperatures.
- Determine the heat transfer rate using an energy balance (first law of thermodynamics).
- Calculate the Log Mean Temperature Difference and correction factor *F*, where applicable to flow pattern within the heat exchanger.
- Determine the overall heat transfer coefficient U_c.
- Calculate the heat transfer surface area.
- Use the above mentioned to determine the performance rating or thermal efficiency.

2.5.1 Basics of Heat Exchanger Design Calculations

The basics of heat transfer equations will be discussed for the thermal analysis (sizing and rating calculations) of shell and tube heat exchangers, as the aqua-ammonia absorption-desorption H&R cycle requires fluid-to-fluid heat transfer. The temperature variations of parallel- and counter-flow heat exchangers are represented in Figure A.1 (Cengel & Ghajar, 2011), where the heat transfer surface area A is plotted along the *x*-axis and the temperature of the inlets and outlets plotted on the *y*-axis. Represented in Figure A.2 is the temperature versus unit surface area lines of condensing and evaporating fluids, respectively, which is extracted from (Cengel & Ghajar, 2011).

Note: The heat capacity, ($\dot{m}\ C_p$), of both condensing and boiling heat exchangers trends towards infinity.

First Law of Thermodynamics

The first law of thermodynamics for a control volume, under steady state conditions between two thermodynamic state changes gives

$$\dot{Q} = \dot{m}(\alpha_2 - \alpha_1) \ \ [W], \tag{2.1}$$

where α_1 and α_2 represents the inlet and outlet enthalpy values of the fluid stream, with known inlet and outlet conditions. When heat transfer between the heat exchanger and its surroundings are neglected, the system is an adiabatic process. If one of the fluids undergo a phase change, the heat transfer rate cannot be approached as

$$\dot{Q} = \dot{m}\ Cp\ (T_2 - T_1)\ \ [W] \tag{2.2}$$

Establishing a mean value of the temperature difference between the 'hot' and 'cold' fluids at their inlets and outlets respectively, as $\Delta T = T_{hot} - T_{cold}$, would result in the equation for calculating the heat transfer rate between the fluids in a heat exchanger as:

$$\dot{Q} = U_c\ A_s \Delta T_m\ [W], \tag{2.3}$$

where A_s represents the total heat transfer area in [m^2], U_c is the overall heat transfer coefficient of both fluids in [$W/m^2.K$], and ΔT_m is the mean temperature difference in [°C]. Thus, it is clear that for the sizing problem it comes down to determining the overall heat transfer coefficient and the mean temperature difference.

2.5.2 Log Mean Temperature Difference Method (LMTD Method)

The temperature difference between the 'hot' and 'cold' fluids varies along the heat exchanger, and the convenience of having a mean temperature difference for the determination of Eq. 2.3 as previously mentioned in section 2.5.1. The log mean temperature difference, which is a further

development of the average temperature difference between two fluids, can be determined by applying an energy balance to a differential area *dA* in the 'hot' and 'cold' fluids. A short proof illustrating the correlations of parallel- and counter-flow log mean temperature differences are shown in the extended theoretical background review in Appendix A 2.2. The log mean temperature difference for a counter-flow heat exchanger is given by solving Eq. 2.2 for 'hot' and 'cold' fluids, substituting into Eq. A.33 and with some rearrangement as:

$$\Delta T_{LMTD} = \frac{\left(T_{h,out} - T_{c,in}\right) - \left(T_{h,in} - T_{c,out}\right)}{\ln\left(\frac{T_{h,out} - T_{c,in}}{T_{h,in} - T_{c,out}}\right)} \quad [°C] \tag{2.4}$$

It can be shown that for parallel-flow HTEX, Eq. 2.4 becomes

$$\Delta T_{LMTD} = \frac{\left(T_{h,in} - T_{c,in}\right) - \left(T_{h,out} - T_{c,out}\right)}{\ln\left(\frac{T_{h,in} - T_{c,in}}{T_{h,out} - T_{c,out}}\right)} \quad [°C] \tag{2.5}$$

Now, the heat transfer rate for a counter-flow heat exchanger can be expressed as

$$\dot{Q} = U_c \, A_s \Delta T_{LMTD,CF} \, [W] \tag{2.6}$$

It should be noted that for the same inlet and outlet temperatures, the LMTD f or counter-flow exceeds that of parallel flow, $\Delta T_{LMTD,\ CF} > \Delta T_{LMTD,\ PF}$ (Thulukakanam, 2000). Counter-flow LMTD represents the maximum temperature potential for heat transfer, thus, the surface area required is smaller for counter-flow arrangement at the same prescribed heat transfer rate.

Cross-Flow and Multi-Pass Heat Exchangers

The log mean temperature difference explained earlier is only limited to parallel- and counter-flow heat exchanger arrangements. Though, similar arrangements have been developed for cross-flow and multi-tube-pass heat exchangers, but the relations created are too convoluted because of the complex flow conditions. According to (Thulukakanam, 2000), a correction factor *F* was introduced to represent cross-flow and multi-pass heat exchangers. Correction factor *F* is dependent on the geometry and the in- and outlet conditions. The log mean temperature difference of cross-flow or multi-pass heat exchangers can be expressed as

$$\Delta T_{LMTD} = F \Delta T_{LMTD,CF} \tag{2.7}$$

The correction factor charts illustrated in Figure A.3 requires the calculation of two temperature ratios, namely, *P* and *R*, which are defined by Eqs. A.37 and A.38 in Appendix A 2.2.

In conclusion, the log mean temperature difference method is highly suited to calculate the heat transfer surface area required from a heat exchanger to realise the pre-assumed outlet temperatures, when the inlet temperatures and mass flow rates are specified.

2.5.3 The Effectiveness Method (NTU Method)

Earlier it was mentioned that a heat exchanger analysis consists of two problems, sizing and rating, and now that the sizing problem has been dealt with, the solution of the rating problem can be clarified. The NTU method mainly focuses on the outlet temperatures and the heat transfer performance of a sized heat exchanger model. The effectiveness-NTU method was developed by Kays and London in 1955 according to (Cengel & Ghajar, 2011). This greatly simplified heat exchanger analysis from the tedious iterative method of using the LMTD method for heat exchanger rating.

Effectiveness relations of heat exchangers involve the dimensionless relations, namely, number of transfer units or NTU and capacity ratio, of which the former can be expressed using the following equation, as found in (Cengel & Ghajar, 2011).

$$NTU = \frac{UA_s}{C_{min}} = \frac{UA_s}{\left(\dot{m}\, C_p\right)_{min}} \tag{2.8}$$

NTU is thus proportional to the heat transfer surface area, therefore the larger the sized heat exchanger model the larger the number of transfer units. The effectiveness of a heat exchanger is a function of two dimensionless parameters, of which the later mentioned capacity ratio can be expressed as

$$c = \frac{C_{min}}{C_{max}}\,, \tag{2.9}$$

where $C_c > C_h$, so that $C_c = C_{max}$ and $C_h = C_{min}$, and vice versa. Lastly, the effectiveness relations are a function of the flow arrangement in the heat exchanger, which is illustrated by Table 2.1.

Standardised effectiveness charts have been created by (Kays & Perkins, 1972) found in (Cengel & Ghajar, 2011), for specific heat exchanger arrangements are illustrated by Fig. A.4 of Appendix A 2.3. The values of $\boldsymbol{\varepsilon}$ and NTU are used as an indicator to determine if the sized heat exchanger model created with the LMTD method is practically viable. The optimum would be to intersect the standardised effectiveness curve with the respective effectiveness, NTU, and capacity ratio values, but any point below the effectiveness curve would indicate to a heat exchanger which is practically viable. However, it is possible to raise the effectiveness and NTU of the sized heat exchanger model to its theoretical maximum performance by determining the maximum outlet temperatures and repeating the effectiveness vs. NTU method. Thus, the NTU method can be utilised as a good indicator for practically realistic temperature boundary conditions especially in determining the commonly unknown secondary refrigerant's outlet temperature.

Table 2.1: Effectiveness relations of (Kays & Perkins, 1972).

Heat exchanger type	Effectiveness relation
1 *Double pipe:*	
Parallel-flow	$\varepsilon = \frac{1 - \exp[-\text{NTU}(1+c)]}{1+c}$
Counter-flow	$\varepsilon = \frac{1 - \exp[-\text{NTU}(1-c)]}{1 - c\exp[-\text{NTU}(1-c)]}$
2 *Shell and tube:*	
One-shell pass 2, 4, . . . tube passes	$\varepsilon = 2\left\{1 + c + \sqrt{1+c^2}\,\frac{1+\exp[-\text{NTU}\sqrt{1+c^2}]}{1-\exp[-\text{NTU}\sqrt{1+c^2}]}\right\}^{-1}$
3 *Cross-flow (single-pass)*	
Both fluids unmixed	$\varepsilon = 1 - \exp\left\{\frac{\text{NTU}^{0.22}}{c}[\exp(-c\ \text{NTU}^{0.78}) - 1]\right\}$
C_{max} mixed, C_{min} unmixed	$\varepsilon = \frac{1}{c}(1 - \exp\{1 - c[1 - \exp(-\text{NTU})]\})$
C_{min} mixed, C_{max} unmixed	$\varepsilon = 1 - \exp\left\{-\frac{1}{c}[1 - \exp(-c\ \text{NTU})]\right\}$
4 *All heat exchangers with* $c = 0$	$\varepsilon = 1 - \exp(-\text{NTU})$

Note: Eq. 4 of Table 2.1 is used for determining the effectiveness relations of phase-change heat exchangers (Cengel & Ghajar, 2011).

2.5.4 Overall Heat Transfer Coefficient

The final piece of the heat exchanger analysis puzzle is the calculation of the overall heat transfer coefficient. It's a single relation that expresses each fluids heat transfer capabilities with its respective thermophysical properties. Within any typical heat exchanger of two fluids, the heat will first be transferred from the 'hot' fluid to the wall separating the fluids, via convection. After which, the heat travels through the wall, via conduction, to heat the 'cold' fluid via convection. Any radiation that could occur is factored into the convective heat transfer coefficients.

The type of heat exchanger geometry greatly influences the overall heat transfer coefficient, the flow Reynolds number, and fluids thermophysical properties. If fouling factors (discussed in Appendix A 2.8) are assumed to have no effect or if the sizing of the heat exchanger is yet to be determine, the overall heat transfer coefficient can be expressed as

$$\frac{1}{U_c} = \frac{1}{h_o} + \frac{1}{h_i}.\frac{d_o}{d_i} + \frac{r_o \ln\left(\frac{r_o}{r_i}\right)}{k_{material}}, \qquad \textbf{(2.10)}$$

where h_o and h_i represents the heat transfer coefficients of the outer- and inner wall of the heat exchanger's tubes respectively in [W/m^2.K] (Thulukakanam, 2000).

The factors of shell side and tube side heat transfer coefficients have far greater influence on the outcome of U_c than the size of the tubes and its material thermal conductivity. Thus, it is of great importance to obtain the correct relation for shell and tube side heat transfer coefficients to match the heat exchanger's geometry, flow conditions, and thermophysical conditions.

2.5.5 Shell Side Heat Transfer Coefficient

The following section deals with the shell side heat transfer coefficient in general and for the specific types of heat exchangers to be designed in this dissertation. Flow through tube bundles have been studied experimentally since it is too complex to be treated analytically. Several correlations, all based on experimental data, have been proposed for the average Nusselt number for flow over tube bundles.

The Nusselt number is named after Wilhelm Nusselt (1882-1957), who defined this dimensionless number in 1915 in his pioneering paper: "*The Basic Laws of Heat Transfer*". The original Nusselt number correlation is defined as:

$$Nu = \frac{h\, L_c}{k} \tag{2.11}$$

Note: The Nusselt number represents the enhancement of heat transfer through a fluid layer as a result of convection relative to conduction across the same fluid layer. A larger Nusselt number ensures more effective convection. If Nu = 1, pure conduction exists across the fluid layer (Cengel & Ghajar, 2011).

Zukauskas – Nusselt Correlation for Tube Bundles

More recently, (Zukauskas, 1987) has proposed a Nusselt number correlation for flow through tube bundles, whose general form is

$$Nu_D = c_n\, Re_D^m\, Pr^n \left(\frac{Pr}{Pr_{wall}}\right)^{0.25}, \tag{2.12}$$

with the constants c_n, m, and n are dependent on the Reynolds number of the fluid flowing through the tube bundle and Pr_{wall} being the Prandtl number estimated at the wall temperature. The average Nusselt number relations proposed by (Zukauskas, 1987) in Table 2.2 can also be used in the calculations of tube bundles less than 16 rows, provided that the correction factor is applied with

$$Nu_{D,N_L<16} = F\, Nu_D \tag{2.13}$$

Table 2.2: Nusselt number correlations for flow over tube bundles for N_L > 16.

Arrangement	Range of Re_D	Correlation	Eq.
In-line	0 - 100	$Nu_D = 0.9\, Re_D^{0.4}\, Pr^{0.36} \left(\frac{Pr}{Pr_{wall}}\right)^{0.25}$	**(2.14)**
	100 - 1000	$Nu_D = 0.52\, Re_D^{0.5}\, Pr^{0.36} \left(\frac{Pr}{Pr_{wall}}\right)^{0.25}$	**(2.15)**
	1000 - 2 * 10^5	$Nu_D = 0.27\, Re_D^{0.63}\, Pr^{0.36} \left(\frac{Pr}{Pr_{wall}}\right)^{0.25}$	**(2.16)**
	2 x 10^5 - 2 x 10^6	$Nu_D = 0.033\, Re_D^{0.8}\, Pr^{0.4} \left(\frac{Pr}{Pr_{wall}}\right)^{0.25}$	**(2.17)**
Staggered	0 - 500	$Nu_D = 1.04\, Re_D^{0.4}\, Pr^{0.36} \left(\frac{Pr}{Pr_{wall}}\right)^{0.25}$	**(2.18)**
	500 - 1000	$Nu_D = 0.71\, Re_D^{0.5}\, Pr^{0.36} \left(\frac{Pr}{Pr_{wall}}\right)^{0.25}$	**(2.19)**
	1000 - 2 * 10^5	$Nu_D = 0.35 \left(\frac{S_T}{S_L}\right)^{0.2} Re_D^{0.6}\, Pr^{0.36} \left(\frac{Pr}{Pr_{wall}}\right)^{0.25}$	**(2.20)**
	2 x 10^5 - 2 x 10^6	$Nu_D = 0.031 \left(\frac{S_T}{S_L}\right) Re_D^{0.8}\, Pr^{0.36} \left(\frac{Pr}{Pr_{wall}}\right)^{0.25}$	**(2.21)**

Note: All properties except Pr_{wall} are evaluated at the bulk fluid temperature, which is the average temperature of the fluid in- and outlet temperatures (Cengel & Ghajar, 2011).

Table 2.3 illustrates the correction factors c_n to be used for tube bundles of less than 16 rows.

Table 2.3: Correction factors c_n.

N_L	1	2	3	4	5	7	10	13
In-line	0.7	0.8	0.86	0.9	0.93	0.96	0.98	0.99
Staggered	0.64	0.76	0.84	0.89	0.93	0.96	0.98	0.99

Nusselt – Nusselt Correlation for Laminar Film Condensation over a Single Horizontal Tube

Nusselt correlation for condensing fluids in a laminar flow state are treated as a case of laminar film condensation of a sluggish vapour on an isothermal horizontal tube, as depicted in Figure 2.4. The motion of the condensing fluid is a balance of viscous and gravitational forces. In the Nusselt (1916) analysis adopted by (Kakaç & Liu, 2002), the convection terms in the energy equation are neglected, so that the local heat transfer coefficient around the tube can be written as

$$h(\varphi) = \frac{k_l}{\delta(\varphi)}, \qquad \textbf{(2.22)}$$

where φ is the circumferential angle function of δ, which is the thickness of the film.

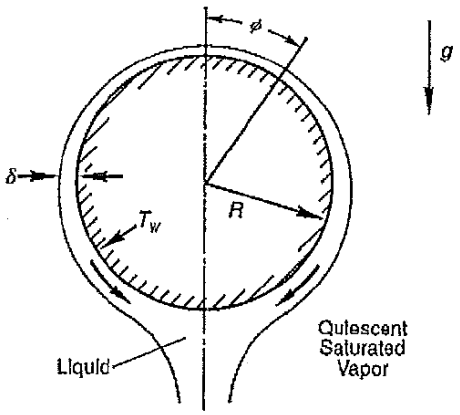

Figure 2.4: Film condensation flow profile on a horizontal tube (Kakac & Liu, 2002).

Logically, the heat transfer coefficient would be maximum at the top of the tube where the film thickness is the lowest. The opposite is true for the bottom of the tube, where the heat transfer coefficient drops to zero as the film thickness increases. The Nusselt correlation for laminar film condensation over a horizontal tube was first introduced in (Nusselt, 1916), which was found in (Kakaç & Liu, 2002), is expressed as

$$h_l = 0.728 * \frac{k_l}{d_o}\left[\frac{\rho_l(\rho_l - \rho_v) * g * \left(\alpha_{fg} * 10^3\right) * d_o^3}{\mu_l * (T_{sat} - T_{wall}) * k_l}\right]^{0.25} \quad \textbf{(2.23)}$$

Film Condensation in Tube Bundles

Film condensation within tube bundles creates several added complexities, as the condensate flow from a given tube is assumed to drain by gravity to the lower adjacent tubes in a laminar continuous sheet. In reality, the condensate may not fall directly vertical to the next tube; it may instead flow sideways (depending on the diameter of the tube and the spacing between tubes), or where vapour velocity is high enough to create shear forces on the condensate as shown by Figure 2.5.

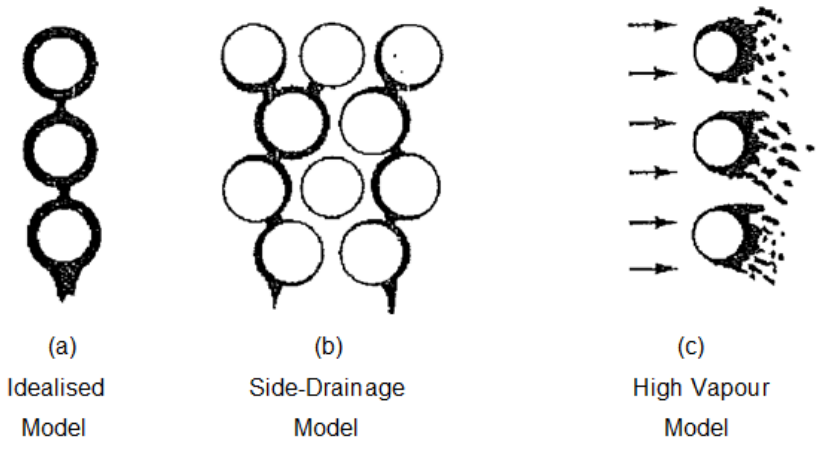

Figure 2.5: Graphic representation of condensate flow through tube bundles (Kakaç & Liu, 2002).

Where there is an absence of vapour velocity the condensate flow by gravity to the lower tubes in the tube bundle (known as condensate inundation), then the film thickness around the lower tubes of the tube bundle should increase and the heat transfer coefficient should decrease (Wolverine Tube Inc, 2014).

Nusselt (1916) added to his film condensation analysis over a single horizontal tube, by introducing an idealised in-line tube column model. Nusselt assumed that the condensate from any given tube in the idealised model would drain to the next tube in a continuous laminar sheet, and that the (T_{sat} – T_{wall}) remains constant across all tubes. With these assumptions Nusselt proposed the average heat transfer coefficient for a vertical column of N tubes, which compares to the top tube of the column as calculated with Eq. 2.23.

$$\frac{h_{m,N}}{h_l} = N^{-1/4} \tag{2.24}$$

According to (Kakaç & Liu, 2002), Nusselt also proposed a correlation for the local coefficient at the Nth tube as

$$\frac{h_N}{h_l} = N^{3/4} - (N-1)^{3/4} \tag{2.25}$$

Kern (1958), as referenced by (Kakaç & Liu, 2002), proposed a less conservative correlation for the mean and local film condensation heat transfer coefficients as

$$\frac{h_{m,N}}{h_l} = N^{-1/6} \tag{2.26}$$

and

$$\frac{h_N}{h_l} = N^{5/6} - (N-1)^{5/6} \tag{2.27}$$

However, the data of numerous experimental measurements have been very scattered and still today there is no successful theoretical model. Thus, for the purposes of design-sizing and rating it's recommended by (Butterworth, 1977) that Eq. 2.26 and Eq. 2.27 are conservative to use for shell side heat transfer coefficient calculation, when there is an absence of vapour velocity. In cases where high vapour velocity is present, the condensate is subjected to vapour shear, as illustrated in Figure 2.5(c). Initially, the effects of vapour shear and condensate inundation where treated separately. However, according to (Kakaç & Liu, 2002), Butterworth proposed an inundation and vapour shear local heat transfer coefficient relationship for the Nth tube row in (Butterworth, 1977) as

$$h_N = \left[\frac{1}{2}h_{sh}^2 + \left(\frac{1}{4}h_{sh}^4 + h_l^4\right)^{\frac{1}{2}}\right]^{1/2} \left[N^{\frac{5}{6}} - (N-1)^{\frac{5}{6}}\right], \tag{2.28}$$

where h_{sh} (condensate vapour shear) can be calculated as

$$h_{sh} = 0.59 \frac{k_l}{d_o} \tilde{R}e^{1/2} \quad \textbf{(2.29)}$$

and $\tilde{R}e$ (two-phase Reynolds number) as

$$\tilde{R}e = \frac{\rho_l u_g d_o}{\mu_l} \quad \textbf{(2.30)}$$

Here u_g represents the mean local velocity of the vapour flowing through the tube bundle and is calculated at the mean flow width, which is the nuclei of the tube bundle layout as shown by Figure A.5. High vapour velocities may exist near the inlet(s) of the condenser, where deeper into the tube bundle the vapour velocities would decrease rapidly as the saturated vapour condenses.

Boiling Regime - Nusselt Correlation

The more popular correlations incorporate both low and high quality behaviour in an adaptive fashion, for instance the plain tube bundle boiling prediction method of (Wolvering Tube Inc, 2014), in which both the convective and nucleate boiling values are determined separately and then added together as

$$h_{bundle} = \left(h_{nb}^2 + h_{cb}^2\right)^{1/2} \quad \textbf{(2.31)}$$

According to (Wolvering Tube Inc, 2014), the nucleate boiling heat transfer coefficient can be predicted by the (Cooper, 1984) dimensional correlation and the convective boiling heat transfer coefficient as proposed by (Cornwell, 1989). Cooper's nucleate boiling heat transfer coefficient can be determined by the following:

$$h_{nb} = 55 \left(P_r^{0.12-0.4343 \ln(R_p)}\right) (-0.4343 \ln(P_r))^{-0.55} M_{NH_3}^{-0.5} \dot{q}_{nucleate}^{0.67} \quad \textbf{(2.32)}$$

where the dimensional correlation is measured in [W/m^2.K], the heat flux of q in [W/m^2], with M is the molecular mass, R_p is the surface roughness in [μm], and P_r is the reduced pressure of the fluid. When the surface roughness of the tubes is unknown, it can be assumed as 1.0 μm (Wolvering Tube Inc, 2014).

The nucleate boiling heat flux term of Eq. 2.32 is determined by utilising the correlation proposed by (Rohsenow, 1952) as found in (Cengel & Ghajar, 2011) as

$$\dot{q}_{nucleate} = \mu_l \alpha_{fg} \left[\frac{g(\rho_l - \rho_v)}{\sigma}\right]^{1/2} \left[\frac{C_{p,l}(T_{wall} - T_{sat})}{C_{sf} h_{fg} Pr_8^n}\right]^3, \quad \textbf{(2.33)}$$

where C_{sf} is the experimental constant that depends on the surface-fluid combination, and n is the experimental constant that depends on the type of fluid. The values of C_{sf} and n are found in Table A.19 in Appendix A 2.4.1.

When designing any boiling heat transfer equipment it's extremely important for the designer to have the critical heat flux in order to avoid the danger of burnout. The critical heat flux can be expressed as

$$\dot{q}_{max} = C_{cr}\alpha_{fg}[\sigma g \rho_v^2(\rho_l - \rho_v)]^{1/4}, \quad \textbf{(2.34)}$$

where C_{cr} is a constant which depends on the tube geometry and is found in Table A.20 in Appendix A 2.4.1.

Cornwell's convective boiling heat transfer coefficient is expressed as

$$h_{cb} = 4.032\left(Re_{\delta}^{0.236}\right)\left(Pr_l^{0.4}\right)\left(\frac{k_l}{\delta}\right) \quad \textbf{(2.35)}$$

In this correlation the Pr_l is the liquid Prandtl number, δ is the liquid film thickness, and Re_{δ} is the liquid film Reynolds number, which is given by the following (Wolvering Tube Inc, 2014):

$$Re_{\delta} = \frac{4\rho_l u_l \delta}{\mu_l} \quad \textbf{(2.36)}$$

The liquid velocity of the film is determined by using the minimum cross-sectional area of the bundle, which is similar to the method used for single-phase cross flows.

An extension of the shell side heat transfer coefficient is available in Appendix A 2.4, which includes the Reynolds number correlations for flow over a horizontal tube and flow through tube bundles.

2.5.6 Tube Side Heat Transfer Coefficient

According to (Cengel & Ghajar, 2011), the well-known problem stated by Wilhelm Nusselt and Leo Graetz for an incompressible fluid with constant properties flowing through a circular duct with a constant wall temperature and fully developed laminar velocity profile was solved numerically in the handbook of Shah & Bhatti (1987). The Nusselt correlations (subscript T) for flow through a circular duct of length L are

$$Nu_T = 1.61\left(\frac{Pe_b d}{L}\right)^{1/3} \quad for\ \frac{Pe_b d}{L} > 10^3 \quad \textbf{(2.37)}$$

and

$$Nu_T = 3.66\ for\ \frac{Pe_b d}{L} < 10^2 \quad \textbf{(2.38)}$$

where the Graetz number or Gz is

$$Gz = \frac{Pe_b d}{L} \tag{2.39}$$

The superposition mean Nusselt number correlation for laminar flow in circular ducts was found in (Kakaç & Liu, 2002), but originally proposed by (Gnielinski, 1983) to give sufficiently good values for most practical applications.

$$Nu_T = \left[3.66^3 + 1.61^3 \left(\frac{Pe_b d}{L}\right)\right]^{1/3} \tag{2.40}$$

Hausen – Nusselt Correlation for Laminar Flow through Circular Ducts

The empirical Nusselt correlation was originally proposed in (Hausen, 1959) as found in (Kakaç & Liu, 2002) and (Thulukakanam, 2000), for laminar flow in the thermal entrance region of a circular duct is comparable to the values of the correlation proposed in Eq. 2.40. The Hausen (1959) Nusselt correlation is

$$Nu_T = 3.66 + \frac{0.19\left(\frac{Pe_b d_i}{L}\right)^{0.8}}{1 + 0.117\left(\frac{Pe_b d_i}{L}\right)^{0.467}} \tag{2.41}$$

The results of Eq. 2.40 and Eq. 2.41 are comparable according to (Kakaç & Liu, 2002), where both equations can be used for liquids and gases in the range of ($0.1 < Pe_b d/L < 10^4$). The Pèclet number (Pe_b) is the Reynolds number multiplied with the bulk fluid Prandtl number.

Gnielinski – Nusselt Correlation for Transitional Flow through Circular Ducts

(Gnielinski, 1976) found in (Thulukakanam, 2000) proposed a modified Petukhov-Kirillov Nusselt correlation of turbulent flow through circular ducts to be applicable to the transitional region of Reynolds numbers between 2300 and 10^4:

$$Nu_T = \frac{\left(\frac{f}{2}\right)(Re_T - 1000)Pr_b}{1 + 12.7\left(\frac{f}{2}\right)^{1/2}\left(Pr_b^{2/3} - 1\right)}, \tag{2.42}$$

where the friction factor is expressed as

$$f = (1.58 \ln Re_T - 3.28)^{-2} \tag{2.43}$$

The thermophysical properties of the tube side heat transfer coefficient equations are evaluated at the bulk fluid temperature of T_{bulk}, defined as

$$T_{bulk} = \frac{T_{in} + T_{out}}{2} \tag{2.44}$$

An extension of the tube side heat transfer coefficient is available in Appendix A 2.5, which includes the Reynolds number correlations for flow though circular ducts.

2.5.7 Heat Transfer Surface Area

The thermodynamic design cannot be completed without the rearranging of Eq. 2.6, which gives the per tube length of heat transfer surface area as

$$L = \frac{\dot{Q}}{U_c \, \Delta T_{LMTD} (N_t \pi d_o)} \tag{2.45}$$

where all the terms of Eq. 2.45 are known, except for the number of tubes, N_t.

Other physical design dimensions such as the shell diameter D_s, and inner- and outer diameter of the tubes can be approached as variable input parameters creating multiple design permutations. These variable input parameters can be standardised sizes of shells and tubes. The number of tubes in a shell and tube heat exchanger depend on the tube bundle layout, number of tube passes, N_p, the pitch ratio, *PR*, the shell inner diameter, D_s, and the tube's outer diameter, d_o. The number of tubes can be determined by using the following (Kakaç & Liu, 2002):

$$N_t = 0.785 \left(\frac{CTP}{CL}\right)\left(\frac{D_s^2}{PR^2 d_o^2}\right), \tag{2.46}$$

where *CTP* is the number tube pass calculation constant that accounts for the incomplete coverage of the tubes in the shell, as recorded parameters in Table 2.4. *CL* is the tube bundle layout constant, with its parameters recorded in Table 2.5.

Table 2.4: Tube pass constant (Kakaç & Liu, 2002).

One Tube Pass	CTP = 0.93
Two Tube Passes	CTP = 0.90
Three Tube Passes	CTP = 0.85

Table 2.5: Tube bundle layout constant (Kakaç & Liu, 2002).

45° and 90°	CL = 1.0
30° and 60°	CL = 0.87

2.6 Extended Theoretical Background and Literature Review

The theoretical background of the shell and tube side pressure drop ratings have been excluded from the main body of this oeuvre, but is available in Appendix A 2.6 & 2.7, respectively. The equations to determine the fouling overall heat transfer coefficient and percentage over design are added to Appendix A 2.8. Furthermore, the mechanical design considerations and rating is

excluded from the main body of text, as it isn't the main focus of the study but does play a fundamental role in the process of heat exchanger designing. The literature review of the mechanical design rating and considerations are available in Appendix A 3, which depict the stress calculations of the pressurised shell, tube bundle sheet, and the number of bolts required for each header. Available in Appendix A 4 is a short literature review of the occupational health and safety of an aqua-ammonia absorption-desorption H&R cycle.

2.7 Conclusion

In conclusion, the literature review and theoretical background study illustrated the methods of obtaining conservative thermophysical properties, which are essential in determining the thermodynamic design and rating model for each of the heat exchangers. The Conde-Petit (2004) & (2011) mathematical models for determining thermophysical properties have shown to be in good accordance with similar properties obtained with EES, and are therefore considered satisfactory for further thermodynamic design purposes. Furthermore, the chapter illustrated the required shell and tube side heat transfer coefficients correlations required to complete the thermodynamic design of the aqua-ammonia heat exchangers. An extension to the theoretical background and literature review was created to keep the main focus of the chapter to the fundamentals of this study. The following chapter deals with the explanation of how the thermophysical properties are calculated combined with an investigation into the two-phase region of aqua-ammonia.

Chapter 3

3 THERMOPHYSICAL PROPERTIES AND THERMODYNAMIC DESIGN SELECTION

Introduction

Chapter 3 focuses on the development of the thermodynamic design selection by investigating each specific heat exchanger's inlet and outlet conditions, be it for aqua-ammonia or ethylene glycol water mixtures. Compiled within Chapter 3 is an in depth investigation into the thermophysical properties of the two-phase and superheated vapour regions of the theoretical maximum mass concentration aqua-ammonia solution, and the conclusions drawn from any anomalies which may occur. The research into the thermophysical properties of 99 wt% aqua-ammonia carries great effect on what the thermodynamic design output will be for each specific heat exchanger. Furthermore, an extension of Chapter 3 is adopted in Appendix C, which deals with the design requirements and the concept generation and evaluation.

3.1 Thermophysical Properties for Aqua-Ammonia Solutions

Figures 3.1 and 3.2 depict the temperature vs. enthalpy of the 99 wt% ammonia refrigerant line and its thermodynamic states, and the weak and strong aqua-ammonia solutions, respectively. Together with Fig. 1.3, these figures will serve as a reference for the subsequent sections of this oeuvre, but remain open to modification and optimisation.

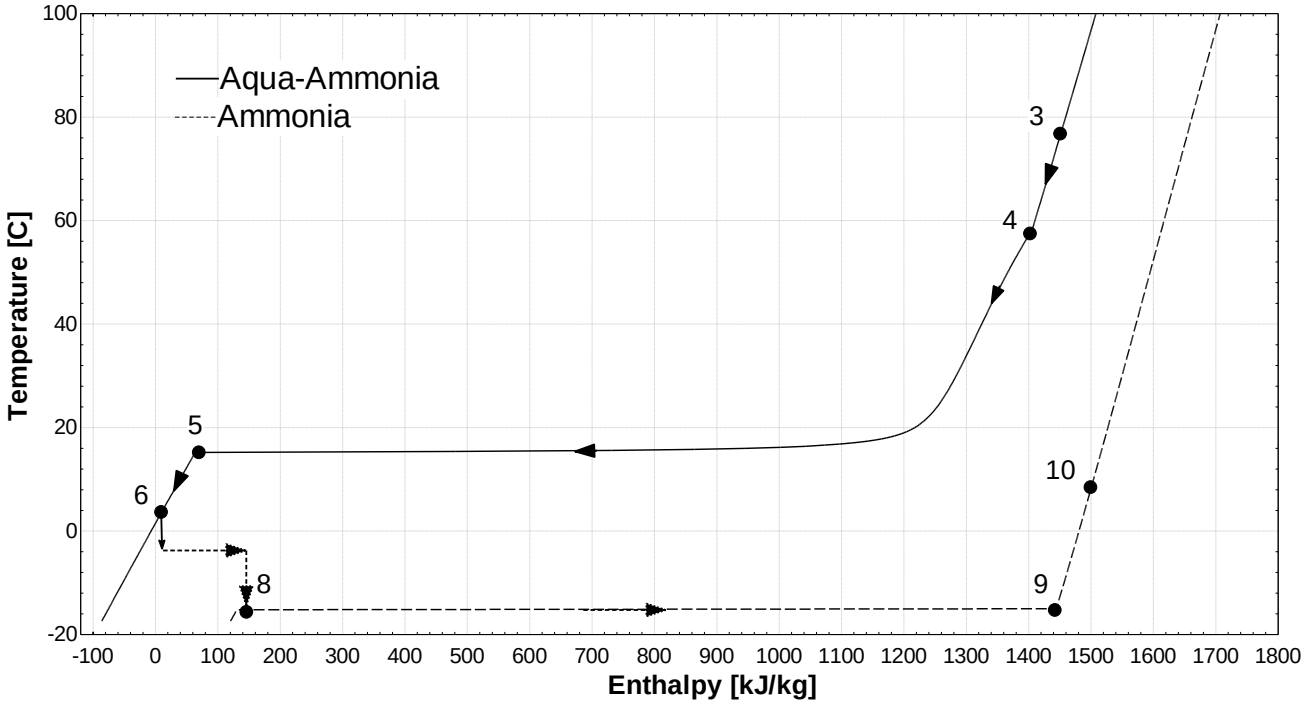

Figure 3.1: Aqua-ammonia absorption-desorption heating and refrigeration heat exchangers temperature vs. enthalpy diagram.

The pressure line of 99 wt% aqua-ammonia is set to a mean system pressure of 7 [bar] and starts off at point 3. Points 1 and 2 form part of the bubble pump generator and rectifier that is out of the scope for this study. The temperature of the superheated vapour state 3 was determined as 77.45 [°C] and is then cooled down to the saturated vapour temperature of state 4. The first anomaly occurs between the latent region of points 4 & 5, as the saturated liquid and vapour temperature isn't a constant temperature. This anomaly was defined by Professor John Tomczyk of Ferris State University as "The temperature difference between the saturated vapour temperature and the saturated liquid at a constant pressure" (Tomczyk et al., 2016). The temperature of state 4 is equal to 54.61 [°C] and condenses to saturated liquid at point 5 with temperature of 15 [°C].

The 'temperature glide' of aqua-ammonia causes a slight problem in calculating the heat transfer coefficient of Eq. 2.48, where Eq. 2.48 requires the use of the saturation temperature, which in this case isn't constant. Thus, further investigation is required. Following state 5, the temperature is lowered by a pre-cool heat exchanger between states 5 to 6. This heat exchanger is

added to the cycle to increase the efficiency of the evaporator and thus the COP of the entire cycle. The sub-cooled liquid of state 6 passes through a venturi to create state 7, whereby the venturi can be approximated as thermostatic (constant enthalpy). State 7 changes to state 8 as the liquid is presented to a state of partial pressure, this is due to the tertiary gas (Helium) in the evaporator module. As the aqueous ammonia feels a partial pressure of 236.2 [kPa] (design requirement), pure ammonia is able to evaporate instantaneously, to which is known as state 9. State 9 is heated to state 10 by the pre-cool heat exchanger.

Figure 3.2 illustrates the weak aqua-ammonia solution at 35.92 wt% ammonia and strong aqua-ammonia solution at 45.3 wt% ammonia at constant pressure of 7 [bar]. Here heat is added to the strong solution at the cost of heat from the weak solution, also known as regenerative heat transfer. This is the most important component of the absorption-desorption H&R cycle in terms of improving the efficiency of the cycle. The cooling of the weak solution liquid line improves the absorption process, as briefly discussed in Chapter 2.1.7.

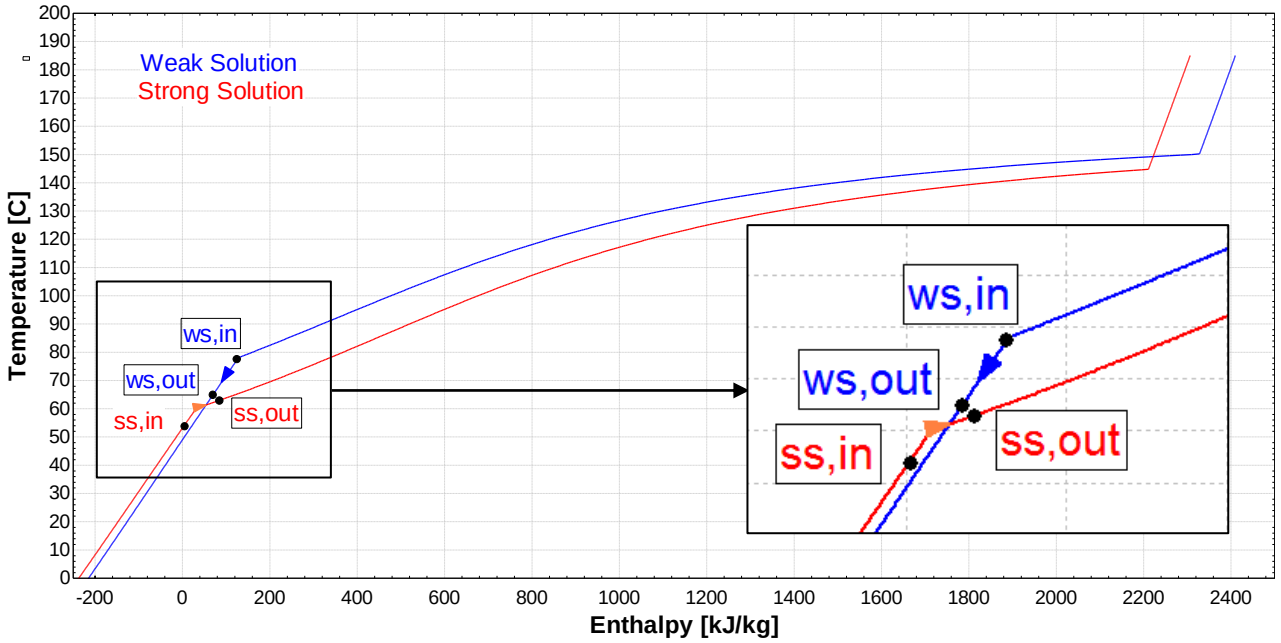

Figure 3.2: Weak and strong solutions aqua-ammonia temperature vs. enthalpy diagram.

3.1.1 Aqua-Ammonia Two-Phase Condensation Investigation

Figure 3.3 illustrates the temperature vs. enthalpy curves of three different constant pressures, with the pressures selected from previous work done by Mr SC van Niekerk as illustrated by the MS Excel 'Clear Sky' data sheet in Appendix D 2.1. The data set obtained from Mr SC van Niekerk depicted an upper and lower boundary of winter and summer ambient conditions, which have a direct influence on the bubble pump generator and its aqua-ammonia outlet conditions (system pressure, temperature, mass flow rate). Therefore, the upper boundary of these conditions were selected at 5 [°C] and 23 [°C], which herein after be known as winter and summer design

conditions, respectively. The third condition selected from the data set is at the average ambient temperature (15 °C) of Potchefstroom, which herein after be known as the average design condition.

The temperature versus enthalpy of Fig. 3.3 appears to remain fairly constant after 1200 [kJ/kg], continuing its way down to saturated liquid state. Therefore, marking the 'turning point' of the temperature glide during the condensation process. The graph of Fig. 3.4 better depicts the turning point of the temperature glide, as it illustrates enthalpy vs. quality of the three design condition curves.

The conclusions drawn from Fig. 3.4 are simply that the enthalpy remains linear with relation to quality until it reaches 1200 [kJ/kg], after which enthalpy becomes non-linear. This change occurs approximately at a quality of 0.94 for each of the three design conditions. Lastly, the graph of Fig. 3.5 depicts the temperature vs. quality of aqueous ammonia at the three design conditions. Figure 3.5 clearly indicates the 'turning point' of the temperature glide created by an aqueous ammonia solution, which is approximated at Q = 0.94 as well. The 'turning point' temperature is approximated to be in the region of 5 [°C] above the saturated liquid temperature for all the ambient conditions. Therefore, it's assumed that state 4 to 5 can be separated into two sections, namely, state 4 to state TP (Turning Point), and state TP to state 5. The thermodynamic design selection would be an engineering decision as to whether: a choice of 2 condensing heat exchangers; or 1 condensing heat exchanger using superposition between states 4 to TP and TP to 5 are designed for.

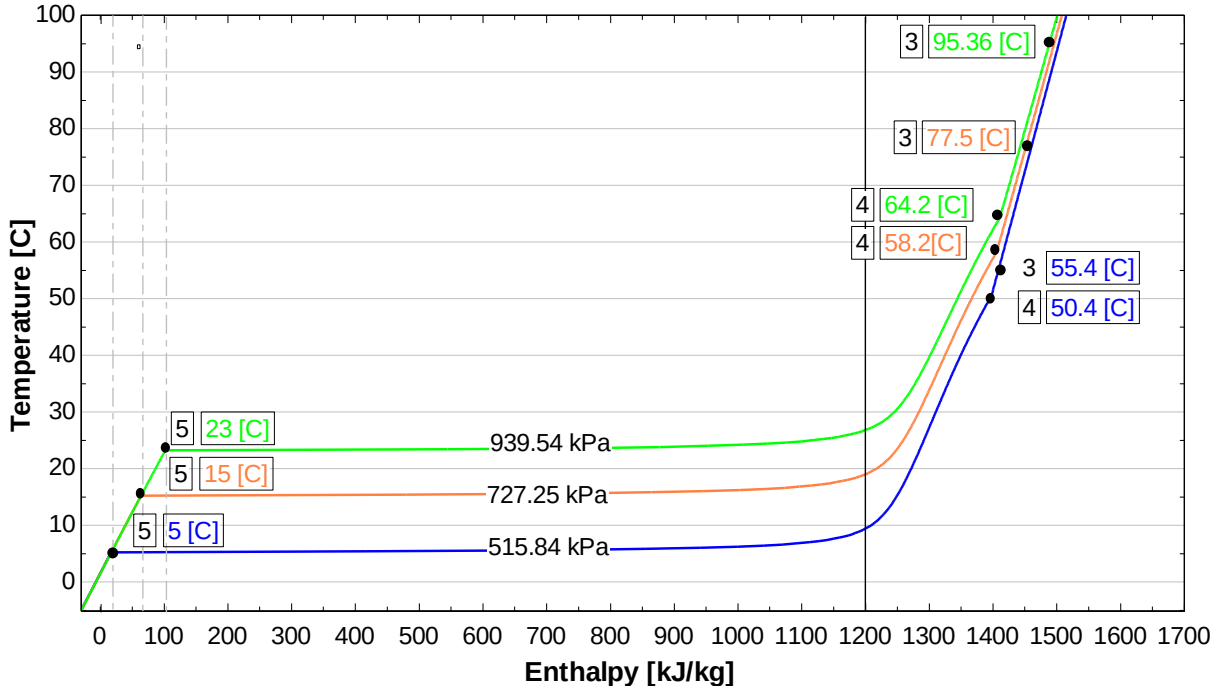

Figure 3.3: Temperature vs. enthalpy of state 3 to 5 for three ambient design conditions.

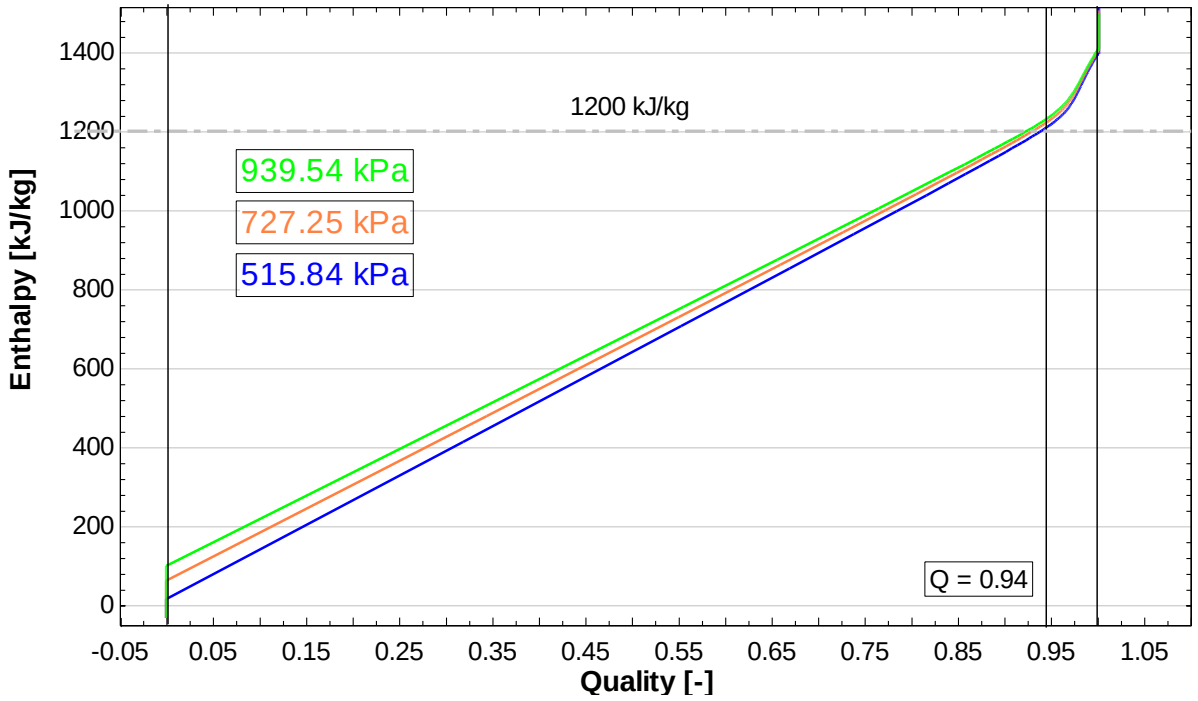

Figure 3.4: Enthalpy vs. quality of the two-phase region for three ambient design conditions of aqua-ammonia.

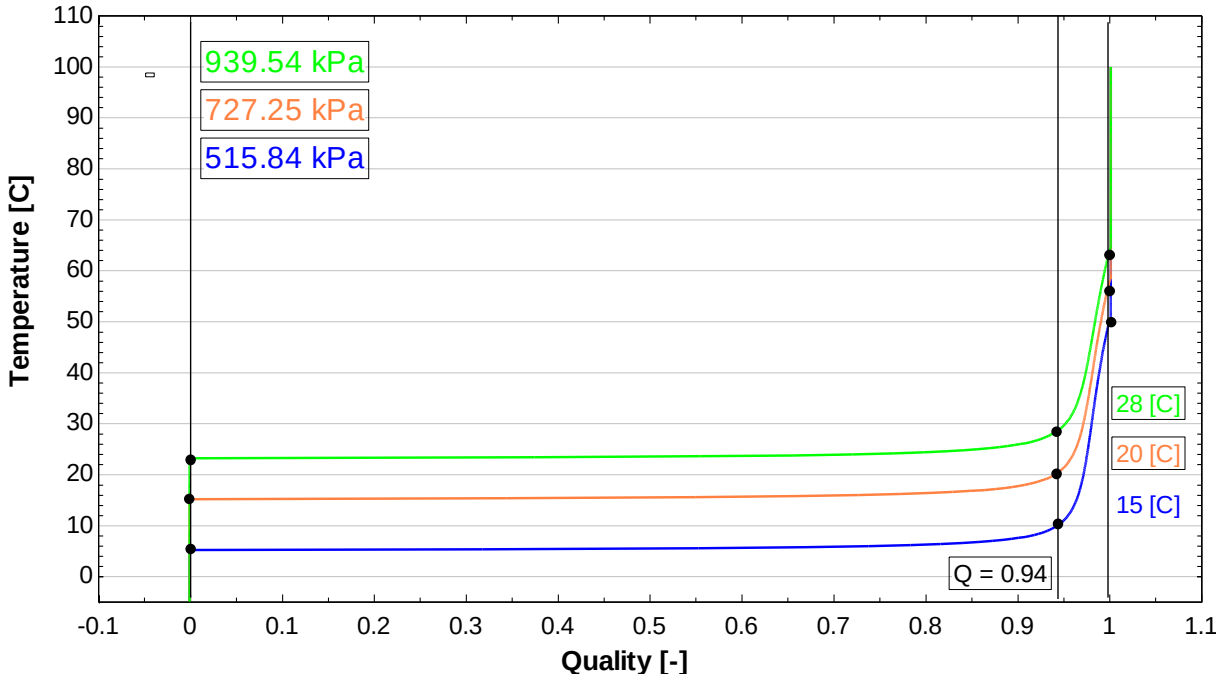

Figure 3.5: Temperature vs. quality of the two-phase region for three ambient design conditions of aqua-ammonia.

Enthalpy of State TP

The enthalpy of state TP at $Q_{x,TP}$ = 0.94 can be approximated as a linear function of quality, as depicted by Fig. 3.6. The black line represents the actual curve of enthalpy as a function of quality, where the red line represents the enthalpy as a linear function of quality. The linear enthalpy approximation is derived by using the grey (dash-dot) construction lines.

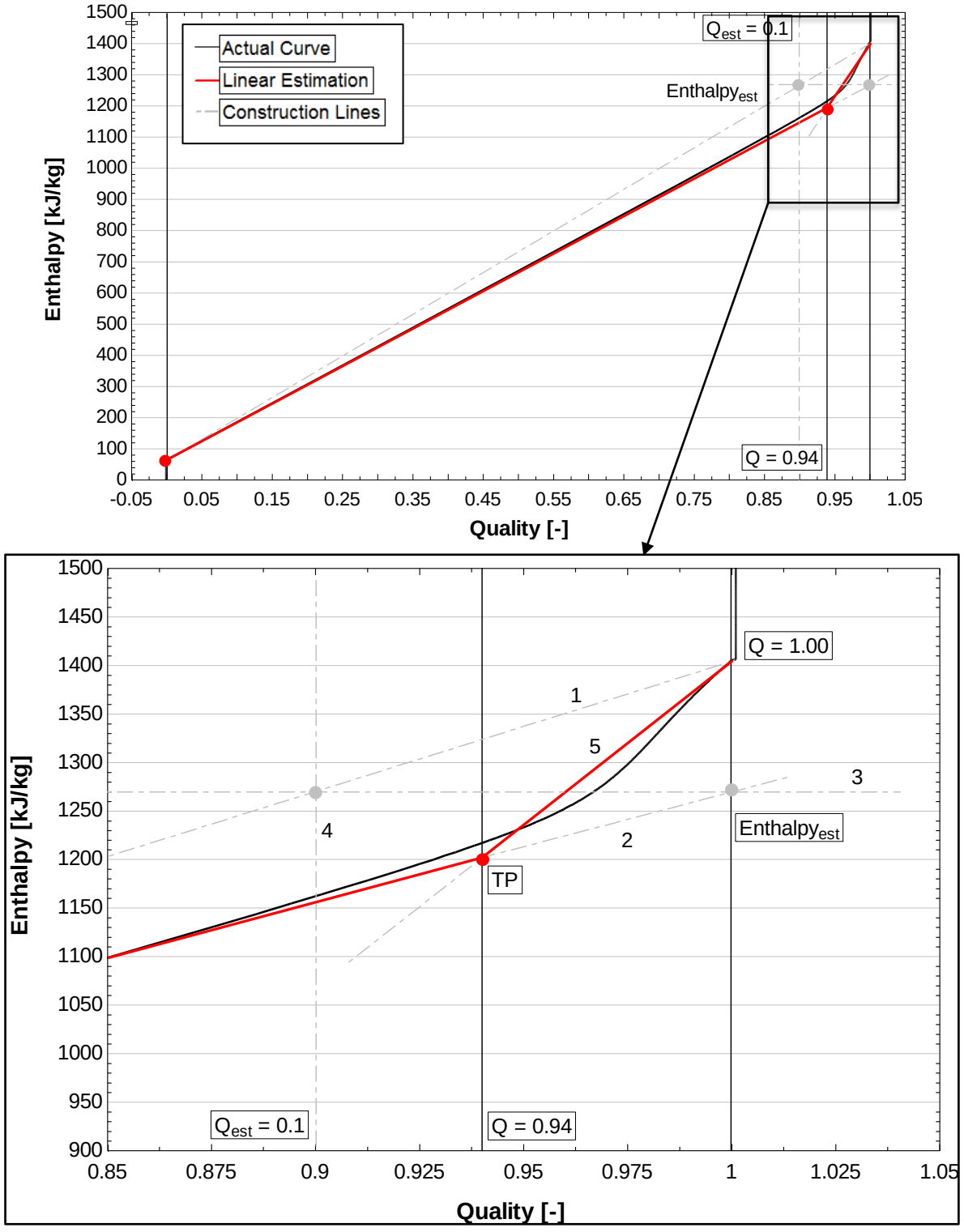

Figure 3.6: Linear enthalpy vs. quality estimation of aqua-ammonia in the two-phase region and the graphical representation of the 'turning point'.

The first construction line to be drawn is from saturated liquid straight to saturated vapour (line numbered; 1), secondly the dotted line under the actual curve is drawn towards the saturated vapour vertical line (line numbered; 2). After which a horizontal line is placed at the intersection of the dotted line and the vertical saturated vapour line (line numbered; 3), this forms the enthalpy estimation if the enthalpy of aqua-ammonia had a linear temperature glide. The horizontal enthalpy estimation line creates an intersection of line number 1 (line numbered; 4), thus creating the quality estimation from the saturated vapour side. Lastly, the intersecting lines of $Q_{x,TP}$ = 0.94 and line number 3 are connected to saturated vapour of the actual enthalpy curve (line numbered 5) to form the new linear estimation of enthalpy.

This process was completed for the average design conditions (727.25 kPa), so that a unified method could be applied to the remaining two conditions. The equations for enthalpy estimation and enthalpy of state TP are derived from a linear weighted function of quality and are expressed as:

$$\alpha_{est} = \alpha_5 + \left(\left(1 - Q_{x,est}\right) * \alpha_4\right) \quad \textbf{(3.1)}$$

and

$$\alpha_{TP} = \alpha_5\left(1 - Q_{x,TP}\right) + \alpha_{est} Q_{x,TP} \quad \textbf{(3.2)}$$

3.1.2 Thermophysical Properties of State 3 to 5

This section focuses on state 3, 4, TP, and 5 of Figure 3.1, with respect to each state's thermophysical properties and what impact it will have on the design selection of each heat exchanger. The thermodynamic design was completed for all three ambient design conditions to confirm which of these conditions yielded the 'worst case' scenario. The 'worst case' is viewed as the condition that demands the largest heat transfer surface area. A trend appeared as to which condition normally yields the 'worst case' scenario, which is a combination of the highest heat transfer rate between states and the refrigerant mass flow rate. Thus, an energy balance is required to determine the 'worst case' scenario between each of the states and their respective mass flow rates as prescribed by Eq. 2.1.

Enthalpy of State 3 through 5

The enthalpy of the superheated vapour state 3 can be obtained as a conservative value by means of EES' built-in property function. As documented by Table A.7, the enthalpy values for saturated liquid and vapour are within good accordance between the mathematical method and EES. Thus, for purposes of consistency the mathematical method will be used for all thermophysical properties within the two-phase region. Enthalpy of state 3 is determined with EES' property function;

enthalpy of state 4 is calculated by using Eq. A.3; the enthalpy of state 5 is calculated using Eq. A.2; and lastly the enthalpy of state TP is calculated using Eq. A.2. Recorded in Table 3.1 are the enthalpy values of states 3, 4, TP, and 5.

Table 3.1: Enthalpy output values for thermodynamic states 3, 4, TP, & 5.

State	Winter Conditions	Average Conditions	Summer Conditions
3	1409 [kJ/kg]	1453 [kJ/kg]	1489 [kJ/kg]
4	1384.169 [kJ/kg]	1391.113 [kJ/kg]	1395.661 [kJ/kg]
TP	1182.205 [kJ/kg]	1235.08 [kJ/kg]	1277.245 [kJ/kg]
5	11.197 [kJ/kg]	58.198 [kJ/kg]	96.515 [kJ/kg]

Now that the enthalpy values of state 3 through 5 have been calculated, it's possible to determine the heat transfer rate of each control volume.

Control volume for state 3 to 4:

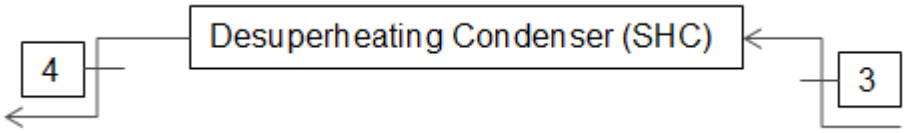

Winter design conditions:

$$\dot{Q}_{WRT} = \dot{m}_{3,WRT}(\alpha_{4,WRT} - \alpha_{3,WRT}) \quad (Eq.2.1)$$
$$\therefore = 0.0005412(1384.169 - 1409)$$
$$\therefore = 13.4385\, W\ (Heat\ Removed)$$

Average design conditions:

$$\dot{Q}_{DSN} = \dot{m}_{3,DSN}(\alpha_{4,DSN} - \alpha_{3,DSN}) \quad (Eq.2.1)$$
$$\therefore = 0.0005839(1391.113 - 1453)$$
$$\therefore = 36.136\, W\ (Heat\ Removed)$$

Summer design conditions:

$$\dot{Q}_{SMR} = \dot{m}_{3,SMR}(\alpha_{4,SMR} - \alpha_{3,SMR}) \quad (Eq.2.1)$$
$$\therefore = 0.0006153(1395.661 - 1489)$$
$$\therefore = 57.431\, W\ (Heat\ Removed)$$

Thus, for state 3 to 4, it is clear that under summer conditions the heat transfer rate is the highest. In this oeuvre, the summer condition thermophysical properties of state 3 will be illustrated within the main document, where the thermophysical properties of the remaining design conditions are added to Appendix B 2.

The control volume for State 4 to 5 is

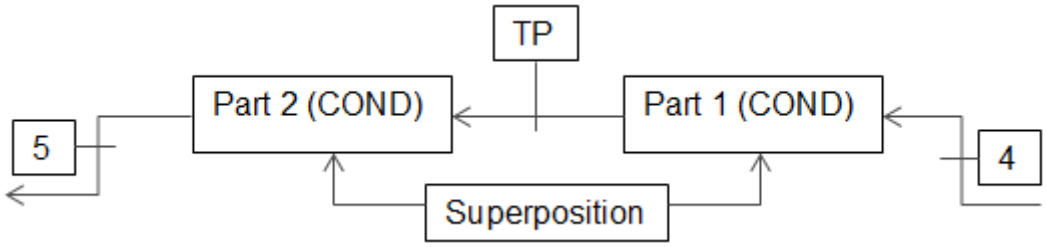

Superposition will be used to determine the highest heat transfer rate of the condenser control volume, as it better represents the enthalpy curve as illustrated in Fig. 3.3.

Winter design conditions 4 to TP:

$$\dot{Q}_{WRT} = \dot{m}_{4,WRT}(\alpha_{TP,WRT} - \alpha_{4,WRT}) \quad (Eq.2.1)$$
$$\therefore = 0.0005412(1182.205 - 1384.169)$$
$$\therefore = 109.303W\ (Heat\ Removed)$$

Winter design conditions TP to 5:

$$\dot{Q}_{WRT} = \dot{m}_{5,WRT}(\alpha_{5,WRT} - \alpha_{TP,WRT}) \quad (Eq.2.1)$$
$$\therefore = 0.0005412(11.197 - 1182.205)$$
$$\therefore = 633.749\ W\ (Heat\ Removed)$$

Average design conditions 4 to TP:

$$\dot{Q}_{DSN} = \dot{m}_{4,DSN}(\alpha_{TP,DSN} - \alpha_{4,DSN}) \quad (Eq.2.1)$$
$$\therefore = 0.0005839(1235.08 - 1391.113)$$
$$\therefore = 91.108\ W\ (Heat\ Removed)$$

Average design conditions TP to 5:

$$\dot{Q}_{DSN} = \dot{m}_{5,DSN}(\alpha_{5,DSN} - \alpha_{TP,DSN}) \quad (Eq.2.1)$$
$$\therefore = 0.0005839(58.198 - 1235.08)$$
$$\therefore = 687.181\ W\ (Heat\ Removed)$$

Summer design conditions 4 to TP:

$$\dot{Q}_{SMR} = \dot{m}_{4,SMR}(\alpha_{TP,SMR} - \alpha_{4,SMR}) \quad (Eq.2.1)$$
$$\therefore = 0.0006153(1277.245 - 1395.661)$$
$$\therefore = 72.862\ W\ (Heat\ Removed)$$

Summer design conditions TP to 5:

$$\dot{Q}_{SMR} = \dot{m}_{5,SMR}(\alpha_{5,SMR} - \alpha_{TP,SMR}) \quad (Eq.2.1)$$
$$\therefore = 0.0006153(96.515 - 1277.245)$$
$$\therefore = 726.503\ W\ (Heat\ Removed)$$

With the total heat transfer rate of each condition adding up to:

- Winter Conditions = 743.052 W (Heat Removed)
- Average Conditions = 778.289 W (Heat Removed)
- Summer Conditions = 799.365 W (Heat Removed)

The thermophysical properties of summer conditions for state 4, TP, and 5 will be illustrated with sample calculations within the main body of the dissertation. The thermophysical properties of remaining states of the absorption-desorption cycle will be tabulated, with sample calculations added to Appendix B.

State 3 Thermophysical Properties

The superheated vapour phase of state 3 proved cumbersome, whereby neither EES' built-in property functions nor (Conde-Petit, 2004) formulae could provide accurate thermophysical properties. It was decided as a conservative approach to determine the thermophysical properties of state 3 as linearly weighted properties with pure ammonia and water at their respective temperatures and ambient design condition pressures. However, it's well known that properties do not necessarily behave linearly in the superheated region, but the thermophysical properties of enthalpy and density can be approximated as linear functions. The temperatures of the pure substances are calculated by using Eqs. A.1 and A.7 for the aqua-ammonia vapour solution temperature.

The Engineering Equation Solver does however provide a conservative value for density in the superheated region of aqueous ammonia. Table 3.2 represents the thermophysical properties of pure ammonia and water at summer design condition pressure, and recorded in Table 3.3 is the linearly weighted thermophysical properties of state 3 at the pre-determined 'worst case' of summer conditions. The transport properties of aqua-ammonia were obtained by using EES' built-in property functions and a linearly weighted property equation according to the mass concentration of aqueous ammonia, which is simply expressed as

$$\theta_{mix} = x\theta_{NH_3} + (1-x)\theta_{H_2O} \tag{3.3}$$

The specific thermal capacity is determined with an energy balance using Eqs. 2.1 and 2.2. The values of dynamic viscosity, thermal conductivity, and Prandtl number are determined as stated above with Eq. 3.3.

Table 3.2: Thermophysical properties of pure ammonia and water for state 3.

Thermophysical Properties (Summer Conditions)						
$T_{3,NH3}$	92.2348	°C		$T_{3,H2O}$	310.114	°C
$P_{3,NH3}$	939.54	kPa		$P_{3,H2O}$	939.54	kPa
$\alpha_{3,NH3}$	1665	kJ/kg		$\alpha_{3,H2O}$	2216	kJ/kg
$Cp_{3,NH3}$	2.462	kJ/kg.K		$Cp_{3,H2O}$	2.701	kJ/kg.K
$\rho_{3,NH3}$	5.522	kg/m^3		$\rho_{3,H2O}$	3.326	kg/m^3
$\mu_{3,NH3}$	0.00001255	kg/m.s		$\mu_{3,H2O}$	0.00002108	kg/m.s
$k_{3,NH3}$	0.03325	W/m.K		$k_{3,H2O}$	0.06675	W/m.K
$Pr_{3,NH3}$	0.9293			$Pr_{3,H2O}$	0.8529	

Table 3.3: Thermophysical properties of aqua-ammonia for state 3.

LINEAR WEIGHTED PROPERTIES		
α_3	1489	kJ/kg
Cp_3	1.1443	kJ/kg.K
ρ_3	5.48	kg/m^3
μ_3	1.264E-05	kg/m.s
k_3	0.033585	W/m.K
Pr_3	0.928536	

State 4 Thermophysical Properties

The saturated vapour properties of state 4 will be calculated by using the mathematical model set out in Appendix A 1.1 for saturated aqua-ammonia vapour. These properties are calculated for summer design conditions, as illustrated by the 'worst case' scenario calculations of states 3 to 4, and 4 to 5. The mathematical method requires several input parameters of which are:

- Pressure
- Mass concentration
- Molar vapour concentration

The saturated vapour aqua-ammonia mixture temperature is calculated using Eq. A.1 by substituting for summer condition pressure (939.54 kPa) and ammonia mass concentration (0.99).

$$T_4(939.54, 0.99) = 333.2048596\ [K] or\ 60.0549\ [°C]$$

The molar vapour concentration is determined by using Eq. A.4 and substituting for summer condition pressure (939.54 kPa) and ammonia mass concentration (0.99).

$$y(939.54, 0.99) = \ 0.999709\ \ [-]$$

Recorded in the box below are the thermophysical properties of saturated aqua-ammonia vapour, of which the sample calculations are available in Appendix B 1.1.

$$Cp_4 = 4.26357\ \left[\frac{kJ}{kg}\right]$$

$$\rho_4 = 8.08943\ \left[\frac{kg}{m^3}\right]$$

$$\mu_4 = 1.18895E(-05)\ \left[\frac{kg}{m.s}\right]$$

$$k_4 = 0.0341137\ \left[\frac{W}{m.K}\right]$$

$$Pr_4 = 1.48596\ [-]$$

State 5 Thermophysical Properties

The saturated liquid properties of state 4 will be calculated by using the mathematical method set out in Appendix A 1.1 for saturated aqua-ammonia liquid. These properties are calculated for summer design conditions, as illustrated by the 'worst case' scenario calculations of states 3 to 4, and 4 to 5.

The mathematical method requires two input parameters of which are:

- Pressure
- Mass concentration

With these input parameters the temperature of the 99 wt% aqua-ammonia mixture can be calculated by using Eq. A.1 and its supporting equation parameters in Table A.2.

$$T(939.54, 0.99) = 296.15\ [K] or\ 23\ [°C]$$

The thermophysical properties of saturated aqua-ammonia liquid are presented by the following:

$$Cp_5 = 4.75161\ \left[\frac{kJ}{kg}\right]$$

$$\rho_5 = 611.081\ \left[\frac{kg}{m^3}\right]$$

$$\mu_5 = 0.000149988\ \left[\frac{kg}{m.s}\right]$$

$$k_5 = 0.489310\ \left[\frac{W}{m.K}\right]$$

$$Pr_5 = 1.45651\ [-]$$

The sample calculations of the mathematical model proposed by Conde-Petit (2004) are available in Appendix B 1.2.

State TP (Turning Point) Thermophysical Properties

The thermophysical properties of state TP has proved to be vague, as state TP falls within the two-phase state of aqua-ammonia. Very few articles exist explaining the characteristics of the two-phase region for aqua-ammonia. As previously iterated, EES does provide a conservative value for the density of aqueous ammonia. Thus, by using EES' built-in property call function for density a graph can be plotted as a function of quality, as illustrated in Fig. 3.7.

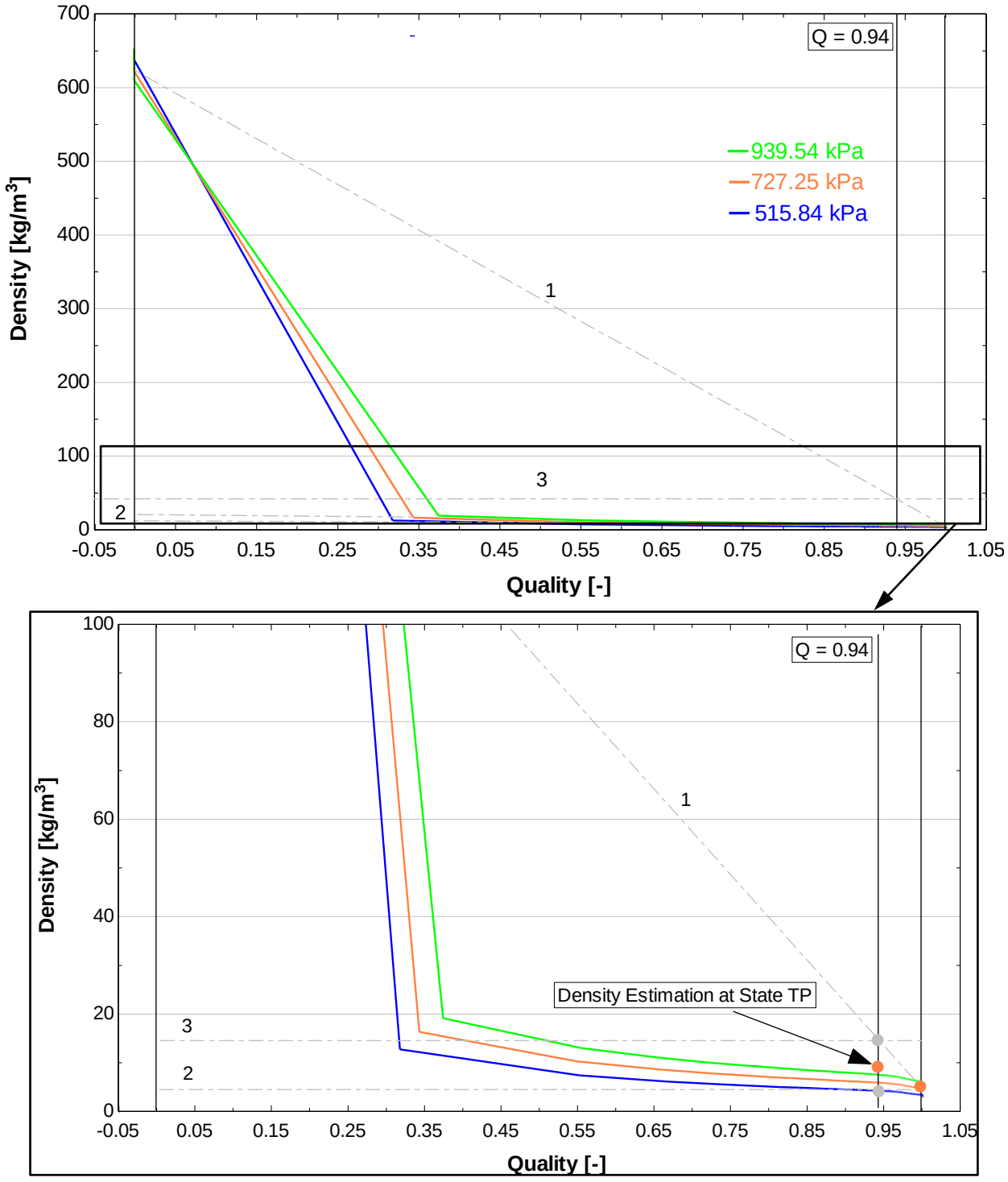

Figure 3.7: Density vs. quality for aqua-ammonia in the two-phase region of three ambient design conditions.

The black line represents the quality at which state TP occurs (Q = 0.94); the orange curve represents the density of 99 wt% aqua-ammonia at 7 [bar] as a function of quality. The linear approximation is made by using the grey construction lines. The first construction line to be drawn is to connect saturated liquid to saturated vapour (line numbered; 1), secondly the line following the density curve (line numbered; 2). The third construction line represent what the density would be if

a point to point linear correlation is made. The density of state TP, would typically be approximated by a simple linear weighted equation, as expressed by the following equation:

$$\rho_{TP} = \rho_4 - ((\rho_4 - \rho_5) * (1 - Q_{x,TP})) \quad \textbf{(3.4)}$$

Although, as illustrated by the construction lines of Figure 3.7, the density of state TP can be approximated by

$$\rho_{TP} = \rho_4 \pm \left(\left(1 - Q_{x,TP}\right) * \rho_4\right) \quad \textbf{(3.5)}$$

With this method the density is approximated from the saturated vapour value, and because the quality of the turning point is close to Q = 1.00 the approximated value of density is much closer to its actual density at Q = 0.94. The density of state TP for summer conditions can be calculated as

$$\rho_{TP} = \rho_4 + \left(\left(1 - Q_{x,TP}\right) * \rho_4\right) \quad (Eq.3.5)$$
$$\therefore = 7.15145 + \left((1 - 0.94) * 7.15145\right)$$
$$\therefore = 7.58054 \left[\frac{kg}{m^3}\right]$$

The remaining properties of dynamic viscosity, thermal conductivity, and Prandtl number have little known two-phase characteristics, or graph interpreting the two-phase region. Thus, as a conservative approach the thermophysical properties are approximated with a point to point linear approximation.

$$\theta_{TP} = \theta_4 - ((\theta_4 - \theta_5) * (1 - Q_{x,TP})) \quad \textbf{(3.6)}$$

The dynamic viscosity can be calculated as

$$\mu_{TP} = \mu_4 - ((\mu_4 - \mu_5) * (1 - Q_{x,TP}))$$
$$\therefore = 1.0512E(-05) - \left((1.0512E(-05) - 0.00014999) * (1 - 0.94)\right)$$
$$\therefore = 1.88805E(-05) \left[\frac{kg}{m.s}\right]$$

The thermal conductivity is approximated as

$$k_{TP} = k_4 - ((k_4 - k_5) * (1 - Q_{x,TP}))$$
$$\therefore = 0.02721628 - \left((0.02721628 - 0.48930958) * (1 - 0.94)\right)$$
$$\therefore = 0.054941882 \left[\frac{W}{m.K}\right]$$

The Prandtl number can be approximated using Eq. A.25, but as the specific thermal capacity is needed and the two-phase specific thermal capacity curve is not known, thus the Prandtl number is calculated using Eq. 3.6.

$$Pr_{TP} = Pr_4 - ((Pr_4 - Pr_5) * (1 - Q_{x,TP}))$$
$$\therefore = 1.3628937 - \big((1.3628937 - 1.45651) * (1 - 0.94)\big)$$
$$\therefore = 1.36851\ [-]$$

Note: The sample calculations of the thermophysical properties of states 5 to 6 and 9 to 10 are available in Appendix B 1.3, as the method of determining the thermophysical properties can be considered trivial.

3.1.3 Thermophysical Properties of State 7 to 8

The sub-cooled liquid of state 6 flows through a venturi nozzle into the evaporator module, whereby the venturi nozzle is isothermal and the sub-cooled liquid would enter the two-phase region with the drop in pressure, now, known as state 7. Added to the drop in pressure, the two-phase liquid feels partial pressure due to Helium in the evaporator module, thus creating state 8. It is assumed that from state 7 to 8 remains isothermal and the quality of two-phase fluid can be determined by a similar but modified method used for the turning point state.

Figure 3.8 depicts the enthalpy curve of 99 wt% aqua-ammonia and pressure of 236.39 [kPa]. The black line indicates the actual enthalpy curve and the red line depicts the linear enthalpy estimation. The blue lines indicate the construction lines needed to form the linear enthalpy estimation. Similar to the turning point, the Q_{est} = 0.1 and the turning point of the curve remains at Q = 0.94. As the enthalpy of state 8 is known, the linear estimation is used to determine the quality of state 8.

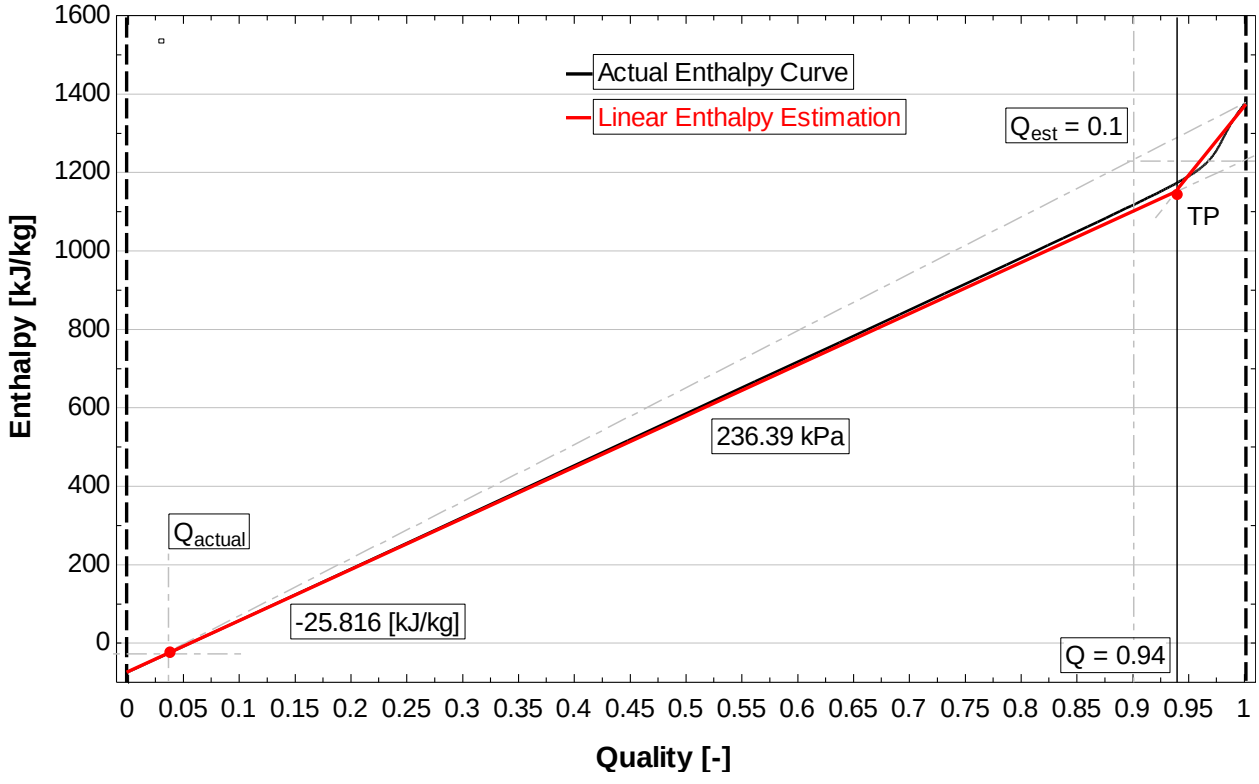

Figure 3.8: Linear enthalpy estimation of aqua-ammonia at 236.39 [kPa].

The enthalpy of the evaporator can be estimated with the method derived in Eq. 3.1. Now, the values of saturated liquid and vapour enthalpy (α_l = -80.43533 kJ/kg and α_g = 1366.0361 kJ/kg as obtained from the mathematical method) are substituted into Eq. 3.1 and the enthalpy estimation is calculated as

$$\alpha_{est} = 1285.601 \left[\frac{kJ}{kg}\right]$$

As state 7 to 8 is a constant enthalpy and has different values for each of the ambient design conditions, the quality of each condition is thus calculated as

$$Q_{x,WRT} = 1 - \left(\frac{\alpha_g - \alpha_8}{\alpha_g - \alpha_{est}}\right)$$

$$\therefore = 1 - \left(\frac{1366.036 - (-25.816)}{1366.036 - 1285.601}\right)$$

$$\therefore = 0.039984$$

$$Q_{x,DSN} = 1 - \left(\frac{\alpha_g - \alpha_8}{\alpha_g - \alpha_{est}}\right)$$

$$\therefore = 1 - \left(\frac{1366.036 - (3.0015)}{1366.036 - 1285.601}\right)$$

$$\therefore = 0.06108$$

$$Q_{x,SMR} = 1 - \left(\frac{\alpha_g - \alpha_8}{\alpha_g - \alpha_{est}}\right)$$

$$\therefore = 1 - \left(\frac{1366.036 - (26.8503)}{1366.036 - 1285.601}\right)$$

$$\therefore = 0.078538$$

Energy Balance of State 8 to 9

Now, it's possible to determine the heat transfer rate of the evaporative two-phase line, now that the enthalpy values of state 8 and 9 are known for all ambient design conditions.

Winter Design Conditions:

$$\dot{Q}_{EVAP,WRT} = \dot{m}_{9,WRT}\left(\alpha_{9,WRT} - \alpha_{8,WRT}\right) \quad (Eq.\,2.1)$$

$$\therefore = 0.0005264(1444 - (-25.816))$$

$$\therefore = 773.711\,W\ (Heat\ Added)$$

Average Design Conditions:

$$\dot{Q}_{EVAP,DSN} = \dot{m}_{9,DSN}\left(\alpha_{9,DSN} - \alpha_{8,DSN}\right) \quad (Eq.2.1)$$
$$\therefore = 0.000568(1444 - 3.0015)$$
$$\therefore = 818.487\, W\ (Heat\ Added)$$

Summer Design Conditions:

$$\dot{Q}_{EVAP,SMR} = \dot{m}_{9,SMR}\left(\alpha_{9,SMR} - \alpha_{8,SMR}\right) \quad (Eq.2.1)$$
$$\therefore = 0.0005986(1444 - 26.8503)$$
$$\therefore = 848.306\, W\ (Heat\ Added)$$

The highest heat transfer is obtained during summer ambient conditions, which is due to the higher mass flow rate of the refrigerant during summer conditions. Under summer ambient conditions the evaporator would need a larger heat transfer surface area, as the evaporator would need to remove more heat from the secondary refrigerant with the warmer ambient conditions.

State 8 Thermophysical Properties

The thermophysical properties of state 8 will be demonstrated for summer design conditions. The values of specific thermal capacity, dynamic viscosity, thermal conductivity, and Prandtl number can be calculated by using a point to point linear relation, similar to the process used to determine the thermophysical properties of state TP with Eq. 3.6.

$$\theta_8 = \theta_l - \left((\theta_l - \theta_g) * (1 - Q_{x,SMR})\right) \quad (Eq\ 3.6)$$

$$Cp_{8,SMR} = 4.53023 - \left((4.53023 - 3.28374) * (1 - 0.078538)\right)$$
$$\therefore = 4.43233\left[\frac{kJ}{kg.K}\right]$$

$$\mu_{8,SMR} = 0.0002324 - \left(\left(0.0002324 - 1.064E(-05)\right) * (1 - 0.078538)\right)$$
$$\therefore = 0.000215\left[\frac{kg}{m.s}\right]$$

$$k_{8,SMR} = 0.574812 - \left((0.574812 - 0.0277249) * (1 - 0.078538)\right)$$
$$\therefore = 0.53188\left[\frac{W}{m.K}\right]$$

$$Pr_{8,SMR} = 1.831384 - \left((1.8313847 - 1.260422) * (1 - 0.078538)\right)$$
$$\therefore = 1.78654[-]$$

3.1.4 Thermophysical Properties of Weak and Strong Aqua-Ammonia Solutions

Figure 3.1 illustrated the regenerative heat exchanger to be between the absorber (absorption) and bubble pump (desorption) components, and it plays an integral role in the absorption – desorption H&R cycle. Figure 3.2 illustrated the regenerative heat exchanger cooling the weak solution aqua-ammonia exiting the bubble pump heading its way to the absorber module, thus, increasing the efficiency of the absorber by increasing the absorbability of ammonia into the weak solution. In turn heat is added to the strong solution exiting the absorber heading towards the bubble pump, increasing the efficiency of the bubble pump by decreasing the heat input needed to boil ammonia out of the strong solution. Thus for the regenerative heat exchanger, collaboration was required with the research project responsible for the thermodynamic design of the absorber module. The weak solution outlet and strong solution inlet parameters of the bubble pump are already known and can be found on the data sheet labelled 'Clear Sky' in Appendix D 8.1.

The temperature of the weak solution entering the absorber was adjusted to the same temperature of the saturated liquid of state 5, which is equivalent to the ambient temperature. Although, another heat exchanger is required to lower the temperature of the weak solution to near ambient temperatures, which hereinafter will be referred to as the auxiliary heat exchanger. Figure 3.9 illustrates temperature vs. enthalpy of the weak and strong solutions to better visualise the revised processes that the weak and strong solutions will undergo. The numbering of the auxiliary and regenerative HTEX's thermodynamic states are changed from in and out to 1, 2, and 3.

The temperature and mass concentration of the strong aqua-ammonia solution could be determined with the use of the absorber simulation model generated by E van Niekerk. The input parameters required by the absorber simulation model are: temperatures for the weak aqua-ammonia solution, state 10, and coolant; mass flow rates of weak solution, state 10, and coolant; and lastly mass concentration of weak solution.

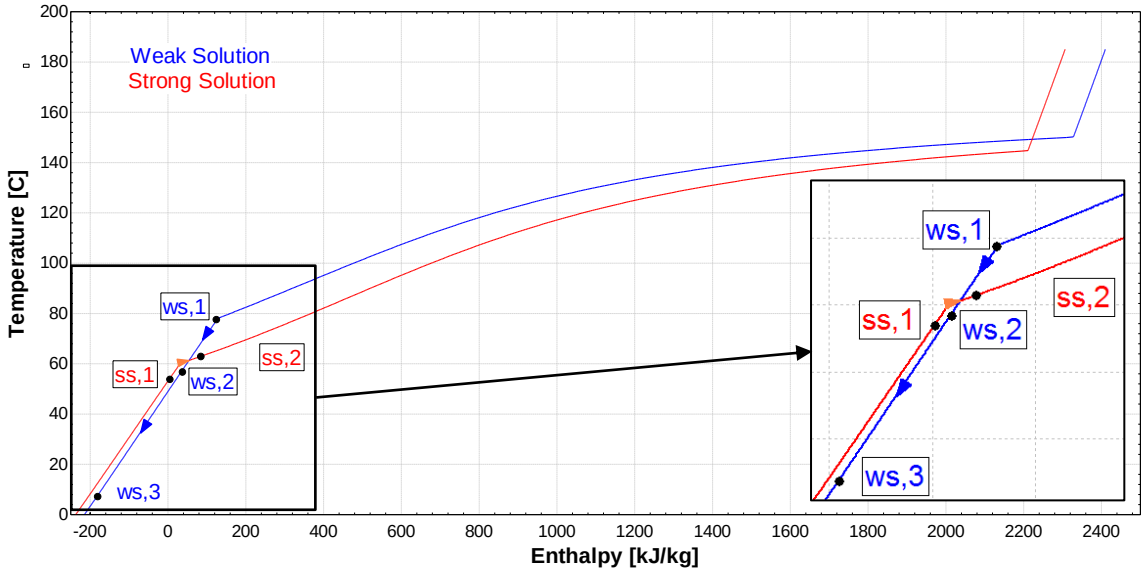

Figure 3.9: Temperature vs. enthalpy of the auxiliary and regenerative heat exchangers.

The temperatures of the strong aqua-ammonia solution into the regenerative heat exchanger are:

$$T_{ss,in,WRT}(515.84, 0.4523) = 33.223\ [°C]$$
$$T_{ss,in,DSN}(727.25, 0.453) = 54.024\ [°C]$$
$$T_{ss,in,SMR}(939.54, 0.4556) = 68.234\ [°C]$$

The inlet temperatures of the strong solution confirm the need for an 'auxiliary' heat exchanger to further cool the weak solution liquid line. The quality parameter of the strong solution out of the regenerative heat exchanger has been pre-determined and is found on the 'Clear Sky' data sheet in Appendix D as

$$T_{ss,out,WRT}(515.84, 0.4523) = 49.55\ [°C]\ with\ Q = 0.008374$$
$$T_{ss,out,DSN}(727.25, 0.453) = 61.46\ [°C]\ with\ Q = 0.01341$$
$$T_{ss,out,SMR}(939.54, 0.4556) = 70.8\ [°C]\ with\ Q = 0.01593$$

The remainder of the weak and strong aqua-ammonia solutions thermophysical properties sample calculations are available in Appendix B 1.4. It's however important to note that the 'worst case' scenario for both heat exchangers is winter ambient conditions, and that for purposes of the design continuity for the regenerative and auxiliary heat exchangers the thermophysical properties will be calculated using EES' thermophysical property call function.

3.1.5 Conclusion of Thermophysical Properties of Aqua-Ammonia Solutions

In conclusion to the thermophysical properties of the aqua-ammonia refrigerant illustrated in Chapter 3 and Appendix B, is that the mathematical method proposed by (Conde-Petit, 2004) falls within good accordance to thermophysical properties obtained from EES' built-in property call function. The mathematical method of calculating thermophysical properties was primarily completed using MS Excel as the preliminary thermodynamic design will firstly be completed in MS Excel. The thermophysical property model coding of MS Excel was verified with no mathematical errors by coding the same Conde-Petit (2004) mathematical models into EES.

3.2 Extended Chapter 3 – Thermophysical Properties and Thermodynamic Design Selection

Omitted from Chapter 3 are the thermophysical property calculations of ethylene glycol water mixtures, which is available in Appendix B 1.5. The reason for the omission of the thermophysical property calculations is that the subject isn't fundamental to this study, but does play an important role in the determination of heat exchanger sizing and rating. Furthermore, the concept design generation and evaluation is omitted from Chapter 3, but is available in Appendix C. This section is fairly large and has a very important role in determining a heat exchanger's configuration, but it

shifts the focus away from the thermodynamic design of a heat exchanger to the physical design of a heat exchanger. The concepts illustrated in Appendix C are the concepts which passed the early elimination hurdle, as the oeuvre tries to be concise and to the point those concepts weren't added to the final report. The concepts of Appendix C are evaluated with a weighted level of importance of the specific heat exchanger's design requirements. Consequently, it's recommended to read through Appendix C before continuing onto Chapter 4 to be able to fully comprehend the thermodynamic design and rating of Chapter 4.

3.3 Conclusion

In conclusion, Chapter 3 has demonstrated all the thermophysical properties and heat exchanger design selections required to complete the thermodynamic design of Chapter 4. Research to investigate the two-phase phenomena of aqueous ammonia was completed, and a linear approach adopted to determine the thermodynamic and transport properties of the two-phase region. The linear approach created in section 3.1.1 was applied to the evaporator's two-phase region as well. Here sub-cooled liquid undergoes a sudden phase change as it passes through the venturi nozzle. Furthermore, an additional heat exchanger was added to the original control volume cycle layout of Fig 1.3.

Chapter 4

4 THERMODYNAMIC DESIGN AND RATING

Introduction

Chapter 4 deals with the specific thermodynamic design and rating calculations required for each of the heat exchangers for an aqua-ammonia absorption-desorption heating & refrigeration unit, including any alternative components assisting the main heat exchangers. The heat exchanger design calculations for all of the heat exchanger designs of this oeuvre are completed under the following set of assumptions:

- Steady state operating conditions exist;
- The heat exchanger is well insulated so that heat loss to the surroundings is negligible.
- The thickness of the tubes is considered negligible since it is thin-walled.
- Changes in potential and kinetic energies of the working fluid streams are negligible.
- The overall heat transfer coefficient is assumed to be uniform across the length of the heat exchanger.

Compiled within each heat exchanger's subsection is the necessary equations and example calculations to determine the heat exchanger's size and performance rating. For the completion of the sizing problem, the log mean temperature difference method was used, with an array of standardised dimensional parameters for the shell's inner diameter and the tube's inner- and outer diameters. The preliminary design-sizing calculation will first be completed using MS Excel and the verification thereof will be completed using EES. The performance rating problem will be completed using the NTU-effectiveness method with MS Excel, after the heat exchanger's preliminary design-sizing model is calculated, but before the preliminary design is verified. The performance rating acts as a benchmark that illustrates whether a heat exchanger is practically viable and whether the assumed coolant outlet temperature is within a practically expected range.

4.1 Overview of the Experimental Setup

The heat exchangers of the solar powered aqua-ammonia absorption-desorption heating and refrigeration package unit is required to fit within a structural housing, with dimensions illustrated in Fig. 4.1. The heat storage setup and the heat sink setup must be stored within the structural housing and the solar collector setup on the outside of the structure. The solar collector has a downstream effect on the absorption-desorption cycle, as it provides the cycle with its heat source. The heat sink setup will directly influence the heat exchangers of the absorption-desorption cycle, as it will house and distribute the ethylene glycol-water solution throughout the most of the cycle (see Fig. 4.2 for coolant flow visualisation).

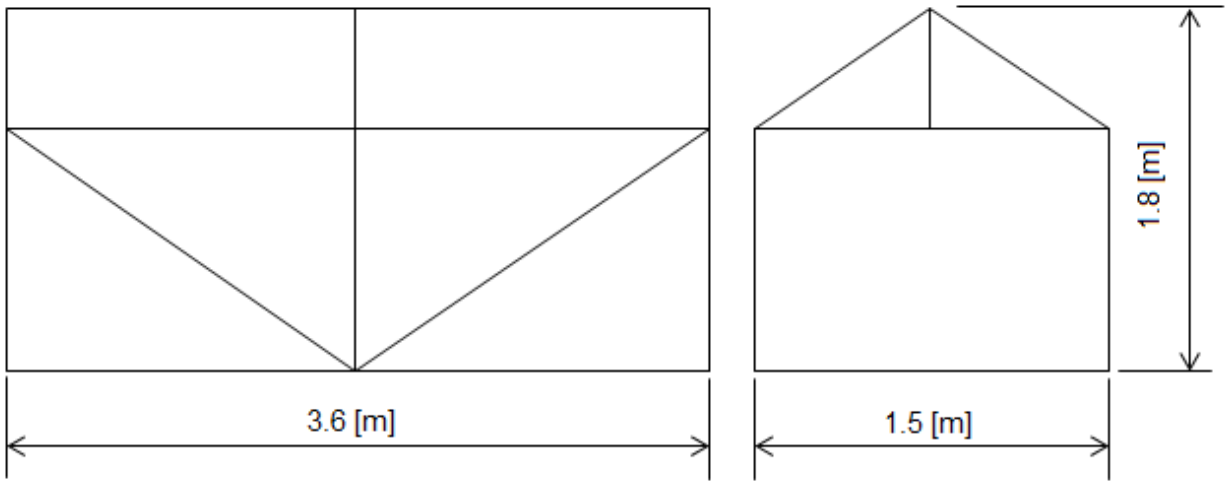

Figure 4.1: Schematic representation of the housing structure for the solar-driven aqua-ammonia absorption-desorption heating & refrigeration package unit.

Although the dimensional parameter that the housing structure creates is 1.5x3.6x1.8, it cannot be used as the dimensional design parameter for each of the heat exchanger designs. Therefore, the cubic size parameter of each heat exchanger is limited to length < 2.5 [m], width < 1 [m], and height < 1 [m]. The housing structure is specified to be able to withstand a load of 750 [kg] suspended from its ceiling, therefore the suspended stage 1 & 2 and de-superheating condensers are limited to a maximum of 500 [kg]. The abovementioned design parameters are focused on the mechanical design of the heat exchangers, but do play an important role regarding the completion of the experimental setup of the solar-powered aqua-ammonia absorption-desorption H&R package unit. The design selection parameters to be considered for the thermodynamic design and rating of the seven heat exchangers are:

- Practically viable thermal heat exchanger efficiency.
- Number of tubes ($2 < N_t < 100$).
- Heat transfer surface tube length < 2 [m].
- Pressure drop < 1 [kPa].

4.2 Introduction to the Heating Side Heat Exchangers (State 3 to 5)

Previously in Chapter 3.1, it was concluded that the heat exchangers needed to cool the refrigerant line from superheated vapour down to saturated liquid, which will require the service of two heat exchanger modules. The heat exchanger between state 4 to 5 can be calculated using superposition, where the heat exchanger surface area is calculated separately and merely added together to form one heat exchanger module. Due to the characteristics of the heating components it's decided that the coolant line will flow in the opposite direction from the aqua-ammonia line. Starting at state 5 and ending at state 3, thus, the design will follow the coolant line's temperature gain through the condenser units. State TP to 5 will hereinafter be known as stage 1 condenser, and state 4 to TP as the stage 2 condenser. State 3 to 4, will hereinafter be known as the de-superheating condenser or DHC as an abbreviation. An illustrative temperature vs. surface area graph is depicted in Figures D 1.1, 1.2, and 1.3 of Appendix D 1, which services as a graphical interpretation of the working fluid streams of the stage 1, 2, and de-superheating condensers.

The outlet temperature of the coolant line of each heat exchanger is an estimation with respect to the ΔT of the coolant inlet- and refrigerant outlet temperatures, which is then iterated using the NTU method to obtain a practically viable outlet temperature. The coolant outlet temperature is required to complete the sizing problem, and serves as the commanding variable for the performance rating of each heat exchanger.

Figure 4.2 illustrates the coolant liquid travelling through the heat exchangers that requires heat energy to be removed, and is represented by the blue lines. The mass flow rates of the coolant can be determined by means of two simple methods; an energy balance of the first law of thermodynamics between the respective refrigerant and coolant in- and outlet conditions, or it can be determined as a conservation of mass. As the 25 wt% ethylene glycol water solution from the heat sink first travels through the absorber module it can be divided into the critical mass flow rate required by the auxiliary heat exchanger and the remaining mass flow rate. The remaining mass flow rate can then be used for the stage 1 condenser, as this module doesn't have a large temperature gain for the coolant. Due to the low temperature gain of the coolant in the stage 1 condenser it is more important for the refrigerant to reach saturated liquid, than the coolant having a critical mass flow rate.

Represented by Fig. 4.2 are the locations where the coolant mass flow rate is divided with the first division occurring after the coolant has travelled through the absorber module. Here the critical mass flow rate required by the auxiliary heat exchanger is calculated. The second division occurs after the stage 1 condenser, where the critical mass flow rate required by the stage 2 condenser is calculated. The coolant mass flow rate remains the same for the de-superheating condenser, as too much heat capacity would be lost if the coolant were to be at critical flow rate for the de-superheating condenser.

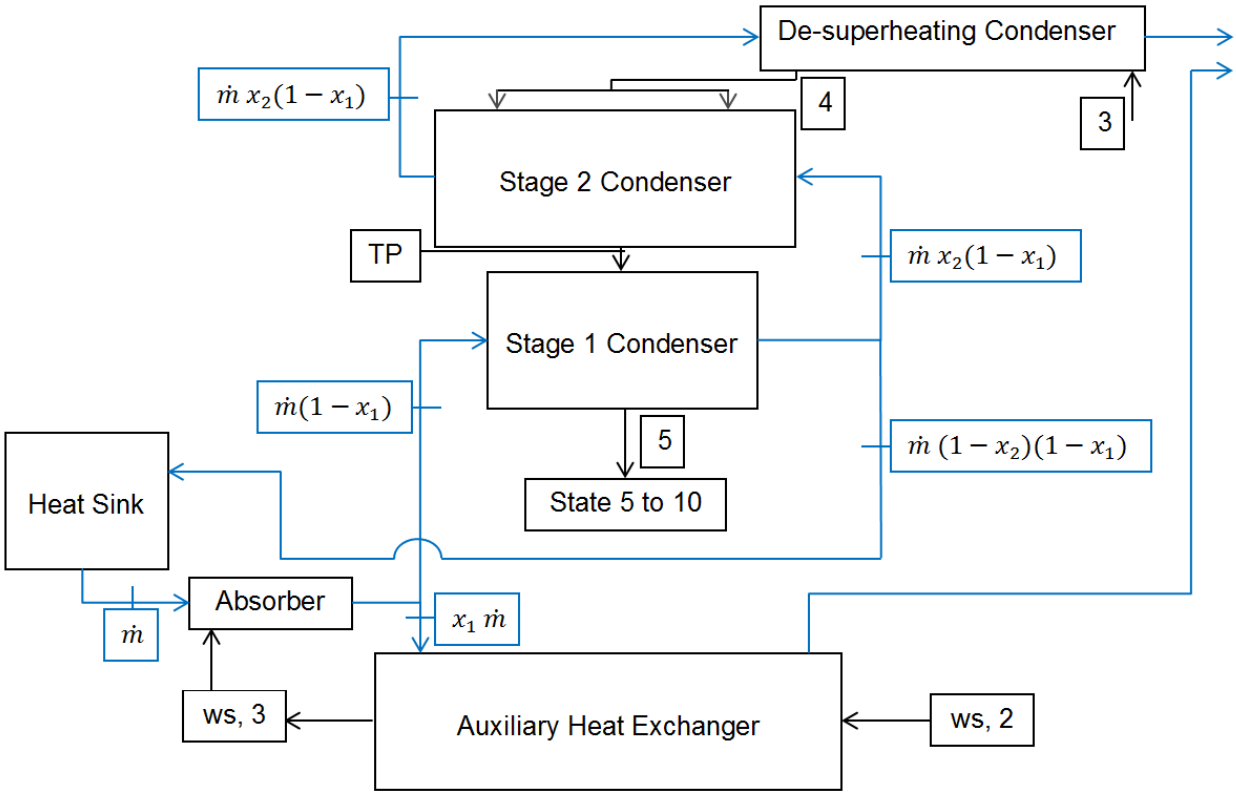

Figure 4.2: Schematic representation of the refrigerant and coolant flow diagram with the heating side components.

The heat sink can deliver a maximum mass flow rate of 0.05 [kg/s] to the system, with the critical mass flow rate of the coolant for the auxiliary heat exchanger is determined as 0.00343 [kg/s] for summer ambient condition. Thus, the mass flow rate for the first stage of the superposition condenser can be calculated as:

$$\sum \dot{m}_{in} = \sum \dot{m}_{out}$$

$$\therefore \dot{m}_{clnt,ABS} = \dot{m}_{clnt,AUX} + \dot{m}_{clnt,S1C}$$

$$\therefore \dot{m}_{clnt,S1C} = \dot{m}_{clnt,ABS} - \dot{m}_{clnt,AUX}$$

$$\therefore \quad = 0.05 - 0.00343$$

$$\therefore \quad = 0.04657 \left[\frac{kg}{s}\right]$$

Now, with the mass flow rate of the coolant through the first stage condenser is pre-determined via a conservation of mass, the coolant outlet temperature can be calculated using Eq. 2.2 and the heat transfer rate obtained in Chapter 3.1.2 as

$$\sum \dot{Q}_{in} = \sum \dot{Q}_{out}$$

$$\therefore \dot{Q}_{S1C,SMR} = \dot{m}_{clnt,S1C} C_{p,clnt,bulk,S1C} \left(T_{clnt,out,S1C} - T_{clnt,in,S1C}\right)$$

$$\therefore 726.503 = (0.04657)(3.7610 \text{ x } 10^3)(T_{clnt,out} - 18.404)$$

$$\therefore T_{clnt,out,S1C} = \frac{726.53}{(0.04657 \text{ x } 3.7610 \text{ x } 10^3)} + 18.404$$

$$\therefore = 22.55\ [°C]$$

Next, it's possible to determine the critical mass flow rate of the coolant flowing through the second stage of the superposition condenser by estimating the outlet temperature and using Eq. 2.2 with the heat transfer rate obtained in Chapter 3.1.2 for state 4 to TP as:

$$\sum \dot{Q}_{in} = \sum \dot{Q}_{out}$$

$$\therefore \dot{Q}_{S2C,SMR} = \dot{m}_{clnt,S2C} C_{p,clnt,bulk,S2C} \left(T_{clnt,out,S2C} - T_{clnt,in,S2C}\right)$$

$$\therefore 72.862 = \left(\dot{m}_{clnt,S2C}\right)(3.79952 \text{ x } 10^3)(56.5 - 22.5520)$$

$$\therefore \dot{m}_{clnt,S2C} = 0.00056\ [kg/s],$$

where the specific thermal capacity is an estimation of the coolant bulk temperature. The coolant line returning to the heat sink will have a mass flow rate of 0.00460 [kg/s] at about 22.55 [°C]. This would mean a large amount of the coolant mass flow circulating in the heating side components has a small temperature range, that would aid the heat sink as it doesn't have to expel large amounts of heat energy into the atmosphere.

The process of designing the condenser unit as a superposition sizing problem ran into an irregularity, where the total heat transfer rate from state 4 to 5 is the largest under summer ambient conditions as mention in Chapter 3.1. Although, this cannot be said if the heat transfer rates are looked at individually, where the heat transfer rate being higher for stage 2 under winter ambient conditions rather than the recommended summer ambient conditions. The higher heat transfer rate of winter conditions would yield a larger coolant critical coolant mass flow rate and subsequently a larger heat transfer surface area for the stage 2 condenser. Therefore, as a conservative approach to the design-sizing of the condenser unit, the sizing of stage 2 condenser will be completed under winter ambient conditions and the thermodynamic design of the stage 1 and 2 condenser will now be considered as separate entities forming two heat exchanger modules. The critical mass flow rate of the coolant can be calculated as:

$$\sum \dot{Q}_{in} = \sum \dot{Q}_{out}$$

$$\therefore \dot{Q}_{S2C,WRT} = \dot{m}_{clnt,S2C} C_{p,clnt,bulk,WRT} \left(T_{clnt,out,WRT} - T_{clnt,in,WRT}\right)$$

$$\therefore 109.303 = \left(\dot{m}_{clnt,S2C}\right)(3.769854 \text{ x } 10^3)(46 - 4.13)$$

$$\therefore \dot{m}_{clnt,S2C} = 0.00069\ [kg/s],$$

where the specific thermal capacity is an estimation at the coolant bulk temperature.

4.3 Stage 1 Condenser (State TP to 5)

4.3.1 Preliminary Thermodynamic Design

The input parameters used to assist the preliminary thermodynamic design calculations of the stage 1 condenser under 'worst case' are illustrated in Table 4.1, with the full perusal of the preliminary design-sizing of all ambient conditions available in Appendix D 2.1.

Table 4.1: Stage 1 condenser – Thermodynamic design input parameters.

Thermodynamic Input Parameters	**Value/Comment**
Summer ambient conditions	
Thermophysical properties of state TP – 5	Section 3.1.2
Shell inner diameter: D_s	264.67 [mm]
Tube dimensions: d_o d_i	31.8 [mm] 28.6 [mm]
Number of tubes: N_t	32 (Calculated Eq. 2.71); 24 (SW est.)
Refrigerant mass flow rate: $\dot{m}_5$	0.0006153 [kg/s]
Coolant mass flow rate: $\dot{m}_{clnt,S1C}$	0.04657 [kg/s]
Fluid Flow Input Parameters	**Comment**
Fluid allocations:	Aqua-ammonia refrigerant – shell side Ethylene glycol water coolant – tube side
Fluid flow pattern	Cross-flow (Appendix C-Figure C.15)
Coolant Thermophysical Properties	**Value [Units]**
$T_{clnt,bulk}$	20.48 [°C]
$C_{p,clnt,bulk}$	3.7610 [kJ/kg.K]
$\rho_{clnt,bulk}$	1038.09 [kg/m^3]
$\mu_{clnt,bulk}$	0.0019977 [kg/m.s]
$k_{clnt,bulk}$	0.499097 [W/m.K]
$Pr_{clnt,bulk}$	15.0930 [-]

The variable to be designed for is the tube's heat transfer surface area, with the only unknown dimension being the length of the tube(s).

Number of Tubes

As the number of tubes is determined using the same equation and input parameters for each of the heat exchangers for the aqua-ammonia absorption-desorption H&R system, the calculation will only be illustrated once with sample values for the stage 1 condenser and hereinafter the calculated value will be given for the remaining heat exchangers. The number of tubes is calculated by using Eq. 2.46, with the input parameters as:

- Single tube pass (CTP = 0.93)
- Tube bundle layout set at 45° (CL = 1.00)
- D_s = 264.67 [mm]
- PR = 1.25 (smallest permitted pitch ratio (Thulukakanam, 2000))
- d_o = 31.8 [mm]

$$N_t = 0.785\left(\frac{CTP}{CL}\right)\left(\frac{D_s^2}{PR^2 d_o^2}\right)$$

$$\therefore \; = 0.785\left(\frac{0.93}{1.00}\right)\left(\frac{264.67^2}{1.25 \text{ x } 31.8^2}\right)$$

$$\therefore \; \cong 32 \; tubes,$$

where the number of tubes are rounded down to the nearest integer. The correlation of Eq. 2.46 doesn't necessarily provide with the exact number of tubes that will fit into a fixed tube sheet, as the formula doesn't account for possible tube sheet stresses and equivalent diameter from shell diameter to the closest tube. Thus, the number of tubes correlation is very conservative for a preliminary thermodynamic design. The parameter of CL for the tube bundle layout is approximated too low, and that the value of 1.34 rather than 1.00 gives a closer result for the actual number of tubes that would fit into the tube sheet. This is determined by constructing the tube sheet component using Computer Aided Design software SolidWorks, where practically only a maximum of 24 tubes will fit into the tube sheet using the tube pitch ratio, tube bundle layout, and tube radial dimensions.

Similar to the number of tubes calculation illustrated above, some thermodynamic design correlations overlap between the seven heat exchanger designs. These overlapping correlations will be illustrated with an example calculation for one heat exchanger and referenced to for the subsequent heat exchanger designs.

Log Mean Temperature Difference

Normal convention for condensing heat exchangers would suggest the use of a mean temperature between the in- and outlets as $\Delta T_m = T_{sat} - T_{wall}$. The mean temperature difference of the stage 1 condenser can be approximated as a log mean temperature difference as the refrigerant undergoes a phase change that doesn't have a constant saturation temperature. The LMTD of the stage 1 condenser is approximated as counter-flow, with the correction factor F = 1.00, due to phase change. Therefore, with Eq. 2.4 the log mean temperature difference is calculated as

$$\Delta T_{LMTD_{S1C}} = \frac{\left(T_{TP,SMR} - T_{clnt,in,SMR}\right) - \left(T_{5,SMR} - T_{clnt,out,SMR}\right)}{\ln\left(\frac{T_{TP,SMR} - T_{clnt,in,SMR}}{T_{5,SMR} - T_{clnt,out,SMR}}\right)}$$

$$\therefore \quad = \frac{(28 - 22.55) - (23 - 18.40)}{\ln\left(\frac{28-22.55}{23-18.40}\right)}$$

$$\therefore \quad = 5.01[°C]\,,$$

where the temperature of the 'Turning Point' is approximated as 5 [°C] above the temperature of state 5 as concluded by the investigation of Chapter 3.1.

Shell Side Heat Transfer Coefficient

State TP to 5 depicted in Fig. 3.3 represents the characteristics of a typical latent two-phase substance. Thus the assumption is made that the shell side heat transfer coefficient for state TP to 5 can be determined by utilising the Nusselt correlation for film condensation in a tube bundle proposed in (Kern, 1958) and the Nusselt correlation for the laminar film condensation originally proposed in (Nusselt, 1916). The heat transfer coefficient for the stage 1 condenser is calculated using Eq. 2.23 & 2.27, where Eq. 2.27 calculates the mean heat transfer coefficient over the tube bundle rows. However, the number of rows of the tube bundle must be determined in order to solve for the heat transfer coefficient. The number of rows can be calculated as the number of tubes divided by the maximum number of tubes to fit in a horizontal line, as illustrated below:

$$N_{t,max} = \frac{D_s}{PR \text{ x } d_o}$$

$$\therefore \quad = \frac{264.67}{1.25 \text{ x } 31.8}$$

$$\therefore \quad = 6.65836$$

$$\therefore \quad \cong 6\ tubes$$

$$N_{rows} = \frac{N_t}{N_{t,max}}$$

$$\therefore \quad = \frac{32}{6}$$

$$\therefore \quad = 5.3333$$

$$\therefore \quad \cong 5\ rows$$

As concluded in Chapter 3.1.1, aqua-ammonia doesn't have a constant saturation temperature. Therefore, it was decided to utilise a modified laminar film condensation Nusselt correlation, which may be untested, but would yield a more conservative heat transfer coefficient. The modification better describes the temperature boundary conditions of the latent two-phase region of aqua-ammonia and the counter-flow ethylene glycol water.

$$h_l = 0.728 * \frac{k_l}{d_o}\left[\frac{\rho_l(\rho_l - \rho_{TP}) * g * (\alpha_{TP-l} * 10^3) * d_o^3}{\mu_l * \left(\Delta T_{LMTD,CF}\right) * k_l}\right]^{\frac{1}{4}} \qquad \textbf{(4.1)}$$

This modification is made with the value of log mean temperature difference, as the log mean temperature difference is a more descriptive representation of the mean temperatures between the in- and outlets of the stage 1 condenser.

Alternatively, the arithmetic average temperature of (T_{sat} – T_{wall}) would have resulted in an under estimation of shell side heat transfer coefficient and the heat transfer surface area, which will

be justified during Chapter 5 of this dissertation. Thus, the laminar film condensation heat transfer coefficient over a single horizontal tube can be calculated as

$$h_5 = 0.728 * \frac{k_5}{d_o}\left[\frac{\rho_5(\rho_5 - \rho_{TP}) * g * (\alpha_{TP-5} * 10^3) * d_o^3}{\mu_5 * (\Delta T_{LMTD,CF}) * k_5}\right]^{\frac{1}{4}}$$

$$\therefore = 0.728 * \frac{0.48931}{0.0318}\left[\frac{611.0805(611.0805 - 8.57479) * 9.81 * (1180.73 * 10^3) * 0.0318}{0.00014988 * (5.00994) * 0.48931}\right]^{\frac{1}{4}}$$

$$\therefore = 8760.97 \left[\frac{W}{m^2.K}\right]$$

The mean heat transfer coefficient for film condensation in a tube bundle of 5 rows can be calculated as

$$\frac{h_o}{h_l} = N^{-1/6} \ (Eq.\ 2.52)$$

$$h_o = h_5 * N^{-1/6}$$

$$\therefore \quad = 8760.97 * 5^{(-1/6)}$$

$$\therefore \quad = 6699.73 \left[\frac{W}{m^2.K}\right]$$

Tube Side Heat Transfer Coefficient

The tube side heat transfer coefficient is determined by using the Hausen method for flow through a circular duct, which is valid for ($0.1 < Gz < 10^4$). This is true for all of the remaining heat exchangers to be designed, no matter the thermodynamic state or chemical composition of the fluid (i.e. aqua-ammonia or ethylene glycol water). This is due to the low mass flow rates of both fluids, which results in Reynolds numbers less than 2300 [-] for flow through a circular duct.

The Hausen tube side heat transfer coefficient will only be illustrated once with sample calculations, and for the remaining heat exchangers the tube side heat transfer coefficients will be tabulated as input parameters and output values of *Re*, *Nu*, and h_i. Now, the tube side heat transfer coefficient can be calculated as

$$Re_T = \frac{4\,\dot{m}_{clnt,S1C}}{N_t\,\pi\,d_i\,\mu_{clnt,bulk}} \quad (Eq.A.49)$$

$$\therefore \quad = \frac{4(0.046569)}{24\,\pi\,(0.0159)(0.0019977)}$$

$$\therefore \quad = 43.2424\,[-]$$

$$Pe_b = Re_T * Pr_{clnt,bulk}$$

$$\therefore = 652.659\,[-]\ (Check)$$

Assume d_i/L = 0.02 for preliminary thermodynamic design.

$$Nu_T = 3.66 + \frac{0.19\left(\frac{Pe_b d_i}{L}\right)^{0.8}}{1 + 0.117\left(\frac{Pe_b d_i}{L}\right)^{0.467}} \quad (Eq.2.41)$$

$$\therefore \quad = 3.66 + \frac{0.19(23.33257)^{0.8}}{1 + 0.117(23.33257)^{0.467}}$$

$$\therefore \quad = 5.22434\ [-]$$

and

$$h_i = \frac{Nu_T\ k_{clnt,bulk}}{d_i} \quad (Eq.2.11)$$

$$\therefore\ = \frac{5.22434(0.499097)}{0.0286}$$

$$\therefore\ = 91.170\ \left[\frac{W}{m^2.K}\right]$$

Overall Heat Transfer Coefficient

Assuming for the preliminary thermodynamic design of each subsequent heat exchanger including the stage 1 condenser that fouling will be excluded from the overall heat transfer coefficient calculation. As fouling factors require the heat transfer surface area to obtain an accurate approximation of fouling. Therefore, by selecting Stainless Steel 304L (with k_{304L} equal to 14.9 [W/m.K] for the specified temperature range of the stage 1 condenser) the overall heat transfer coefficient is calculated by the following:

$$\frac{1}{U_c} = \frac{1}{h_o} + \frac{1}{h_i}.\frac{d_o}{d_i} + \frac{r_o\ \ln\left(\frac{r_o}{r_i}\right)}{k_{material}} \quad (Eq.2.10)$$

$$\therefore = \frac{1}{6699.73} + \frac{1}{91.170}.\frac{0.0318}{0.0286} + \frac{0.0159\ \ln\left(\frac{0.0159}{0.0143}\right)}{14.9}$$

$$\therefore = \left(149.2597E(-06)\right) + \left(10.96856E(-03)\right)\ + \left(113.1776E(-06)\right)$$

$$\therefore U_{S1C} = 80.2681\ \left[\frac{W}{m^2.K}\right]$$

It's clear that the tube side heat transfer coefficient has a far greater influence on the overall heat transfer coefficient than that of the laminar film condensation shell side heat transfer coefficient and the material's thermal conductivity. Thus, the coolant creates the 'bottleneck' of heat flow within the stage 1 condenser, which is a common occurrence for condensing heat exchanger units.

Heat Transfer Surface Area

Now, the thermodynamic sizing problem can be solved by determining the required length of each tube for the stage 1 condenser, by means the following calculation:

$$L = \frac{\dot{Q}_{S1C}}{U_{S1C}\,\Delta T_{LMTD_{S1C}}(N_t \pi d_o)} \quad (Eq.2.45)$$

$$\therefore = \frac{726.503}{80.2681(5.00994)(24 * \pi * 0.0318)}$$

$$\therefore = 0.75586\ [m]$$

Fouling Factors

The fouling factor for the stage 1 condenser is determined by assuming the shell side refrigerant is a pure ammonia gas substance with R_f = 0.00017611 [m^2.K/W], and the tube side coolant has a R_f of 0.000035218 [m^2.K/W]. The fouling factors and percentage over design required are calculated with the same correlation for all the subsequent heat exchanger designs, thus, the fouling factor for overall heat transfer coefficient will only be illustrated once for the stage 1 condenser and given under the design-sizing selection section of the remaining six heat exchanger designs. The overall fouling heat transfer coefficient is

$$\frac{1}{U_f A_s} = \frac{1}{h_o A_o} + \frac{R_{f,o}}{A_o} + \frac{1}{h_i A_i} + \frac{R_{f,i}}{A_i} + \frac{A_o\ \ln(d_o/d_i)}{2\pi L k_{material}} \quad (Eq.A.55)$$

$$U_f A_s = \frac{1}{\frac{1}{6699.73(1.8123)} + \frac{0.00017611}{1.8123} + \frac{1}{91.1697(1.6299)} + \frac{0.000035218}{1.6299} + \frac{1.8123\ \ln(0.0318/0.0286)}{2\pi(0.755861)(14.9)}}$$

$$\therefore U_f = 79.1098\ \left[\frac{W}{m^2.K}\right],$$

where the cleanliness factor (*CF*) calculated as 0.9856 [-] with Eq. A.58. The total fouling resistance (R_{ft}) is calculated as 0.00018242 [m^2.K/W] with Eq. A.57, thus the percentage over design is calculated as

$$OS = 100 U_{S1C} R_{ft} \quad (Eq.A.56)$$

$$\therefore \quad = 100(80.2681)(0.00018242)$$

$$\therefore \quad = 1.46426\ [\%]$$

Although the oversize percentage is very small in this case, the principle will be applied to all the remaining heat exchangers to ensure that the sizing of each heat exchanger is accurate and practically acceptable.

4.3.2 Performance Rating of the Thermodynamic Design

Previously it was mentioned that a heat exchanger analysis consists of two problems, sizing and rating, and now that the preliminary sizing has been completed, the rating problem or performance rating can be solved.

NTU – Effectiveness Performance Rating

The number of heat transfer units and the effectiveness relation can be calculated using the following:

$$NTU = \frac{UA_s}{C_{min}} = \frac{U_{S1C} N_t \pi d_o L_t}{\left(\dot{m}_5\, C_{p,5}\right)_{min}} \quad (Eq.\,2.13)$$

$$\therefore \quad = \frac{80.2681 * 24 * \pi * 0.0318 * 0.755861}{0.0006153 * 4.751615}$$

$$\therefore \quad = 49.5995\ [-]$$

$$\varepsilon = 1 - \exp(-NTU) \quad (Table\ 2.1; Eq.\,4)$$

$$\therefore = 1 - \exp(-49.5995)$$

$$\therefore = 1$$

The effectiveness is equal to 1, which is commonly expected of a condenser unit due to the phase-change, thus satisfying the thermal heat exchanger efficiency requirement. The effectiveness is equal to 100% for all of the ambient design conditions that is illustrated in Figure D 9.1 of Appendix D 9.1.

Pressure Drop

The shell – and tube side pressure drop calculations are irrelevant for the stage 1 condenser, as the layout of the heat exchanger is cross-flow orientated with TEMA shell type J. According to (Walker, 1990) the TEMA shell type J has 1/8th the pressure drop of a regular counter flow heat exchanger.

4.3.3 Thermodynamic Design Verification

The verification of the preliminary thermodynamic design-sizing model was completed using the coding software EES. The verification of the heat exchanger's heat transfer surface area can be completed with two approaches to the formulation of sizing equations. The first method is to duplicate the preliminary sizing as in section 4.2.2, and the second method is to use the heat exchanger model of section 4.2.2 and determine the heat transfer rate. The first method compares the heat exchanger's length obtained by the two software programs, and the second method

compares the heat transfer rate obtained via Eq. 2.1 to the EES heat exchanger heat transfer rate of Eq. 2.6.

The procedure of determining if the thermodynamic design calculations are valid will only be illustrated once for the stage 1 condenser, as the procedure is the same for all succeeding heat exchangers in this oeuvre. As previously mentioned in Chapter 3.1.2, the thermophysical properties of the stage 1 condenser aren't under dispute, as the properties have already been verified. Thus, to fully insure there are no calculation or mathematical errors in the MS Excel coding the same thermophysical property values of the stage 1 condenser will be used for the verification procedure for coding in EES. Full perusal of the EES coding is available in Appendix D 2.2. To keep the oeuvre concise and to the point the coded formatted equations will be illustrated with the value obtained by EES for the said correlation.

Calculating Log Mean Temperature Difference

$$LMTD = \frac{T_{TP} - T_{coolant,out} - [T_5 - T_{coolant,in}]}{\ln\left[\frac{T_{TP} - T_{coolant,out}}{T_5 - T_{coolant,in}}\right]}$$

LMTD = 5.010 [C]

Calculation of the Shell Side Heat Transfer Coefficient

$$h_l = 0.728 \cdot \frac{k_5}{d_{outer}} \cdot \left[\frac{(\rho_5 \cdot [\rho_5 - \rho_{TP}] \cdot 9.81 \cdot [\alpha_{TP} - \alpha_5] \cdot 10^3) \cdot d_{outer}^{\ 3}}{\mu_5 \cdot LMTD \cdot k_5}\right]^{0.25}$$

$$h_o = N^{\left[\frac{-1}{6}\right]} \cdot h_l$$

h_o = 6694.430 [W/m^2·K]

Calculation of the Tube Side Heat Transfer Coefficient using Hausen Method

$$h_i = \frac{Nusselt_t \cdot k_{coolant}}{d_{inner}}$$

h_i = 91.170 [W/m^2·K]

Overall Heat Transfer Coefficient

$$\frac{1}{U} = \frac{1}{h_o} + \frac{1}{h_i} \cdot \frac{d_{outer}}{d_{inner}} + \frac{r_{outer} \cdot \ln\left[\frac{r_{outer}}{r_{inner}}\right]}{k_{ss,304L}}$$

$U = 80.267$ [W/m^2·K]

Calcuating the Heat Transfer Rate(EES & S1C & Comparison Percetage)

$$\dot{Q}_{EES} = U \cdot A_s \cdot LMTD$$

$\dot{Q}_{EES} = 728.788$ [W]

$$\dot{Q}_{S1C} = \dot{m}_5 \cdot [\alpha_{TP} - \alpha_5] \cdot 1000$$

$\dot{Q}_{S1C} = 726.503$ [W]

$$\text{Comparison\%} = \left[\frac{\dot{Q}_{EES}}{\dot{Q}_{S1C}} - 1\right] \cdot 100$$

Comparison% = 0.31447 [%]

The two values of heat transfer rate are within good accordance to one another. Thus, verifying that the MS Excel thermodynamic design model has no mathematical errors and can be considered acceptable for the stage 1 condenser.

4.3.4 Design Sizing Selection

The shell diameter of D_s = 264.67 [mm] was selected for its length over shell diameter ratio being within the 2 to 7 range at 2.89599 [-], as the heat exchanger will be pressurised in excess of 1 [MPa]. The tube diameter was selected based on the low number of tubes (24) the 31.8 [mm] tube requires within the tube bundle, which saves costing in terms of less welding time spent on the stage 1 condenser.

Commonly the tube length obtained with the design-sizing equations are rounded to an easier to measure and manufacturable length. The heat transfer surface length of the tubes are rounded up from 0.75586 [m] to 0.8 [m], which results in a 5.84% overdesign that accounts for ambient conditions that exceed the summer design conditions. The coolant's mass flow rate can be manipulated to reduce the heat transfer rate to accommodate for the required heat of condensation between states 5 to TP for all ambient conditions.

4.4 Stage 2 Condenser (State 4 to TP)

4.4.1 Preliminary Thermodynamic Design

Stage 2 of the condenser unit has the following input parameters to assist the illustration of the thermodynamic design calculations are set in Table 4.2, with full review of the thermodynamic design for all ambient conditions available in Appendix D 3.1.

Table 4.2: Stage 2 condenser – Thermodynamic design input parameters.

Thermodynamic Input Parameters	**Value/Comment**
Winter ambient conditions	
Shell inner diameter: D_s	264.67 [mm]
Tube dimensions: d_o d_i	19.1 [mm] 15.9 [mm]
Number of tubes: N_t	89 (Calculated Eq. 2.46); 68 (SW est.)
Refrigerant mass flow rate: $\dot{m}_4$	0.0005412 [kg/s]
Coolant mass flow rate: $\dot{m}_{clnt,S2C}$	0.00069 [kg/s]
Equivalent diameter: D_e	18.898 [mm] (Eq. A.42)
Clearance: C	4.774 [mm] (Eq. A.45)
Bundle cross-flow area: A_{cs}	0.052936 [m^2] (Eq. A.46)
Mass velocity: G_s	0.010224 [m^2/s]
Number of baffles: N_b	0
Number of tube rows: N_{rows}	8
Tube bundle correction factor: C_n	0.98 (Table 2.3)
Fluid Flow Input Parameters	**Comment**
Fluid allocations:	Aqua-ammonia refrigerant – shell side Ethylene glycol water coolant – tube side
Fluid flow pattern	Cross-flow (Appendix C – Figure C.15)
Coolant Thermophysical Properties	**Value [Units]**
$T_{clnt,bulk}$	25.07 [°C]
$C_{p,clnt,bulk}$	3.76985 [kJ/kg.K]
$\rho_{clnt,bulk}$	1036.268 [kg/m^3]
$\mu_{clnt,bulk}$	0.0017578 [kg/m.s]
$k_{clnt,bulk}$	0.50166 [W/m.K]
$Pr_{clnt,bulk}$	13.2541 [-]

Assumption: It should be noted that the bundle cross-flow area is approximated by splitting the stage 2 condenser into two tube bundle sections with baffle spacing B = 1 [m]. The assumption is justified as the stage 2 condenser has two inlets.

The thermophysical properties of the stage 2 condenser were previously calculated in Chapter 3.1.2 for summer ambient conditions, but recent information suggested that winter ambient conditions would yield the largest heat transfer surface area for the stage 2 condenser. Thus, the thermophysical properties for winter ambient conditions of state 4 and TP, found in Appendix B 2 & 3, are shown in Tables 4.3 & 4.4 as:

Table 4.3: State 4 thermophysical properties for winter ambient conditions.

Thermophysical Properties	Value [Units]
T_4	47.6809 [°C]
P_4	515.84 [kPa]
α_4	1384.1964 [kJ/kg.K]
ρ_4	5.28899 [kg/m^3]
μ_4	1.1317E(-05) [kg/m.s]
k_4	0.031027 [W/m.K]
Pr_4	1.37445 [-]

Table 4.4: State TP thermophysical properties for winter ambient conditions.

Thermophysical Properties	Value [Units]
T_{TP}	10 [°C]
P_{TP}	515.84 [kPa]
α_{TP}	1182.205 [kJ/kg.K]
ρ_{TP}	5.60633 [kg/m^3]
μ_{TP}	2.1851E(-05) [kg/m.s]
k_{TP}	0.060956 [W/m.K]
Pr_{TP}	1.38998 [-]

Log Mean Temperature Difference

The log mean temperature difference of the second stage condenser is calculated with the same equation and correction factor as that of the stage 1 condenser. The correction factor of 1.00, is caused by the specific thermal capacity of the refrigerant trending towards infinity, even though the fluids are in a cross-flow pattern. This is evident when comparing the heat transfer rate of Eq. 2.1 to Eq. 2.2, where the heat transfer rate of Eq. 2.1 is equal to 109.3033 [W], and Eq. 2.2 is equal to 38.4222 [W]. Therefore, with this large difference in heat transfer rate it is a fair assumption that the correction factor F = 1.00 and the log mean temperature difference calculated for counter-flow. The log mean temperature difference is therefore calculated as:

$$\Delta T_{LMTD,CF} = 3.349\ [°C] \quad (Eq.\ 2.4)$$

Shell Side Heat Transfer Coefficient

Similar to stage 1 of the condenser unit, the aqueous ammonia refrigerant is allocated to flow through the tube bundle. Although, the condenser unit has been split into two linear approximations of the two-phase regions of aqua-ammonia, these two stages of the condenser unit aren't best suited to be sized with the same methodology of determining the shell side heat transfer coefficient. As previously illustrated by Figures 3.3 & 3.5, the two-phase region of state 4 to TP has similar behavioural characteristics to the superheated vapour region, where the temperature drops

radically to the contrasting low decline in enthalpy. Thus, it's assumed that the stage 2 condenser can be treated as a 'no-phase change' cooling heat exchanger as the refrigerant remains highly comprised of saturated vapour with little condensation.

The shell side heat transfer coefficient can be approximated using the Zukauskas – Nusselt correlation of flow through a tube bundle. The Zukauskas method will result in a heat transfer coefficient much lower than the Kern – Nusselt correlation of the stage 1 condenser. This can be attributed to the fact that the Kern – Nusselt correlation is based on fluids condensing at a constant temperature. Therefore, nullifying the use of the Kern – Nusselt correlation, as too little condensation occurs within the stage 2 condenser to fully support the use of Eq. 2.23 or Eq. 4.1. The shell side Reynolds number is calculated using Eq. A.47 as 11.6503 [-], which would suggest the use of Eq. 2.18 for calculating the shell side heat transfer coefficient.

$$Nu_D = \left(1.04\, C_n\, Re_D^{0.4} Pr_{bulk}^{0.36} \left(\frac{Pr_{bulk}}{Pr_{wall}}\right)^{0.25}\right) \quad (Eq.\,2.18)$$

$$\therefore h_o = \frac{k_{bulk}}{d_o}\left(1.04 * 0.98\, Re_D^{0.4} Pr_{bulk}^{0.36} \left(\frac{Pr_{bulk}}{Pr_{wall}}\right)^{0.25}\right)$$

$$\therefore \quad = \frac{0.045992}{0.0191}\left(1.04 * 0.98\, (11.6503)^{0.4} (1.38222)^{0.36} \left(\frac{1.38222}{1.38377}\right)^{0.25}\right)$$

$$\therefore \quad = 7.38015\ \left[\frac{W}{m^2.K}\right]$$

Tube Side Heat Transfer Coefficient

As previously illustrated, the tube side heat transfer coefficient is obtained with exactly the same methodology as the stage 1 condenser, therefore the tube side heat transfer coefficient can be expressed as:

$$Re_T = 0.46397\ [-] \quad (Eq.\,A.49)$$

$$Nu_T = 3.68309\ [-] \quad (Eq.\,2.41)$$

$$h_i = 116.489\ \left[\frac{W}{m^2.K}\right] \quad (Eq.\,2.11)$$

Overall Heat Transfer Coefficient

The overall heat transfer coefficient of the stage 2 condenser is calculated with stainless steel 304L as the material of the heat exchanger. The overall heat transfer coefficient is calculated as

$$\frac{1}{U_c} = \frac{1}{h_o} + \frac{1}{h_i}.\frac{d_o}{d_i} + \frac{r_o\, \ln\left(\frac{r_o}{r_i}\right)}{k_{material}} \quad (Eq.\,2.10)$$

$$\therefore = \frac{1}{7.38015} + \frac{1}{116.489} . \frac{0.0191}{0.0159} + \frac{0.00955 \ln\left(\frac{0.00955}{0.000795}\right)}{14.9}$$

$$\therefore = \left(135.499E(-03)\right) + \left(10.3373E(-03)\right) + \left(117.5286E(-06)\right)$$

$$\therefore U_{S2C} = 6.77751 \left[\frac{W}{m^2.K}\right]$$

It's clear from the overall heat transfer coefficient calculation that the shell side heat transfer coefficient has a greater influence, which can be attributed to the high vapour quality of the aqua-ammonia refrigerant. Thus, it can be concluded that the aqua-ammonia refrigerant causes the hindering of heat transfer within the stage 2 condenser, which in turn would mean the stage 2 condenser can't be manipulated in terms of coolant mass flow rates or outlet temperatures.

Heat Transfer Surface Area

The thermodynamic design problem can be solved by determining the required length of each tube for the stage 2 condenser, as illustrated by the following:

$$L = \frac{\dot{Q}_{S2C}}{U_{S2C}\, \Delta T_{LMTD_{S2C}} (N_t \pi d_o)} \quad (Eq. 2.45)$$

$$\therefore \ = \frac{109.3033}{6.77751(3.349)(68 * \ \pi * 0.0191)}$$

$$\therefore \ = 1.1834 \ [m]$$

4.4.2 Performance Rating of the Thermodynamic Design

NTU – Effectiveness Performance Rating

The number of heat transfer units and the effectiveness relation can be calculated using the following:

$$NTU = \frac{U_c A_s}{C_{min}} = \frac{U_{S2C} N_t \pi d_o L_t}{\left(\dot{m}_4\, C_{p,4}\right)_{min}} \quad (Eq. 2.8)$$

$$\therefore \quad = \frac{6.03498 * 68 * \pi * 0.0191 * 1.32897}{0.0006153 * 3.768194}$$

$$\therefore \quad = 16.00493 \ [-]$$

$$c = \frac{C_{min}}{C_{max}} \quad (Eq. 2.9)$$

$$\therefore = \frac{0.0006153 * 3.768194}{0.00069253 * 3.769854}$$

$$\therefore = 0.781139$$

The effectiveness and NTU values are plotted to the standard cross-flow effectiveness vs. NTU curve, which is illustrated in Figure D 9.2 for all ambient conditions to verify the feasibility of the stage 2 condenser.

$$\varepsilon = 1 - \exp\left\{\frac{NTU^{0.22}}{c}\left[\exp(-c\,NTU^{0.78}) - 1\right]\right\} \quad (Table\ 2.1; Eq.3)$$

$$\therefore = 1 - \exp\left\{\frac{16.00493^{0.22}}{0.781139}\left[\exp(-0.781139\,(16.00493)^{0.78}) - 1\right]\right\}$$

$$\therefore = 0.90497\ or\ 90.497\ [\%]$$

Though the number of transfer units stops at 5 on the standard effectiveness vs. NTU chart, the curve can be extrapolated that the capacity ratio of 0.75 could possibly converge to an effectiveness close to the 91% of the stage 2 condenser. If the stage 2 condenser's coolant outlet temperature is lower the critical mass flow rate of the coolant then the coolant mass flow rate would inversely rise and would increase the heat transfer rate of the stage 2 condenser with very little change to the effectiveness. The coolant outlet temperature remains at 46 [°C] and the stage 2 condenser has an estimated effectiveness of 90.497%. Therefore, meeting the thermal heat exchanger efficiency requirements and can be classified as a feasible heat exchanger.

Note: Effectiveness is expected to be near 100% for condensers and boilers, but as the stage 2 condenser is approximated as a cross-flow heat exchanger the effectiveness obtained might be viewed as a high estimation. This should be kept in mind when testing the stage 2 condenser's in- and outlet temperatures within the entire aqua-ammonia heating & refrigeration package unit experimental setup.

Pressure Drop

The shell – and tube side pressure drop are calculated using Eq. A.50 & A.52, with the resulting values shown in Table 4.5.

Table 4.5: Stage 2 condenser – Pressure drop.

Pressure Drop	Output [Units]
Shell side pressure drop: ΔP_s	0.00019 [Pa]
Tube side pressure drop: ΔP_t	0.012 [Pa]

The pressure drop within the stage 2 condenser is too low to have any effect on the thermodynamic design, therefore pressure drop is considered negligible and the stage 2 condenser won't undergo a second iteration of design-sizing.

4.4.3 Thermodynamic Design Verification

As mentioned earlier the preliminary thermodynamic design model of MS Excel can be verified by approximating the heat transfer rate of the sized heat exchanger model in EES. Full perusal of EES coding for the stage 2 condenser is available in Appendix D 3.2. The output parameters of the verification coding are illustrated in Table 4.6, with the conclusion that the comparison between the heat transfer rate from the EES heat exchanger model and the heat transfer rate of Eq. 2.1 are within good accordance to one another. This proves that the preliminary thermodynamic design model is accurate. Slight differences are easily noted when comparing values such as the shell and tube side heat transfer coefficients, where they differ with 0.2602% and 0.0355% respectively between MS Excel and EES. These small differences are accounted to the rounding of output values in succeeding equations in the EES verification model.

Table 4.6: Stage 2 condenser – EES verification output parameters.

Design Parameters	Output [Units]
$\Delta T_{LMTD,CF}$	3.349 [°C]
Shell side heat transfer coefficient: h_o	7.361 [W/m^2.K]
Tube side heat transfer coefficient: h_i	116.165 [W/m^2.K]
Overall heat transfer coefficient: U_c	6.835 [W/m^2.K]
Heat transfer rate: $\dot{Q}_{EES}$	110.516 [W]
Heat transfer rate: $\dot{Q}_{S2C}$	109.303 [W]
Comparison percentage	1.11 [%]

Note: The stage 1 and 2 condensers have been designed for their individual 'worst case' scenarios, at summer and winter ambient conditions respectively. Therefore, for the control of the aqua-ammonia heating cycle the manipulation of coolant mass flow rate of the stage 1 condenser will be fundamental to the effectiveness of the heating cycle at alternative ambient conditions.

4.4.4 Design Sizing Selection

If the tube diameters were to be the same for both the stage 1 and 2 condensers then the length of the stage 2 condenser would've been near 3 [m], which exceeds the design selection parameter of heat transfer surface length. Thus, for the purpose of fluid distribution in both stages of the condenser and shorter shell length of the stage 2 condenser, a tube of d_o = 19.1 [mm] is selected for the stage 2 condenser. The 19.1 [mm] tube gives a total of 68 tubes within the tube bundle, which is within the design selection parameter. The shell housing of both the stages of the condenser are selected with the same inner diameter nominal bore pipe, as it would be more cost effective to purchase one pipe of diameter 264.67 [mm] than different pipe diameters for the shell of the two condenser heat exchangers.

As the design-sizing for the stage 2 condenser was completed for winter ambient conditions, it is decided that the tube length can be rounded down from 1.230 [m] to 1.2 [m], which is to the benefit of yearly ambient conditions being on average higher than winter ambient conditions. Though the fouling factors would suggest an over design percentage of 4.1148%, the stage 2 condenser has an over design percentage of 1.41%. This is a safe design assumption due to the required length of summer ambient conditions is 47.47% lower than the modelled stage 2 condenser.

4.5 De-superheating Condenser (State 3 to 4)

4.5.1 Preliminary Thermodynamic Design

The input parameters for the preliminary design-sizing calculations of the de-superheating condenser are set in Table 4.7.

Table 4.7: De-superheating condenser – Thermodynamic design input parameters.

Thermodynamic Input Parameters	**Value/Comment**
Summer ambient conditions	
Thermophysical properties of state 3 – 4	Section 3.1.2
Shell inner diameter: D_s	134.5 [mm]
Tube dimensions: d_o d_i	19.1 [mm] 15.9 [mm]
Number of tubes: N_t	28 (Calculated Eq. 2.46); 15 (SW est.)
Refrigerant mass flow rate: $\dot{m}_3$	0.0006153 [kg/s]
Coolant mass flow rate: $\dot{m}_{clnt,S2C}$	0.000565 [kg/s]
Equivalent diameter: D_e	18.898 [mm] (Eq. A.42)
Clearance: C	4.774 [mm] (Eq. A.45)
Bundle cross-flow area: A_{cs}	0.006725 [m^2] (Eq. A.46)
Mass velocity: G_s	0.091494 [m^2/s]
Baffle spacing: B	0.25 [m]
Number of tube rows: N_{rows}	5
Tube bundle correction factor: C_n	0.93 (Table 2.3)
Fluid Flow Input Parameters	**Comment**
Fluid allocations:	Aqua-ammonia refrigerant – shell side Ethylene glycol water coolant – tube side
Fluid flow pattern	Counter-flow (Appendix C – Figure C.13)

Table 4.7 Continued:

Thermophysical Properties	Value [Units]
$T_{clnt,bulk}$	69.65 [°C]
$C_{p,clnt,bulk}$	3.86643 [kJ/kg.K]
$\rho_{clnt,bulk}$	1015.979 [kg/m^3]
$\mu_{clnt,bulk}$	0.00072179 [kg/m.s]
$k_{clnt,bulk}$	0.51983 [W/m.K]
$Pr_{clnt,bulk}$	5.40450 [-]

The mass flow rate of the coolant remains the same mass flow received from the stage 2 condenser, and not the de-superheating condenser's critical mass flow rate. This is a design decision to increase the efficiency of the cycle at the cost of possible temperature gains. In other words the coolant's mass flow rate isn't reduced between the stage 2 – and de-superheating condensers to create a single coolant line with a high temperature, rather than having two lines of coolant with stage 2 condenser and de-superheating condenser outlet temperatures. Therefore, the coolant outlet temperature of the de-superheating condenser can be calculated using Eq. 2.2 and the heat transfer rate obtained in Chapter 3.1.2 as

$$\sum \dot{Q}_{in} = \sum \dot{Q}_{out}$$

$$\therefore \dot{Q}_{DHC,SMR} = \dot{m}_{clnt,DHC} C_{p,clnt,bulk,DHC} \left(T_{clnt,out,DHC} - T_{clnt,in,DHC}\right)$$

$$\therefore 57.43125 = (0.000565)(3.86643 \text{ x } 10^3)(T_{clnt,out} - 56.5)$$

$$\therefore T_{clnt,out,S1C} = 82.80\ [°C]$$

The thermodynamic design calculation output values and the corresponding correlation used for the thermodynamic design of the de-superheating condenser are shown in Table 4.8.

Table 4.8: De-superheating condenser – Preliminary thermodynamic design output parameters.

Design Parameters	Output [Units]	Correlation
$\Delta T_{LMTD,CF}$	7.14 [°C]	Eq. 2.4
Re_s	141.007 [-]	Eq. A.47
Shell Side HTC: h_o	13.1496 [W/m^2.K]	Eq. 2.18 & Table 2.2
Re_T	4.17799 [-]	Eq. A.49
Nu_T	3.75452 [-]	Eq. 2.41
Tube Side HTC: h_i	122.7502 [W/m^2.K]	Eq. 2.11
Overall HTC: U_c	11.6347 [W/m^2.K]	Eq. 2.10
Tube length: L	0.768535 [m]	Eq. 2.45

From Table 4.8 it can be concluded that the aqua-ammonia refrigerant is responsible for the hindering of heat transfer within the de-superheating condenser and that any coolant mass flow manipulation would yield little effect on the heat capacity output of the de-superheating condenser.

4.5.2 Performance Rating of the Thermodynamic Design

The number of transfer units and the effectiveness relation is determined by using Eq. 2.8 & 2.9 and equation 1 from Table 2.1 for counter-flow heat exchangers, which is illustrated by the following:

$$NTU = \frac{UA_s}{C_{min}} = \frac{U_{DHC} N_t \pi d_o L_t}{\left(\dot{m}_3\, C_{p,bulk}\right)_{min}}$$

$$\therefore \quad = \frac{10.40337 * 15 * \pi * 0.0191 * 0.855861}{0.0006153 * 2.7039}$$

$$\therefore \quad = 4.83741\ [-]$$

$$c = \frac{C_{min}}{C_{max}}$$

$$c = \frac{\dot{m}_3\, C_{p,bulk}}{\dot{m}_{clnt.S2C}\, C_{p,clnt,bulk}}$$

$$\therefore = \frac{0.0006153 * 2.7039}{0.00056488 * 3.86643}$$

$$\therefore = 0.76175$$

$$\varepsilon = \frac{1 - \exp\left(-NTU(1-c)\right)}{1 - c\exp\left(-NTU(1-c)\right)}$$

$$\therefore = \frac{1 - \exp\left(-4.818065(1-0.75932)\right)}{1 - 0.75932\exp\left(-4.818065(1-0.75932)\right)}$$

$$\therefore = 0.90091\ or\ 90.091\ [\%]$$

The effectiveness and NTU values are plotted to the standard effectiveness vs. NTU curve for counter-flow heat exchangers, available in Appendix D 9.3.

According to Figure D 9.3 the de-superheating condenser is at the limit of performance for a counter-flow heat exchanger, which means the assumed coolant outlet temperature of the de-superheating condenser is at the highest allowable temperature with regards to efficiency. Therefore, the calculated effectiveness of the de-superheating condenser in relation to the summer ambient condition can be considered as a practically feasible heat exchanger.

Pressure Drop

The shell – and tube side pressure drop are calculated using Eqs. A.50 & A.52, with the results recorded in Table 4.9. The pressure drops within the shell – and tube sides of the de-superheating condenser are too small and would have little effect on the design-sizing to substantiate the process of conducting a second design-sizing iteration.

Table 4.9: De-superheating condenser – Pressure drop.

Pressure Drop	Output [Units]
Shell side pressure drop: ΔP_s	0.022 [Pa]
Tube side pressure drop: ΔP_t	0.011 [Pa]

4.5.3 Thermodynamic Design Verification

Full perusal of EES coding for the de-superheating condenser is available in Appendix D 4.2. The output parameters of the verification coding are illustrated in Table 4.10. The comparison of the heat transfer rate obtained from EES' heat exchanger model and the heat transfer rate of Eq. 2.1 are identical. Thus, verifying the coding of MS Excel has no mathematical errors and that the preliminary thermodynamic design is satisfactory.

Table 4.10: De-superheating condenser – EES verification output parameters.

Design Parameters	Output [Units]
$\Delta T_{LMTD,CF}$	7.14 [°C]
Shell side heat transfer coefficient: h_o	13.1497 [W/m^2.K]
Tube side heat transfer coefficient: h_i	122.7502 [W/m^2.K]
Overall heat transfer coefficient: U_c	11.6345 [W/m^2.K]
Heat transfer rate: $\dot{Q}_{EES}$	57.431 [W]
Heat transfer rate: $\dot{Q}_{DHC}$	57.431 [W]
Comparison percentage	-0.0015 [%]

4.5.4 Design Sizing Selection

The selection of a smaller shell diameter for the de-superheating condenser is for space saving purposes in the z-direction, as the refrigerant flows by utilising Gibbs free energy. Thus, the condenser units should not exceed 0.8 [m] in the z-direction within the nock of the housing structure. The tubes are chosen to be the same tube size as the stage 2 condenser, as the smaller 19.1 [mm] tubing has a higher Reynolds number than the 31.8 [mm] tubing. The heat transfer tube length of the de-superheating condenser is increased from 0.768535 [m] to 0.800 [m], which is a 4.094% over design that exceeds the 2.17% over design required for fouling factors.

Now, to conclude the first segment of the heating components of the aqua-ammonia heating cycle, the ethylene glycol water mixture will reach highs of 82.71 [°C] (Summer), 66.71 [°C] (Average), and 51.08 [°C] (Winter) at the respective mass flow rates of 0.565 [g/s], 0.640 [g/s], and 0.693 [g/s].

Note: The outlet temperatures of the coolant at their respective ambient conditions are independent and created with ideal conditions during the thermodynamic design phase. Thus, if a full flow analysis from the heat sink to the outlet of the de-superheating condenser is to be done for all ambient conditions with the modelled heat exchangers, the outlet temperatures achieved won't correspond to the estimated values of the thermodynamic design and rating without the manipulation of coolant mass flow rates. However, it must be iterated that the concluded outlet temperatures are achievable with the modelled stage 1 & 2 and de-superheating condensers proposed in this section, albeit it would be difficult for winter ambient conditions.

Mechanical material note: The subsequent heat exchangers to be designed will either have 19.1 [mm] or 31.8 [mm] stainless steel 304L tubing, and the choice of two shell diameters 264.67 [mm] or 134.5 [mm].

4.6 Pre-Cool Heat Exchanger (State 5 to 6 & 9 to 10)

The pre-cool heat exchanger operates between the states 5 to 6 and 9 to 10, where the pre-cool heat exchanger adds heat from the 'hot' saturated liquid state 5 to the 'cold' saturated vapour state 9, as represented by Figure D 1.4 in Appendix D 1.4. Stated in Chapter 3.1, the pre-cool heat exchanger is merely added to the absorption-desorption cycle to increase the refrigeration coefficient of performance. The pre-cool heat exchanger would increase the refrigeration COP by lowering the evaporator's refrigerant inlet temperature, which means the evaporator would have a larger latent area and a larger cooling capacity.

4.6.1 Preliminary Thermodynamic Design

The preliminary heat exchanger design-sizing incorporates the same shell and tube side heat transfer coefficient correlations as used during the design-sizing of the stage 2 condenser. Therefore, the preliminary design-sizing output values will be tabulated accordingly. The input parameters for the preliminary design-sizing calculations of the pre-cool heat exchanger are set in Table 4.11 as:

Table 4.11: Pre-cool heat exchanger – Thermodynamic design input parameters.

Thermodynamic Input Parameters	**Value/Comment**
Summer ambient conditions	
Thermophysical properties of state 5 – 6	Appendix B 1.3
Thermophysical properties of state 9 – 10	Appendix B 1.3
Shell inner diameter: D_s	134.5 [mm]
Tube dimensions: d_o d_i	19.1 [mm] 15.9 [mm]
Number of tubes: N_t	28 (Calculated Eq. 2.46); 15 (SW est.)
Refrigerant mass flow rate: $\dot{m}_6$	0.0006129 [kg/s]
Refrigerant mass flow rate: $\dot{m}_9$	0.0005986 [kg/s]
Equivalent diameter: D_e	18.898 [mm] (Eq. A.42)
Clearance: C	4.774 [mm] (Eq. A.45)
Bundle cross-flow area: A_{cs}	0.006725 [m^2] (Eq. A.46)
Mass velocity: G_s	0.089011 [m^2/s]
Baffle spacing: B	0.25 [m]
Number of tube rows: N_{rows}	5
Tube bundle correction factor: C_n	0.93 (Table 2.3)
Fluid Flow Input Parameters	**Comment**
Fluid allocations:	Superheated Ammonia – shell side Sub cooled Aqua-ammonia – tube side
Fluid flow pattern	Counter-flow (Appendix C – Figure C.13)

Recorded in Table 4.12 are the thermodynamic design calculation output values and the corresponding correlation used to determine the thermodynamic design of the pre-cool HTEX.

Table 4.12: Pre-cool heat exchanger – Preliminary design output parameters.

Design Parameters	**Output [Units]**	**Correlation**
$\Delta T_{LMTD,CF}$	14.25 [°C]	Eq. 2.4
Re_s	183.953 [-]	Eq. A.47
Shell Side HTC: h_o	9.3079 [W/m^2.K]	Eq. 2.18 & Table 2.2
Re_T	20.0219 [-]	Eq. A.49
Nu_T	3.84190[-]	Eq. 2.41
Tube Side HTC: h_i	122.221 [W/m^2.K]	Eq. 2.11
Overall HTC: U_c	8.51922 [W/m^2.K]	Eq. 2.10
Tube length: L	0.39077 [m]	Eq. 2.45

Full review of the preliminary thermodynamic design is available in Appendix D 5.1.

4.6.2 Performance Rating of the Thermodynamic Design

The performance rating of the pre-cool heat exchanger is determined with the same methodology as with the de-superheating condenser. Thus, to remain concise Table 4.13 depicts the NTU, effectiveness, and pressure drops of the pre-cool heat exchanger with the resulting effectiveness and NTU plotted to the standard counter-flow effectiveness curve in Figure D 9.4.

Table 4.13: Pre-cool heat exchanger – Performance rating.

Performance Rating	Output [Units]	Correlation
NTU	1.039911 [-]	Eq. 2.8
Capacity Ratio: c	0.49601 [-]	Eq. 2.9
Effectiveness: ε	0.5775 or 57.75 [%]	Table 2.1; Eq. 1
Shell side pressure drop: ΔP_s	0.020 [Pa]	Eq. A.50
Tube side pressure drop: ΔP_t	0.004 [Pa]	Eq. A.52

The pressure drops within the shell – and tube sides are too low to substantiate the process of conducting a second design-sizing iteration and can be considered as trivial.

The effectiveness of all the ambient design conditions fall within close proximity to one another, and are at the expected effectiveness for a counter-flow heat exchanger. Therefore, it can be concluded that the temperature boundary conditions are within reasonable ranges of a practical heat exchanger application and satisfy the thermodynamic design requirements.

4.6.3 Thermodynamic Design Verification

Full review of EES coding for the pre-cool heat exchanger is available in Appendix D 5.2, where Table 4.14 depicts the critical output parameters of the EES verification code for the pre-cool heat exchanger.

Table 4.14: Pre-cool heat exchanger – EES verification output parameters.

Design Parameters	Output [Units]
$\Delta T_{LMTD,CF}$	14.25 [°C]
Shell side heat transfer coefficient: h_o	9.3077 [W/m^2.K]
Tube side heat transfer coefficient: h_i	124.563 [W/m^2.K]
Overall heat transfer coefficient: U_c	8.5325 [W/m^2.K]
Heat transfer rate: $\dot{Q}_{EES}$	42.764 [W]
Heat transfer rate: $\dot{Q}_{PC}$	42.698 [W]
Comparison percentage	0.1557 [%]

The comparison of the heat transfer rate obtained from EES' heat exchanger model and the heat transfer rate of Eq. 2.1 are within 0.16% of one another. Thus, verifying the coding of MS Excel thermodynamic design model is without any mathematical errors and the preliminary thermodynamic design as acceptable.

4.6.4 Design Sizing Selection

The shell diameter of 134.5 [mm] and the 19.1 [mm] tubing was selected from same material dimensions used by the de-superheating condenser. The tube length can be increased from 0.39077 [m] to 0.400 [m], which is a 2.363% over design that exceeds the 1.588% over design required for fouling.

4.7 Venturi Nozzle and Orifice (State 6 to 7)

The concept design of the evaporator depicts three inlets, of which one is a venturi nozzle and two orifice nozzles. The venturi nozzle needs to generate a suction force to remove excess helium within the absorber module and re-enter the helium into the evaporator module. Commonly, the thermodynamic design of an orifice or a venturi nozzle is considered as isothermal. The thermodynamic design of an orifice or a venturi nozzle can be determined by using Bernoulli's equation for vertical fluid flow, the continuity equation for pressure drop, and a discharge equation for the drainage mass flow rate (Engineeringtoolbox, 2015).

Bernoulli's equation for vertical fluid flow:

$$P_1 + \frac{1}{2}\rho u_1^2 + \rho g h_1 = P_2 + \frac{1}{2}\rho u_2^2 + \rho g h_2 \quad \textbf{(4.2)}$$

Mass continuity equation:

$$\dot{m} = C_D \frac{\pi}{4} D_2^2 \rho \left[\frac{2(P_1 - P_2)}{\rho(1 - d^4)}\right]^{1/2}, \quad \textbf{(4.3)}$$

where $d = D_2/D_1$.

Volumetric discharge flow rate equation:

$$\dot{V} = C_D A \sqrt{2gh} \quad \textbf{(4.4)}$$

The schematic component diagram of the venturi nozzle and orifice inlets relative to positioning in the evaporator module and liquid column head obtained from the pyramid holding tank is depicted by Figure 4.2.

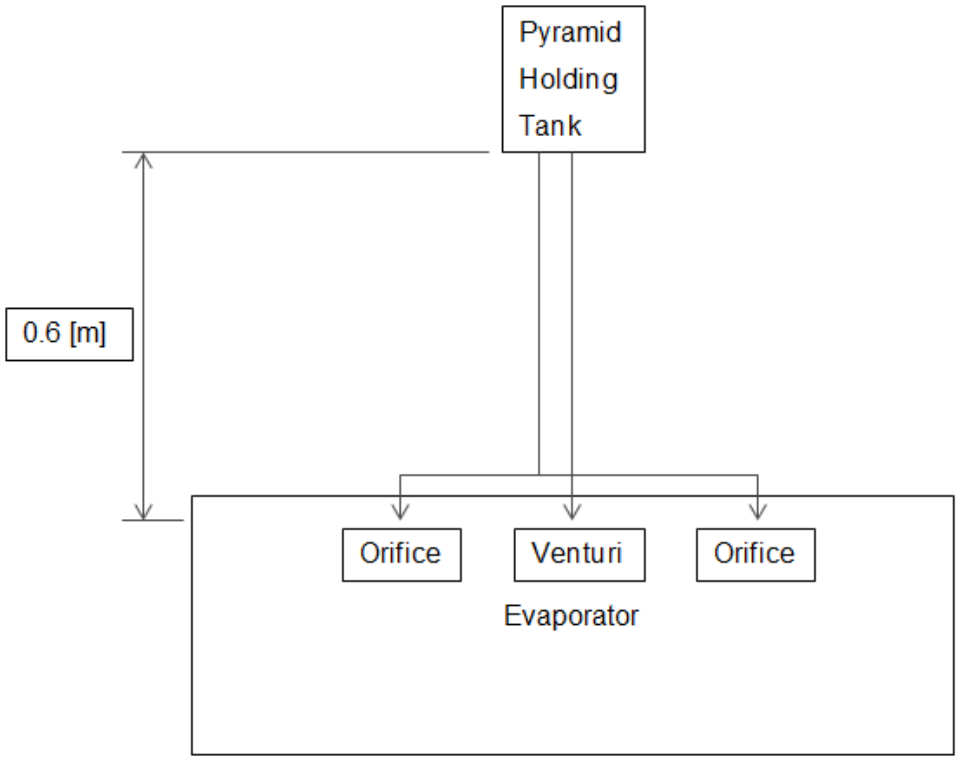

Figure 4.3: Evaporator Inlet Schematic Component Diagram

Full perusal of the venturi nozzle and orifice inlet's control volume diagram and venturi designs are available in Appendix D 6.1.

4.7.1 Venturi Nozzle – Thermodynamic Design

The venturi nozzle is to be designed for winter ambient conditions, as under these conditions the refrigerant mass flow rate is at its lowest, thus, ensuring the venturi will function for the remaining ambient design conditions. Table 4.15 shows the input parameters required to complete the thermodynamic design of the venturi nozzle.

Common practice for smooth nozzles and venturies are that a standardised C_D table found in Table D 6.2 can approximate the discharge coefficient. The discharge coefficient for this application is assumed to be slightly lower than convention, as the venturi's orifice is relatively small (selected as 2 [mm] after practical experimentation with different orifice diameters for the venturi to work effectively) due to the very low mass flow rate and a step-down manufacturing process instead of a smooth cross section reduction.

Table 4.15: Venturi nozzle design input parameters.

Thermodynamic Input Parameters	Value/Comment
Winter ambient conditions	P = 515.84 [kPa]
Thermophysical properties of state 6	Appendix B 6, Table B.6
Tube dimensions: d_o $d_i = D_1$	19.1 [mm] 15.9 [mm]
Orifice diameter: D_2	2 [mm]
Diameter ratio: d	0.125786 [-]
Refrigerant mass flow rate: $\dot{m}_6$	0.000539 [kg/s]
Discharge Coefficient: C_D	0.9 (Assumption)
Head height difference: h_1	0.6 [m]

The pressure drop at the venturi's orifice can be calculated by rearranging Eq. 4.3, as illustrated by the following:

$$\Delta P = \left(\frac{\dot{m}_6}{C_D \frac{\pi}{4} D_2^2 \rho_6}\right)^2 \left(\frac{\rho_6(1-d^4)}{2}\right)$$

$$\therefore \quad = \left(\frac{0.000539}{0.9\frac{\pi}{4}(0.002)^2(648.048)}\right)^2 \left(\frac{648.048(1-0.125786^4)}{2}\right)$$

$$\therefore \quad = 28.02877 \ [Pa]$$

$$\therefore P_2 = P_1 - \Delta P$$

$$\therefore \quad = (515.84 * 10^3) - 28.02877$$

$$\therefore \quad = 515.452 \ [kPa]$$

To calculate the outlet velocity of the venturi nozzle,

$$P_1 + \frac{1}{2}\rho u_1^2 + \rho g h_1 = P_2 + \frac{1}{2}\rho u_2^2 + \rho g h_2 \quad (Eq. 4.2)$$

$$\therefore \ 28.02877 + \frac{1}{2}(648.048)\left(\frac{0.000539}{648.048\frac{\pi}{4}(0.0159)^2}\right)^2 + 648.048(9.81)(0.6) = \frac{1}{2}(648.048)\bar{v}_2^2$$

$$\therefore \ u_2 = 3.44 \ [m/s]$$

To determine the discharge rate of the venturi nozzle,

$$\dot{V} = C_D A \sqrt{2gh} \quad (Eq. 4.4)$$

$$\therefore = 0.9\frac{\pi}{4}(0.002)^2\sqrt{2(9.81)(0.6)}$$

$$\therefore = 9.701 * 10^{-6} \ [m^3/s]$$

The volumetric discharge can be converted to a more desired mass flow rate as

$$\dot{m} = \dot{V}\rho$$
$$\therefore = 0.006287\ [kg/s]$$

The venturi nozzle design can be reviewed in Appendix D 6.1, with experimental setup and results in Appendix D 6.1 & 6.2 respectively.

4.7.2 Orifice – Thermodynamic Design Sizing

The orifice design-sizing uses the same equation set as the venturi nozzle, with the only variance being the orifice diameter (D_2 = 0.0005 m, which is the smallest drill bit that could be used for manufacturing of the orifice nozzle) and the discharge coefficient (C_D = 0.6). Therefore, the output parameters of the orifice design are illustrated by Table 4.16 as

Table 4.16: Orifice design output parameters.

Orifice Design	Output [Units]
Pressure drop: ΔP	4.03755 [kPa]
Velocity: u_2	4.92267 [m/s]
Volume flow rate: $\dot{V}$	4.0421 x 10^{-3} [m^3/s]
Mass flow rate: $\dot{m}$	0.00026195 [kg/s]

4.8 Evaporator (State 8 to 9)

The evaporator operates between the thermodynamic states 8 to 9 of Figure 3.1, which coincidentally means it represents the refrigeration side of the aqua-ammonia absorption-desorption cycle. Between states 8 and 9 the last mass concentration of water is removed from the aqua-ammonia mixture to from pure ammonia, which occurs at the exact moment of evaporation.

The venturi nozzle and orifice inlets are integral to the workings of the evaporator, as the evaporator incorporates a spray/splash evaporation method. To reiterate, the evaporator is filled with auxiliary gas (Helium), which generates a partial pressure that works in on the aqua-ammonia refrigerant. Thus, the refrigerant upon entering the evaporator would ‘flash’ to the thermodynamic state 8 and in theory vaporise upon impacting the coolant filled tube bundle. Figure D 1.5 in Appendix D 1.5 illustrates the fluid temperature variation in the evaporator. The refrigeration side of the aqua-ammonia H&R cycle is illustrated in Figure 4.4, where the required temperatures are shown at the respective components where heat removal is desired. The component diagram is a theoretical representation of a heat source that adds heat to the ethylene glycol water coolant to support boiling within the evaporator. The mean temperature difference of boiling shell and tube heat exchangers are typically calculated as the mean temperature of the secondary fluid minus the saturation temperature ($\Delta T_m = T_{wall} - T_{sat}$), which is also known as the excess temperature. The

mean temperature difference can also be approximated as an arithmetic mean temperature difference of $\Delta T_{am} = ½(\Delta T_1 + \Delta T_2)$, but would result in the same value of mean temperature difference.

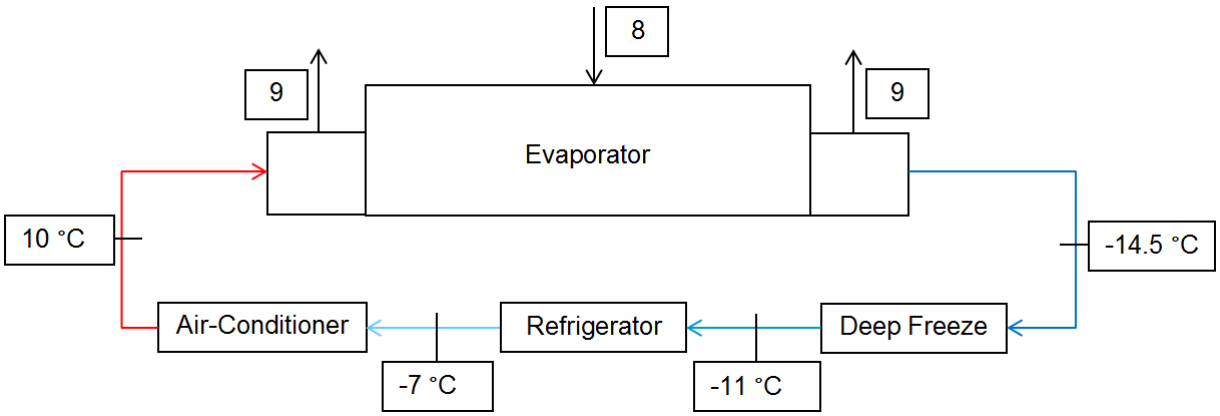

Figure 4.4: Schematic representation of the refrigeration side components.

4.8.1 Preliminary Thermodynamic Design

The input parameters for the preliminary thermodynamic calculations of the evaporator are depicted in Table 4.17. The evaporator's thermodynamic design is approximated as three heat exchanger models joined together, with a calculated length for the venturi inlet and two times the calculated length for the orifice inlets. As the approach for all three sections are identical with only variance illustrate the refrigerant inlet velocities (u_2), as a result, the thermodynamic design will only for the venturi nozzle inlet. Full review of remaining ambient conditions concerning the respective inlets is available in Appendix D 7.1.

Table 4.17: Evaporator – Thermodynamic design input parameters.

Thermodynamic Input Parameters	Value/Comment
Summer ambient conditions	
Thermophysical properties of state 8	Section 3.1.3
Thermophysical properties of state 9	Appendix B 1.3
Mean temperature difference: T_m	12.75 [°C]
Shell inner diameter: D_s	264.67 [mm]
Tube dimensions: d_o d_i	31.8 [mm] 28.6 [mm]
Number of tubes: N_t	32 (Calculated Eq. 2.46); 21 (SW est.)
Refrigerant mass flow rate: $\dot{m}_6$	0.0005986 [kg/s]
Coolant mass flow rate: $\dot{m}_{clnt}$	0.00981 [kg/s]
Inlet Quality: Q_{in} (State 8)	0.078538
Outlet quality: Q_{out} (State 9)	1.00

Table 4.18 Continued:

Fluid Flow Input Parameters	**Comment**
Fluid allocations:	Aqua-ammonia refrigerant – shell side Ethylene glycol water coolant – tube side
Fluid flow pattern	Cross-flow (Appendix C – Figure C.22)
Inlet conditions: 3 Inlets	Central venturi nozzle; 2 adjacent orifices
Coolant Thermophysical Properties	**Value [Units]**
x	35 wt% Ethylene glycol
$T_{clnt,in}$	10 [°C]
$T_{clnt,out}$	-14.5 [°C]
$T_{clnt,bulk}$ / T_{wall}	-2.25 [°C]
$C_{p,clnt,bulk}$	3.52646[kJ/kg.K]
$\rho_{clnt,bulk}$	1063.683 [kg/m^3]
$\mu_{clnt,bulk}$	0.0060436 [kg/m.s]
$k_{clnt,bulk}$	0.45463 [W/m.K]
$Pr_{clnt,bulk}$	46.678 [-]

Shell Side Heat Transfer Coefficient

The flow boiling heat transfer coefficient for tube bundle evaporators can be approached by utilising (Wolvering Tube Inc, 2014) proposed tube bundle boiling prediction method as stated by Eq. 2.31. The nucleate boiling heat transfer coefficient is predicted by using the (Cooper, 1984) correlation given by Eq. 2.32. The convective boiling heat transfer coefficient will thus be approximated by (Cornwell, 1989) correlation represented by Eq. 2.35 with the assumptions of:

- $u_L = 0.01(u_2)$
- $\delta = 0.05\ d_o$
- $C_{sf} = 0.013$ (Stainless Steel)

where u_L is the refrigerant velocity flowing over the tube bundle, δ is the liquid film thickness, and C_{sf} is the experimental constant that is dependent on surface-fluid combination. The refrigerant velocity flowing over the tube bundle is assumed to be 0.01 of the velocity from the venturi nozzle, due to the stream ejected by the venturi will first hit a flat distribution disc before splashing onto the tube bundle.

The nucleate boiling and peak heat flux values are calculated as

$$\dot{q}_{nucleate} = \mu_8 h_{fg} \left[\frac{g(\rho_8 - \rho_9)}{\sigma}\right]^{1/2} \left[\frac{C_{p,8}(T_{wall} - T_{sat})}{C_{sf} h_{fg} Pr_8^n}\right]^3 \quad (Eq.\ 2.33)$$

$$\therefore \quad = 0.00021497(1444 - 26.85032)(10^3)\left[\frac{9.81(611.8465 - 1.966)}{0.0264 + 0.000223(-15)}\right]^{1/2} \left[\frac{4.4323\left(-2.25 - (-15)\right)}{0.013(1444 - 26.8053)(1.7865)}\right]^3$$

$$\therefore \quad = 785569.58\left[\frac{W}{m^2}\right],$$

and

$\dot{q}_{max} = C_{cr}h_{fg}[\sigma g\rho_9^2(\rho_8 - \rho_9)]^{1/4}$ $(Eq.2.34)$, with C_{cr} = 0.12

$$\therefore \quad = 0.12(1444 - 26.85032)(10^3)[0.023055(9.81)(1.966^2)(611.846 - 1.966)]^{1/4}$$

$$\therefore \quad = 817162.53\left[\frac{W}{m^2}\right]$$

The value of peak heat flux for pure ammonia was obtained from EES' critical heat flux function as 822.635 [kW/m^2], which is in great proximity of the value obtained by Eq. 2.34 for aqua-ammonia to pure ammonia ebullition. Thus, validating the peak heat flux value and illustrating that the evaporator lies beneath the critical point in the nucleate boiling regime on the boiling curve, which ensures that 'burnout' doesn't occur.

To calculate the nucleate boiling heat transfer coefficient correlation of Cooper (1984),

$$h_{nb} = 55\left(P_r^{0.12-0.4343\ln(R_p)}\right)(-0.4343\ln(P_r))^{-0.55}M_{NH_3}^{-0.5}\dot{q}_{nucleate}^{0.67} \quad (Eq.2.32)$$

$$\therefore = 55\left(0.020841^{0.12-0.4343\ln(2)}\right)(-0.4343\ln(0.020841))^{-0.55}(17.031^{-0.5})(785569.58^{0.67})$$

$$\therefore = 179796.72\left[\frac{W}{m^2.K}\right]$$

To calculate the liquid film Reynolds number,

$$Re_\delta = \frac{4\rho_8 u_l \delta}{\mu_8} \quad (Eq.2.36)$$

$$\therefore \quad = \frac{4(611.8465)(0.01 * 3.4488)(1.05 * 0.0318)}{0.00021497}$$

$$\therefore \quad = 62.491\,[-]$$

To determine the convective boiling heat transfer coefficient,

$$h_{cb} = 4.032\left(Re_\delta^{0.236}\right)\left(Pr_l^{0.4}\right)\left(\frac{k_l}{\delta}\right) \quad (Eq.2.35)$$

$$\therefore = 4.032\,(62.4905^{0.236})(1.78654^{0.4})\left(\frac{0.53188}{1.05 * 0.0318}\right)$$

$$\therefore = 4512.887\left[\frac{W}{m^2.K}\right]$$

The bundle boiling heat transfer coefficient becomes,

$$h_{bundle} = \left(h_{nb}^2 + h_{cb}^2\right)^{1/2} \quad (Eq.\,2.31)$$
$$\therefore = (179796.72^2 + 4512.89^2)^{1/2}$$
$$\therefore = 179853.35 \left[\frac{W}{m^2.K}\right]$$

Tube Side Heat Transfer Coefficient

The tube side heat transfer coefficient utilises the (Hausen, 1959) Nusselt correlation given in Eq. 2.41, which is the same method used during the previous heat exchanger's thermodynamic design. Thus, the output values of the tube side are represented by Table 4.18 as

Table 4.18: Evaporator – Tube side heat transfer coefficient.

Design Parameters	Output [Units]	Correlation
Re_T	3.444 [-]	Eq. A.49
Nu_T	3.963 [-]	Eq. 2.41
Tube Side HTC: h_i	62.9892 [W/m^2.K]	Eq. 2.11

Now that the tube side heat transfer coefficient is known, it can be concluded that the lower heat transfer coefficient of the coolant will be open to manipulation. The coolant mass flow rate and inlet temperature can be altered when necessary, to keep the refrigeration cycle operating at optimum conditions. In other words, to ensure that the evaporation process takes place within the two-phase region with minimal over evaporation into the superheated region.

Overall Heat Transfer Coefficient and Heat Transfer Surface Area

The calculation of the overall heat transfer coefficient and the length of the tubes aren't concise and have been illustrated, thus the entire evaporator thermodynamic design output results are summarised by Table 4.19. The tube side heat transfer coefficient is considerably lower than its shell side opposite, thus suggesting that the coolant controls the outcome of U_c values.

Table 4.19: Evaporator – Thermodynamic design output parameters.

Design Parameters	Output [Units]
Shell side heat transfer coefficient: h_o	179.853 [kW/m^2.K]
Tube side heat transfer coefficient: h_i	62.9892 [W/m^2.K]
Overall heat transfer coefficient: U_c	56.2769 [W/m^2.K]
Tube length: $L_{Venturi}$	0.5635 [m]
Tube length: $L_{Orifice}$	0.5635 [m]
Tube length: L_{Evap}	1.6905 [m]

4.8.2 Performance Rating of the Thermodynamic Design

Table 4.20, with the NTU, effectiveness, capacity ratio, records the performance rating of the evaporator as:

Table 4.20: Evaporator – Performance rating.

Performance Rating	Output [Units]	Correlation
NTU	32.155 [-]	Eq. 2.8
Capacity Ratio: c	0.05976 [-]	Eq. 2.9
Effectiveness: ε	1.00 or 100 [%]	Table 2.1; Eq. 4

The effectiveness vs. NTU curve of the evaporator's design performance is available in Appendix D 9.5 for all ambient conditions. The effectiveness vs. NTU curve of Figure D 9.5 illustrates that the evaporator has a 100% effectiveness, which is common for boiling heat exchangers. The pressure drops within the shell and tube sides are too small to have any significant effect on the design-sizing and have been excluded from the thermodynamic design calculations of the evaporator module.

4.8.3 Thermodynamic Design Verification

Perusal of EES coding for the evaporator's thermodynamic design verification is available in Appendix D 7.2, with Table 4.21 depicting the critical output parameters thereof. The conclusion that can be drawn from the comparison is that there are no mathematical errors in the determination of the evaporator's thermodynamic design, as the heat transfer rate comparison is within 0.2%. Therefore, the calculation of the thermodynamic design for the evaporator can be considered as acceptable.

Table 4.21: Evaporator – EES verification output parameters.

Design Parameters	Output [Units]
ΔT_m	12.75 [°C]
Shell side heat transfer coefficient: h_o	179.799 [kW/m^2.K]
Tube side heat transfer coefficient: h_i	63.1166 [W/m^2.K]
Overall heat transfer coefficient: U_c	56.385 [W/m^2.K]
Heat transfer rate: $\dot{Q}_{EES}$	849.95 [W]
Heat transfer rate: $\dot{Q}_{EVAP}$	848.31 [W]
Comparison percentage	0.1939 [%]

4.8.4 Design Sizing Selection

The 264.67 [mm] shell diameter was selected for the evaporator as it has a length to diameter ratio that falls within the specified range of 2 to 7. The 31.8 [mm] tubing was selected as it uses approximately 50 less tubes than what the 19.1 [mm] tubing would've used. Although, the larger tube has a slightly lower tube side Reynolds number the manufacturing costs are cut on the assembling and welding times. A fouling factor over design percentage of 13.57% is added to the tube length, thus, resulting in a heat transfer tube length of 1.920 [m].

4.9 Auxiliary-Regenerative Heat Exchanger (Weak and Strong Aqua-Ammonia Solutions)

The auxiliary and regenerative heat exchangers operate between the absorber (absorption) and bubble pump (desorption) components as illustrated in Figure 3.3. The regenerative heat exchanger plays an important role in support of the bubble pump module and the auxiliary heat exchanger increases the absorbability of weak solution aqua-ammonia in the absorber module. The temperature changes versus unit surface area of the regenerative and auxiliary heat exchangers are represented in Figures D 1.6 & 1.7 of Appendix D, respectively.

The thermodynamic design of both the auxiliary and regenerative heat exchangers use the (Zukauskas, 1987) shell side heat transfer coefficient correlation and (Hausen, 1959) tube side heat transfer coefficient correlation. Which are the same correlations used for the stage 2 condenser, de-superheating condenser, and pre-cool heat exchanger.

4.9.1 Regenerative Heat Exchanger – Preliminary Thermodynamic Design

Represented by Table 4.22 are the input parameters required for 'worst case' preliminary design-sizing calculations of the regenerative heat exchanger, with the full review of the remaining ambient condition's preliminary thermodynamic design available in Appendix D 8.1.

Table 4.22: Regenerative heat exchanger – Thermodynamic design input parameters.

Thermodynamic Input Parameters	Value/Comment
Winter ambient conditions	
Thermophysical properties of state (ws: 1 & 2)	Section 3.1.4
Thermophysical properties of state (ss: 1 & 2)	Section 3.1.4
Correction factor: F	0.89 (Figure A.3(b))
Log mean temperature difference: ΔT_{LMTD}	10.6284 [°C]
Shell inner diameter: D_s	0.34768 [mm]
Tube dimensions: d_o d_i	31.8 [mm] 28.6 [mm]
Number of tubes: N_t	49 (Calculated Eq. 2.46); 44 (SW est.)

Table 4.22 continued:

Number of tube rows: Nrows	7 (SW est.)
Tube bundle correction factor: C_n	0.96 (Table 2.3)
Equivalent diameter: D_e	31.464 [mm] (Eq. A.42)
Clearance: C	7.95 [mm] (Eq. A.45)
Bundle cross-flow area: A_{cs}	0.069536 [m^2] (Eq. A.46)
Mass velocity: G_s	0.064677 [m^2/s]
Heat transfer rate: $\dot{Q}_{ss}$	293.2575 [W] (Eq. 2.1)
Refrigerant mass flow rate: $\dot{m}_{ws}$	0.003971 [kg/s]
Secondary refrigerant mass flow rate: $\dot{m}_{ss}$	0.004497 [kg/s]
Inlet Quality: $Q_{ss,1}$	-0.001
Outlet quality: $Q_{ss,2}$	0.0084
Fluid Flow Input Parameters	**Comment**
Fluid allocations:	Strong solution aqua-ammonia – shell side Weak solution aqua-ammonia – tube side
Fluid flow pattern	Cross-flow (Appendix C – Figure C.26)

The preliminary thermodynamic design output values are tabulated in Table 4.23, with the corresponding correlations used for each parameter. In comparison, the shell side heat transfer coefficient is the lower value of the two sided of heat transfer coefficient, which indicates to the shell side heat transfer coefficient being the impeding factor on the outcome of overall heat transfer coefficient. The short tube length is due to a low heat capacity requirement and large shell diameter.

Table 4.23: Regenerative heat exchanger – Preliminary design output parameters.

Design Parameters	Output [Units]	Correlation
$\Delta T_{LMTD,XF}$	10.63 [°C]	Eq. 2.4
Re_s	2.937 [-]	Eq. A.47
Shell Side HTC: h_o	45.4930 [W/m^2.K]	Eq. 2.18 & Table 2.2
Re_T	7.570 [-]	Eq. A.49
Nu_T	4.18143 [-]	Eq. 2.41
Tube Side HTC: h_i	69.4907 [W/m^2.K]	Eq. 2.11
Overall HTC: U_c	26.1364 [W/m^2.K]	Eq. 2.10
Tube length: L	0.2402 [m]	Eq. 2.45

4.9.2 Regenerative Heat Exchanger – Performance Rating of the Thermodynamic Design

The number of transfer units and the effectiveness of the regenerative heat exchanger are demonstrated by Table 4.24 as:

Table 4.24: Regenerative heat exchanger – Performance rating.

Performance Rating	Output [Units]	Correlation
NTU	1.61730 [-]	Eq. 2.8
Capacity Ratio: c	0.88102 [-]	Eq. 2.9
Effectiveness: ε	0.5981 or 59.81%	Table 2.1; Eq. 3

The effectiveness, NTU, and capacity ratio values above are plotted to the standard effectiveness vs. NTU curve in Appendix D 9.6 for all ambient conditions, which can be used to verify the feasibility and temperature boundary conditions of the regenerative heat exchanger. As illustrated by Figure D 9.6, the intersection of the effectiveness and NTU output values fall just beneath the capacity ratio curve, which indicates that the regenerative heat exchanger's in- and outlet temperatures are satisfactory. The effectiveness vs. NTU output parameters strongly advise that the regenerative heat exchanger is feasible and transfers heat to the strong solution with a thermal efficiency of 59.81%.

4.9.3 Regenerative Heat Exchanger – Thermodynamic Design Verification

The EES coding for the regenerative heat exchanger is available in Appendix D 8.2. The critical output parameters of the EES verification code are recorded in Table 4.25.

Table 4.25: Regenerative heat exchanger – EES verification output parameters.

Design Parameters	Output [Units]
$\Delta T_{LMTD,XF}$	10.63 [°C]
Shell side heat transfer coefficient: h_o	45.221 [W/m^2.K]
Tube side heat transfer coefficient: h_i	68.166 [W/m^2.K]
Overall heat transfer coefficient: U_c	25.948 [W/m^2.K]
Heat transfer rate: $\dot{Q}_{EES}$	291.18 [W]
Heat transfer rate: $\dot{Q}_{REGEN}$	293.26 [W]
Comparison percentage	-0.7074 [%]

The comparison of the heat transfer rate obtained from EES' heat exchanger model and the heat transfer rate of Eq. 2.1 vary by less than 0.71%, which would indicate to minute differences in the output values used to obtain the heat transfer rate of the EES heat exchanger model. Input parameters such as d_{inner}/L play a miniscule role in the outcome of the heat transfer rate, but it

might be the reason for the slight difference in the comparison percentage. Therefore, it is concluded that the EES verification model is within acceptable range to the preliminary thermodynamic design model and a secondary thermodynamic design iteration isn't required.

4.9.4 Regenerative Heat Exchanger – Design Selection

The preliminary thermodynamic design was completed for the 'worst case' scenario of winter ambient conditions, but the regenerative heat exchanger has great influence on the functionality of the aqua-ammonia H&R cycle. The remaining ambient conditions require a smaller heat transfer surface area and with the modelled heat exchanger the heat transfer rate can't be manipulated as the previously mentioned heat exchangers would've been. This is due to the working fluids of the regenerative heat exchanger being fixed by the bubble pump generator. Therefore, the regenerative heat exchanger is classified into three heat exchangers that cater for the three ambient conditions. The heat transfer tube lengths with factored over design percentages are recorded in Table 4.26 as:

Table 4.26: Regenerative heat exchanger – Tube lengths.

Ambient Design Condition	Length [m]	Over Design [%]
Summer	0.055	19.794 (19.537% Foul)
Average	0.160	18.624 (16.62% Foul)
Winter	0.280	16.588 (13.696% Foul)

The shell diameter selection will be clarified during the design-sizing selection of the auxiliary heat exchanger as the two heat exchanger entities will be merged to form one heat exchanger module.

4.9.5 Auxiliary Heat Exchanger – Preliminary Thermodynamic Design

The final heat exchanger has its input parameters shown in Table 4.27, which are required to complete the preliminary design calculations of the auxiliary heat exchanger.

Table 4.27: Auxiliary heat exchanger – Thermodynamic design input parameters.

Thermodynamic Input Parameters	Value/Comment
Winter ambient conditions	
Thermophysical properties of state (ws: 2 & 3)	Section 3.1.4
Shell inner diameter: D_s	0.34768 [mm]
Tube dimensions: d_o d_i	31.8 [mm] 28.6 [mm]
Number of tubes: N_t	49 (Calculated Eq. 2.46); 44 (SW est.)
Heat transfer rate: $\dot{Q}_{ss}$	608.834 [W] (Eq. 2.1)

Table 4.27 continued:

Refrigerant mass flow rate: $\dot{m}_{ws}$	0.003971 [kg/s]
Secondary refrigerant mass flow rate: $\dot{m}_{clnt}$	0.003803 [kg/s]
Equivalent diameter: D_e	31.464 [mm] (Eq. A.42)
Clearance: C	7.95 [mm] (Eq. A.45)
Bundle cross-flow area: A_{cs}	0.017384 [m^2] (Eq. A.46)
Mass velocity: G_s	0.21877 [m^2/s]
Baffle spacing: B	0.25 [m]
Number of tube rows: N_{rows}	7
Tube bundle correction factor: C_n	0.96 (Table 2.3)
Fluid Flow Input Parameters	**Comment**
Fluid allocations:	Ethylene glycol water coolant – shell side Weak solution aqua-ammonia – tube side
Fluid flow pattern	Counter-flow (Appendix C – Figure C.28)

The thermodynamic design of the auxiliary heat exchanger resulted in the output values tabulated in Table 4.28 along with the corresponding correlations used for each parameter. The preliminary thermodynamic design of summer ambient condition is considerably less than the winter ambient design, as illustrated by the MS Excel design model in Appendix D 8.1.

Table 4.28: Auxiliary heat exchanger – Preliminary thermodynamic design output parameters.

Design Parameters	Output [Units]	Correlation
$\Delta T_{LMTD,CF}$	3.06 [°C]	Eq. 2.4
Re_s	3.57039 [-]	Eq. A.47
Shell Side HTC: h_o	70.0399 [W/m^2.K]	Eq. 2.18 & Table 2.2
Re_T	3.54601 [-]	Eq. A.49
Nu_T	3.79207 [-]	Eq. 2.41
Tube Side HTC: h_i	61.6875 [W/m^2.K]	Eq. 2.11
Overall HTC: U_c	30.8511 [W/m^2.K]	Eq. 2.10
Tube length: L	1.4672 [m]	Eq. 2.45

The shell and tube side heat transfer coefficients are fairly close to one another, with the tube side heat transfer coefficient being slightly lower than shell side. Thus, the weak aqua-ammonia solution is forming the ‘bottleneck’ on the path of heat transfer.

4.9.6 Auxiliary Heat Exchanger – Performance Rating of the Thermodynamic Design

The number of transfer units and the effectiveness of the auxiliary heat exchanger are demonstrated by Table 4.29, with the resulting output parameters plotted to the standard effectiveness vs. NTU curve in Appendix D 9.7 to verify the practical feasibility of coolant outlet temperature for the auxiliary heat exchanger.

Table 4.29: Auxiliary heat exchanger – Performance rating.

Performance Rating	Output [Units]	Correlation
NTU	11.8119 [-]	Eq. 2.8
Capacity Ratio: c	0.84953 [-]	Eq. 2.9
Effectiveness: ε	0.86717 or 86.717%	Table 2.1; Eq. 1

Fig. D 9.7 demonstrated that the intersection of the effectiveness and NTU values on the standard counter-flow curve is slightly below the expected efficiency of a typical counter-flow heat exchanger. This indicates that the outlet temperature of the coolant could be increased, but would mean an increase in the heat transfer surface area and in the cost of the auxiliary heat exchanger. If the coolant outlet temperature is to be raised by 1 [°C] the length required of a single tube would increase by 473.38 [mm] for 44 tubes, which accumulate to an extra 20.830 [m] of tubing. Thus, the auxiliary heat exchanger's thermodynamic design will remain as calculated.

4.9.7 Auxiliary Heat Exchanger – Thermodynamic Design Verification

The verification design-sizing coding, with formatted equations and solutions for the auxiliary heat exchanger is available in Appendix D 8.3, however the critical output parameters of the EES verification code are shown in Table 4.30.

Table 4.30: Regenerative heat exchanger – EES verification output parameters.

Design Parameters	Output [Units]
$\Delta T_{LMTD,CF}$	3.06 [°C]
Shell side heat transfer coefficient: h_o	70.172 [W/m^2.K]
Tube side heat transfer coefficient: h_i	61.966 [W/m^2.K]
Overall heat transfer coefficient: U_c	30.953 [W/m^2.K]
Heat transfer rate: $\dot{Q}_{EES}$	610.84 [W]
Heat transfer rate: $\dot{Q}_{REGEN}$	608.83 [W]
Comparison percentage	0.3299 [%]

4.9.8 Auxiliary heat exchanger – Design Sizing Selection

The shell diameter selected for the auxiliary and regenerative heat exchanger is larger than the shell diameters proposed for the stage 1 and 2 condensers, and the evaporator module. The reason for the larger shell selection is the L/D_s ratio, which is approximated at 4.22 [-] instead of 8.094 [-] for the 264.67 [mm] shell. The heat transfer tube length of the auxiliary heat exchanger can now be determined as L = 1.7 [m], which falls within the design selection parameter. The auxiliary heat exchanger has a 15.865% over design that exceed the 15.731% required by fouling.

4.10 Conclusion

To conclude the thermodynamic design and rating, a summative sizing and rating table is compiled for the seven heat exchangers for an aqua-ammonia heating and refrigeration package unit in Table 4.31. The thermodynamic design of each heat exchanger resulted in satisfying the design selection requirements for heat transfer tube length, number of tubes, and length over shell diameter for pressurised vessels. The performance rating of the heat exchangers revealed that each heat exchangers were within the expected efficiencies of standard counter/cross-flow heat exchangers, which pointing towards the conclusion that the inlet and outlet temperature conditions of the heat exchangers are satisfactory. Therefore, the heating side heat exchangers will approximately produce a heating capacity of 1.62 [kW] for summer ambient conditions and 1.37 [kW] for winter ambient conditions. The heating side heat exchangers will hence produce a heating capacity COP of 1.5 and 1.4, respectively, and consequently satisfy the requirement for a heating capacity COP > 1.3. The evaporator or cooling side heat exchanger will approximately produce a cooling capacity of 0.85 [kW] for summer ambient conditions and 0.77 [kW] for winter ambient conditions, with cooling capacity COP of 0.76 and 0.77, respectively. Hence, the requirement of the cooling capacity COP is also satisfied.

Table 4.31: Summative thermodynamic design table of the heat exchangers for an aqua-ammonia absorption-desorption heating and refrigeration cycle.

HTEX	Flow Pattern	D_s [mm]	d_o/d_i [mm]	N_t	L [m]	ε [%]	Capacity [W]
S1C	Cross-flow	264.67	31.8 / 28.6	24	0.800	100	726.5
S2C	Cross-flow	264.67	19.1 / 15.9	68	1.200	90.497	72.9
DHC	Counter-flow	134.5	19.1 / 15.9	15	0.800	90.091	57.4
PC	Counter-flow	134.5	19.1 / 15.9	15	0.400	57.75	42.7
EVAP	Cross-flow	264.67	31.8 / 28.6	21	1.920	100	848.3
REGEN	Cross-flow	347.68	31.8 / 28.6	44	0.280	59.81	293.3
AUX	Counter-flow	347.68	31.8 / 28.6	44	1.700	86.741	608.8

Each of the abovementioned heat exchangers were verified to be within good accordance of the heat transfer rate obtained by Eq. 2.1 and the EES heat exchanger model with Eq. 2.6, but further validation is required to prove that accurate correlation selection was utilised in the calculation of each heat exchanger's thermodynamic design model. The following chapter will focus on the validation of the thermodynamic design process, as the sized heat exchanger models will be utilised during the mechanical design of Appendix E. Validation is essential for any design process as it ensures the correct methods were utilised during the design calculation stages.

Chapter 5

5 THERMODYNAMIC DESIGN VALIDATION

Introduction

Chapter 5 of the oeuvre focuses on the validation of the previously sized heat exchangers of Chapter 4. Typical engineering convention dictates that the thermodynamic design of heat exchangers are validated experimentally or by comparing the calculated design models to previously published design models. However, heat exchangers with aqua-ammonia as its refrigerant don't have an undisputed design model to which this study could compare its results. Due to project limitation stressed in Chapter 1, the validation of the thermodynamic design process will be completed mathematically and by utilising standard heat exchanger references. The validation process will see the predicted overall heat transfer coefficient compared to typically expected overall heat transfer coefficient ranges of heat exchangers with similar fluid configurations.

5.1 Thermodynamic Design Validation Process

The correlations used to determine the surface area A_s and the mean temperature difference (ΔT_m or ΔT_{LMTD}) are considered to be truthful, as these correlations are universally applied with their respective governing parameters. The calculated overall heat transfer coefficient U_c of Eq. 2.6 requires a degree of validation to prove that accurate correlations were utilised in determining the shell and tube side heat transfer coefficients. Ideally, the overall heat transfer coefficient is validated by comparing the predicted U_c values to the experimentally obtained values of U_c.

Although, it's possible to validate the predicted overall heat transfer coefficient values by comparing the designed heat exchangers U_c with typically expected ranges of overall heat transfer coefficients. Table 5.1 illustrates the typically expected U_c values of different heat exchanger configurations that are applicable to the heat exchangers of this oeuvre. The overall heat transfer coefficients of condensers and evaporators are commonly 'controlled' or 'bottle necked' by the secondary refrigerant, thus emphasizing the fundamental role that the coolant has to contribute to the U_c value.

Table 5.1: Typical ranges of overall heat transfer coefficients for shell and tube heat exchangers.

Typical Shell and Tube Heat Exchanger Overall Heat Transfer Coefficients					
Application	Working Fluid Allocation		Typical OHTC [W/m^2.K]		Source(s)
	Tube Side	Shell Side	Minimum	Maximum	
	Water	Ammonia	300	1200	[2]
S1C	Water	Aqueous Vapour	1000	1500	[1], [4], [5]
	Water	Gases	20	300	[4]
	Water	Gases	17	280	[2], [3], [5]
	Brine	Gases	15	250	[4]
S2C & DHC	Brine	Gases	17	280	[2], [3], [5]
	Steam	Pool: Aqueous Solution	500	1000	[1]
EVAP	Water	Refrigerant	425	850	[2], [3]
	Water	Water	800	1500	[1], [2], [3], [4], [5]
	Water	Brine	600	1200	[1], [2], [3], [4]
AUX	Liquid	Liquid	150	1200	[2]
	Water	Water	800	1500	[1], [2], [3], [4], [5]
	Aqueous Solution	Aqueous Solution	1400	2800	[5]
REGEN	Liquid	Liquid	150	1200	[2]

The sources of Tables 5.1 & 5.2 are numbered as follows:

1. (Blackmonk Engineering, 2009)
2. (Engineers Edge, 2016)
3. (H&C Heat Transfer Solutions, 2014)
4. (Engineering Page, 2016)
5. (Edwards, 2008)

It is very important to note that these overall heat transfer coefficient ranges are estimated for heat exchangers with higher heat capacities and mass flow rates than that of the heat exchangers of Chapter 4. These ranges are commonly used as indicators to the order of magnitude of U_c values, whereby actual calculation of the overall heat transfer coefficient might result in values lower or higher than the listed values.

In some instances, further validation is possible by comparing the calculated heat transfer coefficients with the typical heat transfer coefficients of Table 5.2. These ranges are guidelines for both the shell and tube side heat transfer coefficients.

Table 5.2: Typical ranges of heat transfer coefficients for shell and tube heat exchangers.

Typical Film Heat Transfer Coefficients				
Application	**Working Fluid**	**Typical HTC [W/m^2.K]**		**Source(s)**
		Minimum	**Maximum**	
S1C	Condensing Ammonia	2840	5680	[2], [3]
S2C & DHC	Gases	15	250	[2], [3]
PC	Gases	15	250	[2], [3]
EVAP	Evaporating Ammonia	1135	2270	[2], [3]
AUX	Water	1700	11350	[2], [3]
REGEN	Water	1700	11350	[2], [3]

5.2 Stage 1 Condenser

The overall heat transfer coefficient of the sized stage 1 condenser model of Chapter 4.3.1 is clearly below the typically expected overall heat transfer coefficient ranges for ammonia outside – water inside of Table 5.1. It was previously concluded in Chapter 4.3.1 that the overall heat transfer coefficient of the stage 1 condenser is haltered by the tube side heat transfer coefficient. The tube side heat transfer coefficient halters the U_c value with its laminar flow regime and low Reynolds number, which is attributed to the low coolant mass flow rates.

Validation of the overall heat transfer coefficient can be achieved by isolating the U_c term of Eq. 2.31, with the assumption that all thermophysical properties and ΔT_{LMTD} remains constant. The

U_c can be increased by increasing the tube side Reynolds number to the governing correlation limitation. Thus, the following can be concluded of the stage 1 condenser's energy balance:

$$\dot{Q}_{S1C} = \dot{m}_5(\alpha_{TP} - \alpha_5) = \dot{m}_{clnt} C_{p,clnt}\left(T_{clnt,out} - T_{clnt,in}\right) = U_c A_s \Delta T_{LMTD.CF}$$

By increasing the mass flow rate of the coolant, it mathematically increases the heat transfer rate, the mass flow rate of the aqueous ammonia refrigerant, and the overall heat transfer coefficient. The surface area (A_s) could either increase or decrease, which would depend on the degree that the heat transfer rate and overall heat transfer coefficient increases. However, the surface area is assumed unimportant for the validation process. To truthfully prove that satisfactory correlations were utilised for the determination of the overall heat transfer coefficient, the mass flow rates of the working fluids can't be increased to the point where it exceeds the shell or tube side heat transfer coefficient correlation limits.

Note: The correlation limitations are mostly the same for all the subsequent heat exchangers, for instance all 7 of the modelled heat exchangers used the (Hausen, 1959) Nusselt correlation for laminar flow through ducts. Therefore, the sample calculation of the tube side heat transfer coefficient correlation limitation is only illustrated once under the stage 1 condenser and tabulated in the subsequent heat exchanger sections. However, the shell side heat transfer coefficient correlation limitations differ between the 7 heat exchangers, where the stage 1 condenser uses the (Kern, 1958) tube bundle laminar film condensation Nusselt correlation, the evaporator uses (Wolverine Tube Inc, 2014) tube bundle boiling heat transfer coefficient, and the remaining heat exchangers uses the (Zukauskas, 1987) Nusselt correlation for tube bundles. Thus, the shell side heat transfer coefficient correlation limitations for Zukauskas will only be illustrated once under the stage 2 condenser's thermodynamic design validation.

5.2.1 Tube Side Heat Transfer Coefficient Correlation Limitations

The tube side heat transfer coefficient correlation of Eq. 2.41 is governed by the range parameter of ($0.1 < Gz < 10^4$), which is entirely based on the assumption that laminar flow is maintained at high Reynolds numbers. The Graetz number is dependent on the heat exchangers tube length, where any increase in heat exchanger tube length would merely keep the Graetz number within range. In some carefully controlled experiments, laminar flow was maintained at Reynolds numbers as high as 100 000 [-] (Cengel & Ghajar, 2011). In the practical application of heat exchangers the flow regime will most probably not remain strictly laminar after Re_t = 2300 [-]. Therefore, it is assumed that the only governing parameter for Hausen's proposed laminar tube side heat transfer coefficient will be Re_t < 2300 [-]. The assumption is based on the applied Reynolds number range for the next applicable Nusselt correlation proposed by (Gnielinski, 1976)

for transitional flow through a circular duct. Thus, the maximum coolant mass flow rate is calculated by re-arranging Eq. A.49 as:

$$\dot{m}_{clnt,max} = \frac{Re_t\, N_t\, \pi\, d_i\, \mu_B}{4}$$

$$\therefore \quad = \frac{2300(24\pi)(0.0286)(0.001997653)}{4}$$

$$\therefore \quad = 2.47694 \left[\frac{kg}{s}\right]$$

5.2.2 Shell Side Heat Transfer Coefficient Correlation Limitations

The tube bundle laminar film condensation heat transfer coefficient output value isn't directly influenced by the increase in refrigerant mass flow rate. However, if the mass flow rate were to be increased to the point where the vapour velocity is larger than 10 [m/s], then vapour shear will occur and demand a definite correlation change from the tube bundle laminar film condensation heat transfer coefficient in Eq. 2.27 proposed by Kern (1958) to the Butterworth (1977) inundation and vapour shear heat transfer coefficient of Eq. 2.28. The vapour velocity is determined at the minimum flow area between the tubes and can be approximated as 5 times the mean inlet velocity. Therefore, by determining the inlet cross-sectional area and factoring it into a simple conservation of mass equation with the mean vapour velocity limit of 2 [m/s], it would result in a maximum inlet mass flow rate of:

$$\dot{m}_{5,max} = \rho_{TP} A_{inlet} u_m$$

$$\therefore \quad = (8.57479)\left(\frac{\pi}{4}(0.0318)^2 + (0.5\ x\ 0.0318)\right)(2)$$

$$\therefore \quad = 0.286295 \left[\frac{kg}{s}\right]$$

5.2.3 Overall Heat Transfer Coefficient Validation Results

The progression of the overall heat transfer coefficient values versus steady incremental increases in tube side Reynolds numbers are plotted and illustrated in Figure 5.1. The tube side Reynolds number is chosen as it represents the controlling factor on U_c value increases. The tube side Reynolds numbers are increased from 40 to 2300 in increments of 0.01 [kg/s], where the initial mass flow rate starts at 0.04 [kg/s] and ends at the maximum of 2.47694 [kg/s]. As illustrated by the legend at the bottom of Figure 5.1, the purple curve with circle symbols represent the U_c values of aqua-ammonia to ethylene glycol water heat transfer. The light blue curve with square symbols represents the overall heat transfer coefficient values of aqua-ammonia to water heat transfer, and the dark blue curve represent ammonia to water heat transfer.

The working fluids of the stage 1 condenser are replaced with pure ammonia and water to better represent U_c values that compare with the typical overall heat transfer coefficient ranges of Table 5.1. The substituted aqua-ammonia with pure ammonia is of comparable thermophysical properties in terms of pressure (939.54 kPa) and saturation temperature (23 °C). Ethylene glycol water is replaced with water of equivalent thermophysical properties in relation to the bulk fluid temperature. The bulk fluid temperature of water is determined with the original heat transfer rate of the stage 1 condenser and an estimated specific heat capacity.

Points 1 and 3 mark the initial and limit of aqua-ammonia to ethylene glycol water's overall heat transfer coefficient values. Points 2 and 4 represent the initial and limit values of both the aqua-ammonia-to-water and ammonia-to-water overall heat transfer coefficients. The two curves are identical in shape as they lie on top of each other. This would suggest that the overall heat transfer coefficient does not differentiate between pure ammonia and 99 wt% aqua-ammonia, as water has control over the outcome of the U_c simulation.

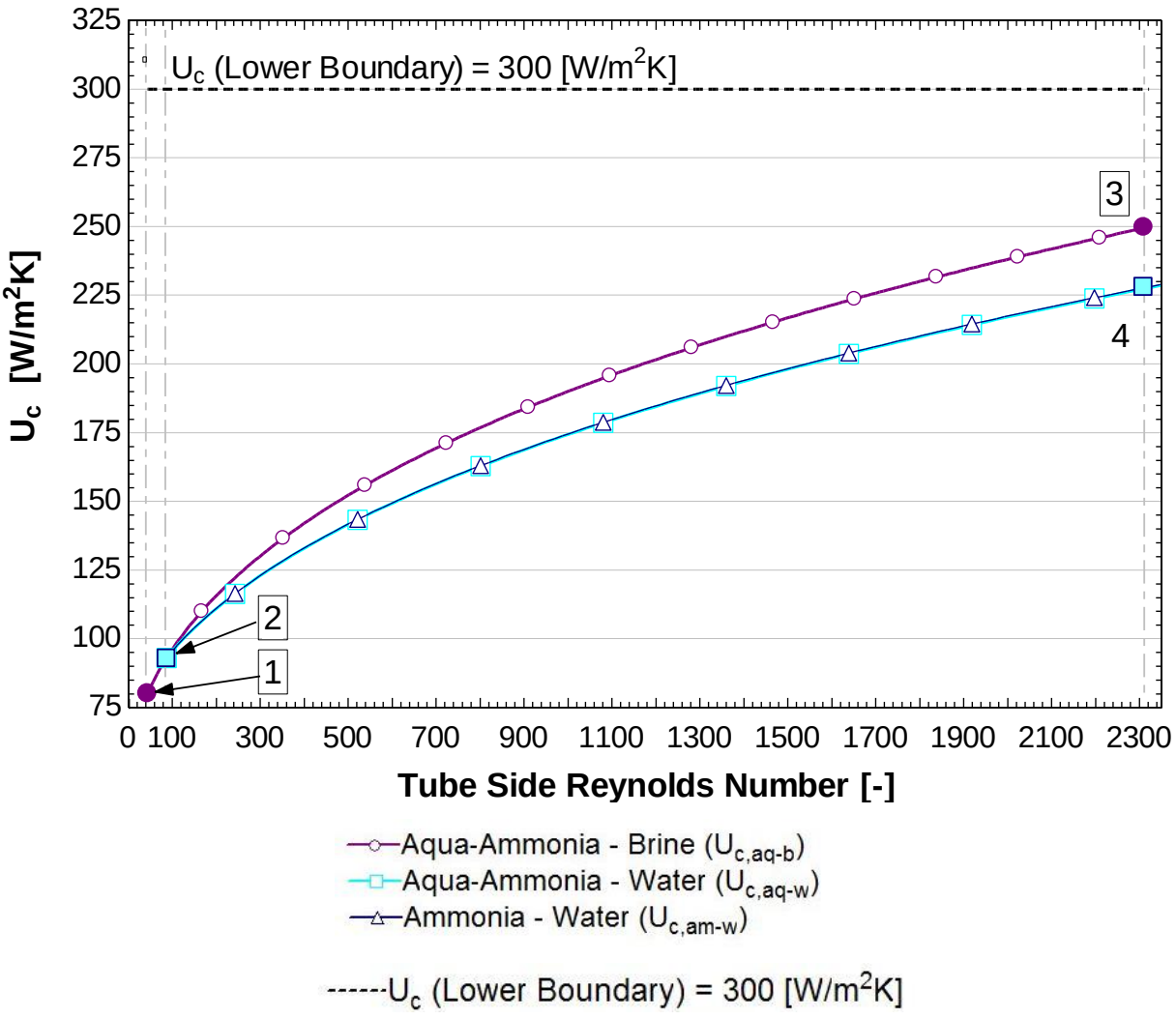

Figure 5.1: Stage 1 Condenser - Overall heat transfer coefficient vs. tube side Reynolds number simulation model output plot.

The results of the U_c simulation curves are illustrated in Tables 5.3 and 5.4, where Table 5.3 represents the initial conditions of the stage 1 condenser and Table 5.4 shows the limiting boundary conditions. The initial input parameters of the aqua-ammonia-to-water and ammonia-to-water condenser simulations are calculated at the original heat transfer rate of the stage 1 condenser, as calculated in Chapter 3.1.2. The limiting boundary condition occurs where the shell or tube side heat transfer coefficients meet their respective correlation limits.

The results of Table 5.3, supports the claim that the overall heat transfer coefficient does not discriminate between the 99 wt% aqua-ammonia and 100% pure ammonia to water heat transfer. This is evident with the 0.2% difference in initial U_c values.

Table 5.3: Stage 1 condenser - The initial boundary conditions for 3 permutations of working fluids.

Initial boundary conditions:	Aq - B	Aq - W	Am - W
Coolant mass flow rate: $\dot{m}_{clnt}$	0.046569 [kg/s]	0.041871 [kg/s]	0.041871 [kg/s]
Tube side: Re_t	43.24 [-]	77.78 [-]	77.78 [-]
Tube side HTC: h_i	91.17 [W/m^2.K]	103.91 [W/m^2.K]	103.91 [W/m^2.K]
Refrigerant mass flow rate: $\dot{m}_5$	0.0006153 [kg/s]	0.0006153 [kg/s]	0.0006185 [kg/s]
Shell side HTC: h_o	6694.43 [W/m^2.K]	6694.43 [W/m^2.K]	8156.89 [W/m^2.K]
Heat transfer rate: $\dot{Q}_{S1C}$	726.503 [W]	726.503 [W]	726.552 [W]
Overall heat transfer coefficient: U_c	80.27 [W/m^2.K]	91.214 [W/m^2.K]	91.438 [W/m^2.K]

Further investigation was conducted with lower mass concentrations of ammonia in water mixtures, of which the results are shown in Table 5.5.

It's evident from Table 5.4 that at higher Reynolds numbers the ethylene glycol water mixture creates a higher U_c value than the equivalent water coolant fluid. The Reynolds numbers of both ethylene glycol water and water are at 2300 [-], but their respective Prandtl numbers differ considerably with water having a much lower Prandtl number. This is the main contributing factor that ethylene glycol water has a higher heat transfer coefficient.

The three working fluid permutations of U_c are lower than the typically expected overall heat transfer coefficient for condensing ammonia-to-water. This can be attributed to the tube side heat transfer coefficient reaching its correlation limit Re_t = 2300 [-], before the shell side could reach its mass flow rate and mean vapour velocity limits. Therefore, the optimal operating conditions of the modelled stage 1 condenser, with aqua-ammonia and ethylene-glycol water, results in a maximum U_c of 249.090 [W/m^{2}K]. If the tube side heat transfer coefficient correlation were to be changed to (Gnielinski, 1976) Nusselt correlation for transitional flow through circular ducts, the overall heat transfer coefficients would easily enter the typical U_c ranges of Table 5.1.

Table 5.4: Stage 1 condenser - The limit boundary conditions for 3 permutations of working fluids.

Limit boundary conditions:	Aq - B	Aq - W	Am - W
Coolant mass flow rate: $\dot{m}_{clnt}$	2.47694 [kg/s]	1.235 [kg/s]	1.235 [kg/s]
Tube side: Re_t	2300 [-]	2300 [-]	2300 [-]
Tube side HTC: h_i	296.30 [W/m^2.K]	268.45 [W/m^2.K]	268.45 [W/m^2.K]
Refrigerant mass flow rate: $\dot{m}_5$	0.032720 [kg/s]	0.018149 [kg/s]	0.017091 [kg/s]
Shell side HTC: h_o	6694.43 [W/m^2.K]	6694.43 [W/m^2.K]	8156.89 [W/m^2.K]
Heat transfer rate: $\dot{Q}_{S1C}$ (Eq. 2.26)	38.6335 [kW]	21.4291 [kW]	20.0785 [kW]
Overall heat transfer coefficient: U_c	249.090 [W/m^2.K]	227.044 [W/m^2.K]	228.433 [W/m^2.K]

The curves of Figure 5.2 illustrate the temperature versus enthalpy of aqueous ammonia at different ammonia mass concentrations and their respective 'turning points'. As previously claimed in Chapter 3.1.1, to the right of the 'turning point' is where the temperature decreases more rapidly than enthalpy, and to the left of the 'turning point' the temperature vs. enthalpy exhibits the characteristics of a typical latent two-phase substance. Thus, the assumption of 2 stages of the condenser was created.

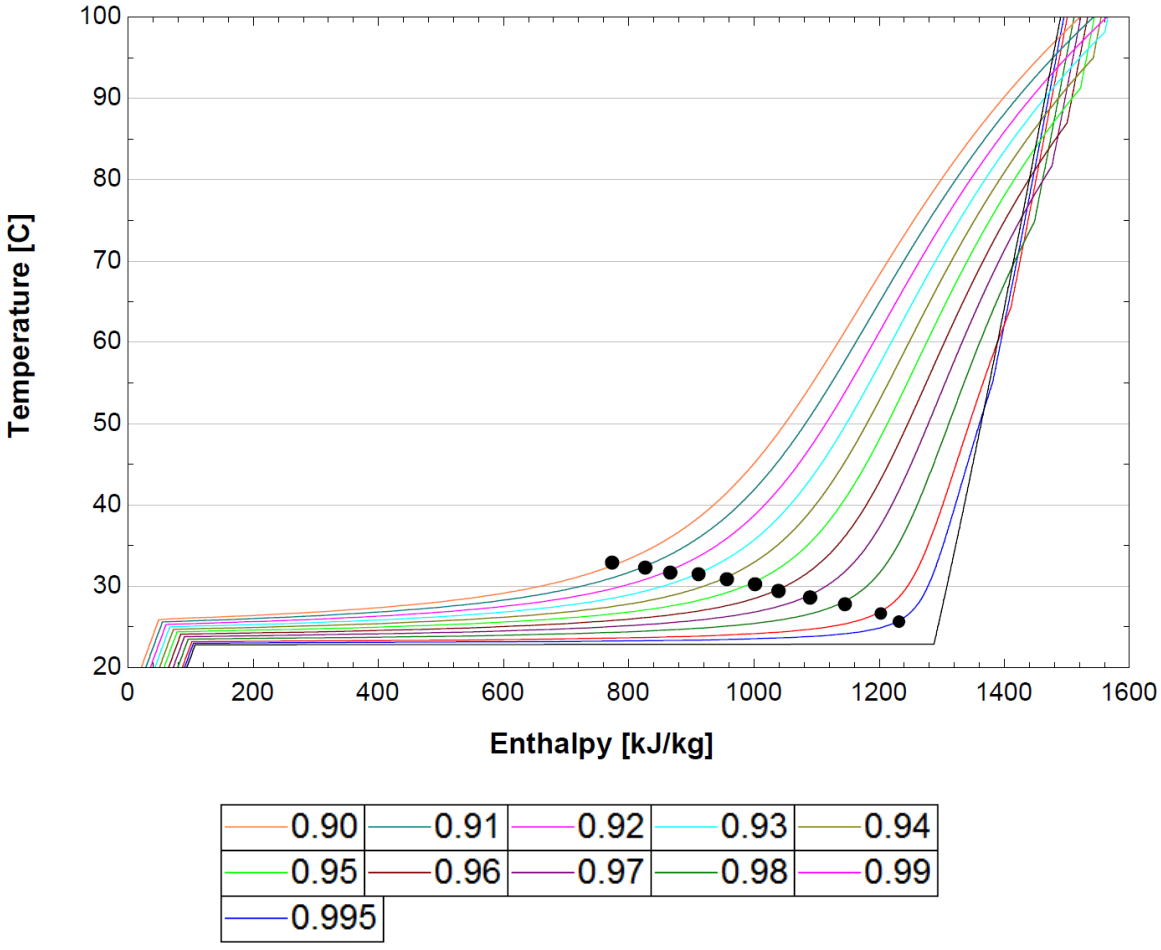

Figure 5.2: Temperature vs. enthalpy of different mass concentrations of ammonia in water mixtures.

Closer investigation was conducted at 90 wt% ammonia in water, where the 'turning point' was found to be at the quality of Q = 0.63. Figure 5.3 illustrates the linear enthalpy estimation of both the 90 and 99 wt% ammonia in water. The red line represents the linear enthalpy estimation of the 90 wt% aqua-ammonia, and the blue line represents the 99 wt% ammonia in water. The dot-dash lines illustrate construction lines similar to that of the 'turning point' investigation of Chapter 3.1.1.

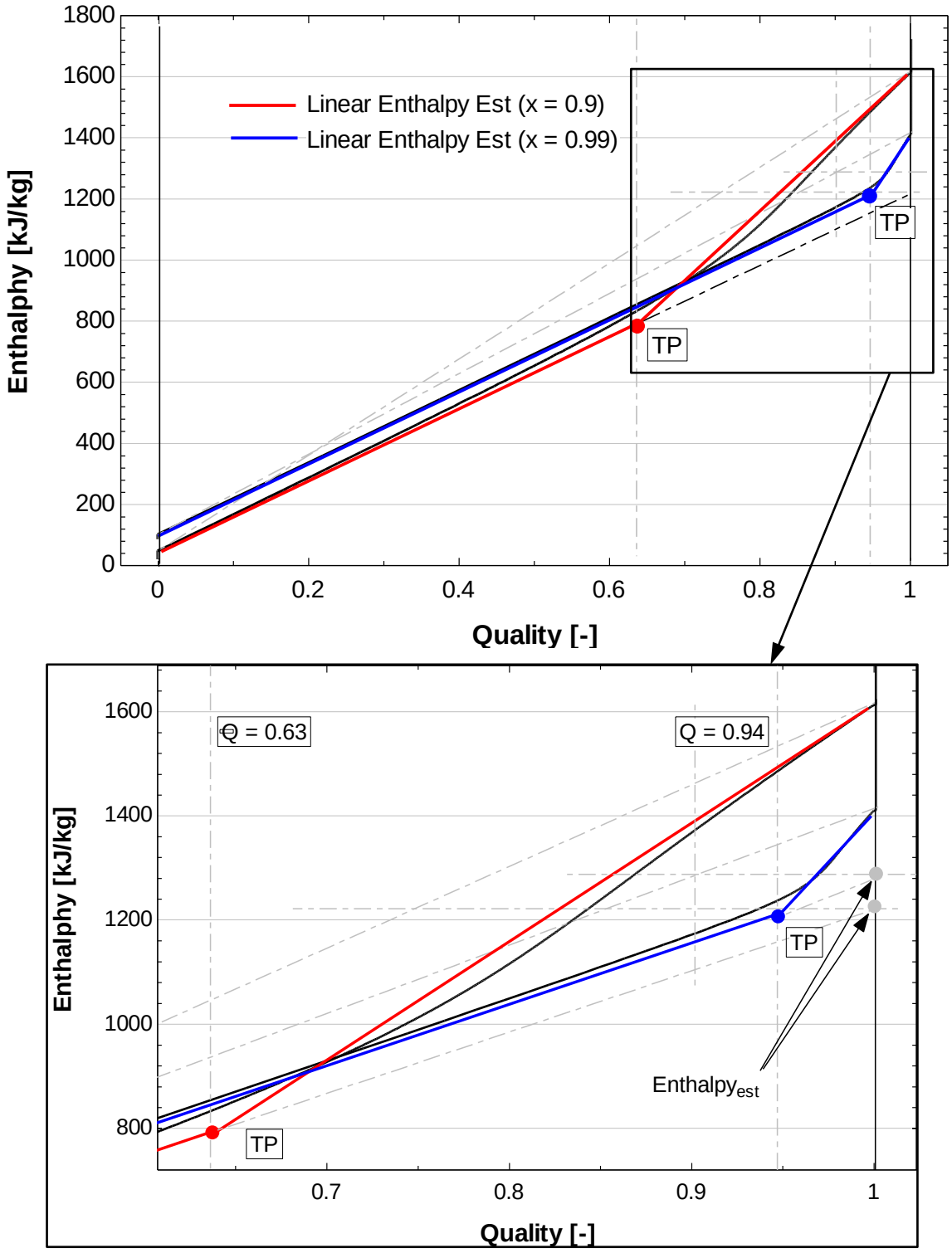

Figure 5.3: Enthalpy vs. quality investigation of 'turning point' for 0.9 and 0.99 mass concentrations ammonia in water.

The temperature boundary conditions of the coolant for the 90 wt% simulation are calculated to equate the log mean temperature difference of the 99 wt% stage 1 condenser. Entering the thermophysical properties of state $TP_{0.9}$ and the same refrigerant mass flow rate as the 99 wt% stage 1 condenser into the stage 1 condenser thermodynamic design model yielded the results tabulated in Table 5.5.

Table 5.5: The comparison table of the stage 1 condenser simulation model with 90 & 99 wt% aqua-ammonia and water as coolant.

S1C: Mass concentration comparison	x = 0.9	x = 0.99
$\Delta T_{LMTD,CF}$	5.098 [°C]	5.099 [°C]
Coolant mass flow rate: $\dot{m}_{clnt}$	0.01211 [kg/s]	0.041871 [kg/s]
Tube side: Re_t	11.25 [-]	77.78 [-]
Tube side HTC: h_i	74.905 [W/m^2.K]	103.91 [W/m^2.K]
Refrigerant mass flow rate: $\dot{m}_5$	0.0006153 [kg/s]	0.0006153 [kg/s]
Shell side HTC: h_o	6152.92 [W/m^2.K]	6694.43 [W/m^2.K]
Heat transfer rate: $\dot{Q}_{S1C}$ (Eq. 2.27)	455.594 [W]	726.503 [W]
Heat transfer rate: $\dot{Q}_{Total}$ (Eq. 2.27)	961.78 [W]	799.36 [W]
Overall heat transfer coefficient: U_c	66.139 [W/m^2.K]	91.214 [W/m^2.K]

It can be concluded from Table 5.5 that the 0.9 mass concentration has a lower overall heat transfer coefficient, which is due to the lower tube side heat transfer coefficient. The low tube side heat transfer coefficient can be attributed to the lower coolant mass flow rate, which is directly connected to the refrigerant mass flow rate. The mass flow rate of the aqua-ammonia remains constant for both mass concentrations due to the assumption that the bubble pump generator will boil-off aqua-ammonia at the same rate for both mass concentrations.

The differing overall heat transfer coefficient results from Tables 5.4 and 5.5 clearly support the claim that the stage 1 condenser can't be sized by assuming pure ammonia thermophysical properties, when there is a mass concentration lower than 98 wt% aqua-ammonia. The differences in heat transfer rates of Table 5.4 also indicates to the reality that the stage 1 condenser can't be sized by assuming pure ammonia thermophysical properties, even if the mass concentration is 0.99. As the heat transfer surface area could result in an over estimation of the required heat transfer surface area. The differences in heat transfer rates of Table 5.5 and the behavioural characteristics of two-phase aqua-ammonia can support the assumption that an aqua-ammonia condenser can be split into two stages of the condenser unit (latent condensing heat exchanger and vapour cooling heat exchanger). In section 5.3 the assumption that the second stage of the condenser unit may be approached as a gas-to-brine heat exchanger will be proved to be acceptable.

5.2.4 Shell Side Heat Transfer Coefficient Validation Results

As previously mentioned, the tube bundle laminar film condensation HTC isn't influenced by mass flow rates and Reynolds numbers, but it is greatly influences by the wall temperature of the tubes. The ethylene glycol water solution's inlet and outlet temperatures effect the wall temperature. Assuming the coolant outlet temperature remains the same as the initial stage 1 condenser model and the inlet temperature is decreased in small increments, the shell side heat transfer coefficient would theoretically decrease. Figure 5.4 and the results in Table 5.6 support the assumption that the laminar film condensation heat transfer coefficient proposed by (Nusselt, 1916) can be approached as a log mean temperature difference, as proposed by Eq. 4.1.

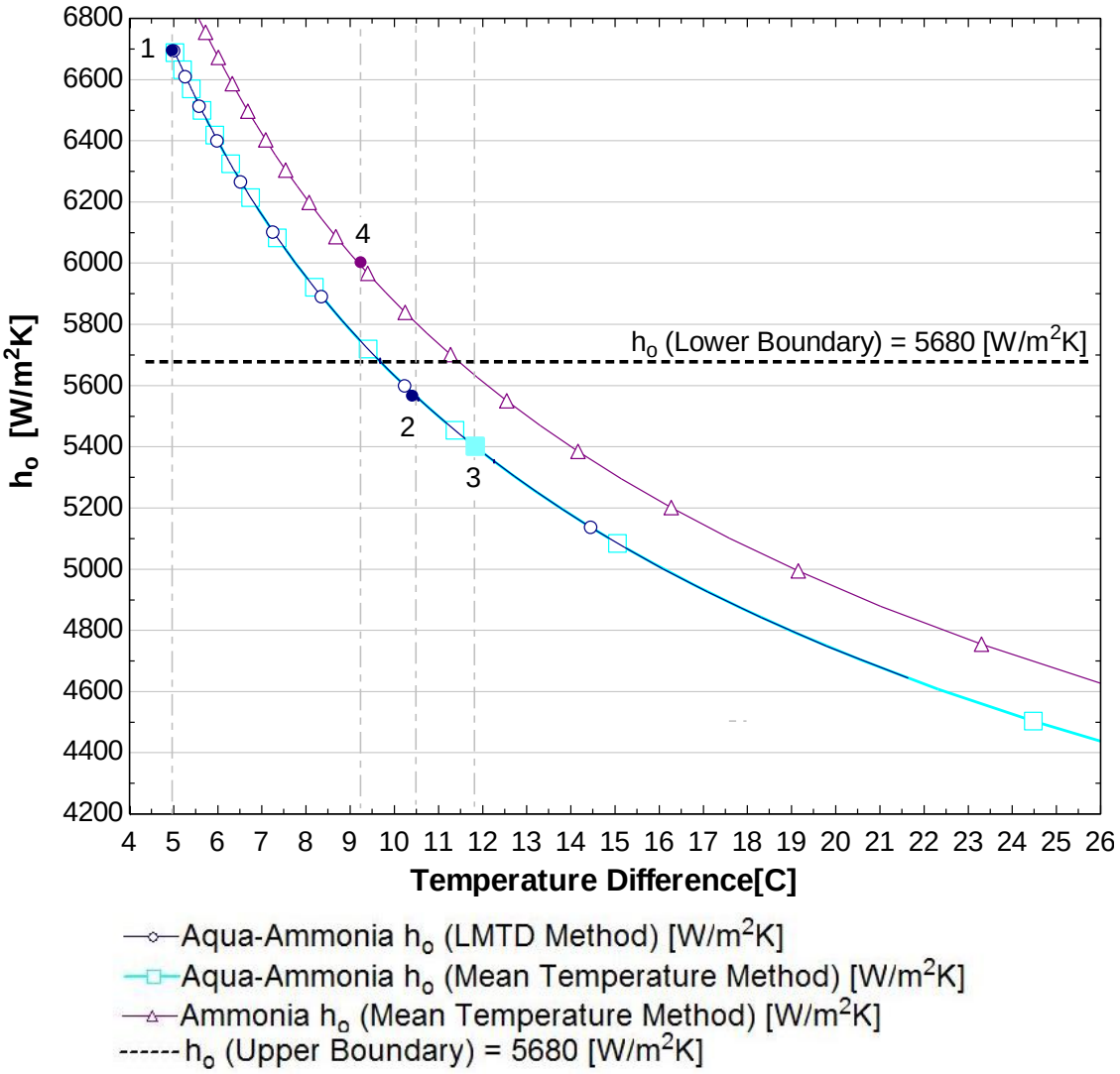

Figure 5.4: Stage 1 condenser – Shell side heat transfer coefficient vs. temperature difference simulation model output plot.

The dark blue curve with circle symbols represent the results of Eq. 4.1 (log mean temperature difference method), the light blue square symbol curve represents the results obtained by Eq. 2.23 (mean temperature difference method). These two curves are identically shaped and occupy the

same coordinates, though the two methods yield different results for the same input parameters. The third curve, with triangular symbols, represents the results obtained with pure ammonia substance and the mean temperature difference method.

The three points of comparison of Fig. 5.4 are set at a coolant inlet temperature of 5 [°C]. The heat transfer coefficient output value of the (aqua-ammonia) log mean temperature difference method (at point 2) is slightly less conservative by 2.788%, than the result of the (aqua-ammonia) mean temperature difference method (at point 3). Although, the log mean temperature difference method is slightly less conservative than the mean temperature difference method, the counter-flow log mean temperature better represents the two-phase mean temperature difference between aqua-ammonia solutions (with temperature glide) and the secondary refrigerant. Point 4 of Figure 5.4 illustrates the equivalent to points 2 & 3 with pure ammonia as refrigerant, which has a shell side heat transfer coefficient approximately 6.02% higher than that of point 2 and 8.98% higher than that of point 3.

Table 5.6: Stage 1 condenser – Shell side heat transfer coefficient output values.

Points	$T_{clnt,in}$	$\Delta T_{LMTD\ or\ MTD}$	h_o	U_c
1	18.404 [°C]	5.01 [°C] (LMTD)	6699.73 [W/m^2.K]	80.27 [W/m^2.K]
2	5 [°C]	10.503 [°C] (LMTD)	5563.48 [W/m^2.K]	65.442 [W/m^2.K]
3	5 [°C]	11.72 [°C] (MTD)	5412.56 [W/m^2.K]	65.420 [W/m^2.K]
4	5 [°C]	9.224 [°C] (MTD)	5898.36 [W/m^2.K]	65.442 [W/m^2.K]

As shown in Table 5.6 the overall heat transfer coefficient of points 2 and 3 are near identical, which would only leave the mean temperature difference to influence the heat transfer surface area. If it were assumed that for points 2 and 3 the heat transfer rates are identical, then the heat transfer surface area of point 2 would be 11.59% larger than that of point 3. Thus supporting the decision to use Eq. 4.1 and the counter-flow log mean temperature difference as a conservative and elegant approach to determine the thermodynamic design for first segment of the latent two-phase region of aqua-ammonia solutions.

5.2.5 Thermodynamic Design Validation Conclusion

The conclusions that can be made from the results obtained in section 5.2 are:

- The assumption that the condenser unit can't be sized by assuming pure ammonia thermophysical properties is valid.
- The mean temperature difference of the laminar film condensation heat transfer coefficient is better represented with a counter-flow log mean temperature difference when dealing with temperature-glide in aqua-ammonia solutions, despite the fact it is 2.788% less conservative.

- The mean temperature difference of the heat transfer rate in Eq. 2.3 is better represented with the counter-flow log mean temperature difference when dealing with temperature gliding mixtures, as it is 11.59% more conservative. Therefore, the mean temperature difference method would underestimate the total heat transfer surface area required for the thermodynamic design of the latent like region of aqueous ammonia solutions.
- The overall heat transfer coefficient of a condensing heat exchanger is greatly influenced by the secondary refrigerant (coolant).
- The overall heat transfer coefficient output values were below the typical U_c range values, which are to be expected of a condensing heat exchanger with low refrigerant and coolant mass flow rates with laminar flow regimes.

Therefore, it can be concluded that accurate correlations were utilised in calculating the stage 1 condenser's thermodynamic design. The design-sizing parameters of the stage 1 condenser are now utilised in the mechanical design consideration phase, with which the manufacturing and assembly drawings are created. The mechanical design considerations of the stage 1 condenser are available in Appendix E 1, and the manufacturing and assembly drawings are available in Appendix E 2.

5.3 Stage 2 Condenser

The heat transfer coefficient results from the modelled stage 2 condenser in Chapter 4.4.1 indicate that the shell side heat transfer coefficient impedes heat from being transferred. Thus, for the validation of the stage 2 condenser the mass flow rate of the refrigerant will be increased, whilst maintaining constant thermophysical properties for both aqua-ammonia and ethylene-glycol water. The energy balance of the stage 2 condenser is

$$\dot{Q}_{S2C} = \dot{m}_4(\alpha_4 - \alpha_{TP}) = \dot{m}_{clnt} C_{p,clnt}\left(T_{clnt,out} - T_{clnt,in}\right) = U_c A_s \Delta T_{LMTD.CF}$$

The U_c simulation will start at the Re_s of the original sized stage 2 condenser model of Chapter 4.4.1 and will continue increasing until one of the correlation limits are reached.

The heat transfer coefficient correlation limitations of the second stage of the condenser unit are determined similarly to the limitations of the stage 1 condenser, therefore the tube side heat transfer coefficient correlation limitations are tabulated into Table 5.7.

Table 5.7: Stage 2 condenser – Tube side heat transfer coefficient correlation limitations.

Correlation Limit Parameters	Limit
Tube side: Re_t	2300
Maximum coolant mass flow rate: $\dot{m}_{clnt.max}$	2.1048 [kg/s]

The shell side staggered tube bundle Nusselt correlation proposed in (Zukauskas, 1987) is largely influenced by the Reynolds number for flow across the tube bundle. The incremental increase of refrigerant mass flow rate will increase the Re_s and consequently the heat transfer coefficient. The correlation of Eq. 2.18 has its limitation recorded in Table 5.8 as:

Table 5.8: Stage 2 condenser – Shell side heat transfer coefficient correlation limitations.

Correlation Limit Parameters	Limit
Shell side: Re_s	500
Maximum coolant mass flow rate: $\dot{m}_{4.max}$	0.02323 [kg/s]

5.3.1 Overall Heat Transfer Coefficient Validation Results

Figure 5.5 represents the growth of the overall heat transfer coefficient values versus steady incremental increases of shell side Reynolds numbers. The shell side Reynolds number was chosen for the *x*-axis as it signifies the governing factor of the U_c correlation output value increases. The shell side Reynolds numbers are increased from an initial 11.7 to the limit of 500 [-], with 0.01 [kg/s] increments. The initial position, represented by point 1 on Figure 5.5, is the original stage 2 condenser model as illustrated in Chapter 4.4.1.

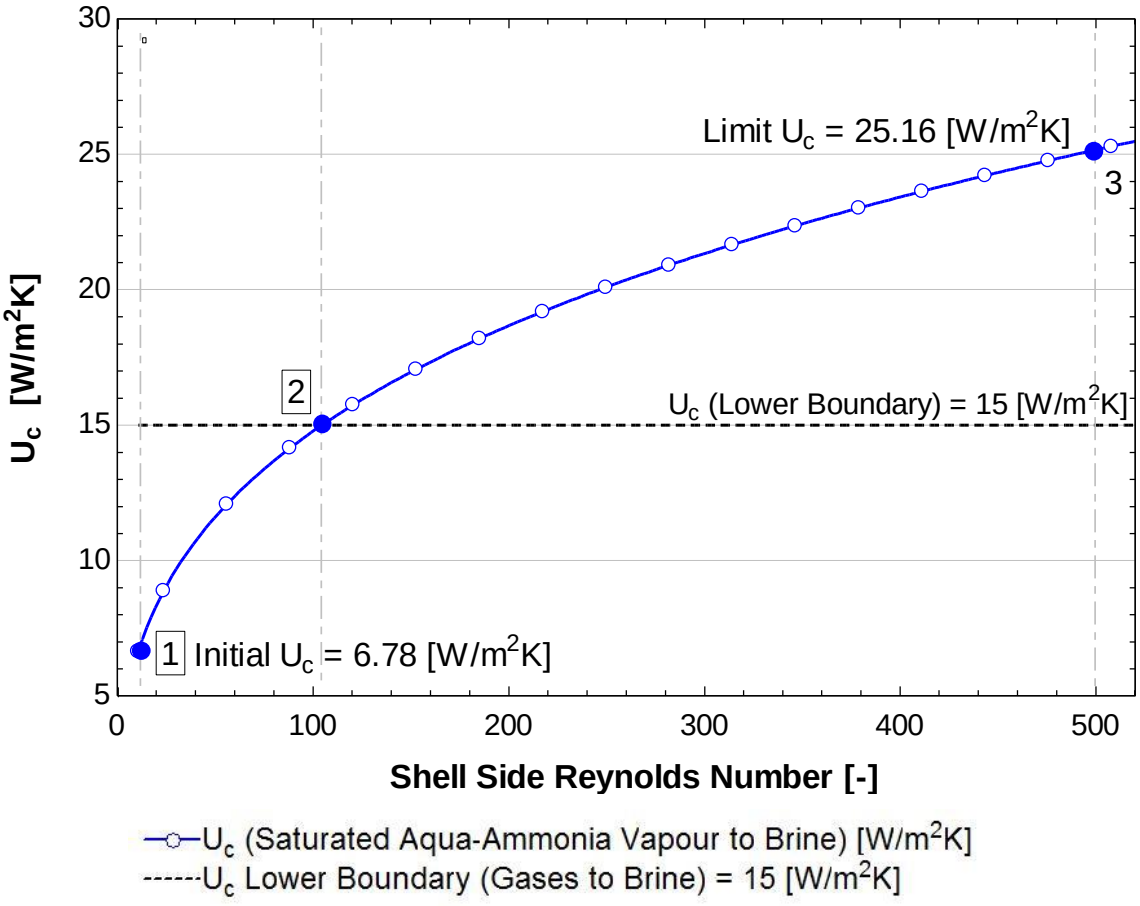

Figure 5.5: Stage 2 condenser – Overall heat transfer coefficient vs. shell side Reynolds number simulation model output plot.

The initial overall heat transfer coefficient is fairly lower than the lower boundary of typical U_c ranges, which can be attributed to the very low mass flow rates achieved by an absorption-desorption cycle. The overall heat transfer coefficient simulation reaches the shell side heat transfer coefficient correlation limit at 25.16 [W/m^2.K], which falls inside the expected U_c ranges of gases-to-brine heat transfer. Presented in Table 5.9 are the output values of points 1, 2, and 3.

Table 5.9: Stage 2 Condenser – Overall heat transfer coefficient vs. shell side Reynolds numbers simulation model output values.

Stage 2: U_c Simulation	**1**	**2**	**3**
Coolant mass flow rate: $\dot{m}_{clnt}$	0.0006925 [kg/s]	0.006219 [kg/s]	0.029726 [kg/s]
Tube side: Re_t	0.464 [-]	4.166 [-]	19.915 [-]
Tube side HTC: h_i	116.165 [W/m^2.K]	119.237 [W/m^2.K]	127.508 [W/m^2.K]
Refrigerant mass flow rate: $\dot{m}_4$	0.0005412 [kg/s]	0.004860 [kg/s]	0.02323 [kg/s]
Shell side: Re_s	11.7 [-]	104.6 [-]	500 [-]
Shell side HTC: h_o	7.3610 [W/m^2.K]	17.711 [W/m^2.K]	33.114 [W/m^2.K]
Heat transfer rate: $\dot{Q}_{S2C}$	109.303 [W]	981.548 [W]	4691.64 [W]
Overall heat transfer coefficient: U_c	6.78 [W/m^2.K]	15 [W/m^2.K]	25.165 [W/m^2.K]

The shell side heat transfer coefficient does have a sharp increase in response to the gains in Reynolds numbers. This is due to two factors: Reynolds numbers increase more rapidly with a gas state fluid than a liquid state fluid; and transitional flow occurs at lower Reynolds numbers for shell side than that of tube side. The U_c simulation model limit of point 3 doesn't exceed the tube side heat transfer coefficient correlation limit of Re_t = 2300. If the shell side heat transfer coefficient were substituted with Eqs. 2.19 or 2.20 the overall heat transfer coefficient could in theory increase even further. This however isn't recommended, as a steady increase in refrigerant mass flow rate would only result in larger heat transfer rate requirements and impractically large heat exchangers. Therefore, if the heat capacity of the stage 2 condenser is to be increased, it should be increased well into the turbulent flow regime.

Recorded in Table 5.10 is the heat exchanger comparison made between 0.9 and 0.99 mass concentration aqua-ammonia. The comparison is made at the initial conditions of the stage 2 condenser simulation model, that way the comparison is equivalent to the sized stage 2 condenser model of Chapter 4.4. Included is the assumption that the mass flow rate of aqua-ammonia remains constant for both stage 2 condenser's mass concentrations simulations. The temperature boundary conditions of the coolant for the 90 wt% simulation are calculated to equate the log mean temperature difference of the 99 wt% stage 2 condenser.

The overall heat transfer coefficient of the 90 wt% aqua-ammonia is near four times greater than the 99 wt% aqua-ammonia, which can be attributed to the slightly higher liquid quality of bulk

fluid thermophysical properties of the 90 wt% aqua-ammonia. The overall heat transfer coefficient of the 90 wt% aqua-ammonia does however fall within the typical range of gas-to-brine heat exchangers.

The required heat transfer rate to cool the 90 wt% stage 2 condenser is more than four times greater than the 99 wt% stage 2 condenser. The heat transfer surface area of the 90 wt% stage 2 condenser would be 31.12% larger than its counterpart.

Table 5.10: The comparison table of the sized stage 2 condenser model with 90 & 99 wt% aqua-ammonia and ethylene glycol water as coolant.

S2C: Mass concentration comparison	x = 0.9	x = 0.99
$\Delta T_{LMTD,CF}$	3.434 [°C]	3.348 [°C]
Coolant mass flow rate: $\dot{m}_{clnt}$	0.0015227 [kg/s]	0.0006925 [kg/s]
Tube side: Re_t	1.664 [-]	0.464 [-]
Tube side HTC: h_i	119.050 [W/m^2.K]	116.165 [W/m^2.K]
Refrigerant mass flow rate: $\dot{m}_4$	0.0005412 [kg/s]	0.0005412 [kg/s]
Shell side: Re_s	2.098 [-]	11.7 [-]
Shell side HTC: h_o	30.125 [W/m^2.K]	7.3610 [W/m^2.K]
Heat transfer rate: $\dot{Q}_{S2C}$ (Eq. 2.27)	487.017 [W]	109.30 [W]
Overall heat transfer coefficient: U_c	23.040 [W/m^2.K]	6.780 [W/m^2.K]

5.3.2 Thermodynamic Design Validation Conclusion

In conclusion, the overall heat transfer coefficient validation of section 5.3.1 yielded coherent results that proved that adequate correlations were utilised in the thermodynamic design of the second stage of the condenser unit. The knowledge obtained from the mass concentration comparison results supported the assumption that the condenser unit using an aqua-ammonia refrigerant can be split into two thermodynamic heat exchanger designs and that the second stage of the condenser unit be treated as a gas-to-brine heat exchanger. Furthermore, it can be concluded that the stage 1 condenser will decrease in surface area with decreasing wt% of ammonia in water and the stage 2 condenser would increase in heat transfer surface area with decreasing wt% of ammonia in water.

The performance rating proves that the sized stage 2 condenser model can be implemented as a practical application with an expected thermal efficiency around 90%. Consequently, the sizing model of Chapter 4.4 may be utilised to further the mechanical design considerations and manufacturing drawings of Appendix E 3.

5.4 De-superheating Condenser

The modelled de-superheating condenser of Chapter 4.5 indicated that the shell side heat transfer coefficient impedes the heat from being transferred, and thus is considered as the controlling factor of the overall heat transfer coefficient. The U_c simulation will see the increase of shell side Reynolds numbers from the originally modelled Re_s = 141.007 [-] (as presented in Table 4.9) to the Re_s limit in 0.01 [kg/s] increments. Thus, the de-superheating condenser's energy balance is:

$$\dot{Q}_{DHC} = \dot{m}_3(\alpha_3 - \alpha_4) = \dot{m}_{clnt} C_{p,clnt}\left(T_{clnt,out} - T_{clnt,in}\right) = U_c A_s \Delta T_{LMTD.CF}$$

As the de-superheating condenser uses the exact same correlations to determine its shell and tube side heat transfer coefficients as the stage 2 condenser; the correlation limitations will be the same. Therefore, recorded in Tables 5.11 and 5.12 are the tube side correlation limitations and the shell side correlation limitations, respectively.

Table 5.11: De-superheating condenser – Tube side heat transfer coefficient correlation limitations.

Correlation Limit Parameters	Limit
Tube side: Re_t	2300 [-]
Maximum coolant mass flow rate: $\dot{m}_{clnt.max}$	0.31097 [kg/s]

Table 5.12: De-superheating condenser – Shell side heat transfer coefficient correlation limitations.

Correlation Limit Parameters	Limit
Shell side: Re_s	500 [-]
Maximum refrigerant mass flow rate: $\dot{m}_{3,max}$	0.002182 [kg/s]

5.4.1 Overall Heat Transfer Coefficient Validation Results

Presented in Figure 5.6 is the overall heat transfer coefficient simulation of the de-superheating condenser. The overall heat transfer coefficient reaches the shell side Reynolds number limit at 18.064 [W/m^2.K], which falls within the typical U_c range of a gas-to-brine heat exchanger. Table 5.13 illustrates the input and output values of the points one, two, and three in Fig. 5.6. The tube side Reynolds number remain noticeably low throughout the U_c simulation, which is to be expected from the small increases in refrigerant mass flow rates. As the coolant and refrigerant mass flow rates are co-dependent. The shell side Reynolds numbers increase rapidly with the small increases in mass flow rate, due to its superheated vapour state. Therefore, the overall heat transfer coefficient simulation model doesn't exceed the tube side heat transfer coefficient correlation limit of Re_t = 2300 [-].

Thus, to further the U_c value of the de-superheating condenser the shell side heat transfer coefficient correlation needs to be changed to Eq. 2.19 for Reynolds numbers between 500 and

1000 [-]. Although, it should be noted that further increases in refrigerant mass flow rate in the laminar regime will only cause the heat transfer surface area to increase to impractical sizes. Therefore, if the mass flow rate and heat capacity of the refrigerant is to be increased, it should be increased to Reynolds numbers in the turbulent regime. The output values of turbulent heat transfer coefficients are typically much higher than that of laminar heat transfer coefficients.

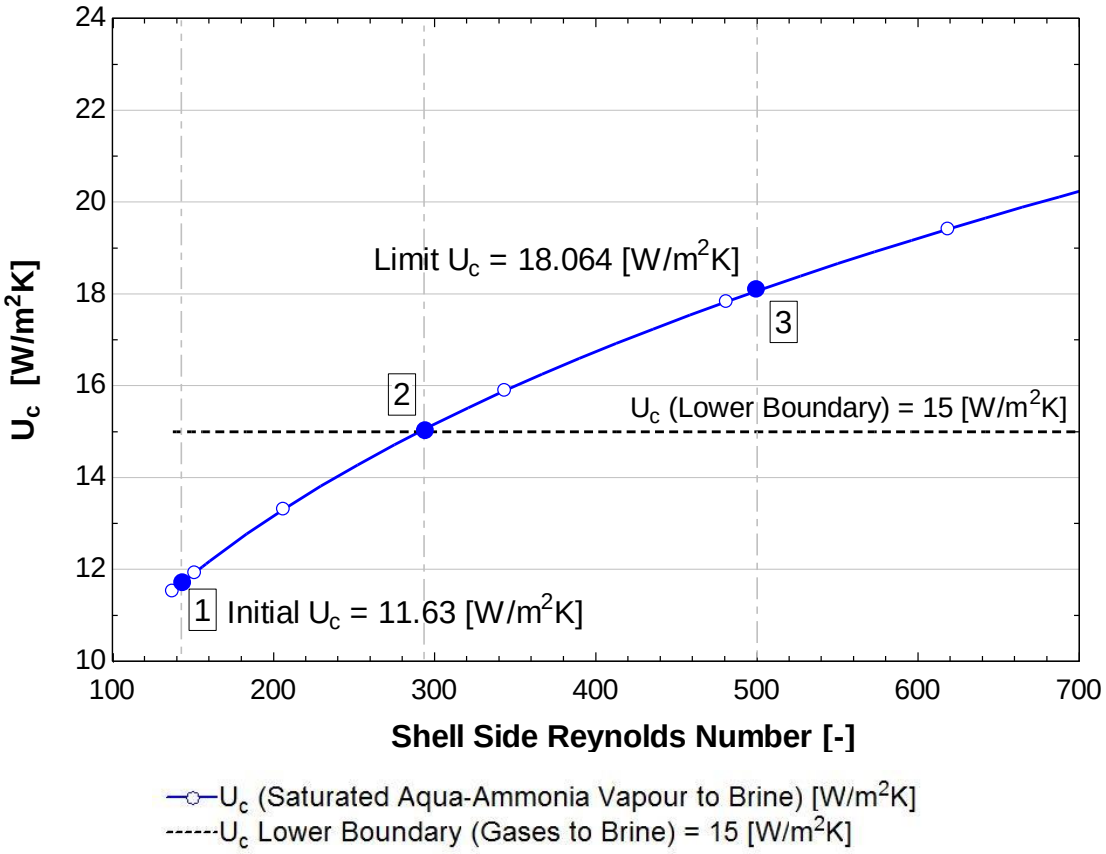

Figure 5.6: De-superheating condenser – Overall heat transfer coefficient vs. shell side Reynolds number simulation model output plot.

Table 5.13: De-superheating condenser – Overall heat transfer coefficient vs. shell side Reynolds numbers simulation model output values.

De-superheating: U_c Simulation	**1**	**2**	**3**
Coolant mass flow rate: $\dot{m}_{clnt}$	0.0005649 [kg/s]	0.0011650 [kg/s]	0.0020032 [kg/s]
Tube side: Re_t	4.178 [-]	8.617 [-]	14.82 [-]
Tube side HTC: h_i	122.75 [W/m^2.K]	125.012 [W/m^2.K]	127.681 [W/m^2.K]
Refrigerant mass flow rate: $\dot{m}_3$	0.0006153 [kg/s]	0.001269 [kg/s]	0.002182kg/s]
Shell side: Re_s	141.007 [-]	290.82 [-]	500 [-]
Shell side HTC: h_o	13.150 [W/m^2.K]	17.566 [W/m^2.K]	21.818 [W/m^2.K]
Heat transfer rate: $\dot{Q}_{DHC}$	57.431 [W]	118.447 [W]	203.667 [W]
Overall heat transfer coefficient: U_c	11.635 [W/m^2.K]	15 [W/m^2.K]	18.064 [W/m^2.K]

5.4.2 Thermodynamic Design Validation Conclusion

In conclusion, the U_c simulation model proves that the thermodynamic design process of the de-superheating condenser to be acceptable. The calculated performance rating supports the claim that the thermodynamic design of the de-superheating condenser is practically feasible, with realistically expected coolant outlet temperatures. Therefore, the sizing model concluded in Chapter 4.5.4 may be utilised to further the mechanical design considerations of the de-superheating condenser in Appendix E 1, and help create the manufacturing and assembly drawings of Appendix E 4.

5.5 Pre-Cool Heat Exchanger

The fluid configuration of the pre-cool heat exchanger doesn't have a corresponding typical overall heat transfer coefficient range in Table 5.1, but its shell and tube side heat transfer coefficients can be validated individually. As the pre-cool heat exchanger uses exactly the same equations for the shell and tube heat transfer coefficient correlations as the de-superheating condenser, the correlations limitations will be similar. The sized heat exchanger model of Chapter 4.6 suggests that the shell side heat transfer coefficient impedes heat transfer from occurring and is therefore considered as the controlling factor. Presented in Table 5.14 is the shell side heat transfer coefficient correlation limitation to be used in the validation simulation model. The tube side heat transfer coefficient correlation is assumed as proven to be acceptable, due to the previous work of sections 5.2, 5.3 and 5.4.

Table 5.14: Pre-cool heat exchanger – Shell side heat transfer coefficient correlation limitations.

Correlation Limit Parameters	Limit
Shell side: Re_s	500 [-]
Maximum refrigerant mass flow rate: $\dot{m}_9$	0.0016273 [kg/s]

The validation process of the pre-cool heat exchanger doesn't require an energy balance or constant tube side thermophysical properties, although it does require the incremental increase of shell side Reynolds numbers and constant ammonia thermophysical properties. Shell side Reynolds numbers increase from an initial value of 183.943 [-] to the correlation limit of 500 [-] in 0.01 [kg/s] increments. The lower boundary of the typical range of heat transfer coefficient for gases is 15 [W/m^2.K] (Engineers Edge, 2016).

5.5.1 Shell Side Heat Transfer Coefficient Validation Results

Demonstrated in Figure 5.7 is the shell side heat transfer coefficient simulation versus shell side Reynolds numbers, where the simulated increase in heat transfer coefficient reaches its correlation limit before entering the typical expected range of gas heat transfer.

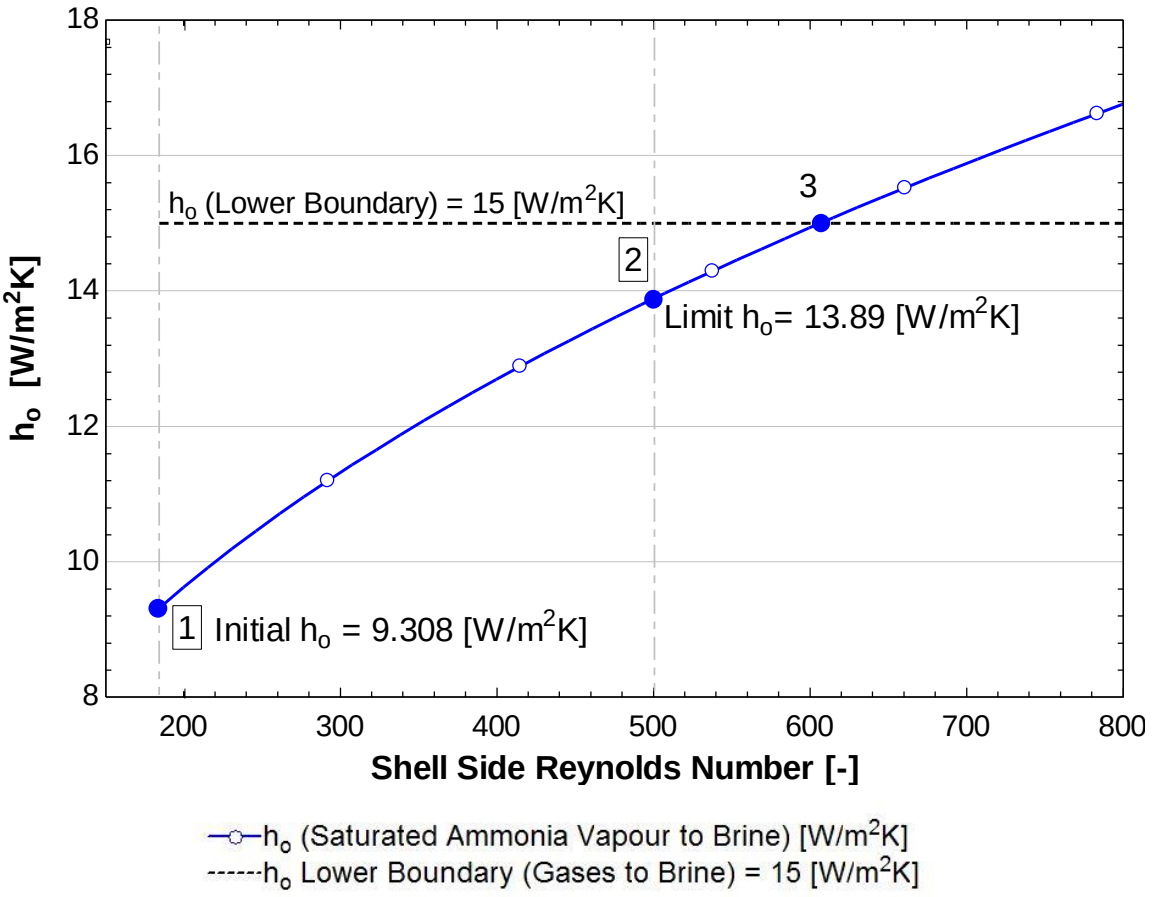

Figure 5.7: Pre-Cool heat exchanger – Shell side heat transfer coefficient vs. shell side Reynolds number simulation model output plot.

A simulation limit lower than the typical range of heat transfer coefficient can be attributed to the lower density and dynamic viscosity of pure ammonia, which would mathematically increase the Reynolds numbers at a higher accelerated rate than that of the de-superheating condenser. The shell side heat transfer coefficient can be increased further by increasing the shell side mass flow rate, but this would require the use of correlation that can accommodate Re_s > 500 [-]. Again, the same problem of the de-superheating condenser arises, where any further increases in shell side mass flow rate would increase the heat transfer surface area to impractical sizes. Therefore, increases in mass flow rate should be into the turbulent regime to obtain sensible heat transfer surface areas for large heat capacities.

5.5.2 Thermodynamic Design Validation Conclusion

In conclusion, the shell side heat transfer coefficient simulation model proves that an accurate shell side correlation was utilised in the thermodynamic design process of the pre-cool heat exchanger. The tube side heat transfer coefficient is proved to be valid by the previous heat exchangers that used the same correlation under similar conditions. Further thermodynamic design validation was obtained with the performance rating of the pre-cool heat exchanger, proving that the pre-cool heat

exchanger is feasible in a real world application. Therefore, the thermodynamic design and rating model calculated in Chapter 4.6 can be utilised to determine the mechanical considerations of the pre-cool heat exchanger as illustrated in Appendix E 1, and the manufacturing and assembly drawings recorded in Appendix E 5.

5.6 Evaporator

The working fluid configuration of the evaporator doesn't have a direct overall heat transfer coefficient range match in Table 5.1, but the U_c simulation model of the evaporator could be validated for a refrigerant-to-water evaporative heat exchanger. Secondly, the shell side boiling heat transfer coefficient will be validated against the typical heat transfer coefficient range of convective pool boiling pure ammonia in Table 5.2. The nucleate boiling heat transfer coefficient can be considered as validated, due to the comparison of heat flux versus peak heat flux in Chapter 4.8.

The sized evaporator model obtained in Chapter 4.8 indicated that the tube side heat transfer coefficient impeded heat from being transferred. Thus, the mass flow rate of the 35 wt% ethylene glycol water mixture will be increased until it reaches the tube side heat transfer coefficient correlation limit, as recorded in Table 5.15. The increase in coolant mass flow rate would mathematically increase the mass flow rate of the refrigerant, but the increase in venturi inlet velocity will have an insignificant effect on the outcome of U_c value. Thus, the evaporator's energy balance is:

$$\dot{Q}_{EVAP} = \dot{m}_9(\alpha_9 - \alpha_8) = \dot{m}_{clnt} C_{p,clnt}\left(T_{clnt,out} - T_{clnt,in}\right) = U_c A_s \Delta T_{LMTD.CF}$$

The U_c validation process will see the increase of tube side Reynolds numbers from the original modelled refrigerant Re_s = 3.444 [-] to the Re_t limit of 2300 [-] in 0.01 [kg/s] increments.

Table 5.15: Evaporator – Tube side heat transfer coefficient correlation limitations.

Correlation Limit Parameters	Limit
Tube side: Re_t	2300
Maximum coolant mass flow rate: $\dot{m}_{clnt.max}$	6.556 [kg/s]

5.6.1 Overall Heat Transfer Coefficient Validation Results

Recorded in Figure 5.6 is the U_c simulation curve, which reaches the shell side Reynolds number limit at 251.73 [W/m^2.K], which falls just short of the typical U_c range of a refrigerant to water boiling heat exchanger. The overall heat transfer coefficient limit of the evaporator looks comparable to the U_c limit of the stage 1 condenser. This could be due to the characteristics of the proposed

Nusselt correlation of (Hausen, 1959) for laminar flow through circular ducts, which seems to have a limit ranging between 250 and 300 [W/m^2.K] for Re_t = 2300 [-].

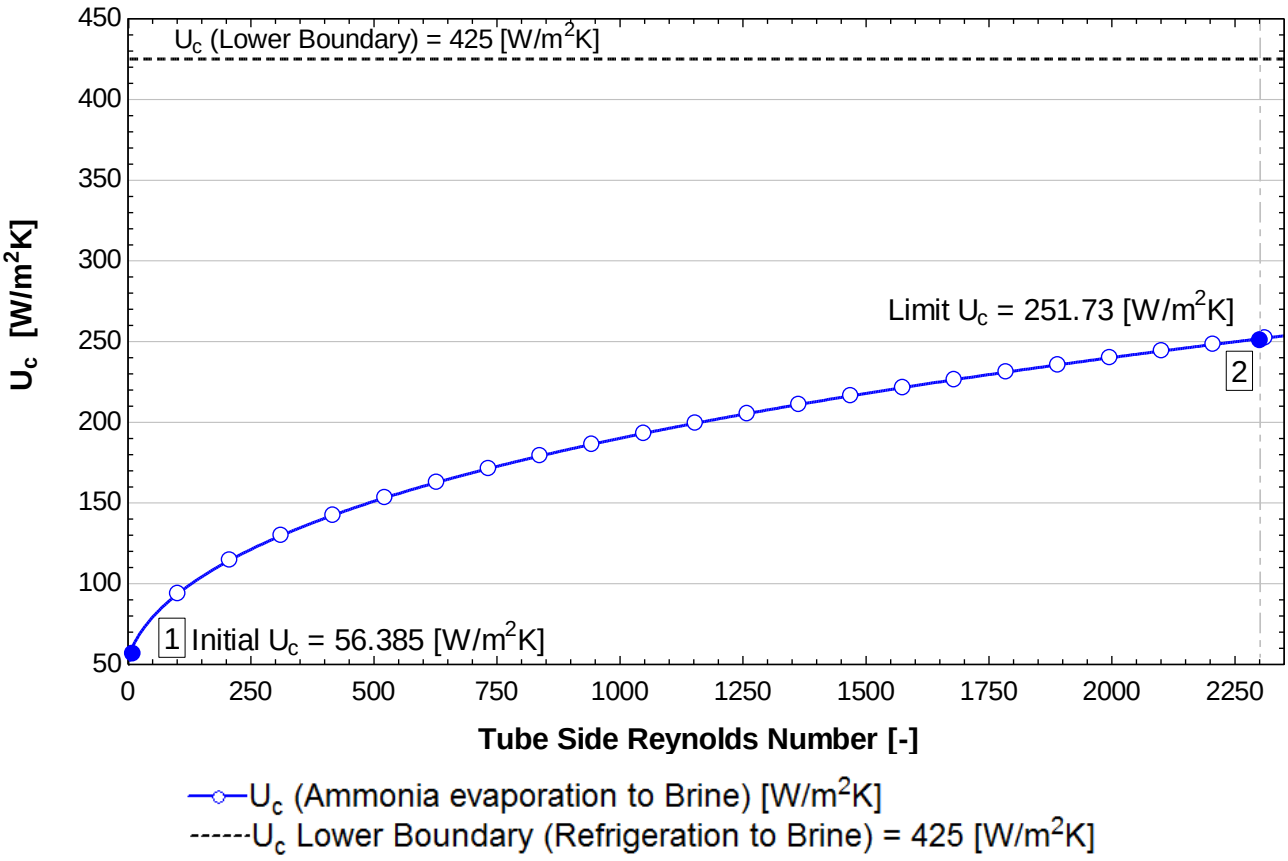

Figure 5.8: Evaporator – Overall heat transfer coefficient vs. tube side Reynolds number simulation model output plot.

Recorded in Table 5.16 are the thermodynamic output values of the U_c simulation. It should be noted that the orifice diameter of the venturi nozzle required adjustment, as the mass flow rate of the refrigerant exceeded the mathematical limits of the Bernoulli equation. Therefore, the orifice diameter of the venturi nozzle is re-sized to 16 [mm], which would result in equivalent entry velocity and Reynolds number as that of the sized evaporator model in Chapter 4.8. The shell side heat transfer coefficient remains unaffected throughout the overall heat transfer coefficient simulation, which only leaves the tube side heat transfer coefficient to influence the outcome of overall heat transfer coefficient.

It is possible for the overall heat transfer coefficient to fall within the typical U_c ranges, as it can be accomplished by increasing the tube side Reynolds number to the transition regime and substituting the tube side heat transfer coefficient correlation with the transitional flow in circular ducts Nusselt correlation proposed in (Gnielinski, 1983). Nevertheless, it should be noted that the significant increase in mass flow rate of both refrigerant and coolant has a far greater influence on the heat transfer rate than the overall heat transfer coefficient, which would result in a ridiculously large heat transfer surface area. If the evaporator were to have a cooling capacity in excess of

566.427 [kW], it would be of great importance for sensible heat transfer surface areas to reconsider the tube side heat transfer coefficient correlation to suit turbulent flow through circular ducts and to re-evaluate the wall temperature of the shell side heat transfer coefficient correlation to suit film boiling.

Table 5.16: Evaporator – Overall heat transfer coefficient vs. tube side Reynolds number simulation model output values.

Evaporator: U_c Simulation	**1**	**2**
Coolant mass flow rate: $\dot{m}_{clnt}$	0.009819 [kg/s]	6.556 [kg/s]
Tube side: Re_t	3.444 [-]	2300 [-]
Tube side HTC: h_i	63.116 [W/m^2.K]	288.504 [W/m^2.K]
Refrigerant mass flow rate: $\dot{m}_9$	0.0005986 [kg/s]	0.3997 [kg/s]
Venturi orifice: d_2	2 [mm]	16 [mm]
Shell side: Re_s	62.429 [-]	62.429 [-]
Convective boiling: h_{cb}	4512.88 [W/m^2.K]	4512.88 [W/m^2.K]
Nucleate boiling: h_{nb}	179792.8 [W/m^2.K]	179792.8 [W/m^2.K]
Shell side HTC: h_o	179849.4 [W/m^2.K]	179849.4 [W/m^2.K]
Heat transfer rate: $\dot{Q}_{EVAP}$	808.306 [W]	566.427 [kW]
Overall heat transfer coefficient: U_c	56.385 [W/m^2.K]	251.72 [W/m^2.K]

5.6.2 Convective Boiling Heat Transfer Coefficient Validation Results

Proper validation of the convective boiling heat transfer coefficient correlation requires that the refrigerant mass flow rate is decreased and consequently the Re_s, as this would emulate the conditions of convective pool boiling. Previously, the velocity of the tiny aqua-ammonia droplets forming a thin falling film was assumed to be equal to gravitational flow, but to emulate the conditions of convective pool boiling the evaporator is assumed to have a submerged tube bundle. Illustrated in Fig. 5.9 is the convective boiling heat transfer coefficient versus liquid film Reynolds numbers, which incorporates the typical heat transfer coefficient ranges of Table 5.2.

Fig. 5.9 clearly indicates to Re_δ values below 5 [-] for typical convective boiling heat transfer coefficients, where such low Reynolds numbers are to be expected from convective pool boiling. The convective boiling curve suggests that it would plateau at higher Reynolds numbers, thus illustrating the possibility of Re_δ limitations.

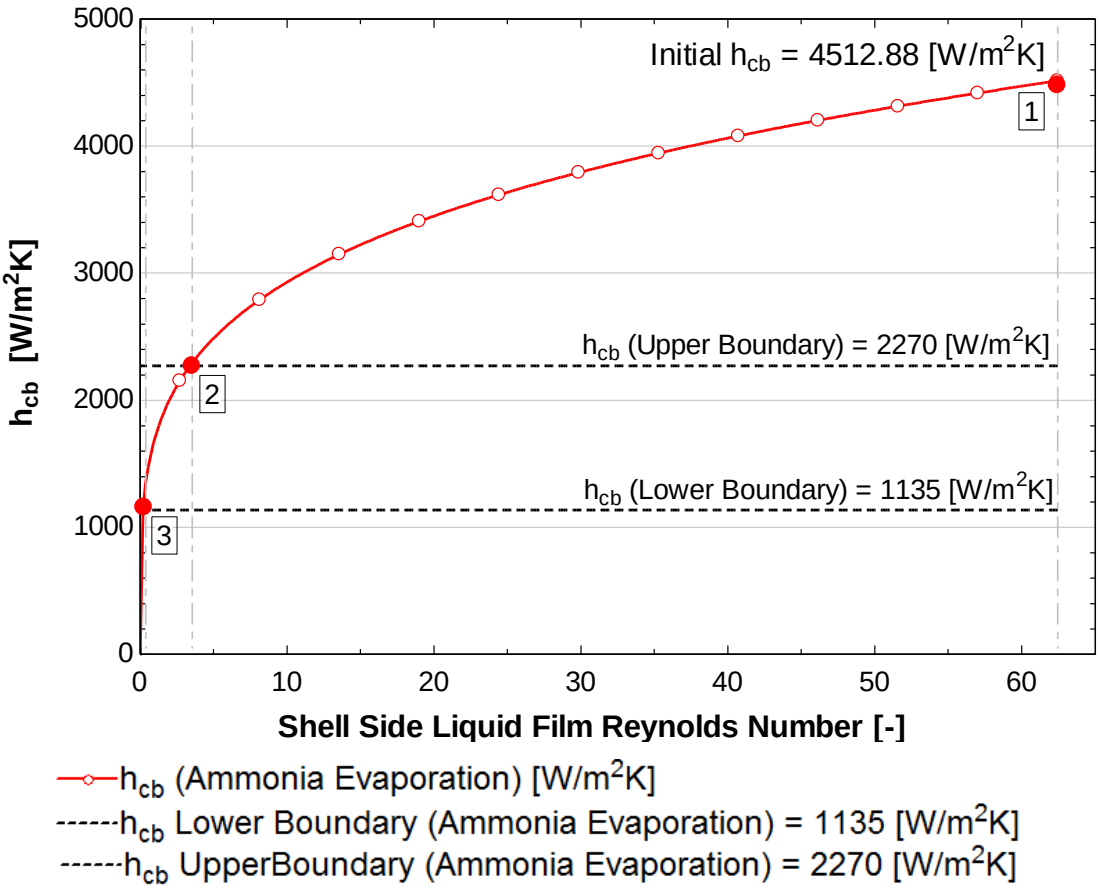

Figure 5.9: Evaporator – Convective boiling heat transfer coefficient vs. shell side liquid film Reynolds numbers.

5.6.3 Thermodynamic Design Validation Conclusion

To conclude the evaporator's validation processes, it should be noted that very little undisputed information (or is under intellectual property protection) on falling film aqua-ammonia (under partial pressure) boiling exists to make sensible conclusions of the evaporator's thermodynamic design. However, the heat flux vs. peak heat flux comparison indicated that the nucleate boiling heat transfer coefficient was correctly utilised. Overall heat transfer coefficient simulation proved that the convective boiling heat transfer coefficient has an infinitesimal role in the U_c outcome. And lastly, the convective boiling heat transfer coefficient correlation proposed in (Cornwell, 1989) gave sensible results when subjected to convective pool boiling conditions.

The performance rating of Chapter 4.8.2 did however yield conclusive results, which suggests that the thermodynamic design model would produce a practically viable evaporation heat exchanger. The evaporator's mechanical design considerations of Appendix E 1 utilised the sized evaporator model of Chapter 4.8 to create the manufacturing and assembly drawings that are available in Appendix E 6.

5.7 Auxiliary-Regenerative Heat Exchanger

The overall heat transfer coefficient validation of the auxiliary-regenerative heat exchanger will be completed by investigating the overall heat transfer coefficients individually. Thus, for the regenerative heat exchanger, the Reynolds number of the (strong aqua-ammonia solution) shell side heat transfer coefficient will be incrementally increased to see whether the U_c limit falls within typical Table 5.1 ranges. The closest typical U_c range that represents the fluid configuration of both the auxiliary and regenerative heat exchangers is a liquid-to-liquid heat transfer heat exchanger. The energy balance of the regenerative heat exchanger is illustrated by the following:

$$\dot{Q}_{REGEN} = \dot{m}_{ws}(\alpha_{ws,1} - \alpha_{ws,2}) = \dot{m}_{ss}(\alpha_{ss,2} - \alpha_{ss,1}) = U_c A_s \Delta T_{LMTD.XF}$$

The U_c simulation will start off at Re_s of the original sized regenerative heat exchanger model represented in Chapter 4.9.1 and will continue until one of the heat transfer coefficient correlation limitations are reached.

The heat transfer coefficient sides of the auxiliary heat exchanger are extremely close to one another, therefore it can't be expressed with complete certainty that the tube side heat transfer coefficient will remain the controlling factor on the outcome of U_c. Thus, it's impossible to predict which of the heat transfer coefficient will have control over heat from being transferred. Therefore, it is decided that the (coolant) shell side Reynolds number will be incrementally increased from its initial value of 3.5873 [-] to the probable limit of 500 [-]. The auxiliary heat exchanger's energy balance is

$$\dot{Q}_{AUX} = \dot{m}_{ws}(\alpha_{ws,2} - \alpha_{ws,3}) = \dot{m}_{clnt} C_{p,clnt}(T_{clnt,out} - T_{clnt,in}) = U_c A_s \Delta T_{LMTD.CF}$$

Both of the individual heat exchanger models utilises the Hausen (1959) laminar flow through circular ducts Nusselt correlation and Zukauskas' (1987) tube bundle Nusselt correlation for calculating the overall heat transfer coefficient. Thus, both of the individual heat exchanger models will have the same correlation limitation, but with varying maximum mass flow rates.

Recorded in Tables 5.18 and 5.19 are the tube side and shell side correlation limitations, respectively.

Table 5.17: Tube side heat transfer coefficient correlation limitations.

Correlation Limit Parameters	Limit
Tube side: Re_t	2300 [-]
Regenerative maximum mass flow rate: $\dot{m}_{ws.max}$	1.2060 [kg/s]
Auxiliary maximum mass flow rate: $\dot{m}_{ws.max}$	2.5756 [kg/s]

Table 5.18: Shell side heat transfer coefficient correlation limitations.

Correlation Limit Parameters	Limit
Shell side: Re_s	500 [-]
Regenerative maximum mass flow rate: $\dot{m}_{ss,max}$	0.76232 [kg/s]
Auxiliary maximum mass flow rate: $\dot{m}_{clnt,max}$	0.530 [kg/s]

5.7.1 Regenerative Heat Exchanger – Overall Heat Transfer Coefficient Validation Results

Recorded in Figure 5.9 is the U_c simulation curve of the regenerative heat exchanger, which has an initial overall heat transfer coefficient of 25.949 [W/m^2.K]. The initial value of U_c is very low in comparison to the simulation limit of 125.66 [W/m^2.K], which is due to the very low shell side Reynolds number. It should be noted that these low Reynolds numbers are to be expected from the absorption-desorption cycle, which flows entirely by thermo siphoning (buoyancy flow) generated by the bubble-pump generator and differences in fluid densities.

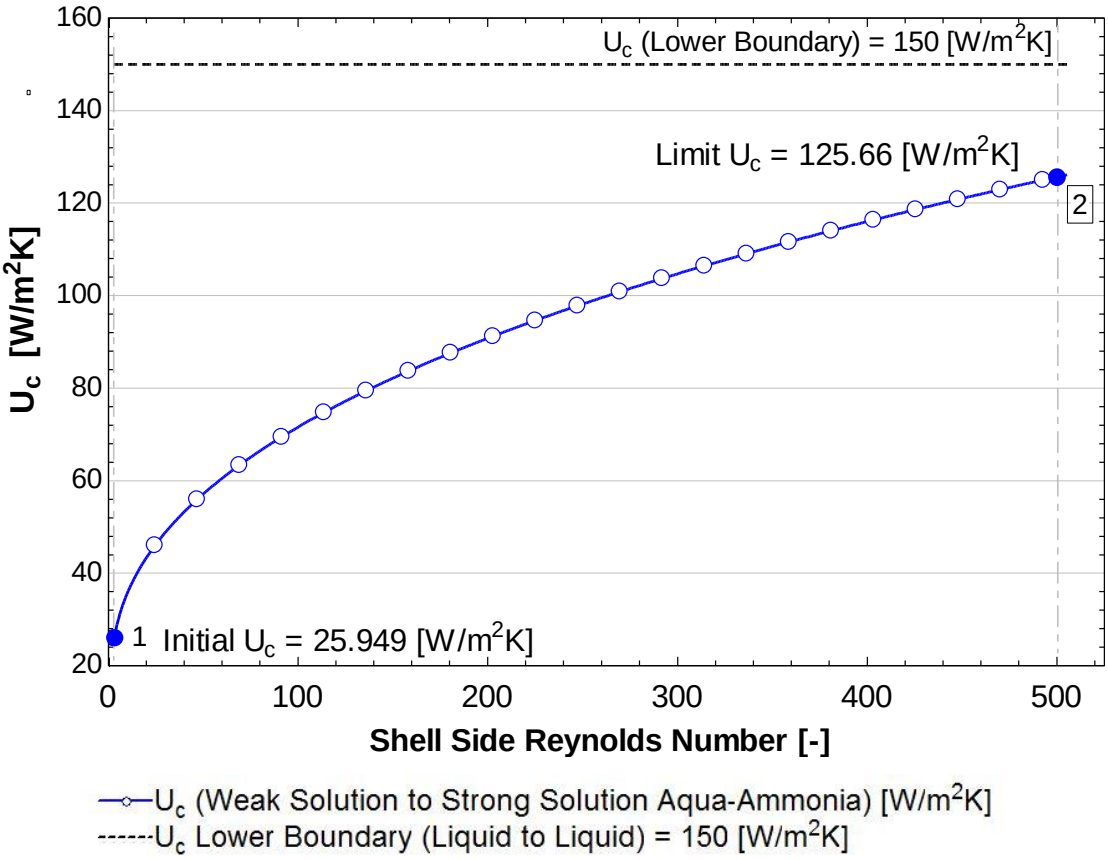

Figure 5.10: Regenerative heat exchanger – Overall heat transfer coefficient vs. shell side Reynolds number simulation model output plot.

The U_c simulation model reached the shell side heat transfer coefficient correlation limit first, with the tube side Reynolds number only reaching 1283 [-]. Results entered into Table 5.20 suggest that the controlling heat transfer coefficient has shifted towards the tube side HTC. The

222.075 [W/m^2.K] of the tube side heat transfer coefficient further strengthens the hypothesis that Hausen's (1959) Nusselt correlation for laminar flow through circular ducts has a output limit in the region of 250 to 300 [W/m^2.K].

Table 5.19: Regenerative heat exchanger – Overall heat transfer coefficient vs. shell side Reynolds number simulation model output values.

Regenerative: U_c Simulation	**1**	**2**
Tube side mass flow rate: $\dot{m}_{ws}$	0.003971 [kg/s]	0.673 [kg/s]
Tube side: Re_t	7.573 [-]	1283 [-]
Tube side HTC: h_i	68.1661 [W/m^2.K]	222.075 [W/m^2.K]
Shell side mass flow rate: $\dot{m}_{ss}$	0.004497 [kg/s]	0.7623 [kg/s]
Shell side: Re_s	2.951 [-]	500 [-]
Shell side HTC: h_o	45.224 [W/m^2.K]	352.380 [W/m^2.K]
Heat transfer rate: $\dot{Q}_{REGEN}$	293.3 [W]	49.7078 [kW]
Overall heat transfer coefficient: U_c	25.949 [W/m^2.K]	125.66 [W/m^2.K]

5.7.2 Auxiliary Heat Exchanger – Overall Heat Transfer Coefficient Validation Results

Figure 5.11 represents the overall heat transfer coefficient simulation for the auxiliary heat exchanger with the lower boundary of the typical U_c range at 150 [W/m^2.K] for liquid-to-liquid heat exchangers. The initial overall heat transfer coefficient of 30.851 [W/m^2.K] increases quite rapidly to 50 [W/m^2.K], after which it tends towards a more linear increase with increasing Re_s. The U_c simulation model reached its limit at 91.97 [W/m^2.K], which evidently occurred at the shell side heat transfer coefficient correlation limit of Re_s = 500 [-].

Presented in Table 5.22 are the results of the U_c simulation model, which clearly shows the Reynolds numbers of both sides remain in fair proximity to one another. Although, the same isn't true for the heat transfer coefficients, which started fairly close to one another. Initially the shell side heat transfer coefficient impeded heat from being transferred, but at the simulation limit it's the tube side heat transfer coefficient with the control of the overall heat transfer coefficient. The output of overall heat transfer coefficient could be further increased by substituting the shell side heat transfer coefficient of Eq. 2.18 for Eq. 2.20, which will remain valid until the tube side heat transfer coefficient correlation limit of Re_t = 2300 is reached. It's however recommended to increase both the refrigerant and coolant's mass flow rate into the transitional or turbulent regimes and opt for a correlation change for the tube side heat transfer coefficient as well. In doing so the overall heat transfer coefficient would be greatly increased well into the typical U_c ranges of liquid-to-liquid heat exchangers and inherently obtain sensible heat transfer areas.

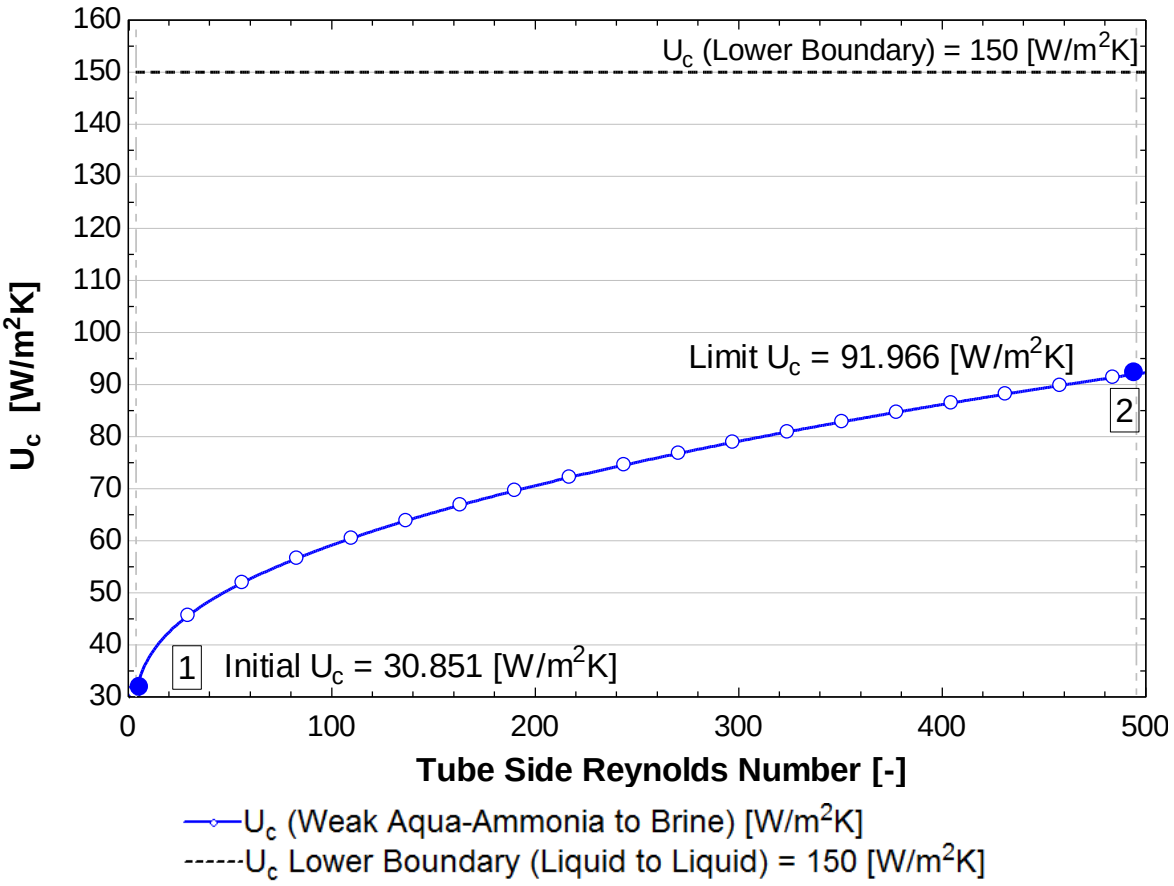

Figure 5.11: Auxiliary heat exchanger – Overall heat transfer coefficient vs. shell side Reynolds number simulation model output plot.

Table 5.20: Auxiliary heat exchanger – Overall heat transfer coefficient vs. shell side Reynolds number simulation model output values.

Auxiliary: U_c Simulation	**1**	**2**
Tube side mass flow rate: $\dot{m}_{ws}$	0.003971 [kg/s]	0.5535 [kg/s]
Tube side: Re_t	3.546 [-]	494.27 [-]
Tube side HTC: h_i	61.966 [W/m^2.K]	126.600 [W/m^2.K]
Shell side mass flow rate: $\dot{m}_{clnt}$	0.003803 [kg/s]	0.53002 [kg/s]
Shell side: Re_s	3.587 [-]	500 [-]
Shell side HTC: h_o	70.172 [W/m^2.K]	505.665 [W/m^2.K]
Heat transfer rate: $\dot{Q}_{REGEN}$	608.834 [W]	84.863 [kW]
Overall heat transfer coefficient: U_c	30.851 [W/m^2.K]	91.966 [W/m^2.K]

5.7.3 Aux-Regen Heat Exchanger – Thermodynamic Design Validation Conclusion

Although both the heat exchangers had initial and limit U_c values below the typically expected U_c range, it doesn't discredit the correlations used in determining the overall heat transfer coefficient of the auxiliary heat exchanger. The low U_c output values are expected of liquid-to-liquid heat

exchangers with extremely low mass flow rates, especially the heat exchangers of an absorption-desorption H&R cycle that isn't driven by a pump.

Furthermore, the performance ratings of both heat exchanger compartments indicate to practically viable heat exchanger temperature conditions. Therefore, it can be concluded that thermodynamic design models of Chapter 4.9 can be considered accurate and acceptable. The mechanical considerations, available in Appendix E 1, are calculated by utilising the design-sizing models of Chapter 4 sections 4.9.4 and 4.9.8 to create the manufacturing and assembly drawings of the auxiliary-regenerative heat exchanger. The manufacturing and assembly drawings of the auxiliary-regenerative heat exchanger are available in Appendix E 7.

5.8 Conclusion

In conclusion, the validation process of this chapter aimed to prove that sufficient design assumptions were made and that accurate correlations were utilised in the calculation of the thermodynamic design of the heat exchangers in an aqua-ammonia absorption-desorption H&R cycle. The overall heat transfer coefficient simulations of the stage 2 and de-superheating condensers exhibited U_c limits within the typically expected ranges of gas-to-brine heat exchanger configurations. This is attributed to the ease with which the Reynolds numbers of gaseous state fluids can increase. The remaining five heat exchangers all exhibited overall heat transfer coefficient simulation limits below the lower boundary of expected U_c ranges, which is expected from liquid-to-liquid or two-phase-to-liquid heat transfer configurations with essentially laminar flow regimes. The overall heat transfer coefficient simulation models are good indicators that accurate correlations were utilised in calculating the thermodynamic design models and that the output values of the thermodynamic designs are truthful and satisfactory.

Chapter 6

6 CLOSURE

Introduction

Chapter 6 focuses on the conclusions of this study and recommendations for future work. The conclusions are based on the knowledge and results obtained throughout the course of the study. The research project required the design of seven heat exchangers used in an aqua-ammonia absorption-desorption cycle, with the main focus on the thermodynamic design and rating. Furthermore, Chapter 6 identifies potential areas that warrant further investigation and attention.

6.1 Conclusions

The research project required for the thermodynamic design of seven heat exchangers used in an aqua-ammonia absorption-desorption heating and refrigeration cycle. The thermodynamic design requirements were set with heat transfer capacity, thermal heat exchanger efficiency, and fluid stream allocation amongst the most important requirements. The mechanical design requirements were set with safety as the highest regarded requirements.

The literature review and theoretical background study created the opportunity to extend engineering knowledge in terms of the inner workings of the aqua-ammonia absorption-desorption H&R cycle and its components. Previous research papers such as (Conde-Petit, 2004) and (Conde-Petit, 2011) provided the methods of obtaining conservative thermophysical properties, which are essential in determining the thermodynamic design of a heat exchanger. Literature and background of heat exchanger designs were found in textbooks such as (Cengel & Ghajar, 2011), (Kakaç & Liu, 2002), (Thulukakanam, 2000), and (Walker, 1990), which greatly aided the thermodynamic design and rating of the heat exchangers of this oeuvre.

The thermophysical properties of the aqua-ammonia refrigerant illustrated in Chapter 3 and Appendix B 1 were calculated using the mathematical model proposed by (Conde-Petit, 2004), where it was found that the thermophysical properties obtained fall within good accordance to the thermophysical properties obtained from EES' built-in property call function. The two-phase phenomena of aqueous ammonia was investigated, where a linear approach was adopted to determine the thermodynamic and transport properties of the two-phase region. The linear approach was applied to the evaporator's latent region as well, where sub-cooled liquid undergoes a sudden phase change as it passes through the venturi nozzle.

The preliminary thermodynamic design of each heat exchanger resulted with the required length of the tubes, whereby the sized heat exchanger could then undergo a performance rating to determine whether the heat exchanger's assumed outlet temperatures are satisfactory. The performance rating of the heat exchangers revealed that each heat exchanger falls within the expected efficiencies of standard counter/cross-flow heat exchangers. Therefore, the performance rating indicated that the inlet and outlet temperature conditions of the heat exchangers are sufficient. After the preliminary design's boundary conditions were confirmed the thermodynamic design could undergo a verification process of heat transfer rate comparison. The verification process pitted the heat transfer rates of equations 2.1 & 2.4 against each other with good accordance, but further validation was required to prove accurate correlations were utilised in the calculation of each heat exchanger's sizing model.

The validation process brought forth the conclusion that laminar flow regimes are exceptional at transferring heat at high thermal efficiencies, but does occur at the cost of heat transfer surface area. The overall heat transfer coefficient simulation models produced limit values

that are in good accordance to the standard expected U_c ranges, where all the heat exchangers exhibited U_c simulation limits near the lower boundary of the standard expected U_c ranges. These standard expected ranges of overall heat transfer coefficients are available at (Blackmonk Engineering, 2009), (Engineers Edge, 2016), (H&C Heat Transfer Solutions, 2014), (Engineering Page, 2016). The U_c simulation model and its limits were used as an indicator to determine whether the initial U_c value (which is the overall heat transfer coefficients of the sized heat exchangers in Chapter 4) is calculated with shell and tube side heat transfer coefficient correlations that provide accurate and satisfactory results.

Furthermore, the validation process of the stage 1 and 2 condenser produced results that supported the initial assumptions of separating the two-phase region of state 4 to 5 into two segments. The comparison of the 99 wt% aqua-ammonia to the 90 wt% aqua-ammonia supported the initial hypothesis that the stage 1 condenser can be treated as a latent condensing heat exchanger and the stage 2 condenser can be treated as a gaseous state cooling heat exchanger. The comparison between condensing aqua-ammonia and pure ammonia supported the hypothesis that the thermodynamic design of the two-phase region can't be approached with pure ammonia thermophysical properties. The mean temperature difference versus log mean temperature difference comparison of the Nusselt correlation for laminar film condensation produced encouraging results that the laminar film condensation Nusselt correlation is better represented by the counter-flow log mean temperature difference. Now, with the validation process and the sizing of the heat exchangers complete it was possible to complete the mechanical design of the heat exchangers.

The mechanical considerations were based on first order principle calculations to ensure the safe operation of the heat exchangers under 1.5 times its operating conditions. The mechanical considerations produced the necessary material requirements for the CAD design of the seven heat exchangers, which included manufacturing drawings of non-standard components and assembly drawings of each heat exchanger. Thus, concluding the design of the heat exchangers for a solar-powered aqua-ammonia absorption-desorption heating and refrigeration package unit.

6.2 Recommendations

Based on the results of this study the following thermodynamic design and rating aspects were identified as potential areas that warrant further research to expand the limited knowledge of:

- The two-phase region of aqua-ammonia solutions requires further investigation particularly into the experimental analysis of the stage 1 and 2 condensers to improve the thermodynamic design of condensing heat exchangers using aqua-ammonia as refrigerant.

- The laminar film evaporation of aqua-ammonia under partial pressure requires further research to formulate an undisputed heat transfer coefficient correlation for the thermodynamic design of boiling heat exchangers using aqua-ammonia as refrigerant.
- Further investigation is required into the thermophysical properties of superheated aqua-ammonia vapour as there are no mathematical models to predict the exact thermophysical properties beyond saturated aqua-ammonia vapour. These thermophysical properties are essential for the thermodynamic design of pre-condenser cooling heat exchangers.
- The designed heat exchangers of this oeuvre should be applied to an experimental aqua-ammonia absorption-desorption H&R package unit to truly evaluate the validity of the thermodynamic design models.

Based on the conclusions made of this study the following was identified as potential areas that require further attention to complete the experimental setup of the solar-powered aqua-ammonia absorption-desorption heating and refrigeration package unit.

- As the operating pressure of the aqua-ammonia absorption-desorption cycle exceeds the SABS standard for non-pressure vessels at 400 [kPa], it's recommended that the heat exchangers are certified before pressure testing commences.
- The pressure testing process for all of the manufactured heat exchangers can be completed using two accepted methods, namely, hydrostatic and pneumatic pressure tests. The first method involves filling the heat exchanger vessel with a liquid, usually water, and applying pressure with compressed air or nitrogen. The second method involves filling the heat exchanger vessel with compressed air or nitrogen to test the vessels capability to withhold the pressure. The hydrostatic method of pressure testing a heat exchanger vessel is the preferred method since it's relatively safe in comparison to a pneumatic pressure test. The heat exchanger vessel should be able to withstand 1.5 times the maximum operating pressure.
- An integrated control system is required to control the coolant mass flow rates that manipulate the temperatures and mass flow rates of the aqua-ammonia absorption-desorption cycle. The control system for the heat exchangers can be coded using the EES mathematical models to determine the thermophysical properties in addition with the EES design verification model of each heat exchanger.

Finally but most importantly, the thermodynamic design models in this oeuvre can be implemented in designing heat exchangers that utilise aqua-ammonia refrigerant.

LIST OF REFERENCES

29CFR1910.119, O., 1992. *Process Safety Management of Highly Hazardous Chemicals 29CFR1910.119*. Washington, DC: Occupational Health and Safety Administration.

Agency for Toxic Substances & Disease Registry, 2014. [Online] Available at: http://www.atsdr.cdc.goc/MHM/mhmi_v1_2_3.pdf [Accessed 29 April 2015].

Althouse, A.D., Turnquist, C.H. & Bracciano, A.F., 1992. Modern Refrigeration and Air Conditioning. South Holland, Illinois: The Goodheart-Willcox Company. pp.611-631; 1005-1029.

ASHRAE, 1994. Safety Code for Mechanical Refrigeration. *American Society of Heating, Refrigeration and Air-conditioning Engineers*, pp.std 15-94.

ASHRAE, 2001. Thermodynamics and refrigeration cycles. *The American Society of Heating, Refrigeration and Air-Conditioning Engineers, Inc*, ASHRAE Handbook Fundamentals SI Edition(U.S.A. ASHRAE), p.Chapter 1.

Blackmonk Engineering, 2009. *Overall Heat Transfer Coefficients*. [Online] Available at: http://www.blackmonk.co.uk/2009/10/22/overall-heat-transfer-coefficients/ [Accessed 17 June 2016].

Borgnakke, C. & Sonntag, R., 2009. *Fundamentals of Thermodynamics*. 7th ed. Hoboken: John Wiley & Sons.

Britannica, 2006. [Online] Available at: https://global.britannica.com/technology/heat-exchanger [Accessed 27 March 2016].

Budynas, R.G. & Nisbett, J.K., 2011. *Shigley's Mechanical Engineering Design*. 9th ed. Singapore: McGraw-Hill.

Butterworth, D., 1977. Developments in the design of shell and tube condensers. *ASME Winter Annual Meeting*, ASME Preprint 77-WA/HT-24.

Cengel, Y. & Ghajar, A., 2011. Fundamentals and Application. In *Heat and Mass Transfer*. 4th ed. New York: McGraw-Hill. pp.Chapter 6 (373-408); Chapter 7 (417-437); Chapter 8 (466-518); Chapter 11 (630-681).

Conde-Petit, M.R., 2004. [Online] M. Conde Engineering Available at: http://www.mrc-eng.com/news.htm [Accessed 10 May 2015].

Conde-Petit, M.R., 2011. [Online] M. Conde Engineering Available at: http://www.mrc-eng.com/news.htm [Accessed 10 May 2015].

Cooper, M.G., 1984. Heat Flow Rates in Saturated Nucleate Pool Boiling - A Wide Ranging Examination using Reduced Properties. In J.P. Hartnett & T.F. Irvine, eds. *Advances in Heat Transfer*. 16th ed. Princeton: Academic Press. pp.157-239.

Cornwell, K., 1989. The Influence of Bubbly Flow on Boiling from Tube in a Bundle. In *Advances in Pool Boiling Heat Transfer*. 1112th ed. Paderborn: Eurotherm No.8. pp.177-84.

Dossat, R., 1984. Principles of Refrigeration. In *Absorption Refrigeration*. 4th ed. New York: John Wiley and Sons. pp.225-43.

Edwards, J.E., 2008. Teeside, UK.: P&I Design LTD.

El-Sayed, Y.M. & Tribus, M., 1985. Thermodynamic Properties of Water-Ammonia Mixtures. In *Theoretical Implementation for Use in Power Cycles Analysis, ASME-AES - Vol. 1 - Analysis of Energy Systems*. pp.17-22, 89-95.

Engineering Page, 2016. [Online] Available at: http://www.engineeringpage.com/technology/thermal/transfer.html [Accessed 17 June 2016].

Engineeringtoolbox, 2015. [Online] Available at: http://www.engineeringtoolbox.com/orifice-nozzle-venturi-d_590.html [Accessed 18 Augustus 2015].

Engineers Edge, 2016. *Overall Heat Transfer Table*. [Online] Available at: http://www.engineersedge.com/thermodynamics/overall_heat_transfer-table/htm [Accessed 17 June 2016].

Fenghour, A. & al, e., 1995. The Viscosity of Ammonia. J. Phys. Chem. Ref. Data. pp.24(5), 1649-1667.

Forley, G., 2000. [Online] Advanced Building Systems Available at: www1.eere.energy.gov/manufacturing/distrubutedenergy/pdfs/absorption_future.pdf [Accessed 14 January 2014].

Gnielinski, V., 1976. New equations for heat and mass transfer in turbulent pipe and channel flow. *Int. Chem. Eng.*, 16, p.359.

Gnielinski, V., 1983. Forced convection ducts. In E.U. Schlünder, ed. *Heat Exchanger Design Handbook*. Washington, D.C: Hemisphere. pp.2.5.1-.3.

H&C Heat Transfer Solutions, 2014. *Coefficients*. [Online] Available at: http://www.hcheattransfer.com/coefficients.html [Accessed 17 June 2016].

Haar, L. & Gallagher, J.S., 1978. Thermodynamic properties of Ammonia. *Journal of Physical and Chemical Reference Data*, pp.635-792.

Hausen, H., 1959. Neue Gleichungen für die Warmeübertragung bei freier oder erzwungener Stromung. pp.9, 75.

Hibbeler, R.C., 2010. *Engineering Mechanics - Statics*. 12th ed. Singapore: Pearson.

HRS Heat Exchangers, 2016. [Online] Available at: http://www.hrs-heatexchangers.com/en/products/components/corrugated-tube-heat-exchangers/hrs-g-series/default.aspx [Accessed 27 March 2016].

IAPWS, 1997. Release on the IAPWS Industrial Formulation 1997 for Thermodynamic Properties of Water and Steam. *The International Association for Properties of Water and Steam*, (IAPWS, London).

Ibrahim, O.M. & Klein, S.A., 1993. Thermodynamic Properties of Ammonia-Water Mixtures. In *ASHRAE Transactions, 99*. pp.1495-502.

Indiamart, 2016. [Online] Available at: http://www.indiamart.com/arhtechnologies/plate-heat-exchanger.html [Accessed 27 March 2016].

Jiawei-Phe, 2016. [Online] Available at: www.jiawei-phe.com/Gasket-Plate-Heat-Exchanger.html [Accessed 27 March 2016].

Kakaç, S. & Liu, H., 2002. Heat Exchangers Selection, Rating, and Thermal Design. In *Chapter 8: Shell and Tube Heat Exchanger*. 2nd ed. Boca Raton: CRC Press LLC. pp.283-348.

Kays, W.M. & Perkins, H.C., 1972. Handbook of Heat Transfer. New York: McGraw-Hill. p.Chap 7.

Kern, D.Q., 1950. *Process Heat Transfer*. New York: McGraw-Hill.

Kern, D.Q., 1958. In *Mathematical development of loading in horizontal condensers*. AIChE J. p.157.

Laesecke, A. & al, e., 1999. Viscosity measurements of Ammonia, R32, and R134a. In *Vapor Buoyancy and Radial Accelaration in Capillary Viscometers*. Int. J. Thermophysics. pp.20(2), 401-434.

Martin, H., 1992. *Heat Exchangers*. 1st ed. New York: Hemisphere Publishing Corporation.

Mason, E.A. & Saxena, C.S., 1958. Physics of Fluids. p.361.

Moody, L.F., 1994. Friction factor for pipe flow. *ASME*, pp.66, 671.

N.I.S.T, 2016. *Standard Reference Data*. [Online] Available at: http://www.nist.gov/srd/nist23.cfm [Accessed 27 March 2015].

Nusselt, W., 1916. In *The condensation of steam on cooled surfaces*. Z.d. Ver. Deut. Ing. pp.60, 541.

Pátek, J. & Klomfar, J., 1995. Simple functions for fast calculations of selected thermodynamic properties of the ammonia-water system. Int. J. Refrig. pp.18(4), 228-234.

Perez-Blanco, H., 1988. *A Model of an Ammonia-Water Falling Film Absorber*. ASHRAE Tranactions, Vol 95(1), 467-483.

Perry, R.H. & Chilton, C.H., 1973. *Chemical Engineers' Handbook*. 5th ed. New York: McGraw-Hill.

Pinevic, G., 1948. Kholodilnaya Teknika. pp.Reproduced in Kaltetecnik, 1950(1), 29-30.

Rohsenow, W.M., 1952. A Method of Correlating Heat Transfer Data for Surface Boiling of Liquids. *ASME Transactions*, 74, pp.969-75.

Sassen, C.L., van Kwartel, R.A.C., van der Kooi, H.J. & de Swan Arons, J., 1990. Liquid Equilibria for the System Ammonia-Water up to Critical Region. J. Chem. Eng. Data. pp.140 - 144.

Shah, R.K. & Bhatti, M.S., 1987. Laminar convective heat transfer in ducts. In S. Kakac, R.K. Shah & W. Aung, eds. *Handbook of Single-Phase Convective Heat Transfer*. New York: John Wiley & Sons. p.Chap 3.

Srikhirin, P., Aphornratana, S. & Chungpaibulpatana, S., 2001. A review of absorption refrigeration technologies.. In *Chapter 5 Renewable & sustainable energy reviews*. pp.343-72.

Stoecker, W. & Jones, J., 1983. Refrigeration and Air Conditioning. In *Chapter 17 Absorption Refrigeration*. 2nd ed. New York: McGraw-Hill. pp.328-51.

Thevenot, R., 1979. *A History of Refrigeration Throughout the World*. Paris: International Institute of Refrigeration (IIR).

Thulukakanam, K., 2000. *Heat Exchanger Design Handbook*. 1st ed. New York: Taylor & Franscis.

Tilner-Roth, R. & Friend, D.G., 1998. A Helmoltz Free Energy Formulation of the Thermodynamic Properties of Mixture

Tilner-Roth, R. & Friend, D.G., 1998. Survey and Assesment of Available Measurrements on Thermodynamic Properties of the Mixture

Tomczyk, J.A., Silberstein, E., Whitman, W.C. & Johnson, W.M., 2016. *Refrigeration and Air Conditioning Technology*. 8th ed. Boston: Cengage Learning.

Vicatos, G., n.d. *Design of absorption refrigeration machines*. Mechanical Engineering Dpt, University of Cape Town, South Africa, Tel: 021 650 2492.

Walker, G., 1990. *Industrial Heat Exchangers: A Basic Guide*. 2nd ed. New York: Hemisphere Publishing Corporation.

Wassiljewa, A., 1904. Physik Zeitschrift. pp.Chapter 5, 737.

White, F.M., 2011. *Fluid Mechanics*. 7th ed. New York: McGraww-Hill.

Wolverine Tube Inc, 2014. *Heat Transfer Databook*. [Online] Available at: http://www.wlv.com/wp-content/uploads/2014/06/data/db3ch7.pdf [Accessed 27 Augustus 2015].

Wolvering Tube Inc, 2014. *Heat Transfer Databook*. [Online] Available at: http://www.wlv.com/wp-content/uploads/2014/06/data/db3ch9.pdf [Accessed 27 Augustus 2015].

Ziegler, B., 1982. Wärmetransforamtion durch einstifige Sorptionsprozisse mit dem Stoffpaar Ammoniak - Wasser. (Dissertation ETH Zürich Nr. 7070).

Zukauskas, A., 1987. Heat Transfer from Tubes on Cross Flow. In R.K. Kakac, R.K. Shah & W. Aung, eds. *Handbook of Single Phase Convective Heat Transfer*. New York: Wiley Interscience.

The appendices are available in electronic format only on the compact disc (CD) below.

Appendix A

Extended Chapter 2 – Literature Review and Theoretical Background Study

Summary

Compiled within Appendix A is the omitted literature and theoretical background from Chapter 2 that is required to complete the design of a heat exchanger. The literature surveyed will be divided into the following categories:

- Thermophysical properties of aqua-ammonia solutions.
- Thermophysical properties of ethylene glycol solutions.
- Thermodynamic design and rating.
- Mechanical design rating and considerations
- Occupational health and safety of an aqua-ammonia absorption-desorption cycle.

Table of Contents

List of Tables

List of Figures

1 EXTENDED LITERATURE REVIEW AND THEORETICAL BACKGROUND STUDY

1.1 Thermophysical Properties of Aqua-Ammonia Solutions

Fundamental Parameters of Pure Substances

Table A.1 contains the parameters of the pure substances, namely, ammonia and water, which will be used in the determination of thermophysical property equations.

Table A.1: Fundamental parameters of ammonia and water (Conde-Petit, 2004).

	H_2O	NH_3
T_{crit} [K]	647.14	405.4
P_{crit} [bar]	220.64	113.336
ρ_{crit} [kg/m^3]	322	225
M [kg/kmol]	18.015268	17.03026

According to Conde-Petit (2004), the simplified formulation proposed by Patek and Klomfar in (Pátek & Klomfar, 1995) can be used to determine the thermodynamic properties of the saturated liquid and saturated vapour phase of a mixture. These equations, though completely empirical, they allow for the calculation of properties of the ammonia-to-water mixture with accuracy conservative enough to be considered acceptable for thermodynamic design calculations.

Temperature for saturated liquid and vapour aqua-ammonia solutions can be calculated as

$$T(P,x) = T_o\left(\sum_i A_i (1-x)^{mi} \left[\ln\left(\frac{Po}{P}\right)\right]^{ni}\right) \qquad [K]\,, \tag{A.1}$$

with equation parameters (m_i, n_i, and A_i) are available in Tables A.2 and A.3.

Enthalpy for saturated aqua-ammonia liquid mixtures can be approximated as

$$\alpha_l(T,x) = \alpha_o \sum_i A_i \left(\frac{T}{To} - 1\right)^{mi} * (x^{ni}) \qquad \left[\frac{kJ}{kg}\right], \tag{A.2}$$

where its equation parameters are illustrated in Table A.4.

Now, the enthalpy for saturated vapour mixtures is

$$\alpha_v(T,x) = \alpha_o \sum_i A_i \left(1 - \frac{T}{To}\right)^{mi} * (1-x)^{ni/4} \qquad \left[\frac{kJ}{kg}\right], \tag{A.3}$$

with the equation parameters as shown in Table A.5.

Lastly, the molar concentration, used to determine the transport properties of a saturated vapour mixture can be calculated as

$$y(P,x) = 1 - \exp\left(ln(1-x)\sum_i A_i \left(\frac{P}{P_0}\right)^{mi} * x^{\frac{n_i}{3}}\right) \quad [-] \tag{A.4}$$

and the equation parameters as illustrated in Table A.6. The following tables demonstrate the required parameters to determine the thermodynamic properties for the abovementioned saturated aqua-ammonia mixtures.

Table A.2: Saturated aqua-ammonia liquid temperature parameters (Conde-Petit, 2004).

i	m_i	n_i	A_i
1	0	0	3.22302
2	0	1	-0.384206
3	0	2	0.0460965
4	0	3	-0.00378945
5	0	4	0.00013561
6	1	0	0.487755
7	1	1	-0.120108
8	1	2	0.0106154
9	2	3	-0.000533589
10	4	0	7.85041
11	5	0	-11.5941
12	5	1	-0.052315
13	6	0	4.89596
14	13	1	0.0421059
T_0 = 100 K			P_0 = 2000 kPa

Table A.3: Saturated aqua-ammonia vapour temperature parameters (Conde-Petit, 2004).

i	m_i	n_i	A_i
1	0	0	3.24004
2	0	1	-0.395
3	0	2	0.043562
4	0	3	-0.00219
5	1	0	-1.43526
6	1	1	1.05256
7	1	2	-0.07193
8	2	0	12.2362
9	2	1	-2.24368
10	3	0	-20.178
11	3	1	1.10834
12	4	0	14.5399
13	4	2	0.644312
14	5	0	-2.21246
15	5	2	-0.75627
16	6	0	-1.35529
17	7	2	0.183541
T_0 = 100 K			P_0 = 2000 kPa

Table A.4: Saturated aqua-ammonia liquid enthalpy parameters (Conde-Petit, 2004).

i	m_i	n_i	A_i
1	0	1	-7.6108
2	0	4	25.6905
3	0	8	-247.092
4	0	9	325.952
5	0	12	-158.854
6	0	14	61.9084
7	1	0	11.4314
8	1	1	1.18157
9	2	1	2.84179
10	3	3	7.41609
11	5	3	891.844
12	5	4	-1613.09
13	5	5	622.106
14	6	2	-207.588
15	6	4	-6.87393
16	8	0	3.50716
T_0 = 273.15 K			**α_0 = 100 kJ/kg**

Table A.5: Saturated aqua-ammonia vapour enthalpy parameters (Conde-Petit, 2004).

i	m_i	n_i	A_i
1	0	0	1.28827
2	1	0	0.125247
3	2	0	-2.08748
4	3	0	2.17696
5	0	2	2.35687
6	1	2	-8.86987
7	2	2	10.2635
8	3	2	-2.3744
9	0	3	-6.70155
10	1	3	16.4508
11	2	3	-9.36849
12	0	4	8.42254
13	1	4	-8.58807
14	0	5	-2.77049
15	4	6	-0.96125
16	2	7	0.988009
17	1	10	0.308482
T_0 = 324 K			**α_0 = 1000 kJ/kg**

Table A.6: Molar concentration of saturated aqua-ammonia parameters (Conde-Petit, 2004).

i	m_i	n_i	A_i
1	0	0	19.8022017
2	0	1	-11.8092669
3	0	6	27.747998
4	0	7	-28.8634277
5	1	0	-59.1616608
6	2	1	578.091305
7	2	2	6.21736743
8	3	2	-3421.98402
9	4	3	11940.3127
10	5	4	-24541.3777
11	6	5	29159.1865
12	7	6	-18478.229
13	7	7	23.4819434
14	8	7	4803.10617
			P_0 = 2000 kPa

The numerical mathematical method proposed by (Conde-Petit, 2004) is considerably simpler than the formulation adopted by the IAPWS of which is based upon the equations developed by (Tilner-Roth & Friend, 1998) and (Ziegler, 1982). According to Conde-Petit (2004), the fore mentioned equations can be effortlessly solved both implicitly and explicitly. Recorded in Table A.7 are the comparisons of enthalpy at saturated liquid and vapour of the fore mentioned equations and the results obtained from EES. The comparisons of the two methods are made with a 99 wt% aqua-ammonia solution and are within acceptable range to one another, thus boasting well for the mathematical method.

Table A.7: Enthalpy comparison of EES and the (Conde-Petit, 2004) mathematical method.

Saturated Liquid Enthalpy Comparison			
Pressure [kPa]	EES	Mathematical Method	Δ [%]
510.8	15.89 [kJ/kg.K] @ 5°C	11.1974 [kJ/kg.K] @ 5°C	29.53
721.3	62.66 [kJ/kg.K] @ 15°C	58.198 [kJ/kg.K] @ 15°C	7.121
933.4	100.7 [kJ/kg.K] @ 23°C	96.515 [kJ/kg.K] @ 23°C	4.156

Saturated Vapour Enthalpy Comparison			
Pressure [kPa]	EES	Mathematical Method	Δ [%]
515.84	1397 [kJ/kg.K] @ 50.26°C	1384.2 [kJ/kg.K] @ 47.68°C	0.9163
727.25	1405 [kJ/kg.K] @ 58.03°C	1391.1 [kJ/kg.K] @ 54.61°C	0.9893
939.54	1410 [kJ/kg.K] @ 64.11°C	1395.7 [kJ/kg.K] @ 60.05°C	1.014

Critical Temperature and Pressure of Ammonia – Water Solution

The formulation of the equations to determine the critical temperature and pressure is derived from (Sassen et al., 1990), furthermore the critical temperature and pressure of a mixture solution is dependent on its concentration. The critical temperature of the aqua-ammonia is formulated as

$$T_{crit,mix} = \sum_{i}^{4} A_i * x^i \quad [K], \tag{A.5}$$

with the parameters of A_i demonstrated in Table A.8. The critical temperatures of 0.99 mass concentration of aqua-ammonia was determined at 408.87 [K] and for the 0.99 molar concentration of ammonia in water at 405.52 [K].

Table A.8: Critical temperature parameters of aqua-ammonia mixtures (Conde-Petit, 2004).

i	A_i
0	647.14
1	-199.822371
2	109.035522
3	-239.626217
4	88.689691

The critical pressure of ammonia – water mixture can be formulated as

$$P_{crit,mix} = \sum_{i}^{4} B_i * x^i \quad [bar] \tag{A.6}$$

and the parameters of B_i are shown in Table A.9.

Table A.9: Critical pressure parameters of aqua-ammonia mixtures (Conde-Petit, 2004).

i	B_i
0	220.64
1	-37.923795
2	36.424739
3	-41.851597
4	-63.805617

The critical pressure is calculated as 113.584 [bar] for 99 wt% ammonia in water.

1.1.1 Specific Thermal Capacity of Saturated Aqua-Ammonia Liquid

Conde-Petit (2004) adopted a practical approach by considering the solution as quasi-ideal for the calculation of specific thermal capacity, that showed to be in good agreement with values obtained by (Tilner-Roth & Friend, 1998). The equation set used to calculate specific thermal capacity starts

with the calculation of theta in Eq. A.7, which represents the temperature of the solution and its critical temperature as a fraction.

$$\theta \equiv \frac{T_{mix}}{T_{crit,mix}} = \frac{T_{NH3}}{T_{c,NH3}} = \frac{T_{H2O}}{T_{c,H2O}} \quad \textbf{(A.7)}$$

Using the mixture temperature fraction, the saturated liquid dimensionless temperature fraction is calculated as:

$$\tau = 1 - \theta \quad \textbf{(A.8)}$$

The specific thermal capacity of pure ammonia and water are calculated as:

$$Cp_T = A_{cp} + B_{cp} * \tau^{-1} \quad \textbf{(A.9)}$$

The values for saturated liquid specific thermal capacity is calculated by using parameters for pure substances obtained on the basis of (IAPWS, 1997) for water and data by (Haar & Gallagher, 1978), as demonstrated in Table A.10.

Table A.10: Saturated liquid specific thermal capacity parameters of pure substances.

	Equation Parameters	
	A_{Cp}	B_{Cp}
NH_3	3.875648	0.242125
H_2O	3.665785	0.236312

Finally, the saturated liquid specific thermal capacity of the mixture can be calculated using

$$Cp_l = x * Cp_{T,NH3} + (1-x)Cp_{T,H2O} \quad \left[\frac{kJ}{kg.K}\right] \quad \textbf{(A.10)}$$

1.1.2 Specific Thermal Capacity of Saturated Aqua-Ammonia Vapour

Specific thermal capacity of saturated vapour aqua-ammonia is determined with an ideal solution of real gases, which would require the use of the molar concentration as calculated in Eq. A.4. Derived from the examples in (Conde-Petit, 2004), a new solution temperature fraction (*Θ*) is required to determine the saturated vapour temperature fraction of Eq. A.7. The saturated vapour temperature fraction is determined with the solution vapour temperature calculated by Eq. A.1, and then substituting into Eq. A.7. Conde-Petit (2004) suggested that the values of specific thermal capacity of pure ammonia and water, at saturated vapour state, are calculated by using

$$Cp_T = A + B\tau^{-\frac{1}{3}} + C\tau^{-\frac{2}{3}} + D\tau^{-\frac{5}{3}} + E\tau^{-\frac{7.5}{3}} \quad \textbf{(A.11)}$$

The parameters for A to E were obtained from (Haar & Gallagher, 1978) for pure ammonia, and for water from (IAPWS, 1997). The equation parameters are illustrated in Table A.11.

Table A.11: Saturated vapour specific thermal capacity parameters of pure substances.

	Equation Parameters				
	A	**B**	**C**	**D**	**E**
NH_3	-1.1991971	1.240129495	0.924818752	0.0182	0.00024503
H_2O	3.46182565	-4.987788063	2.99438177	0.006259	-8.263E-06

Lastly, the specific thermal capacity of the saturated vapour solution is determined by using

$$Cp_v = y * Cp_{T,NH3} + (1-y)Cp_{T,H2O} \quad \left[\frac{kJ}{kg.K}\right] \tag{A.12}$$

1.1.3 Density of Saturated Solutions in the Liquid Phase

Conde-Petit (2004) suggested that the density of the saturated aqueous ammonia liquid is determined by assuming a quasi-ideal solution, where the equation is simply expressed as

$$\rho_l = x\left(\rho_{NH3,T_{NH3}}\right) + (1-x)\left(\rho_{H2O,T_{H2O}}\right) + \Delta\rho^*_{T_{m,x}} \quad \left[\frac{kg}{m^3}\right], \tag{A.13}$$

where the third term of Eq. A.13 represents the 'excess' density in relation to the ideal solution, and can be approximated with the function

$$\Delta\rho^*_{T_{m,x}} = [x(1-x) - Ax^2(1-x)] * (\rho^{0.5}_{NH3,T_{NH3}} * \rho^{0.5}_{H2O,T_{H2O}}) \tag{A.14}$$

Here, the parameter variable *A* is a function of the dimensionless solution temperature calculated as

$$T^*_{mix} \equiv \left(\frac{T_{mix}}{T_{c,H2O}}\right) \tag{A.15}$$

Eq. A.15 defers from Eq. A.7, where it is made dimensionless with the critical temperature of water and not the solution. Parameter variable *A* can be defined by

$$A = \sum_{i=0}^{2} A_{1,i} T^{*\,i}_{mix} + \frac{\sum_{i=0}^{2} A_{2,i} T^{*\,i}_{mix}}{x}, \tag{A.16}$$

where the A_1 and A_2 components of Eq. A.16 are illustrated in Table A.12.

Table A 12: Parameters A_1 and A_2

i	A_1	A_2
0	-2.41	2.118
1	8.31	-4.05
2	-6.924	4.443

The density of the pure substances of the aqua-ammonia mixture can be obtained from corresponding substance temperatures in Table A-11 for ammonia and Table A-9 for water in (Cengel & Ghajar, 2011), by linear interpolation method.

1.1.4 Density of Saturated Solutions in the Vapour Phase

The saturated vapour density calculations proposed by Conde-Petit (2004) are modelled to a quasi-ideal solution for real gases, with the density equation as

$$\rho_v = y\rho_{NH3,T_{NH3}} + (1-y)\rho_{H2O,T_{H2O}} + \Delta\rho^*_{T_{m,x}} \quad \left[\frac{kg}{m^3}\right] \tag{A.17}$$

The excess density can be approximated with the following functions and equation parameters for A, B, C, D, J, and K

$$\Delta\rho^*_{T_{m,x}} = A(1-y)^B\left(1-e^{Cy^D}\right)\Delta\rho_{max,T_m} \tag{A.18}$$

$$\Delta\rho_{max,T_m} = e^{J-K/T^*_m},$$

with T_m^* determined by Eq. A.15 and the input values of parameters A, B, C, D, J, and K are illustrated in Table A.13.

Table A.13: Excess density parameters (Conde-Petit, 2004).

Equation Parameters Excess Density			
A	82	**D**	2.75
B	0.5	**J**	9.952
C	-0.05	**K**	3.884

The density of pure ammonia and water can be calculated by

$$\rho_G = \rho_{crit} * \exp\left(\sum_{i=1}^{6} A_i \tau^{b_i}\right), \tag{A.19}$$

with the parameters of A_i and b_i shown in Table A.14.

Table A.15 depicts the comparison of densities at saturated liquid and saturated vapour state for 99 wt% aqua-ammonia. The comparison is drawn with the fore mentioned equations and the results obtained from EES' built-in transport property function. Density is the only transport property that EES' property call function can provide output values for a fluid higher than saturated liquid. The comparisons of the two methods are in good accordance to one another, more so with saturated liquid than with saturated vapour densities. This is due to the excess density calculation with the mathematical method.

Table A.14: Density parameters A_i and b_i of pure ammonia and water (Conde-Petit, 2004).

	H_2O		NH_3	
i	**A**	**b**	**A**	**b**
1	-2.0254501	1/3	-1.4309743	1/3
2	-2.7013142	2/3	-3.3127364	2/3
3	-5.3591618	4/3	-4.4442577	4/3
4	-17.343965	3	-16.844664	3
5	-44.618327	37/6	-37.797135	37/6
6	-64.869053	71/6	-97.828538	71/6

Table A.15: Density comparison of EES and the (Conde-Petit, 2004) mathematical method.

Saturated Liquid Density Comparison			
Pressure [kPa]	EES	Mathematical Method	Δ [%]
510.8	637.7 [kg/m^3] @ 5°C	636.998 [kg/m^3] @ 5°C	0.110
721.3	622.4 [kg/m^3] @ 15°C	622.765 [kg/m^3] @ 15°C	0.059
933.4	609.7 [kg/m^3] @ 23°C	611.081 [kg/m^3] @ 23°C	0.227

Saturated Vapour Density Comparison			
Pressure [kPa]	EES	Mathematical Method	Δ [%]
515.84	3.38 [kg/m^3] @ 50.26°C	5.289 [kg/m^3] @ 47.68°C	56.48
727.25	4.721 [kg/m^3] @ 58.03°C	6.839 [kg/m^3] @ 54.61°C	44.86
939.54	6.07 [kg/m^3] @ 64.11°C	8.089 [kg/m^3] @ 60.05°C	33.26

1.1.5 Dynamic Viscosity of Saturated Liquid Aqua-Ammonia Solutions

According to Conde-Petit (2004), the experimental data for dynamic viscosity of aqua-ammonia mixtures are scarce to say the least, with the largest set of experimental data published by (Pinevic, 1948). Conde-Petit (2004) stated that due to the large number of uncertainties reported for the measurement of dynamic viscosity the data wasn't considered for the formulation of a new calculation model. This new model is compared to (Fenghour & al, 1995) and (Laesecke & al, 1999).The dynamic viscosity model for saturated aqua-ammonia liquid can be described by the following equation as

$$\ln \mu_l = x\left(\ln\left(\mu_{NH3,T_{NH_3}}\right)\right) + (1-x)\ln\left(\mu_{H2O,T_{H_2O}}\right) + \Delta\mu(T_{mix}, x) \quad \left[\frac{kg}{m.s}\right] \qquad \textbf{(A.20)}$$

Similar to the mathematical model for density the saturated liquid dynamic viscosity model proposed in (Conde-Petit, 2004) has an excess term in the main equation, which is calculated by using the following equations.

$$\Delta\mu(T_{mix}, x) = \left(0.534 - 0.815\left(\frac{T_m}{T_{c,H2O}}\right)\right) * F(x), \quad \textbf{(A.21)}$$

with function *F(x)* as

$$F(x) = 6.38(1-x)^{1.125x}\left(1 - e^{-0.585x(1-x)^{0.18}}\right)\ln(\mu_{NH3}^{0.5} * \mu_{H2O}^{0.5})$$

The values of pure substances are obtained via a linear interpolation of data in Tables A-9 & A-11 of (Cengel & Ghajar, 2011) at the specific substance temperature as calculated by using Eq. A.7. Thus, a comparison portrayed in Table A.16 can be made for dynamic viscosity between EES' property call function and the mathematical method given in (Conde-Petit, 2004), though it should be noted that the comparison table is only valid for a 99 wt% aqua-ammonia solution at saturated liquid.

Table A.16: Dynamic viscosity comparison of EES and the (Conde-Petit, 2004) mathematical method.

Saturated Liquid Dynamic Viscosity Comparison			
Pressure [kPa]	EES	Mathematical Method	Δ [%]
515.84	0.0001651 [kg/m.s] @ 5°C	0.0001869 [kg/m.s] @ 5°C	11.66
727.25	0.0001494 [kg/m.s] @ 15°C	0.0001674 [kg/m.s] @ 15°C	10.75
939.54	0.0001384 [kg/m.s] @ 23°C	0.0001500 [kg/m.s] @ 23°C	7.733

The values of the mathematical method are slightly higher than the property model of EES, which could be due to linear interpolation of pure ammonia and water properties that are measured at saturation temperature of the pure substance. Thus, the model can be improved upon, with more accurate pure substance properties, but for purposes of this oeuvre the values obtained by the mathematical model is conservative and sufficient for the thermodynamic design calculation of Chapter 4.

1.1.6 Dynamic Viscosity of Saturated Vapour Aqua-Ammonia Solutions

Conde-Petit (2004) suggested that the dynamic viscosity of saturated vapour mixtures can be calculated using (Wassiljewa, 1904) proposed equation, but modifications introduced by (Mason & Saxena, 1958) should be taken into consideration.

$$\mu_v = \frac{y\mu_{NH3}}{y + (1-y)\varphi_{12}} + \frac{(1-y)\mu_{H2O}}{(1-y) + y\varphi_{21}} \quad \left[\frac{kg}{m.s}\right], \quad \textbf{(A.22)}$$

with

$$\varphi_{12} = \frac{\left[1 + \left(\frac{\mu_{NH3}}{\mu_{H_2O}}\right)^{0.5} \left(\frac{M_{H2O}}{M_{NH3}}\right)^{0.25}\right]^2}{\left[8\left(1 + \frac{M_{NH3}}{M_{H2O}}\right)\right]^{0.5}}$$

$$\varphi_{21} = \varphi_{21} \frac{\mu_{NH_3}}{\mu_{H_2O}} \frac{M_{NH_3}}{M_{H_2O}}$$

Note: The values of the pure substances of ammonia and water are of similar origins as that of the saturated liquid dynamic viscosity's pure substances, with the only exception being the temperature at which the values are measured. The temperatures of the substances are calculated using the molar concentration as function of temperature, i.e. Eq. A.4.

1.1.7 Thermal Conductivity of Saturated Aqua-Ammonia Liquid Solutions

Conde-Petit (2004) proposed the formulation of a quasi-ideal solution that is used to determine the thermal conductivity of saturated aqua-ammonia liquid, which corresponds to the values of thermal conductivity for pure ammonia and water and can be described with the following:

$$k_l = x\left(k_{NH3(\rho^+_{NH3})}\right) + (1-x)\left(k_{H2O(T_{H2O})}\right) \left[\frac{W}{m.K}\right], \quad \textbf{(A.23)}$$

with the density as a function of substance temperature

$$\rho^+_{NH3} = \rho_{NH3}(T_{NH3})(x^{0.425})$$

The values of pure ammonia and water are obtained with the same method as that of the dynamic viscosity for saturated liquid solutions. Although the thermal conductivity of pure ammonia is a function of density, it too is calculated with the linear interpolation method. Table A.17 demonstrates the comparison made between EES' thermal conductivity property and the mathematical method proposed in (Conde-Petit, 2004) by Eq. A.23 above. The comparison is made with a 99 wt% aqua-ammonia solution.

Table A.17: Thermal conductivity comparison of EES vs. mathematical method.

Saturated Liquid Thermal Conductivity Comparison			
Pressure [kPa]	EES	Mathematical Method	Δ [%]
515.84	0.5442 [W/m.K] @ 5°C	0.5298 [W/m.K] @ 5°C	2.646
727.25	0.5133 [W/m.K] @ 15°C	0.5072 [W/m.K] @ 15°C	1.188
939.54	0.4895 [W/m.K] @ 23°C	0.4893 [W/m.K] @ 23°C	0.0409

The comparison values are within a small delta percentage to one another, even though a linear interpolation method is used to determine the values of the pure substances for the mathematical method.

1.1.8 Thermal Conductivity of Saturated Aqua-Ammonia Vapour Solutions

According to Conde-Petit (2004), the thermal conductivity of a saturated vapour solution can be calculated using Eq. A.22, with substituting for thermal conductivity as a function of temperature and not dynamic viscosity.

$$k_v = \frac{y k_{NH_3}}{y + (1-y)\varphi_{12}} + \frac{(1-y)k_{H_2O}}{(1-y) + y\varphi_{21}} \quad \left[\frac{W}{m.K}\right], \tag{A.24}$$

with

$$\varphi_{12} = \frac{\left[1 + \left(\frac{k_{NH3}}{k_{H_2O}}\right)^{0.5} \left(\frac{M_{H2O}}{M_{NH3}}\right)^{0.25}\right]^2}{\left[8\left(1 + \frac{M_{NH3}}{M_{H2O}}\right)\right]^{0.5}}$$

$$\varphi_{21} = \varphi_{21} \frac{k_{NH_3}}{k_{H_2O}} \frac{M_{NH_3}}{M_{H_2O}}$$

The thermal conductivity values of pure ammonia and water are calculated similarly as previously discussed with the dynamic viscosity of saturated vapour solutions.

1.1.9 Prandtl Number Aqua-Ammonia Solutions

The Prandtl number was formulated by Ludwig Prandtl (1875-1953), where it is a dimensionless parameter and accounts for “the relative thickness of the velocity and thermal boundary layers” (Cengel & Ghajar, 2011). A very low Prandtl number is the result of a very high thermal conductivity.

The Prandtl number is essentially the ratio between molecular diffusivity of momentum and molecular diffusivity of heat or the ration between dissipation and conduction. The Prandtl number for fluids has a range between 0.01 to greater than 100 000. The Prandtl number for an ammonia-water mixture is a simple correlation with the specific thermal capacity, the dynamic viscosity, and thermal conductivity, which can be expressed as

$$Pr = \frac{\mu_{mix} Cp_{mix}}{k_{mix}} \quad [-] \tag{A.25}$$

Note: Eq. A.25 is valid for both the saturated liquid and saturated vapour solutions.

Hereby, completing the thermophysical properties of aqua-ammonia needed to calculate the thermodynamic design of the refrigerant working fluid. The following section will discuss the thermophysical properties of the secondary working fluid (coolant) required for the thermodynamic design of the heat exchanger for the absorption-desorption H&R cycle.

1.2 Thermophysical Properties of Ethylene Glycol Water Solutions

The thermophysical properties of brines can be calculated by mathematical models proposed in (Conde-Petit, 2011), which include specific thermal capacity, density, dynamic viscosity, thermal conductivity, and Prandtl number.

Freezing Temperature

An ethylene glycol water solution will be used as the secondary fluid (coolant) for the thermodynamic design of the absorption-desorption cycle, only variable to consider is the concentration of ethylene glycol in water. The concentration of ethylene glycol in water is dependent on the risk of freezing, thus the freezing temperature is calculated first using the following equation:

$$\frac{T_F}{273.15} = A_0 + A_1 x + A_2 x^2 \quad [K] \tag{A.26}$$

Specific Thermal Capacity, Density, and Thermal Conductivity

The specific thermal capacity, density, and thermal conductivity are all calculated by the same formula, where the property is represented by f as a function of temperature (*T*) and mass concentration (*x*) (Conde-Petit, 2011).

$$f(x,T) = A_1 + A_2 x + A_3 \left(\frac{273.15}{T}\right) + A_4 x \left(\frac{273.15}{T}\right) + A_5 \left(\frac{273.15}{T}\right)^2 \tag{A.27}$$

Dynamic Viscosity and Prandtl Number

Similar to the aforementioned properties the dynamic viscosity and Prandtl number can be calculated with the same equation, only with varying equation parameters.

$$\ln\big(f(x,T)\big) = A_1 + A_2 x + A_3 \left(\frac{273.15}{T}\right) + A_4 x \left(\frac{273.15}{T}\right) + A_5 \left(\frac{273.15}{T}\right)^2 \tag{A.28}$$

Each property to be calculated has its own set of equation parameters, of which is depicted in Table A.18. Thus, completing the thermophysical properties of the working fluids within an aqua-ammonia absorption-desorption cycle. The following section discusses the equations required to determine the sizing of the heat exchangers and their performances.

Table A.18: Equation parameters ethylene glycol water solution (Conde-Petit, 2011).

Equation Parameters						
Order	**Specific Heat C_p [kJ/kg.K]**	**Density [kg/m3]**	**Dynamic Viscosity [kg/m.s]**	**Thermal Conductivity [W/m.K]**	**Prandtl Number [-]**	**Freezing Temp [K]**
0						1.0
1	5.36449	658.49825	-4.63024	0.83818	3.96951	-0.06982
2	0.78863	-54.81501	-2.14817	-1.3762	0.70076	-0.35780
3	-2.59001	664.71643	-12.70106	-0.07629	-12.98045	
4	-2.73187	232.72605	5.40536	1.0772	2.64789	
5	1.43759	-322.6166	10.989	-0.20174	11.589	

2 EXTENDED THEORECTICAL BACKGROUND - THERMODYNAMIC DESIGN AND RATING

2.1 Basics of Heat Exchanger Design Calculations

The temperature variations of parallel- and counter-flow heat exchangers are represented in Figure A.1 (Cengel & Ghajar, 2011), and represented in Figure A.2 is the temperature versus unit surface area lines of condensing and evaporating fluids, respectively, which is extracted from (Cengel & Ghajar, 2011). The heat transfer surface area A is plotted along the *x*-axis and the temperature of the inlets and outlets plotted on the *y*-axis.

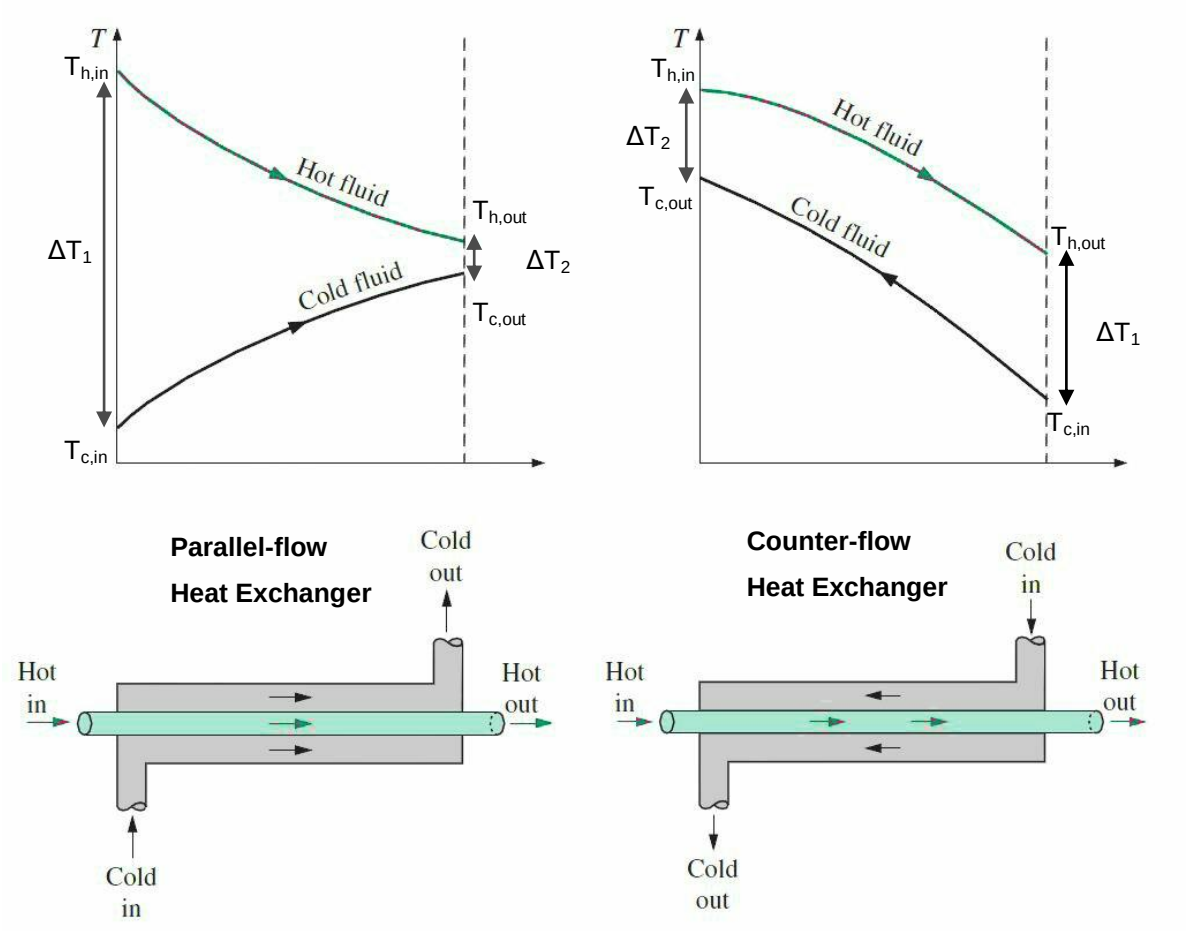

Figure A.1: Temperature vs. unit surface area of parallel- and counter-flow heat exchangers.

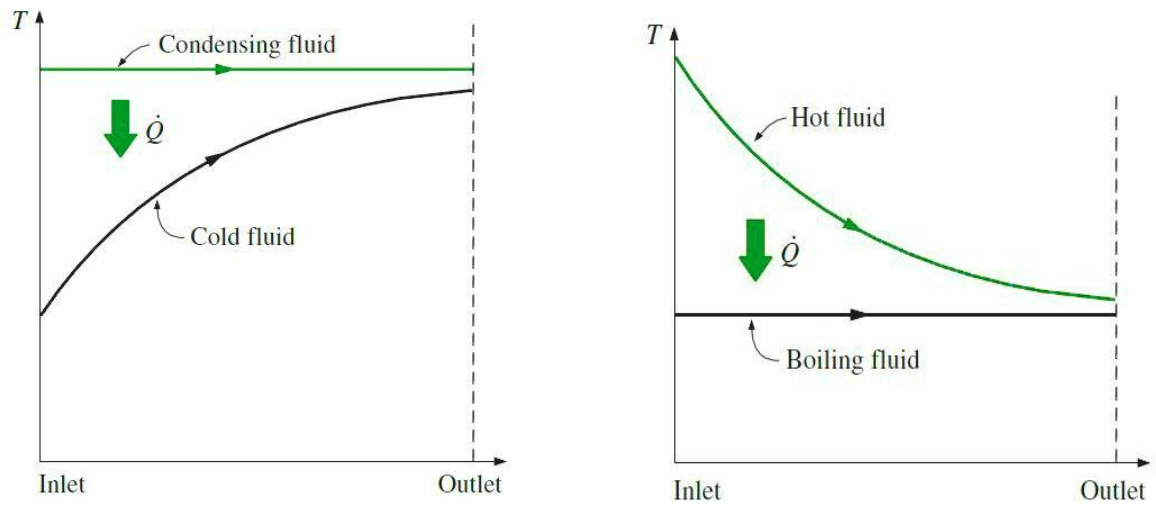

Figure A.2: Temperature vs. unit surface area of condensing and boiling heat exchangers.

2.2 Log Mean Temperature Difference Method

The log mean temperature difference can be calculated by applying a differential area to the first law of thermodynamics. As seen with Figure A.1 the temperature of the 'hot' fluid will drop by dT_h and similar with the 'cold' fluid, which rises with dT_c. Now, considering the counter-flow heat exchanger illustrated in Figure A.1, and taking the differential forms of Eq. 2.2 for 'hot' and 'cold' fluids for adiabatic steady state, single phase heat transfer, the energy balance yields step 1 (Cengel & Ghajar, 2011):

$$\delta\dot{Q} = -\left(\dot{m}\, C_p\right)_h dT_h = \pm\left(\dot{m}\, C_p\right)_c dT_c \qquad \textbf{(A.29)}$$

The heat transfer rate of δQ may also be expressed as the rate of heat transfer from the 'hot' fluid to the 'cold' fluid across the heat transfer area dA, with step 2 in the following equation:

$$\delta\dot{Q} = U(T_h - T_c)dA \qquad \textbf{(A.30)}$$

Solving Eq. 2.3 for dT_h and dT_c, results in

$$dT_h - dT_c = \delta\dot{Q}\left(\frac{1}{\dot{m}_c\, C_{pc}} - \frac{1}{\dot{m}_h C_{ph}}\right) \qquad \textbf{(A.31)}$$

Now, substitute Eq. A.6 into Eq. A.5 and rearranging it gives

$$\frac{d(T_h - T_c)}{T_h - T_c} = U\left(\frac{1}{\dot{m}_c\, C_{pc}} - \frac{1}{\dot{m}_h C_{ph}}\right)dA\ , \qquad \textbf{(A.32)}$$

which when integrated from inlet of the heat exchanger to the outlets with constant values for overall heat transfer coefficient, mass flow rates, and specific thermal capacity, results in

$$\ln\left(\frac{T_{h,out}-T_{c,in}}{T_{h,in}-T_{c,out}}\right)= UA\left(\frac{1}{\dot{m}_c\, C_{pc}}-\frac{1}{\dot{m}_h C_{ph}}\right) \quad \textbf{(A.33)}$$

Finally, solving Eq. 2.2 for 'hot' and 'cold' fluids, substituting into Eq. A.33 and after some rearrangement gives

$$\Delta T_{LMTD,CF}=\frac{\left(T_{h,out}-T_{c,in}\right)-\left(T_{h,in}-T_{c,out}\right)}{\ln\left(\frac{T_{h,out}-T_{c,in}}{T_{h,in}-T_{c,out}}\right)} \quad \textbf{(A.34)}$$

It can be shown that for parallel-flow HTEX, Eq. A.9 becomes

$$\Delta T_{LMTD}=\frac{\left(T_{h,in}-T_{c,in}\right)-\left(T_{h,out}-T_{c,out}\right)}{\ln\left(\frac{T_{h,in}-T_{c,in}}{T_{h,out}-T_{c,out}}\right)} \quad \textbf{(A.35)}$$

Log mean temperature differences have thus far been limited to parallel- and counter-flow heat exchanger arrangements. For the arrangements of cross-flow and multi-pass heat exchanger a correction factor *F* is required. The log mean temperature difference of cross-flow or multi-pass heat exchangers can be expressed as

$$\Delta T_{LMTD}=F\Delta T_{LMTD,CF} \quad \textbf{(A.36)}$$

The correction factor charts illustrated in Figure A.3 requires the calculation of two temperature ratios, namely, *P* and *R*, which are defined as:

$$P=\frac{T_{c,out}-T_{c,in}}{T_{h,in}-T_{c,in}} \quad \textbf{(A.37)}$$

$$R=\frac{T_{h,in}-T_{h,out}}{T_{c,out}-T_{c,in}} \quad \textbf{(A.38)}$$

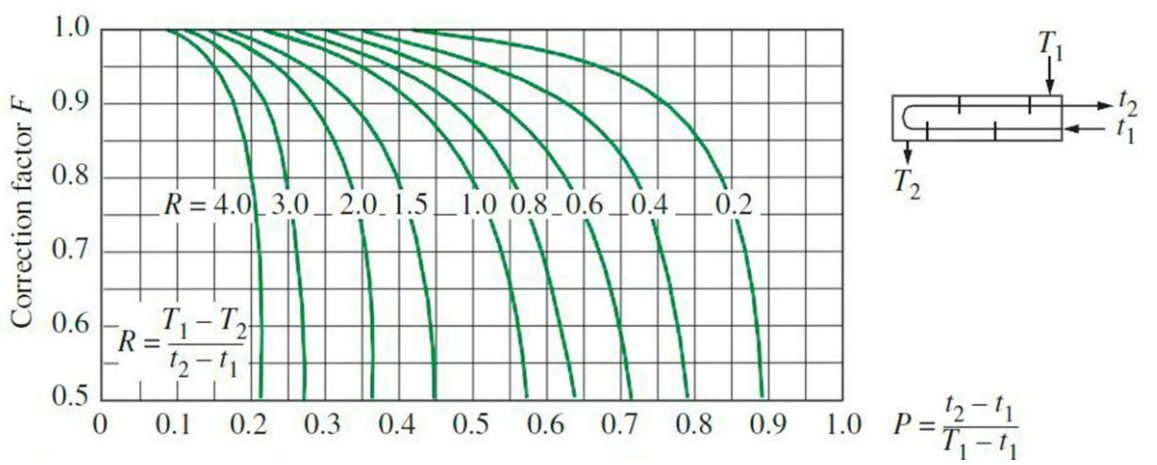

(a) One-shell pass and any multiple of 2 tube passes

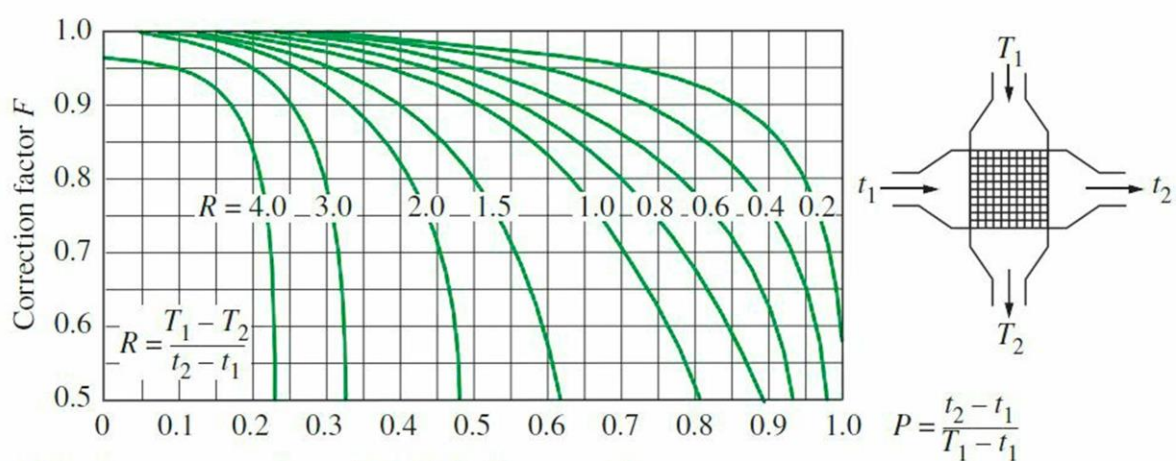

(b) Single-pass cross-flow with both fluids unmixed

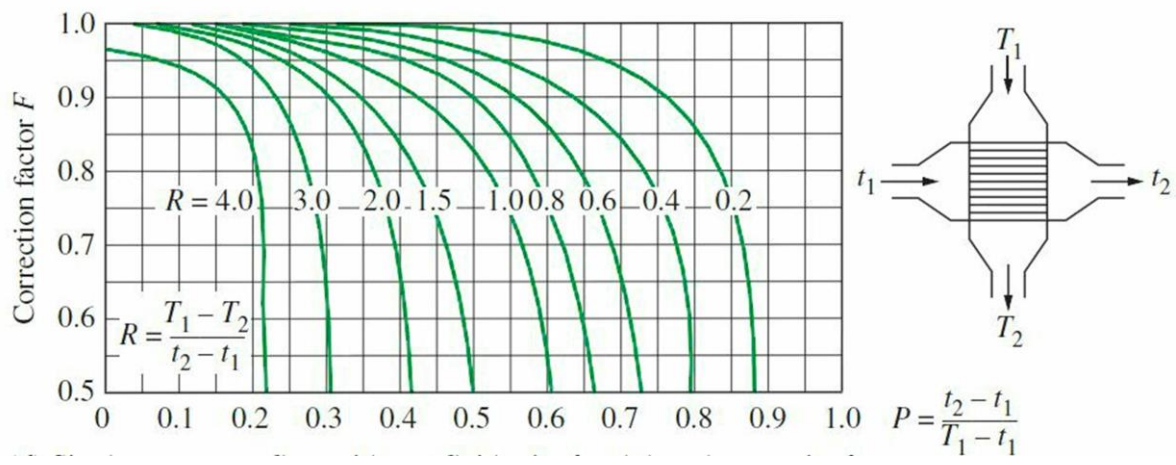

(c) Single-pass cross-flow with one fluid mixed and the other unmixed

Figure A.3: Correction factor F charts (Cengel & Ghajar, 2011).

2.3 The Effectiveness Method (NTU Method)

Standardised effectiveness charts have been created by (Kays & Perkins, 1972) found in (Cengel & Ghajar, 2011), for specific heat exchanger arrangements, which are illustrated by Figure A.4.

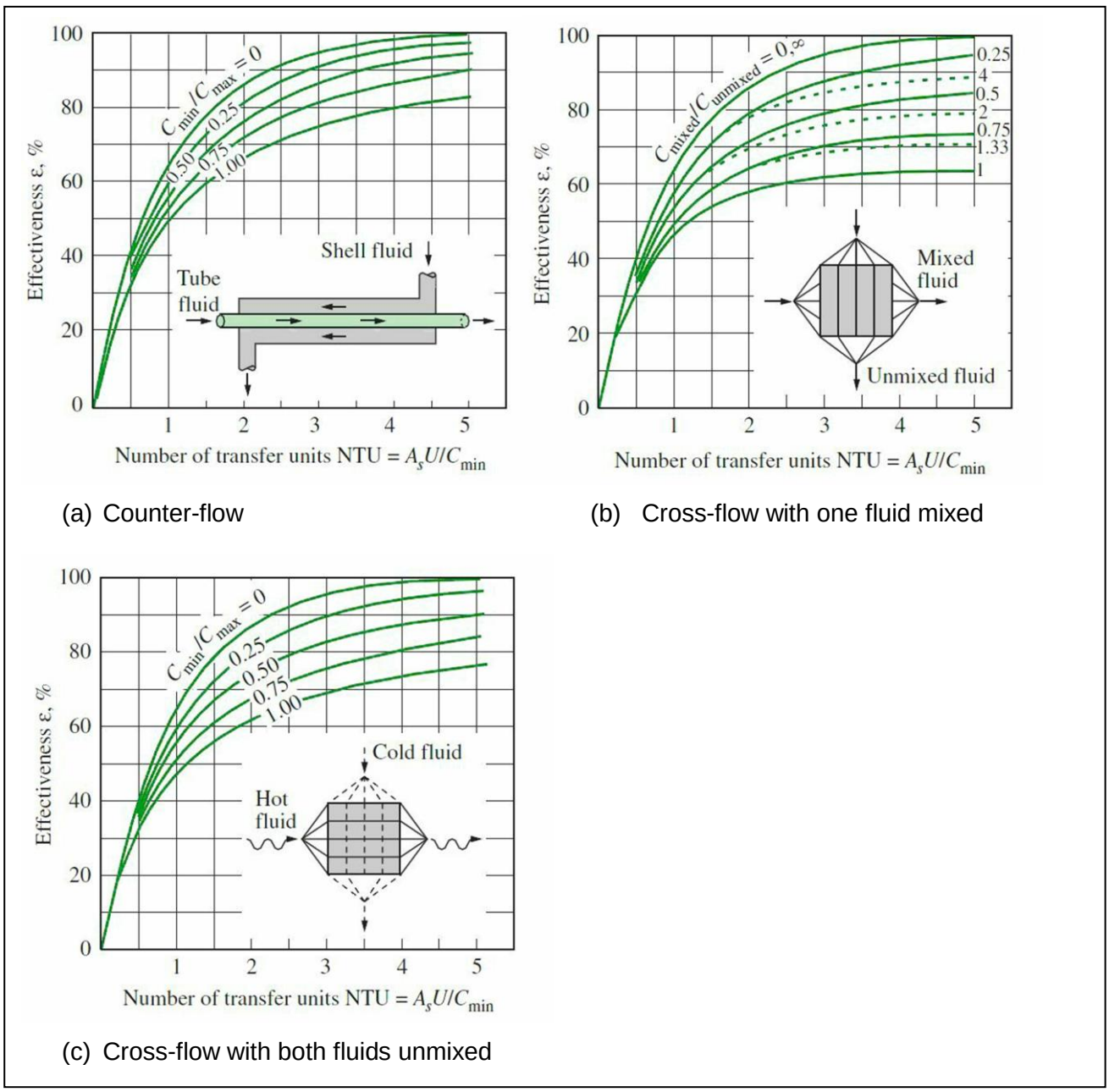

(a) Counter-flow

(b) Cross-flow with one fluid mixed

(c) Cross-flow with both fluids unmixed

Figure A.4: Effectiveness vs. NTU charts (Cengel & Ghajar, 2011).

2.4 Shell Side Heat Transfer Coefficient

2.4.1 Boiling Regime – Nusselt Number Correlation

The experimental values of the surface fluid combination constant C_{sf} and the fluid type constant n is recorded in Table A.19, which is used in the calculation of nucleate boiling heat flux.

Table A.19: Experimental constants of surface-fluid combination (Cengel & Ghajar, 2011).

Fluid-Heating Surface Combination	C_{sf}	n
Water–copper (polished)	0.0130	1.0
Water–copper (scored)	0.0068	1.0
Water–stainless steel (mechanically polished)	0.0130	1.0
Water–stainless steel (ground and polished)	0.0060	1.0
Water–stainless steel (teflon pitted)	0.0058	1.0
Water–stainless steel (chemically etched)	0.0130	1.0
Water–brass	0.0060	1.0
Water–nickel	0.0060	1.0
Water–platinum	0.0130	1.0
n-Pentane–copper (polished)	0.0154	1.7
n-Pentane–chromium	0.0150	1.7
Benzene–chromium	0.1010	1.7
Ethyl alcohol–chromium	0.0027	1.7
Carbon tetrachloride–copper	0.0130	1.7
Isopropanol–copper	0.0025	1.7

The geometry constant C_{cr} illustrated in Table A.20, is used in the calculation of the critical heat flux and requires the calculation of the dimensionless parameter L^*. The dimensionless parameter is calculated with

$$L* = L\left[\frac{g(\rho_l - \rho_v)}{\sigma}\right]^{1/2}$$

Table A.20: Heater geometry constant (Cengel & Ghajar, 2011).

Heater Geometry	C_{cr}	Charac. Dimension of Heater, L	Range of L^*
Large horizontal flat heater	0.149	Width or diameter	$L^* > 27$
Small horizontal flat heater[1]	$18.9K_1$	Width or diameter	$9 < L^* < 20$
Large horizontal cylinder	0.12	Radius	$L^* > 1.2$
Small horizontal cylinder	$0.12L^{*-0.25}$	Radius	$0.15 < L^* < 1.2$
Large sphere	0.11	Radius	$L^* > 4.26$
Small sphere	$0.227L^{*-0.5}$	Radius	$0.15 < L^* < 4.26$

2.4.2 Reynolds Number Correlation for Flow over a Horizontal Tube

The dimensionless Reynolds number was derived by Osborne Reynolds (1842 – 1912). It is essentially based on the ratio of inertia forces to viscous forces in a fluid (Cengel & Ghajar, 2011). Reynolds number can be expressed for external flow as:

$$Re_D = \frac{\rho u D}{\mu}, \tag{A.39}$$

with *u* as the velocity of the fluid stream, and *D* the outer diameter of the tube.

Laminar flow occurs at low Reynolds numbers < 1000 and fully developed turbulent flow occurs at *Re* = 2 x 10^5, at namely, the critical Reynolds number (Re_{cr}). This, however, is dependent on flow geometry, surface roughness and the level of fluctuations in the inlet stream (White, 2011).

2.4.3 Reynolds Number Correlation through Tube Bundles

The Reynolds number for flow through a tube bundle can be calculated for two scenarios of shell and tube heat exchanger, namely, baffled or no baffle heat exchangers. If the heat exchanger has no baffles, the heat transfer coefficient may be based on the equivalent diameter, D_e, where the equivalent diameter is taken as four times the net flow area of the layout (tube pitch layout) divided by the wetted perimeter:

$$D_e = \frac{4 \text{ x } free - flow\ area}{wetted\ perimeter} \tag{A.40}$$

(Kakaç & Liu, 2002) suggested a heat transfer correlation for shell side heat transfer of a baffle less shell and tube heat exchanger as:

$$\frac{h_o D_e}{k_b} = 0.36(Re_s)^{0.55} \left(\frac{C_p \mu}{k}\right)^{\frac{1}{3}} \left(\frac{\mu_b}{\mu_{wall}}\right)^{0.14}, \tag{A.41}$$

with 2 x 10^3 < (Re_s) < 1 x 10^6

A new relation is introduced, G_s, the shell side mass velocity, which is the mass flow rate of the shell side fluid divided by the bundle cross flow area (A_{cs}). The equivalent diameter is dependent on the pitch-tube layout, either square- or triangular-pitch layout. Thus, for the square pitch the following equation is used to determine the equivalent diameter:

$$D_{e,square} = \frac{4(P_T^2 - \pi d_o^2/4)}{\pi d_o} \tag{A.42}$$

and for the triangular tube pitch:

$$D_{e,triangular} = \frac{4\left(P_T^2\sqrt{3}/4 - \pi d_o^2/8\right)}{\pi d_o/2} \tag{A.43}$$

Figure A.5 depicts a graphical representation of the pitch tube bundle layout, but more importantly shows where the equivalent diameter lies (equivalent diameter lies within the hashed areas of Figure A.5).

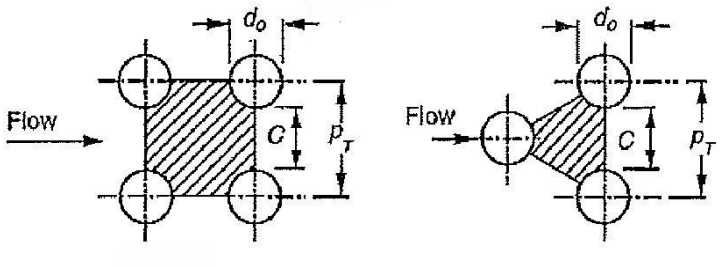

Figure A.5: Pitch tube layouts (Kakaç & Liu, 2002).

where the pitch size and clearance (*C*) are calculated with

$$P_T = d_o \text{ x } PR \;\; (PR = Pitch\ Ratio) \tag{A.44}$$

$$C = P_T - d_o \tag{A.45}$$

Heat exchangers that are baffled have the same set of equations, with a slight tweak to the bundle cross flow area equation at the centre of the shell. Now, the baffle spacing (*B*) is added to the equation, where conventionally the baffle spacing is set at 0.4 to 0.6 of the shell diameter.

$$A_{cs} = \frac{D_s C B}{P_T} \tag{A.46}$$

Thus, the Reynolds number of baffled shell and tube heat exchangers can be calculated by using the following equation extracted from (Kakaç & Liu, 2002):

$$Re_s = \frac{G_s D_e}{\mu} \tag{A.47}$$

2.5 Tube Side Heat Transfer Coefficient

Reynolds Number Correlation for Flow through Circular Ducts

The Reynolds number correlation for flow through a circular tube can be derived from the Reynolds number correlation of external flow as

$$Re_T = \frac{\rho u D_h}{\mu}, \tag{A.48}$$

where D_h is the hydraulic diameter, which is equal to the inner diameter of the tube.

(Kakaç & Liu, 2002) suggested the rearranging of Eq. A.48 and substituting velocity with a mass flow rate relation yields a far simpler correlation for Reynolds number calculation as

$$Re_T = \frac{4\,\dot{m}}{\pi\, d_i\, \mu} \tag{A.49}$$

The flow through a tube for most practical applications is laminar when Re < 2300, turbulent when Re > 10 000, and in the transitional range for 2300 ≤ Re ≤ 10 000. It's possible to maintain laminar flow for Reynolds numbers above 2300 in very smooth tubes by avoiding tube vibrations and flow disturbances (Cengel & Ghajar, 2011). In the transitional range of Reynolds number the flow can switch between laminar and turbulent randomly.

2.6 Shell Side Pressure Drop

Pressure drops from the shell side depend on the geometrical layout of the shell and tube heat exchanger, namely, the number of tubes in the tube bundle, and the baffle spacing and baffle cut. Kern (1950) as found in (Kakaç & Liu, 2002) proposed that the pressure drop be a product of friction factor *f*, the shell diameter D_s, the number of baffles N_b, and the mass velocity G_s, where the equivalent diameter is calculated by Eq. A.32 & A.33. Thus, the pressure drop on the shell side can be calculated using the following:

$$\Delta P_s = \frac{f G_s^2 (N_b + 1) D_s}{2\rho De\left({}^{\mu_{bulk}}/_{\mu_{wall}}\right)^{0.14}} \tag{A.50}$$

The friction factor *f* is calculated with

$$f = \exp(0.576 - 0.19\, ln(Re_s))\,, \tag{A.51}$$

where ($400 < Re_s < 10^6$). The friction factor correlation for the shell has been tested based on data obtained from actual heat exchangers, and takes entrance and exit losses into account (Kakaç & Liu, 2002).

2.7 Tube Side Pressure Drop

The pressure drop of the tube side can be determined by knowing the number of tube passes, N_p, and the length of the tubes (*L)*. The pressure drop for single tube pass heat exchanger can be calculated using the following two equations, which were extracted from (Moody, 1994).

$$\Delta P_t = 4f \frac{LN_p}{d_i} \rho \frac{U_m^2}{2} \tag{A.52}$$

$$\Delta P_t = 4f\frac{LN_p}{d_i}\frac{G_i^2}{2\rho} \tag{A.53}$$

The friction factor in the laminar region is calculated using

$$f = \frac{16}{Re_t}, \tag{A.54}$$

where the Reynolds number is limited to 2300.

2.8 Fouling Factor

The performance of a heat exchanger deteriorates with the course of its operation life as a result of accumulating deposits or material corrosion. The extra layer of deposits represents additional resistance from heat being transferred between the two fluids. The total effect of these accumulations on the heat transfer is represented by a fouling factor R_f, which is a measure of thermal resistance (Cengel & Ghajar, 2011).

In applications where fouling is likely to occur it should be considered in the thermodynamic design and selection of the heat exchanger. In such applications where fouling is unavoidable, it will be required that the total heat transfer surface area is increased by an over design percentage to meet the heat transfer design requirements. Fouling factors are obviously zero for a new heat exchanger, but with the course of operating time the performance slowly decreases. The fouling factor depends on the operating temperature and fluid velocity, in other words fouling increases with low fluid velocities and high fluid temperatures.

Thulukakanam (2000) proposed the overall heat transfer coefficient with fouling factors is

$$\frac{1}{U_f A_s} = \frac{1}{h_o A_o} + \frac{R_{f,o}}{A_o} + \frac{1}{h_i A_i} + \frac{R_{f,i}}{A_i} + \frac{A_o \ln(d_o/d_i)}{2\pi L k_{material}} \tag{A.55}$$

Kakaç and Liu (2002) suggested that the over design percentage can be expressed by

$$OS = 100 U_{S1C} R_{ft}, \tag{A.56}$$

with the total resistance factor and cleanliness factor as

$$R_{ft} = \frac{1 - CF}{U_c CF} \tag{A.57}$$

$$CF = \frac{U_f}{U_c} \tag{A.58}$$

3 MECHANICAL DESIGN RATING AND CONSIDERATIONS

Although, the main focus of this study is the thermodynamic design and rating of seven heat exchangers for an aqua-ammonia absorption-desorption H&R cycle, the heat exchangers still need to be manufactured and the mechanical rating still needs to be considered. Especially, since a volatile refrigerant will be used under 10-to-14 times atmospheric pressure. Among the considerations to be made are the thicknesses of the heat exchangers shells, the thicknesses of the tubes in the tube bundle, the thicknesses of the tube sheets, and lastly the number of bolts for the flanges of the connecting pipes.

First order stress calculations and standardised codes, such as ASME and TEMA, will be used to determine whether the mechanical designs of the heat exchangers are deemed safe for operation.

3.1 Tube Sheet Stress Calculations and TEMA Codes

The tube sheet of a fixed shell and tube heat exchanger plays an integral role of keeping the fluids separate and containing the pressure to the inside of the heat exchanger. The minimum tube sheet thickness can be determined by completing simple first order stress calculations from (Hibbeler, 2010) coupled with verification from the TEMA rule for tube sheet thicknesses (Thulukakanam, 2000). If the tube sheet is to be assumed as a circular disk with uniform loading, which is clamped at its edges, the thickness can be calculated by a rearrangement of Eq. A.59 as

$$\sigma_{allow} = \frac{3P_D r^2}{4t^2} \tag{A.59}$$

to

$$t = \sqrt{\frac{3P_D r^2}{4\sigma_{allow}}}\,, \tag{A.60}$$

with P_D as the effective design pressure, r as the radius of the tube sheet disk, and σ_{allow} as the ASME allowable stress for the selected material. The TEMA rule for minimum tube sheet thickness can be calculated using the following (Thulukakanam, 2000):

$$t = F\frac{G}{3}\sqrt{\frac{P_D}{\eta\sigma_{allow}}}, \tag{A.61}$$

with

$$F = \begin{cases} 1.0 - \ if\ the\ tubesheet\ is\ clamped \\ 1.25 - if\ the\ tubesheet\ is\ simply\ supported \end{cases}$$

and

$$\eta = \begin{cases} 0.42 - triangular\ pitch \\ 0.5 - square\ pitch \end{cases}$$

F is the parameter used to account for the restraint of the tube sheet; *G* is the diameter of the tube sheet disk; and *η* is the TEMA ligament efficiency.

3.2 Tube Stress Calculations and ASME Codes

3.2.1 Thick Walled Cylinder

The thickness of the shell and of the tubes within each heat exchanger designs is highly important, as the wall thickness is the only material separating the fluids from one another and the outside environment. The outer shell of the heat exchanger can be viewed as a vessel, which experiences internal pressure from the working fluids. When a vessel is under internal pressure then there are stresses acting in on the wall of the vessel in the axial, radial, and circumferential direction, as illustrated in Figure A.6 as available from (Engineeringtoolbox, 2015).

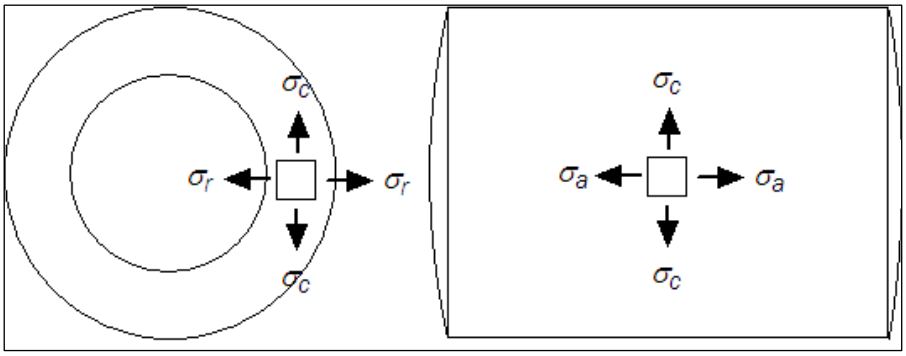

Figure A.6: Stress diagram of thick walled cylinders subjected to design pressure.

The following equations are derived from first order principles and can be used to determine the stresses of a thick walled cylinder under pressure as

Axial stress:

$$\sigma_a = \frac{(P_i r_i^2 - P_o r_o^2)}{(r_o^2 - r_i^2)} \quad \textbf{(A.62)}$$

Hoop stress:

$$\sigma_c = \left[\frac{(P_i r_i^2 - P_o r_o^2)}{(r_o^2 - r_i^2)}\right] - \left[\frac{r_i^2 r_o^2 (P_o - P_i)}{\left(r^2 (r_o^2 - r_i^2)\right)}\right] \quad \textbf{(A.63)}$$

Radial stress:

$$\sigma_r = \left[\frac{(P_i r_i^2 - P_o r_o^2)}{\left(r_o^2 - r_i^2\right)}\right] + \left[\frac{r_i^2 r_o^2 (P_o - P_i)}{\left(r^2\left(r_o^2 - r_i^2\right)\right)}\right] \quad \textbf{(A.64)}$$

Where:

P_i = the internal pressure;

P_o = the external pressure;

r_i = the inner radius of the shell;

r_o = the outer radius of the shell;

r = mean radius of the shell;

A safety factor can be obtained from the stress calculations above by simply dividing by the standardised allowable stress obtained from the ASME codes.

To verify the safety factor obtained from first principles, the ASME codes can be used to determine the minimum thickness of the shell and tube walls. These codes are the industry standard and used worldwide, where the equation for determining the minimum wall thickness according to ASME B31.3 is

$$t_{min} = \frac{PD_o}{2(SEW + PY)}, \quad \textbf{(A.65)}$$

where:

P = the internal gauge pressure;

D_o = the outer diameter of the shell;

S = the allowable stress according to ASME pipe design tensile strength;

E = weld quality factor;

W = weld joint strength reduction factor;

Y = coefficient from Table 304.1.1 in ASME, 2014

The first order principles are used to determine a safety factor with standard sizes of pipes and tubing, whereas the ASME wall thickness calculations act as confirmation that the standard pipe is thick enough for the application.

$$SF = \frac{\sigma_{allow}}{\sigma_{max}} \quad \textbf{(A.66)}$$

3.2.2 Thin Walled Cylinder

Tubes are classified as thin walled cylinders when the wall thickness is approximately one tenth the tubes radius. The stress calculations for thin walled cylinders are formulated to determine the stresses of a pressure working on the inside of the cylinder.

Thin walled hoop stress:

$$\sigma_h = \frac{P_D d_i}{2t} \tag{A.67}$$

Thin walled longitudinal stress:

$$\sigma_l = \frac{P_D d_i}{4t} \tag{A.68}$$

To determine whether a tube wouldn't collapse from pressure on the outside of the tube, a thick walled analysis can be used as a conservative method of calculating the maximum stress and comparing it to the allowable stress.

3.3 Header Bolt Calculations

The number of bolts needed to suitably fasten the headers and pipe flanges are calculated using simple first principle equations obtained from (Budynas & Nisbett, 2011) with the internal pressure acting on the end plate of the header, as illustrated by Figure A.7.

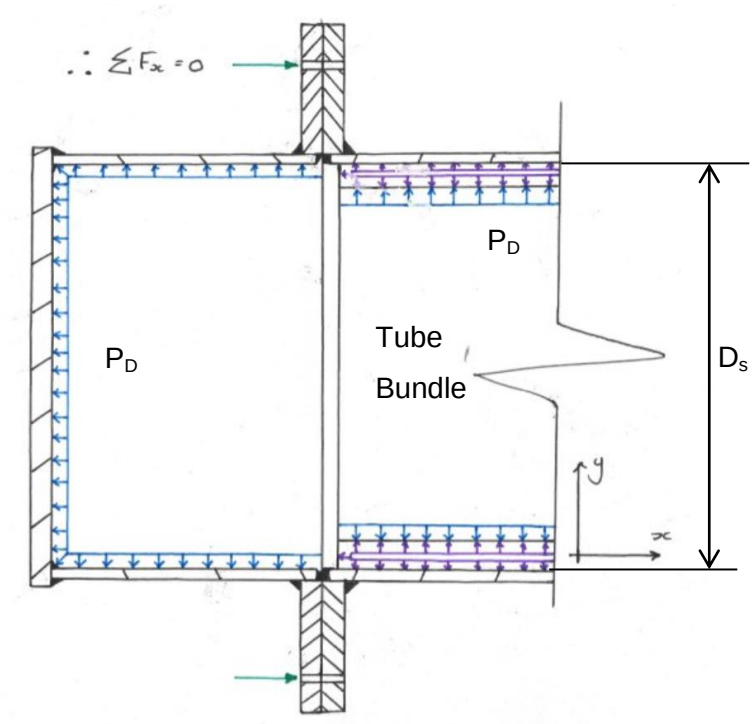

Figure A.7: Simplified heat exchanger header force diagram.

The force exerted on the end plate of the header is calculated using the following:

$$F_{end} = P_D \left(\frac{\pi}{4} D_s^2\right) \quad \textbf{(A.69)}$$

The force acting on the flange of the header due to the fasteners can be calculated using the following:

$$F_{flange} = P_D \frac{\pi}{4}\left(D_{flange}^2 - D_s^2\right), \quad \textbf{(A.70)}$$

where D_{flange} is the outer diameter of the flange.

The operating force of the bolts are determined as

$$F_{op} = 2.75 P_D \pi D_{flange} W_{flange}, \quad \textbf{(A.71)}$$

where W_{flange} is the width of the flange component.

The design force is a culmination of the operating force and the largest force between the flange and end plate forces, where the design force is then used to determine the number of bolts required as

$$N_{bolts} = \frac{F_D}{\sigma_Y \left(\frac{\pi}{4} D_{bolt}^2\right)}, \quad \textbf{(A.72)}$$

with:

σ_Y = the yield strength of the bolt

D_{bolt} = the diameter of the bolt

4 OCCUPATIONAL HEALTH AND SAFETY OF AN AQUA-AMMONIA ABSORPTION-DESORPTION CYCLE

The social, legal, health, safety, and environmental impact of products and designs have become an important parameter to determine the success of a design in today's day and age. Due to the increasing demand for safer and cleaner designs, it is important to ensure that all legal aspects are abided by, and that fatalities are not caused by the design product. This section will investigate the social, legal, health, safety, and environmental impacts of the heat exchanger modules to be designed.

4.1 Social and Legal Impacts

The physiological affects aqua-ammonia on humans are serious at high concentrations. Refrigerant R717 becomes an explosive mixture in air between 20-30% mass concentration (ANSI/ASHRAE, 1994). While South Africa seeks to finalise a SANS standard for ammonia as a refrigerant under SANS 10400. A standard does not exist in South Africa, therefore, the design of an aqua-ammonia absorption-desorption refrigeration plant will be designed according to the United States of America's Occupational Health and Safety Act for Process Safety Management 29CFR1910,119. This code provides comprehensive guidelines to designing and developing an ammonia absorption refrigeration plant.

Codes and standards are also required when designing the mechanical components of the aqua-ammonia absorption-desorption cycle. Since SANS 10400 is not yet in existence, the structural design of the support mountings and welds for this project has been based on SANS Code in (Parrot, 2005), and the module thickness based on design pressure accompanied by a large safety factor. Sound levels are not a legal issue, as all the heat exchangers won't be in close proximity to people, but sound levels should be kept below 85 [dB].

4.2 Health Impacts

As it is now known that pure ammonia is a toxic substance, it can have different affects to the human body at different levels of concentration when mixed with the air. At 100-200 ppm the eyes start to feel agitated, when moving passed 500 ppm the human eye could have permanent. An ammonia concentration of 5000 and above the human skin will attain second degree burns, at 400 ppm the human lunges will be agitated and start to blister, at 1700 ppm coughing will start and at 2400 ppm it becomes life threatening when inhaled (www.atsdr.cdc.gov, 2014).

4.3 Safety Impacts

According to the Kyoto Protocol the safety requirements for designing an ammonia refrigeration plant are that (29CFR1910.119, 1992):

- All power to all circuits within of the absorption-desorption cycle should be automatically shut-down should the ammonia reach 3% volume.
- All circuits in which power should be maintained during high ammonia concentrations, for instance the condenser, should have intrinsically safe fittings.

During maintenance of the several heat exchangers of the aqua-ammonia package unit would be shut-down, during the inspection of the modules, as a safety precaution the licensed inspector should wear the appropriate eye, mouth, and skin protection.

4.4 Environmental Impacts

Ammonia is an “environmentally friendly” refrigerant in other words ammonia is not contributing to the depletion of the ozone layer (O_3), greenhouse effect, or to global warming. Ammonia has a very short atmospheric lifetime and therefore has no cumulative effect on the environment. It is also known as a biodegradable substance. Ammonia is one of only few alternative refrigerants with zero ODP (Ozone Depletion Potential) and zero GWP (Global Warming Potential) accepted by all governments, ASHRAE, UNEP, International Institution of Refrigeration, and almost all Institutes of Refrigeration worldwide (ANSI/ASHRAE, 1994).

Energy and efficiency of a system is highly important due to a lack of energy or high energy demands. Energy in the form of mechanical work is normally much more expensive than in the form of heat. Since the absorption-desorption H&R cycle uses less expensive thermal (heat) energy, lower COP values are acceptable. Therefore, the aqua-ammonia absorption-desorption H&R cycle is a viable alternative to the conventional energy thirsty vapour-compression cycle.

Appendix B

Extended Chapter 3 – Thermophysical Properties

Summary

Appendix B is mainly focused on the thermophysical properties of the thermodynamic states in the aqua-ammonia absorption-desorption H&R cycle that have been excluded from the main body of text. Some of the thermophysical property sample calculations of a thermodynamic state were omitted due to the trivial nature of the sample calculation.

Table of Contents

List of Tables

1 EXTENDED THERMOPHYSICAL PROPERTIES

1.1 Thermophysical Properties of State 4

Compiled within this section are the thermophysical property sample calculations of saturated aqua-ammonia vapour under summer ambient conditions. The specific thermal capacity for saturated vapour is calculated as

$$\theta = \frac{T_{mix}}{T_{crit,mix}} \quad (Eq\ 2.7)$$

$$\therefore = \frac{333.2049}{405.5173}$$

$$\therefore = 0.821679$$

$$\tau = 1 - \theta \quad (Eq\ 2.8)$$

$$\therefore = 1 - 0.821679$$

$$\therefore = 0.178321$$

$Cp_{T,NH_3} = A + B\tau^{-\frac{1}{3}} + C\tau^{-\frac{2}{3}} + D\tau^{-\frac{5}{3}} + E\tau^{-\frac{7.5}{3}}$ $(Eq\ 2.11)$ with parameters (Table 2.6)

$$\therefore = -1.199197 + \left(1.240129495 * 0.178321^{-\frac{1}{3}}\right) + \left(0.924818752 * 0.178321^{-\frac{2}{3}}\right) + \left(0.0182 * 0.178321^{-\frac{5}{3}}\right) + \left(0.000245 * 0.178321^{-\frac{7.5}{3}}\right)$$

$$\therefore = 4.2635966 \left[\frac{kJ}{kg}.K\right]$$

$$Cp_{T,H_2O} = A + B\tau^{-\frac{1}{3}} + C\tau^{-\frac{2}{3}} + D\tau^{-\frac{5}{3}} + E\tau^{-\frac{7.5}{3}}$$

$$\therefore = 3.4618257 + \left(-4.987788063 * 0.178321^{-\frac{1}{3}}\right) + \left(2.99438177 * 0.178321^{-\frac{2}{3}}\right) + \left(0.006259 * 0.178321^{-\frac{5}{3}}\right) + \left(0.00000826 * 0.178321^{-\frac{7.5}{3}}\right)$$

$$\therefore = 4.16210333 \left[\frac{kJ}{kg}.K\right]$$

Finally, the specific thermal capacity of the mixture can be calculated using

$$Cp_4 = yCp_{T,NH3} + (1-y)Cp_{T,H2O} \quad (Eq.2.12)$$

$$\therefore = 0.999709(4.2635966) + \left((1 - 0.999709) * 4.16210333\right)$$

$$\therefore = 4.26357 \left[\frac{kJ}{kg}.K\right]$$

The density of saturated vapour state 4 is determined as

$\Delta\rho_{max,T_m} = e^{J-K/T_m^*}$ with parameters Table 2.8

$\therefore = 11.118577 \left[\frac{kg}{m^3}\right]$

$\Delta\rho^*_{T_{m,x}} = A(1-y)^B\left(1-e^{Cy^D}\right)\Delta\rho_{max,T_m}$ $(Eq\ 2.18)$ with parameters Table 2.8

$\therefore = 0.7579289 \left[\frac{kg}{m^3}\right]$

Using Eq. 2.19 and parameters set in Table 2.9 the densities of pure ammonia and water are calculated as

$\rho_{NH_3,T_{NH3}} = 7.3313701 \left[\frac{kg}{m^3}\right]$ and $\rho_{H_2O,T_{H2O}} = 7.7712887 \left[\frac{kg}{m^3}\right]$

Substituting the above values into Eq. 2.17 yields the density of the aqueous ammonia mixture.

$\rho_4 = y\rho_{NH3,T_{NH3}} + (1-y)\rho_{H2O,T_{H2O}} + \Delta\rho^*_{T_{m,x}}$

$\therefore = (0.999709 * 7.3313701) + \left((1-0.999709) * 7.17712887\right) + 0.7579289$

$\therefore = 8.08943 \left[\frac{kg}{m^3}\right]$

The dynamic viscosity of saturated vapour of state 4 (summer design conditions) are:

$\varphi_{12} = \frac{\left[1+\left(\frac{\mu_{NH3}}{\mu_{H_2O}}\right)^{0.5}\left(\frac{M_{H2O}}{M_{NH3}}\right)^{0.25}\right]^2}{\left[8\left(1+\frac{M_{NH3}}{M_{H2O}}\right)\right]^{0.5}}$ $(Eq\ 2.22)$,where μ_{NH3} = 1.18881(-05) kg/m.s and μ_{H2O} = 1.78265E(-05) kg/m.s

$\therefore = 0.8472279$

$\varphi_{21} = \varphi_{21}\frac{\mu_{H_2O}}{\mu_{NH_3}}\frac{M_{NH_3}}{M_{H_2O}}$

$\therefore = 1.2009746$

$\mu_4 = \frac{y\mu_{NH3}}{y+(1-y)\varphi_{12}} + \frac{(1-y)\mu_{H2O}}{(1-y)+y\varphi_{21}}$

$\therefore = \frac{0.999709 * 1.18881E(-05)}{0.999709 + (1-0.999709) * 0.8472279} + \frac{(1-0.999709) * 1.78265E(-05)}{(1-0.999709) * 1.2009746}$

$\therefore = 1.188948E-05 \left[\frac{kg}{m.s}\right]$

The thermal conductivity of state 4 is determined using similar equation to dynamic viscosity, only exception is the substituting of values of thermal conductivity for pure ammonia and water.

$$\varphi_{12} = \frac{\left[1+\left(\frac{k_{NH3}}{k_{H_2O}}\right)^{0.5}\left(\frac{M_{H2O}}{M_{NH3}}\right)^{0.25}\right]^2}{\left[8\left(1+\frac{M_{NH3}}{M_{H2O}}\right)\right]^{0.5}} \quad (Eq\ 2.24)$$,where k_{NH3} = 0.0341093 W/m.K and k_{H2O} = 0.0536266 W/m.K

$$\therefore = 0.829371$$

$$\varphi_{21} = \varphi_{21}\frac{k_{H_2O}}{k_{NH_3}}\frac{M_{NH_3}}{M_{H_2O}}$$

$$\therefore = 1.232643$$

$$k_4 = \frac{yk_{NH3}}{y+(1-y)\varphi_{12}} + \frac{(1-y)k_{H2O}}{(1-y)+y\varphi_{21}}$$

$$\therefore = \frac{0.999709 * 0.0341093}{0.999709 + (1-0.999709) * 0.829371} + \frac{(1-0.999709) * 0.0536266}{(1-0.999709) * 1.232643}$$

$$\therefore = 0.034114\ \left[\frac{W}{m.K}\right]$$

Lastly, the Prandtl number for state 4 is calculated using the values of $C_{p,4}$, μ_4, and k_4.

$$Pr_4 = \frac{\mu_{mix}Cp_{mix}}{k_{mix}} \quad (Eq.2.25)$$

$$\therefore = \frac{4.26258 * 10^3 * 1.188948E-05}{0.034114}$$

$$\therefore = 1.485959\ [-]$$

1.2 Thermophysical Properties of State 5

Compiled within this section are the thermophysical property sample calculations of saturated aqua-ammonia liquid under summer ambient conditions. The specific thermal capacity of state 5 can be calculated as

$$\theta = \frac{T_{mix}}{T_{crit,mix}} \quad (Eq\ 2.7)$$

$$\therefore = \frac{296.15}{408.86745}$$

$$\therefore = 0.724318$$

$$\tau = 1-\theta \quad (Eq\ 2.8)$$

$$\therefore = 1-0.724318$$

$$\therefore = 0.275682$$

$Cp_{T,NH_3} = A_{cp} + B_{cp} * \tau^{-1}$ $(Eq\ 2.9)$ with parameters (Table 2.5)

$\therefore = 3.875648 + (0.242125 * 0.275682^{-1})$

$\therefore = 4.753924 \left[\frac{kJ}{kg}.K\right]$

$Cp_{T,H_2O} = A_{cp} + B_{cp} * \tau^{-1}$ $(Eq\ 2.9)$ with parameters (Table 2.5)

$\therefore = 3.665785 + (0.236312 * 0.275682^{-1})$

$\therefore = 4.522975 \left[\frac{kJ}{kg}.K\right]$

Now, the specific thermal capacity of the mixture can be calculated using

$Cp_5 = xCp_{T,NH3} + (1-x)Cp_{T,H2O}$ $(Eq.2.10)$

$\therefore = 0.99(4.753924) + \big((1-0.99) * 4.522975\big)$

$\therefore = 4.75161 \left[\frac{kJ}{kg}.K\right]$

The density of saturated liquid state 5 can be calculated as

$\Delta\rho^*_{T_{m,x}} = [x(1-x) - Ax^2(1-x)] * \left(\rho^{0.5}_{NH3,T_{NH3}} * \rho^{0.5}_{H2O,T_{H2O}}\right)$ $(Eq.2.14)$

Where variable *A* is determined using Eqs. 2.15 & 2.16, Table 2.7, and ρ_{NH3} = 609.477 [kg/m^3] and ρ_{H2O} = 869.642 [kg/m^3]

$\therefore = [0.99(1-0.99) - 1.1499893(0.99^2)(1-0.99)](609.477^{0.5} * 869.642^{0.5})$

$\therefore = -0.998161 \left[\frac{kg}{m^3}\right]\ excess$

Substituting the above values into Eq. 2.13 yields the density of the aqueous ammonia mixture.

$\rho_5 = x\left(\rho_{NH3,T_{NH3}}\right) + (1-x)\left(\rho_{H2O,T_{H2O}}\right) + \Delta\rho^*_{T_{m,x}}$

$\therefore = (0.99 * 609.477) + \big((1-0.99) * 869.642\big) - 0.998161$

$\therefore = 611.081 \left[\frac{kg}{m^3}\right]$

Dynamic viscosity for saturated liquid of state 5 can be approximated as

$F(x) = 6.38(1-x)^{1.125x}\left(1 - e^{-0.585x(1-x)^{0.18}}\right)\ln(\mu^{0.5}_{NH3} * \mu^{0.5}_{H2O})$

Where the values of μ_{NH3} = 0.0001519 [kg/m.s] and μ_{H2O} = 0.000142 [kg/m.s] are determined via linear interpolation as a function of substance temperature.

$\therefore = -0.074496 \left[\frac{kg}{m.s}\right]$

$$\Delta\mu(T_{mix}, x) = \left(0.534 - 0.815\left(\frac{T_m}{T_{c,H2O}}\right)\right) * F(x) \quad (Eq.\ 2.21)$$

$$\therefore = \left(0.534 - 0.815\left(\frac{296.15}{647.14}\right)\right) * (-0.074496)$$

$$\therefore = -0.011996304 \left[\frac{kg}{m.s}\right]$$

Using Eq. 2.20 and substituting for the value of excess dynamic viscosity, the saturated liquid dynamic viscosity is obtained as

$$ln\,\mu_5 = x\left(ln\left(\mu_{NH3,T_{NH3}}\right)\right) + (1-x)\,ln\left(\mu_{H2O,T_{H2O}}\right) + \Delta\mu(T_{mix}, x)$$

$$\therefore = 0.99(\ln(0.0001519)) + (1 - 0.99)\ln(0.000142) - 0.011996304$$

$$\therefore \ln(\mu_5) = -8.804958$$

$$\therefore = 0.000149988 \left[\frac{kg}{m.s}\right]$$

Thermal conductivity of state 5 saturated liquid:

$\rho^{+}_{NH3} = \rho_{NH3}(T_{NH3})(x^{0.425})$,where ρ_{NH3} = 610.3259 [kg/m^3]

$$\therefore = 610.3259(0.99^{0.425})$$

$$\therefore = 607.725 \left[\frac{kg}{m^3}\right]$$

The thermal conductivity of pure ammonia is a function of density and has been determined via linear interpolation as $k_{NH3}(\rho_{NH3})$ = 0.48749 [W/m.K], and for water as a function of temperature k_{H2O} = 0.669 [W/m.K].

Substituting the above values into Eq. 2.23 yields the thermal conductivity of the aqueous ammonia mixture.

$$k_5 = x\left(k_{NH3(\rho^{+}_{NH3})}\right) + (1-x)\left(k_{H2O(T_{H2O})}\right)$$

$$\therefore = (0.99 * 0.48749) + \left((1 - 0.99) * 0.669\right)$$

$$\therefore = 0.48931 \left[\frac{W}{m.K}\right]$$

Lastly, the Prandtl number for state 5 is calculated using the values of Cp, μ, and k.

$$Pr_5 = \frac{\mu_{mix} Cp_{mix}}{k_{mix}} \quad (Eq\ 2.25)$$

$$\therefore = \frac{4.75161 * 10^3 * 0.000149988}{0.48931}$$

$$\therefore = 1.4561\ [-]$$

1.3 Thermophysical Properties of States 5 to 6 and 9 to 10

This section focuses on the thermophysical properties of the inlet and outlet conditions of the pre-cool heat exchanger control volume for state 5 to 6 and 9 to 10, as depicted in Figures 3.1 and 3.3.

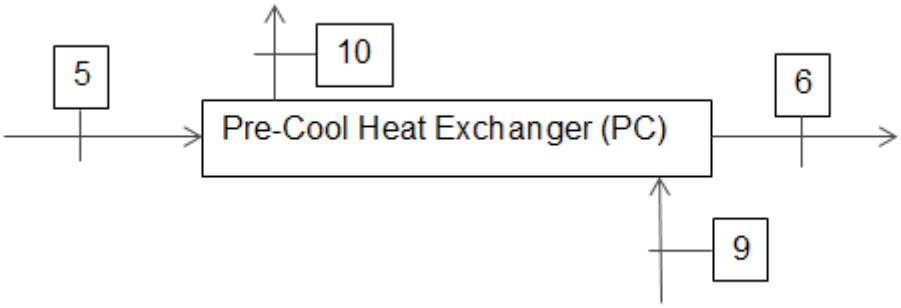

Enthalpy of State 5 to 6

The enthalpy values of state 5 are already known as previously calculated in Chapter 3.1.2, though the enthalpy of state 6 is to be determined. EES can provide with the enthalpy values for sub-cooled liquid aqua-ammonia, but for purposes of consistency the mathematical method is used to determine the enthalpy of state 6. Using Eq. 2.3 and equation parameters in Table A.3, the enthalpy of state 6 is calculated as

$$\alpha_{6,WRT}(270.141, 0.99) = -25.8159 \quad \left[\frac{kJ}{kg}\right]$$
$$\alpha_{6,DSN}(276.386, 0.99) = 3.00148 \quad \left[\frac{kJ}{kg}\right]$$
$$\alpha_{6,SMR}(281.503, 0.99) = 26.8503 \quad \left[\frac{kJ}{kg}\right]$$

The temperatures of state 6 for the three ambient conditions were obtained from the MS Excel 'Clear Sky' data sheet in Appendix D 2.1.

Now, that the enthalpy values of state 6 have been calculated it is possible to determine the heat transfer rate of the sub-cooled liquid line of aqueous ammonia.

Winter design conditions:

$$\dot{Q}_{PC,WRT} = \dot{m}_{6,WRT}\left(\alpha_{6,WRT} - \alpha_{5,WRT}\right) \quad (Eq.\,2.27)$$
$$\therefore = 0.000539(-25.8159 - 11.1974)$$
$$\therefore = 19.9502\,W\ (Heat\ Removed)$$

Average design conditions:

$$\dot{Q}_{PC,DSN} = \dot{m}_{6,DSN}\left(\alpha_{6,DSN} - \alpha_{5,DSN}\right) \quad (Eq.\,2.27)$$
$$\therefore = 0.0005816(3.00148 - 58.1984)$$
$$\therefore = 32.1026\,W\ (Heat\ Removed)$$

Summer design conditions:

$$\dot{Q}_{PC,SMR} = \dot{m}_{6,SMR}(\alpha_{6,SMR} - \alpha_{5,SMR}) \quad (Eq. 2.27)$$
$$\therefore = 0.0006129(26.8503 - 96.5153)$$
$$\therefore = 42.6977\ W\ (Heat\ Removed)$$

Therefore, for state 5 to 6, it is clear that summer conditions has the highest heat transfer rate and should yield the largest heat transfer surface area when calculating the thermodynamic design sizing. Thus, in this oeuvre, the summer condition thermophysical properties of state 6 will be calculated and illustrated in below, and the remaining conditions thermophysical properties are added to section 4 of Appendix B.

The temperature of state 10 is unknown and can be calculated by an energy balance between state 5 to 6 and 9 to 10.

$$\sum \dot{Q}_{in} = \sum \dot{Q}_{out}$$
$$\dot{Q}_{PC,SMR} = \dot{m}_{9,SMR}(\alpha_{10,SMR} - \alpha_{9,SMR}) \quad (Eq. 2.27)$$
$$\therefore\ 42.6977 = 0.0005986(\alpha_{10,SMR} - 1444) * 10^3$$
$$\therefore\ \alpha_{10,SMR} = 1515.3292\ \left[\frac{kJ}{kg}\right]$$

The temperature of state 10 can be determined via EES' temperature function for pure ammonia by substituting the variables of pressure and enthalpy (P_{10} = 236.2 kPa, α_{10} = 1515.3292 kJ/kg).

$$T_{10,SMR}(236.2, 1515.3292) = 15.11\ [°C]$$

State 6 Thermophysical Properties

The sub-cooled liquid phase of state 6 is determined by means of the mathematical method set out in Chapter 2.4.1 for saturated liquid. As a liquid is incompressible the values obtained by mathematical method are within good accordance to EES' thermophysical properties. Thus, the thermophysical properties of state 6 under summer ambient conditions, with temperature and pressure at 8.353 °C and 939.54 [kPa], respectively, are:

$Cp_6 = 4.6506 \left[\frac{kJ}{kg}\right]$

$\rho_6 = 632.288 \left[\frac{kg}{m^3}\right]$

$\mu_6 = 0.000176853 \left[\frac{kg}{m.s}\right]$

$k_6 = 0.52233 \left[\frac{W}{m.K}\right]$

$Pr_6 = 1.5746[-]$

State 9 Thermophysical Properties

As depicted by Figure 3.1, state 9 is at the saturated vapour state of pure ammonia, this is due to a tertiary gas in the evaporator module which creates a partial pressure of the aqua-ammonia mixture. The partial pressure of aqua-ammonia assists the evaporation process whereby pure ammonia can evaporate first out of the mixture, thus, creating the pure ammonia saturated vapour state 9. As state 9 and 10 consists of pure ammonia vapour the thermophysical properties are determined by use of EES' property call function. Under state 9, the thermophysical properties are determined as a function of pressure and quality for summer ambient conditions. The partial pressure of 236.2 [kPa] is desired for all ambient design conditions, thus the thermophysical properties of state 9 are valid for winter, average, and summer design conditions.

$Cp_9(236.2, 1.00) = 2.481 \left[\frac{kJ}{kg}\right]$

$\rho_9(236.2, 1.00) = 1.966 \left[\frac{kg}{m^3}\right]$

$\mu_9(236.2, 1.00) = 0.0000086 \left[\frac{kg}{m.s}\right]$

$k_9(236.2, 1.00) = 0.02212 \left[\frac{W}{m.K}\right]$

$Pr_9(236.2, 1.00) = 0.9645\ [-]$

State 10 Thermophysical Properties

The transport properties of superheated state 10 are obtained by using EES' property call function, with input parameters of pressure and enthalpy. The remaining thermophysical properties of winter and average design conditions are available in section 4.

$$Cp_{10}(236.2, 1515.3292) = 2.294 \left[\frac{kJ}{kg}\right]$$

$$\rho_{10}(236.2, 1515.3292) = 1.728 \left[\frac{kg}{m^3}\right]$$

$$\mu_{10}(236.2, 1515.3292) = 9.689E(-06) \left[\frac{kg}{m.s}\right]$$

$$k_{10}(236.2, 1515.3292) = 0.02425 \left[\frac{W}{m.K}\right]$$

$$Pr_{10}(236.2, 1515.3292) = 0.9167 [-]$$

1.4 Thermophysical Properties of Weak and Strong Aqua-Ammonia Solutions

The enthalpy values of the strong aqua-ammonia solution can be determined by means of the mathematical method, but the thermophysical properties of the weak aqua-ammonia solution can't be calculated using the mathematical method proposed in (Conde-Petit, 2004). Thus, it was decided that for purposes of the design continuity for the regenerative and auxiliary heat exchangers the thermophysical properties will be calculated using EES' property call function. This does create a problem for the strong solution's transport properties out of the regenerative heat exchanger as the fluid is in a two-phase state at its outlet. The quality is low enough that a conservative assumption can be made for the values of the thermophysical properties. It's therefore assumed that the thermophysical properties of the outlet of strong solution be calculated at Q = 0.00. In other words the properties of dynamic viscosity and thermal conductivity are calculated at saturated liquid for the strong aqua-ammonia solution.

But first the values of enthalpy for the strong solution's in and outlet conditions are determined with EES, where enthalpy requires three input parameters: pressure, mixture temperature, and mass concentration.

$$\alpha_{ss,in,WRT}(515.84, 33.223, 0.4523) = -69.03 \left[\frac{kJ}{kg}\right]$$

$$\alpha_{ss,in,DSN}(727.25, 54.024, 0.453) = 3.968 \left[\frac{kJ}{kg}\right]$$

$$\alpha_{ss,in,SMR}(939.54, 68.234, 0.4556) = 68.12 \left[\frac{kJ}{kg}\right]$$

$$\alpha_{ss,out,WRT}(515.84, 49.55, 0.4523) = -3.824 \left[\frac{kJ}{kg}\right] \; with \; Q = 0.008374$$

$$\alpha_{ss,out,DSN}(727.25, 61.46, 0.453) = 56.07 \left[\frac{kJ}{kg}\right] \; with \; Q = 0.01341$$

$$\alpha_{ss,out,SMR}(939.54, 70.8, 0.4556) = 102 \left[\frac{kJ}{kg}\right] \; with \; Q = 0.01593$$

Energy Balance of Regenerative Heat Exchanger

Using the mass flow rates obtained from the MS Excel 'Clear Sky' data sheet in Appendix D 8.1 and the enthalpy values obtained above, the heat transfer rate of the regenerative heat exchanger can be calculated.

Winter design conditions:

$$\dot{Q}_{REGEN,WRT} = \dot{m}_{ss,WRT}\left(\alpha_{ss,out,WRT} - \alpha_{ss,in,WRT}\right) \; (Eq. 2.26)$$

$$\therefore = 0.0044974(-3.824 - (-69.03))$$

$$\therefore = \; 293.2575 \, W \; (Heat \; Added)$$

Average design conditions:

$$\dot{Q}_{REGEN,DSN} = \dot{m}_{ss,DSN}\left(\alpha_{ss,out,DSN} - \alpha_{ss,in,DSN}\right) \; (Eq. 2.26)$$

$$\therefore = 0.0036046(102 - 68.12)$$

$$\therefore = \; 122.1238 \, W \; (Heat \; Added)$$

Summer design conditions:

$$\dot{Q}_{REGEN,SMR} = \dot{m}_{ss,SMR}\left(\alpha_{ss,out,SMR} - \alpha_{ss,in,SMR}\right) \; (Eq. 2.26)$$

$$\therefore = 0.003879(56.07 - 3.968)$$

$$\therefore = \; 202.1037 \, W \; (Heat \; Added)$$

It's clear that for winter design conditions the heat transfer rate has the highest output and would require the largest surface area. Thus, the thermophysical properties of the regenerative heat exchanger can be calculated for winter design conditions and implemented in the thermodynamic design of Chapter 4.

The only unknown at the regenerative heat exchanger is the outlet conditions of the weak solution, whereby the temperature of (ws, out) can be calculated by means of an energy balance determining the enthalpy of state (ws, out).

$$\dot{Q}_{REGEN,WRT} = \dot{m}_{ws,WRT}\left(\alpha_{ws,out,WRT} - \alpha_{ws,in,WRT}\right) \; (Eq. 2.26)$$

$$\therefore \; 293.2575 = 0.003971\left(\alpha_{ws,out,WRT} - 50.48\right)$$

$$\therefore \; \alpha_{ws,out,WRT} = \; -23.3697 \left[\frac{kJ}{kg}\right]$$

Energy Balance of the Auxiliary Heat Exchanger

The heat transfer rates of the auxiliary heat exchanger can be calculated as

Winter design condition:

$$\dot{Q}_{AUX,WRT} = \dot{m}_{ws,WRT}\left(\alpha_{ws,3,WRT} - \alpha_{ws,2,WRT}\right) \quad (Eq.2.26)$$
$$\therefore = 0.003971\left(-176.7 - (-23.38)\right)$$
$$\therefore = 608.834\, W\ (Heat\ Removed)$$

Average design condition:

$$\dot{Q}_{AUX,DSN} = \dot{m}_{ws,DSN}\left(\alpha_{ws,3,DSN} - \alpha_{ws,2,DSN}\right) \quad (Eq.2.26)$$
$$\therefore = 0.003311\left(-148.5 - (65.95)\right)$$
$$\therefore = 710.044\, W\ (Heat\ Removed)$$

Summer design conditions:

$$\dot{Q}_{AUX,SMR} = \dot{m}_{ws,SMR}\left(\alpha_{ws,3,SMR} - \alpha_{ws,2,SMR}\right) \quad (Eq.2.26)$$
$$\therefore = 0.003006\left(-109.1 - (146.2)\right)$$
$$\therefore = 767.432\, W\ (Heat\ Removed)$$

Though the values of heat transfer rate are larger for summer and average design conditions, the winter design condition has a larger mass flow rate at a lower operating pressure, which will result in a larger heat transfer surface area.

Weak Solution Thermophysical Properties

The transport properties of the weak solutions fluid states were determined by using EES' property call function for aqueous ammonia, where the input parameters are: pressure, temperature in [°C], and mass concentration. The remaining design conditions' properties are added to section 5 of Appendix B.

Weak solution state 1:

$$Cp_{ws,1,WRT}(515.84, 61.72, 0.378) = 4.31478\ \left[\frac{kJ}{kg.K}\right] \quad (Eq\ 2.10)$$
$$\rho_{ws,1,WRT}(515.84, 61.72, 0.378) = 840.9\left[\frac{kg}{m^3}\right]$$
$$\mu_{ws,1,WRT}(515.84, 61.72, 0.378) = 0.0004314\left[\frac{kg}{m.s}\right]$$
$$k_{ws,1,WRT}(515.84, 61.72, 0.378) = 0.51\left[\frac{W}{m.K}\right]$$
$$Pr_{ws,1,WRT}(515.84, 61.72, 0.378) = 3.6498[-] \quad (Eq\ 2.25)$$

Weak solution state 2:

$$Cp_{ws,2,WRT}(515.84, 44.94, 0.378) = 4.2777 \left[\frac{kJ}{kg.K}\right] \quad (Eq\ 2.10)$$

$$\rho_{ws,2,WRT}(515.84, 44.94, 0.378) = 855.7 \left[\frac{kg}{m^3}\right]$$

$$\mu_{ws,2,WRT}(515.84, 44.94, 0.378) = 0.0006301 \left[\frac{kg}{m.s}\right]$$

$$k_{ws,2,WRT}(515.84, 44.94, 0.378) = 0.4406 \left[\frac{W}{m.K}\right]$$

$$Pr_{ws,2,WRT}(515.84, 44.94, 0.378) = 6.1176[-] \quad (Eq\ 2.25)$$

Weak solution state 3:

$$Cp_{ws,3,WRT}(515.84, 5, 0.378) = 4.20632 \left[\frac{kJ}{kg.K}\right] \quad (Eq\ 2.10)$$

$$\rho_{ws,3,WRT}(515.84, 5, 0.378) = 875.2 \left[\frac{kg}{m^3}\right]$$

$$\mu_{ws,3,WRT}(515.84, 5, 0.378) = 0.001636 \left[\frac{kg}{m.s}\right]$$

$$k_{ws,3,WRT}(515.84, 5, 0.378) = 0.4899 \left[\frac{W}{m.K}\right]$$

$$Pr_{ws,3,WRT}(515.84, 5, 0.378) = 14.047[-] \quad (Eq\ 2.25)$$

Strong Solution Thermophysical Properties

The strong aqua-ammonia solution's thermophysical properties are approximated using the input parameters of: pressure, temperature, and mass concentration into EES' property call function.

Strong solution state 1:

$$Cp_{ss,1,WRT}(515.84, 33.223, 0.4523) = 4.2876 \left[\frac{kJ}{kg.K}\right] \quad (Eq\ 2.10)$$

$$\rho_{ss,1,WRT}(515.84, 33.223, 0.4523) = 870.3 \left[\frac{kg}{m^3}\right]$$

$$\mu_{ss,1,WRT}(515.84, 33.223, 0.4523) = 0.0008615 \left[\frac{kg}{m.s}\right]$$

$$k_{ss,1,WRT}(515.84, 33.223, 0.4523) = 0.4321 \left[\frac{W}{m.K}\right]$$

$$Pr_{ss,1,WRT}(515.84, 33.223, 0.4523) = 8.5484[-] \quad (Eq\ 2.25)$$

Strong solution state 2:

$$Cp_{ss,2,WRT}(515.84, 49.55, 0.4523) = 4.3238 \left[\frac{kJ}{kg.K}\right] \quad (Eq\ 2.10)$$

$$\rho_{ss,2,WRT}(515.84, 49.55, 0.4523) = 274.7 \left[\frac{kg}{m^3}\right]$$

$$\mu_{ss,2,WRT}(515.84, 49.55, Q = 0) = 0.0005241 \left[\frac{kg}{m.s}\right]$$

$$k_{ss,2,WRT}(515.84, 49.55, Q = 0) = 0.4302 \left[\frac{W}{m.K}\right]$$

$$Pr_{ss,2,WRT}(515.84, 49.55, 0.4523) = 5.2675[-] \quad (Eq\ 2.25)$$

1.5 Thermophysical Properties of Ethylene Glycol Water Mixtures

Ethylene glycol water solution acts as the secondary refrigerant or coolant of the absorption-desorption cycle, and the calculation of the thermophysical properties of ethylene glycol water mixture is constant throughout the design process. Therefore, the calculation of the thermophysical properties will only be demonstrated once for the coolant inlet and outlet of the auxiliary heat exchanger. The inlet temperature has been pre-determined as the coolant comes from the absorber module. The outlet temperature is an iterative estimation, which influences the efficiency of the heat exchanger. Thus, if the efficiency is to low the outlet temperature is adjusted accordingly. The thermophysical properties of the coolant is determined at the fluid bulk temperature and mass concentration of ethylene glycol in water, thus, for the conditions of: $T_{clnt,bulk,WRT}$ = 21.7275 [°C] or 294.8775 [K] and x = 0.25. Thus, the thermophysical properties are:

$$f(x,T) = A_1 + \mathrm{A_2 x} + \mathrm{A_3}\left(\frac{273.15}{\mathrm{T}}\right) + \mathrm{A_4 x}\left(\frac{273.15}{\mathrm{T}}\right) + \mathrm{A_5}\left(\frac{273.15}{\mathrm{T}}\right)^2 \quad (Eq\ A.2),$$

with parameters from Table A.6.

$$Cp_{clnt,bulk,WRT}(0.25, 294.8775)$$

$$= 5.36449 + 0.78863(0.25) - 2.59001\left(\frac{273.15}{294.8775}\right) - 2.73187(0.25)\left(\frac{273.15}{294.8775}\right) + 1.43759\left(\frac{273.15}{294.8775}\right)^2$$

$$\therefore = 3.7634 \left[\frac{kJ}{kg.K}\right]$$

$\rho_{clnt,bulk,WRT}(0.25,294.8775)$

$$= 658.49825 - 54.81501(0.25) + 664.71643\left(\frac{273.15}{294.8775}\right) + 232.72605(0.25)\left(\frac{273.15}{294.8775}\right) - 322.61661\left(\frac{273.15}{294.8775}\right)^2$$

$\therefore = 1037.6 \left[\frac{kg}{m^3}\right]$

$k_{clnt,bulk,WRT}(0.25,294.8775)$

$$= -4.63024 - 2.14817(0.25) - 12.70106\left(\frac{273.15}{294.8775}\right) + 5.40536(0.25)\left(\frac{273.15}{294.8775}\right) + 10.989\left(\frac{273.15}{294.8775}\right)^2$$

$\therefore = 0.4998\left[\frac{W}{m.K}\right]$

$\ln(f(x,T)) = A_1 + \mathrm{A_2 q} + \mathrm{A_3}\left(\frac{273.15}{\mathrm{T}}\right) + \mathrm{A_4 q}\left(\frac{273.15}{\mathrm{T}}\right) + \mathrm{A_5}\left(\frac{273.15}{\mathrm{T}}\right)^2 \quad (Eq\ A.3)$,

with parameters from Table A.6.

$\ln\left(\mu_{clnt,bulk,WRT}(0.25,294.8775)\right)$

$$= 0.8318 - 1.3762(0.25) - 0.07629\left(\frac{273.15}{294.8775}\right) + 1.0772(0.25)\left(\frac{273.15}{294.8775}\right) - 0.20174\left(\frac{273.15}{294.8775}\right)^2$$

$\therefore = 0.000192763\left[\frac{kg}{m.s}\right]$

$\ln\left(Pr_{clnt,bulk,WRT}(0.25,294.8775)\right)$

$$= 3.96951 + 0.70076(0.25) - 12.98045\left(\frac{273.15}{294.8775}\right) + 2.64789(0.25)\left(\frac{273.15}{294.8775}\right) + 11.589\left(\frac{273.15}{294.8775}\right)^2$$

$\therefore = 14.5556[-]$

2 REMAINING THERMOPHYSICAL PROPERTIES OF STATE 3, 4, AND 5

This section focuses on the thermophysical properties of state 3, 4, and 5 which are omitted from the main text, but did play an integral role in calculating the thermodynamic design and rating of Appendices D 2.1, 3.1, and 4.1.

Table B.1: Thermophysical properties of state 3, 4, and 5 for average ambient condition.

Aqua-Ammonia Thermophysical Properties								
T_3	77.45	°C	T_4	54.6101	°C	T_5	15	°C
P_3	727.25	kPa	P_4	727.25	kPa	P_5	727.25	kPa
α_3	1453	kJ/kg	α_4	1391.113	kJ/kg	α_5	58.1984	kJ/kg
Cp_3	1.490532	kJ/kg.K	Cp_4	4.02682	kJ/kg.K	Cp_5	4.69343	kJ/kg.K
ρ_3	4.445	kg/m^3	ρ_4	6.83864	kg/m^3	ρ_5	622.765	kg/m^3
μ_3	1.1951E-05	kg/m.s	μ_4	1.1634E-05	kg/m.s	μ_5	0.00016736	kg/m.s
k_3	0.0311455	W/m.K	k_4	0.0326865	W/m.K	k_5	0.507217	W/m.K
Pr_3	0.932801		Pr_4	1.433302		Pr_5	1.548668	

Table B.2: Thermophysical properties of state 3, 4, and 5 for winter ambient condition.

Aqua-Ammonia Thermophysical Properties								
T_3	55.43	°C	T_4	47.6809	°C	T_5	5	°C
P_3	515.84	kPa	P_4	515.84	kPa	P_5	515.84	kPa
α_3	1409	kJ/kg	α_4	1384.169	kJ/kg	α_5	11.1974	kJ/kg
Cp_3	2.7191	kJ/kg.K	Cp_4	3.768195	kJ/kg.K	Cp_5	4.63071	kJ/kg.K
ρ_3	3.351	kg/m^3	ρ_4	5.28899	kg/m^3	ρ_5	636.998	kg/m^3
μ_3	1.1116E-05	kg/m.s	μ_4	1.1317E-05	kg/m.s	μ_5	0.00018688	kg/m.s
k_3	0.0284156	W/m.K	k_4	0.0310749	W/m.K	k_5	0.539840	W/m.K
Pr_3	0.934832		Pr_4	1.374453		Pr_5	1.633274	

3 REMAINING THERMOPHYSICAL PROPERTIES STATE TP

This section focuses on the remaining thermophysical properties of state TP, which are omitted from the main text, but did play an integral role in the calculation of the stage 1 condenser's thermodynamic design of Appendices D 2.1 and 3.1.

Table B.3: Thermophysical properties of state TP for average ambient condition.

Aqua-Ammonia Thermophysical Properties		
T_{TP}	20	°C
P_{TP}	727.25	kPa
α_{TP}	1235.081	kJ/kg
Cp_{TP}		kJ/kg.K
ρ_{TP}	7.248959	kg/m^3
μ_{TP}	2.0978E-05	kg/m.s
k_{TP}	0.0611583	W/m.K
Pr_{TP}	1.440224	

Table B.4: Thermophysical properties of state TP for winter ambient condition.

Aqua-Ammonia Thermophysical Properties		
T_{TP}	10	°C
P_{TP}	515.84	kPa
α_{TP}	1182.205	kJ/kg
Cp_{TP}		kJ/kg.K
ρ_{TP}	5.606328	kg/m^3
μ_{TP}	2.1851E-05	kg/m.s
k_{TP}	0.0609562	W/m.K
Pr_{TP}	1.389982	

4 REMAINING THERMOPHYSICAL PROPERTIES STATE 6, 8, AND 10

This section focuses on the remaining thermophysical properties of state 6, 8, and 10, which are omitted from the main text, but did play an integral role in the calculation of the pre-cool heat exchanger's thermodynamic design and rating of Appendix D 5.1.

Table B.5: Thermophysical properties of state 6, 8, & 10 for average ambient condition.

Aqua-Ammonia Thermophysical Properties								
T_6	3.236	°C	T_8	-15	°C	T_{10}	8.681	°C
P_6	727.25	kPa	P_8	236.39	kPa	P_{10}	727.25	kPa
α_6	3.00148	kJ/kg	α_8	3.001478	kJ/kg	α_{10}	1500.519	kJ/kg
Cp_6	4.62062	kJ/kg.K	Cp_8	4.45409	kJ/kg.K	Cp_{10}	2.317	kJ/kg.K
ρ_6	639.456	kg/m^3	ρ_8	632.439	kg/m^3	ρ_{10}	1.773	kg/m^3
μ_6	0.0001868	kg/m.s	μ_8	0..00021884	kg/m.s	μ_{10}	9.454E-06	kg/m.s
k_6	0.533840	W/m.K	k_8	0.541433	W/m.K	k_{10}	0.02373	W/m.K
Pr_6	1.617245		Pr_8	1.79651		Pr_{10}	0.9231	

Table B.6: Thermophysical properties of state 6, 8, & 10 for winter ambient condition.

Aqua-Ammonia Thermophysical Properties								
T_6	-3.009	°C	T_8	-15	°C	T_{10}	0.7104	°C
P_6	515.84	kPa	P_8	236.39	kPa	P_{10}	515.84	kPa
α_6	-25.81591	kJ/kg	α_8	-25.8159	kJ/kg	α_{10}	1481.899	kJ/kg
Cp_6	4.58699	kJ/kg.K	Cp_8	4.48039	kJ/kg.K	Cp_{10}	2.357	kJ/kg.K
ρ_6	648.048	kg/m^3	ρ_8	637.446	kg/m^3	ρ_{10}	1.832	kg/m^3
μ_6	0.0002085	kg/m.s	μ_8	0.00022352	kg/m.s	μ_{10}	9.164E-06	kg/m.s
k_6	0.547786	W/m.K	k_8	0.552975	W/m.K	k_{10}	0.02314	W/m.K
Pr_6	1.745595		Pr_8	1.80855		Pr_{10}	0.9331	

5 THERMOPHYSICAL PROPERTIES OF WEAK SOLUTION STATE 1, 2, AND 3

This section focuses on the remaining thermophysical properties of weak solution state 1, 2, and 3, which are omitted from the main text, but did play an integral role in calculating the auxiliary and regenerative heat exchanger's thermodynamic design of Appendix D 8.1.

Table B.7: Thermophysical properties of weak solution state 1, 2, & 3 for summer ambient condition.

Aqua-Ammonia Thermophysical Properties								
$T_{ws,1}$	90.32	°C	$T_{ws,2}$	81.28	°C	$T_{ws,3}$	23	°C
$P_{ws,1}$	939.51	kPa	$P_{ws,2}$	939.51	kPa	$P_{ws,3}$	939.51	kPa
$\alpha_{ws,1}$	186.8	kJ/kg	$\alpha_{ws,2}$	146.2	kJ/kg	$\alpha_{ws,3}$	-109.1	kJ/kg
$Cp_{ws,1}$	4.12038	kJ/kg.K	$Cp_{ws,2}$	4.13012	kJ/kg.K	$Cp_{ws,3}$	4.20715	kJ/kg.K
$\rho_{ws,1}$	821.3	kg/m^3	$\rho_{ws,2}$	831.9	kg/m^3	$\rho_{ws,3}$	879.8	kg/m^3
$\mu_{ws,1}$	0.0002566	kg/m.s	$\mu_{ws,2}$	0.0003018	kg/m.s	$\mu_{ws,3}$	0.001151	kg/m.s
$k_{ws,1}$	0.7504	W/m.K	$k_{ws,2}$	0.6632	W/m.K	$k_{ws,3}$	0.4465	W/m.K
$Pr_{ws,1}$	1.41116		$Pr_{ws,2}$	1.88072		$Pr_{ws,3}$	10.8453	

Table B.8: Thermophysical properties of weak solution state 1, 2, & 3 for average ambient condition.

Aqua-Ammonia Thermophysical Properties								
$T_{ws,1}$	77.79	°C	$T_{ws,2}$	64.04	°C	$T_{ws,3}$	15	°C
$P_{ws,1}$	727.25	kPa	$P_{ws,2}$	727.25	kPa	$P_{ws,3}$	727.25	kPa
$\alpha_{ws,1}$	127	kJ/kg	$\alpha_{ws,2}$	65.95	kJ/kg	$\alpha_{ws,3}$	-148.5	kJ/kg
$Cp_{ws,1}$	4.13504	kJ/kg.K	$Cp_{ws,2}$	4.15101	kJ/kg.K	$Cp_{ws,3}$	4.22087	kJ/kg.K
$\rho_{ws,1}$	831.2	kg/m^3	$\rho_{ws,2}$	845.6	kg/m^3	$\rho_{ws,3}$	879.4	kg/m^3
$\mu_{ws,1}$	0.0003186	kg/m.s	$\mu_{ws,2}$	0.0004183	kg/m.s	$\mu_{ws,3}$	0.001436	kg/m.s
$k_{ws,1}$	0.6302	W/m.K	$k_{ws,2}$	0.5296	W/m.K	$k_{ws,3}$	0.4688	W/m.K
$Pr_{ws,1}$	2.09048		$Pr_{ws,2}$	3.27871		$Pr_{ws,3}$	12.9291	

6 THERMOPHYSICAL PROPERTIES OF STRONG SOLUTION STATE 1 AND 2

This section focuses on the remaining thermophysical properties of strong solution state 1 and 2, which are omitted from the main text, but did play an integral role in calculating the regenerative heat exchanger's thermodynamic design of Appendix D 8.1.

Table B.9: Thermophysical properties of strong solution state 1 & 2 for summer ambient condition.

Aqua-Ammonia Thermophysical Properties					
$T_{ss,1}$	68.234	°C	$T_{ss,2}$	70.8	°C
$P_{ss,1}$	939.51	kPa	$P_{ss,2}$	939.51	kPa
$\alpha_{ss,1}$	68.12	kJ/kg	$\alpha_{ss,2}$	102	kJ/kg
$Cp_{ss,1}$	4.18637	kJ/kg.K	$Cp_{ss,2}$	4.13788	kJ/kg.K
$\rho_{ss,1}$	803.8	kg/m^3	$\rho_{ss,2}$	256.6	kg/m^3
$\mu_{ss,1}$	0.0003424	kg/m.s	$\mu_{ss,2}$	90.0003355	kg/m.s
$k_{ss,1}$	0.529	W/m.K	$k_{ss,2}$	0.5362	W/m.K
$Pr_{ss,1}$	6.30641		$Pr_{ss,2}$	2.58907	

Table B.10: Thermophysical properties of strong solution state 1 & 2 for average ambient condition.

Aqua-Ammonia Thermophysical Properties					
$T_{ss,1}$	54.024	°C	$T_{ss,2}$	61.46	°C
$P_{ss,1}$	727.25	kPa	$P_{ss,2}$	727.25	kPa
$\alpha_{ss,1}$	3.968	kJ/kg	$\alpha_{ss,2}$	56.07	kJ/kg
$Cp_{ss,1}$	4.17017	kJ/kg.K	$Cp_{ss,2}$	4.14788	kJ/kg.K
$\rho_{ss,1}$	820.1	kg/m^3	$\rho_{ss,2}$	250.1	kg/m^3
$\mu_{ss,1}$	0.0004639	kg/m.s	$\mu_{ss,2}$	0.0004055	kg/m.s
$k_{ss,1}$	0.449	W/m.K	$k_{ss,2}$	0.4795	W/m.K
$Pr_{ss,1}$	4.30949		$Pr_{ss,2}$	3.51207	

Appendix C

Extended Chapter 3 - Concept Design Generation and Evaluation

Summary

Appendix C deals with the design requirements and technical specifications of the seven heat exchanger designs omitted from Chapter 3 to keep the oeuvre concise. The requirements are ranked according to the level of importance to which the concept designs can be evaluated according to the ranked requirement system. Typically, a functional analysis is required before the design requirements and specifications, but for the purpose of this oeuvre the functional analysis can be construed from the literature in Chapter 2.1.

Table of Contents

List of Tables

List of Figures

1 DESIGN REQUIREMENTS AND TECHNICAL SPECIFICATIONS

The design must consist of a large number of standard components to minimise the cost of each heat exchanger, such standard components include the outer shell, inner tubing, valves, fittings, bolts and nuts, and seals. The elements to be designed for are the heat transfer surface area (i.e. tube length), tube layout, tube bundle type, and shell inlet-to-outlet type. The entire system layout must be designed, in other words the design of each heat exchanger connecting to the next to complete the absorption-desorption heating and refrigeration cycle.

Other important requirements to consider are total size and mass, thermal efficiency, cost effectiveness, and heat transfer capacity. Furthermore, the requirements to keep in consideration are the maintainability, the ease of manufacturing, and how reliable the design will be. The designs of the several heat exchangers must all adhere to legislation governing aqua-ammonia absorption-desorption refrigeration systems, and most important requirement to assess is the impact on human and environmental safety.

Each of the above mentioned requirements are ranked according to the level of importance, with which the concepts generated will be evaluated. A rating system of 1 to 10 is used, where 1 indicates a low level of importance and 10 indicates the highest level of importance. The thermodynamic requirements are the most important for the scope of work set out in this dissertation, where this oeuvre does not focus on the mechanical design in infinitesimal detail, but there is still need for the mechanical design to consider operational safety and feasible.

The design requirements of the de-superheating condenser, the pre-cool HTEX, the regenerative HTEX, and the auxiliary HTEX have the same ranked design requirements due to all consisting of single phase refrigerant designs, which are tabulated in Table C.1. The design ranked requirements of the evaporator and condenser cannot be tabulated on the same table, as the characteristic of both heat exchangers are vastly different. Thus, the condenser’s ranked requirements are in Table C.2. Lastly, the ranked requirements of the evaporator module is tabulated in Table C.3.

Table C.1: No-phase change heat exchanger – Ranked design requirements.

Requirement	Level	Comments
Thermodynamic Requirements:		
• Heat transfer rating	10	Maximum for all design conditions.
• Sensible overall heat transfer coefficient	10	Overall heat transfer coefficient within expected ranges.
• Stream allocation	7	Allocation of refrigerant in or over tubes.
• Thermal HTEX efficiency	8	As high possible to expected efficiencies.
• Outlet temperatures of secondary fluids	8	Outlet temperatures of secondary fluid are connected directly to thermal efficiency.
• Number of tubes	7	Within a sensible number for manufacturing and heat transfer purposes $2 < N_t < 100$.
• Number of tube passes	7	Restricted to single tube pass.
• Heat transfer surface length	8	< 2 m
• Minimisation of pressure drops within each HTEX module	4	< 1 kPa
Fluid Flow Requirements:		
• Distribution of fluid flowing through each HTEX module	7	Fluids must be able to reach all areas within HTEX module.
• Blockage or back pressure prevention	7	HTEX components should not create a blockage or back pressure preventing flow.
• Thermo siphoning flow	8	The cycle's thermal syphoning must be optimal for high levels of efficiency.
Mechanical Module Requirements:		
• Size	5	Height < 1m, Width < 1m, Length < 2.5m.
• Mass	5	< 500kg per module.
• Safety requirement	9	Static and Dynamic stresses of all components must have a SF > 2
• L/D_s	9	$(2 < L/D_s < 7)$
• Cost effectiveness	8	Design must be as cheap as possible without compromising safety and thermal efficiency.
• Maintainability	6	Design must be easily maintained.
• Seal	10	Modules must be sealed off to the environment.
• Keeping refrigerant and coolant separate	9	Refrigerant and coolant must be kept separate at all times.
• Piping and fittings	8	The piping and fittings must adhere to the safety requirements.
• Manufacturability	7	Each design must be easily manufactured.

Table C.2: Superposition condenser – Ranked design requirements.

Requirement	Level	Comments
Thermodynamic requirements:		
• Heat transfer rating	10	Maximum for all design conditions.
• Sensible overall heat transfer coefficient	9	Overall heat transfer coefficient within expected ranges.
• Aqua-ammonia outlet quality $Q \leq 0.00$	10	The outlet of the condenser must be lower or equal to saturated liquid.
• Stream allocation	10	Allocation of refrigerant in or over tubes.
• Thermal HTEX efficiency	9	As high possible to expected efficiencies.
• Outlet temperatures of secondary fluids	8	Outlet temperatures of secondary fluid are connected directly to thermal efficiency.
• Number of tubes	7	Within a sensible number for manufacturing and heat transfer purposes $2 < N_t < 100$.
• Number of tube passes	7	Restricted to single tube pass.
• Heat transfer surface length	8	< 2 m
• Minimisation of pressure drops within each HTEX module	4	< 1 kPa
Fluid flow requirements:		
• Distribution of fluid flowing through each HTEX module	7	Fluids must be able to reach all areas within HTEX module.
• Blockage or back pressure prevention	7	HTEX components should not create a blockage or back pressure preventing flow.
• Thermo siphoning flow	8	The cycle's thermal syphoning must be optimal for high levels of efficiency.
Mechanical module requirements:		
• Size	5	Height < 1m, Width < 1m, Length < 2.5m.
• Mass	5	< 500kg per module.
• Safety requirement	9	Static and Dynamic stresses of all components must have a SF > 2
• L/D_s	9	$(2 < L/D_s < 7)$
• Cost effectiveness	8	Design must be as cheap as possible without compromising safety and thermal efficiency.
• Maintainability	6	Design must be easily maintained.
• Seal	10	Modules must be sealed off to the environment.
• Keeping refrigerant and coolant separate	9	Refrigerant and coolant must be kept separate at all times.
• Piping and fittings	8	The piping and fittings must adhere to the safety requirements.
• Manufacturability	7	Each design must be easily manufactured.

Table C 3: Evaporator – Ranked design requirements.

Requirement	Level	Comments
Thermodynamic requirements:		
• Heat transfer rating	8	Maximum for all design conditions.
• Sensible overall heat transfer coefficient	9	Overall heat transfer coefficient within expected ranges.
• Ammonia outlet quality $Q \geq 1.00$	10	The outlet of the evaporator refrigerant must be higher or equal to saturated vapour.
• Stream allocation	10	Allocation of refrigerant in or over tubes.
• Thermal HTEX efficiency	9	As high possible to expected efficiencies.
• Outlet temperatures of secondary fluids	8	Outlet temperatures of secondary fluid are connected directly to thermal efficiency.
• Number of tubes	7	Within a sensible number for manufacturing and heat transfer purposes $2 < N_t < 100$.
• Number of tube passes	10	Restricted to single tube pass.
• Heat transfer surface length	8	< 2 m
• Minimisation of pressure drops within each HTEX module	4	< 1 kPa
Fluid flow requirements:		
• Distribution of fluid flowing through each HTEX module	7	Fluids must be able to reach all areas within HTEX module.
• Blockage or back pressure prevention	7	HTEX components should not create a blockage or back pressure preventing flow.
• Thermal syphoning flow	8	The cycle's thermal syphoning must be optimal for high levels of efficiency.
Mechanical module requirements:		
• Size	5	Height < 1m, Width < 1m, Length < 2.5m.
• Mass	5	< 500kg per module.
• L/D_s	9	$(2 < L/D_s < 7)$
• Safety requirement	9	Static and Dynamic stresses of all components must have a SF > 2
• Cost effectiveness	8	Design must be as cheap as possible without compromising safety and thermal efficiency.
• Maintainability	6	Design must be easily maintained.
• Seal	10	Modules must be sealed off to the environment.
• Keeping refrigerant and coolant separate	9	Refrigerant and coolant must be kept separate at all times.
• Piping and fittings	8	The piping and fittings must adhere to the safety requirements.
• Manufacturability	7	Each design must be easily manufactured.

2 CONCEPT DESIGN, EVALUATION, AND SELECTION

The following section focuses on the generation and evaluation of design concepts for all of the heat exchangers within the scope of work. The concept design are generated with the background obtained from (Kakac & Liu, 2002) and (Thulukakanam, 2000) (with the basics of heat exchangers discussed during Chapter 2.2). A brief discussion will be given for each basic component and main heat exchanger concepts. It was decided that to keep the design of each heat exchanger as simple as possible, due to the little documented cases of thermodynamic designs of heat exchangers for aqua-ammonia refrigeration. This boasted well for the cost of manufacturing as simple designs would be cheaper to manufacture. Furthermore, it was decided that the heat exchangers will consists of single tube and shell passes, with counter- or cross-flow. With these design selection it's possible to prove a complex subject matter without over complicating the thermodynamic design calculations.

2.1 Standardised Heat Exchanger Shell Types

The shell types of shell and tube heat exchangers have been standardised by TEMA (Tubular Exchanger Manufacturers Association) found on (Engineering Page, 2016). The standardised shell types are identified by a letter system and will be illustrated in the following section.

Single Shell Pass – Type E

The type E shell is the most commonly used due to its simplicity and low cost to manufacture. Fluid enters the shell at one end and exits at the opposite end, in other words a single pass of fluid in the shell.

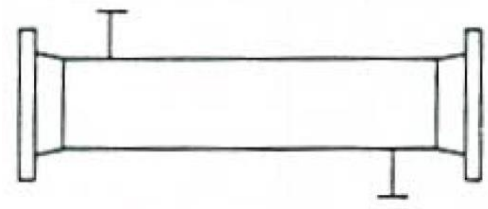

Figure C.1: Shell type E.

Split Cross-flow Shell – Type G

The split flow of type G has horizontal baffles which are approximately 75% of the tube length, the pressure drop of type G is similar to the pressure drop of type E. Because type G has cross-flow of fluids it does have a higher LMTD temperature and thus a higher effectiveness for the same surface area.

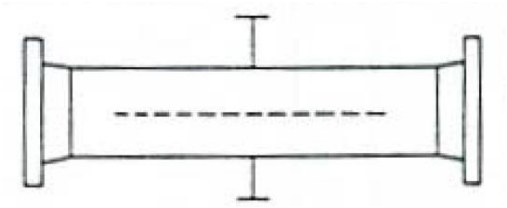

Figure C.2: Shell type G.

Double Split Flow Shell – Type H

Type H has similar characteristics to that of type G, but has two inlets, two outlets, and two separating horizontal baffles.

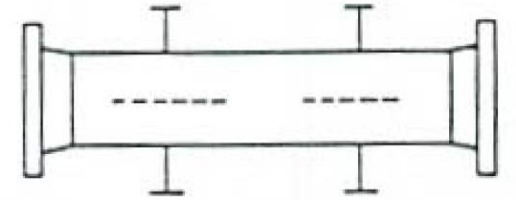

Figure C.3: Shell type H.

Divided Flow Shell – Type J

The divided flow shell has two inlets and one central outlet, this type of shell is used for low pressure drop design applications such as condensers. Type J has approximately 1/8 the pressure drop of type E.

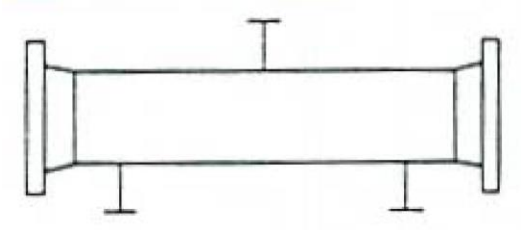

Figure C.4: Shell type J.

Kettle Type Boiler – Type K

Type K is mainly used for the application of vaporisation of the fluid line, the tube bundle covers the lower half of the shell. The saturated vapour to superheated vapour would then exit the top half of the shell.

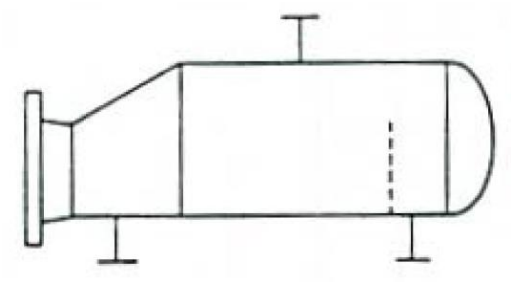

Figure C.5: Shell type K.

Cross-flow Shell – Type X

The shell characteristics of type X is similar to type J, only now type X has one inlet and one outlet concentric to one another. The inlet and outlet is divided with a single distribution impingement plate near the inlet.

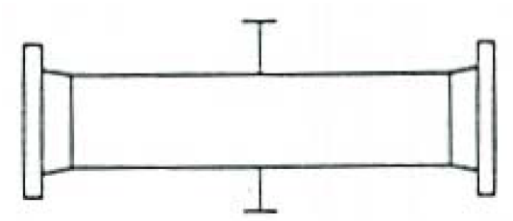

Figure C.6: Shell type X.

2.2 Standardised Heat Exchanger Tube Bundle Layouts

Figure C.7 depicts the standard tube bundle layout, which illustrates the angle between tubes.

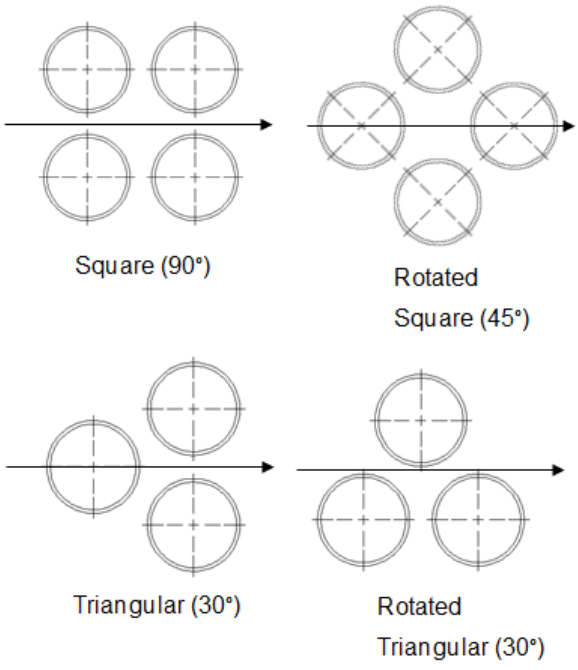

Figure C.7: Standard tube bundle layout angles.

The 30° layout gives the highest tube density, but if the pitch ratio is lower than 1.25 the tube plate will become structurally weak. The pitch ratio is standardised to be between 1.25 and 1.5 (Kakac & Liu, 2002). The 45° and 90° tube layouts are used when external cleaning is required. The 45° tube layout would perform similarly to the 30° tube layout in terms of flow pattern. A higher tube density would mean a higher number of tubes at a shorter heat transfer length, but would result in more welding time which increases the cost. Thus, for the thermodynamic design sizing and mechanical design of the heat exchangers a 45° tube bundle will be used.

2.3 Standardised Heat Exchanger Transverse Baffle Types

Transverse baffle types adapted from (Thulukakanam, 2000). Optimum baffle is between 0.4 and 0.6 of the shell diameter and the baffle cut of 25% to 35% is recommended by (Thulukakanam, 2000). The single and double segment baffles are the most commonly used, with the triple segment used in for low pressure drop applications (Kakac & Liu, 2002).

Single-Segmental Transverse Baffle

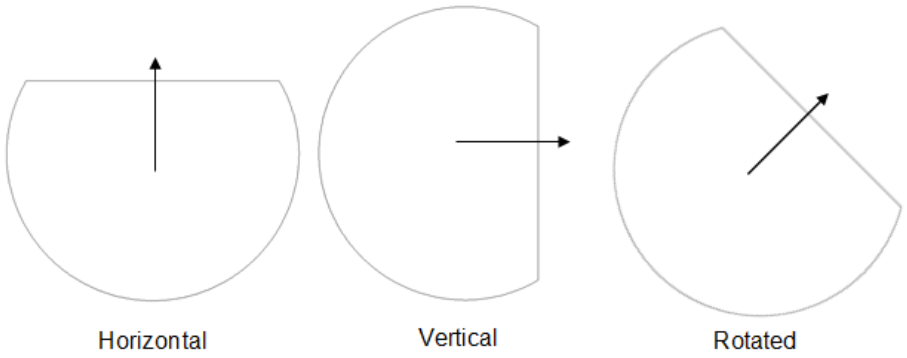

Figure C.8: Single segment baffle.

Double-Segmental Transverse Baffle

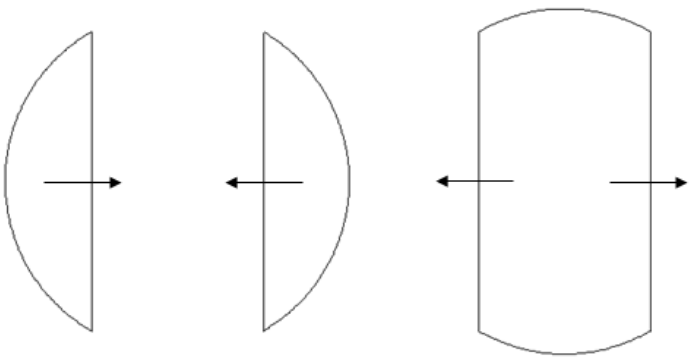

Figure C.9: Double segment baffle.

Triple-Segmental Transverse Baffle

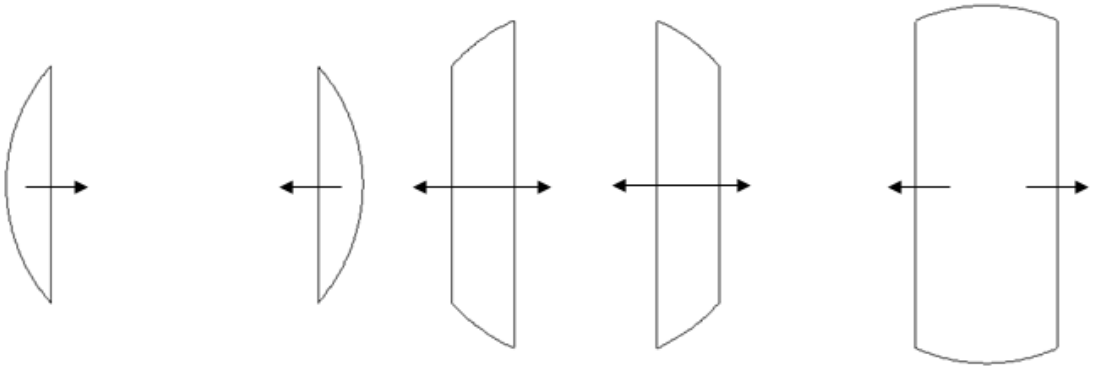

Figure C.10: Triple segment baffle.

2.4 De-superheating Condenser and Pre-Cool Heat Exchanger Concept Designs

The concepts of the de-superheating condenser and the pre-cool heat exchanger can be the same concepts as both heat exchangers are vapour vs. liquid fluid lines. It was decided that the superheated vapour be within the shell flowing over the tubes, thus, turbulent flow is created more easily resulting in better heat transfer coefficient. The concepts will be evaluated according to the specific design requirements set out in section 1.1.

Concept 1 depicted in Figure C.11 is a permutation of shell type E and double segmented transverse baffles. The superheated refrigerant vapour enters the shell at the opposite end to the coolant inlet, creating a counter-flow heat exchanger. The inside of the tubes can be easily cleaned as result of any material build-up of the ethylene glycol water mixture. Concept 1 can be easily assembled and therefore manufactured. The double segmented baffles are more expensive to manufacture in comparison to a single segmented baffle.

Concept 1:

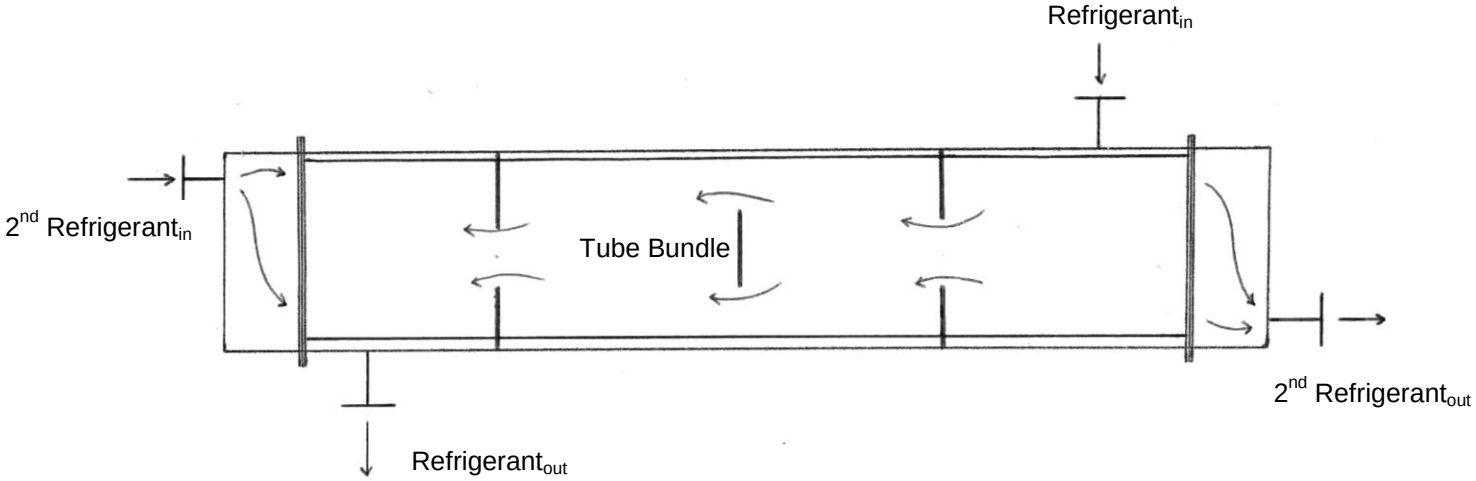

Figure C.11: DHC and PC – Concept 1

Concept 2:

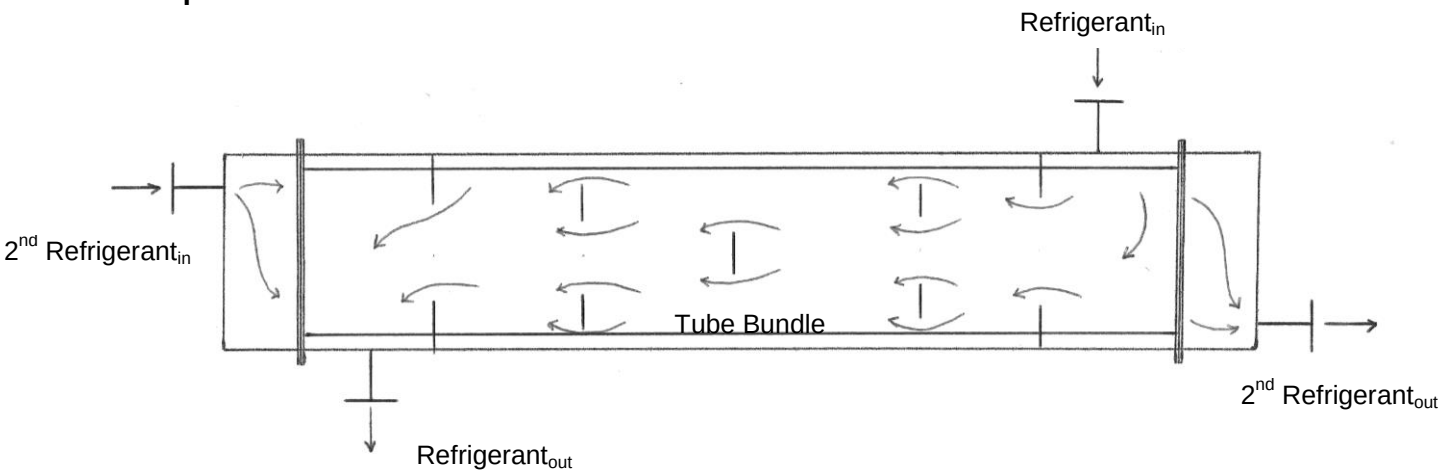

Figure C.12: DHC and PC – Concept 2

Concept 2 is depicted by Figure C.12 is a permutation of shell type E and triple segmented baffles, creating a counter-flow heat exchanger. The refrigerant and coolant streams have the same characteristics as concept 1, with the only difference being the lower pressure drop of concept 2. The cost of manufacturing of concept 2 would be the highest of the 4 concept designs.

Concept 3:

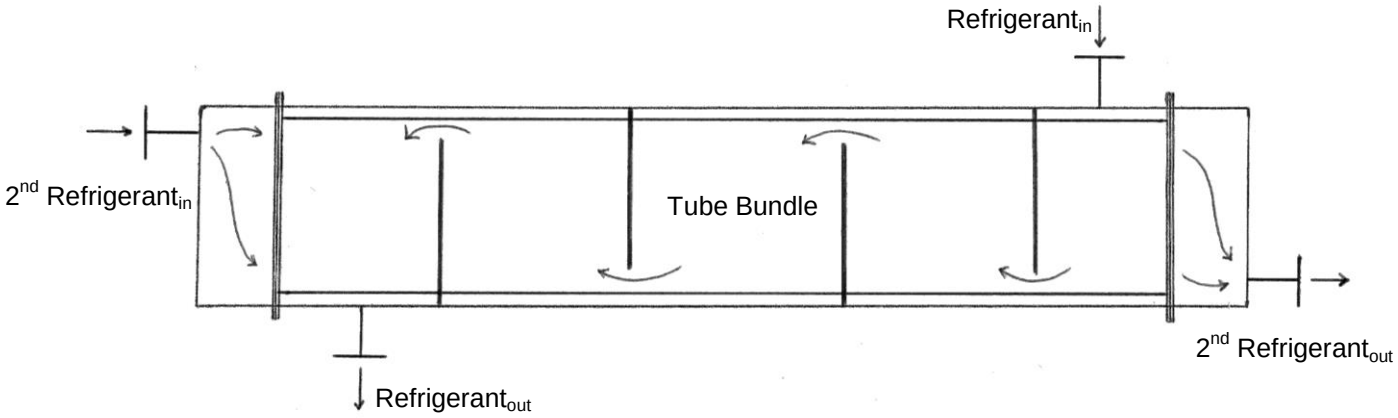

Figure C.13: DHC and PC – Concept 3

Concept 3 is illustrated by Figure C.13, which is a permutation of the shell type E and single segmented transverse baffles, creating a counter-flow heat exchanger. Concept 3 would be the simplest to manufacture and the also the cheapest, though the pressure drop would be the highest of the design concepts. Similar to concept 1, concept 3 would be easily cleaned at the tube side.

Concept 4:

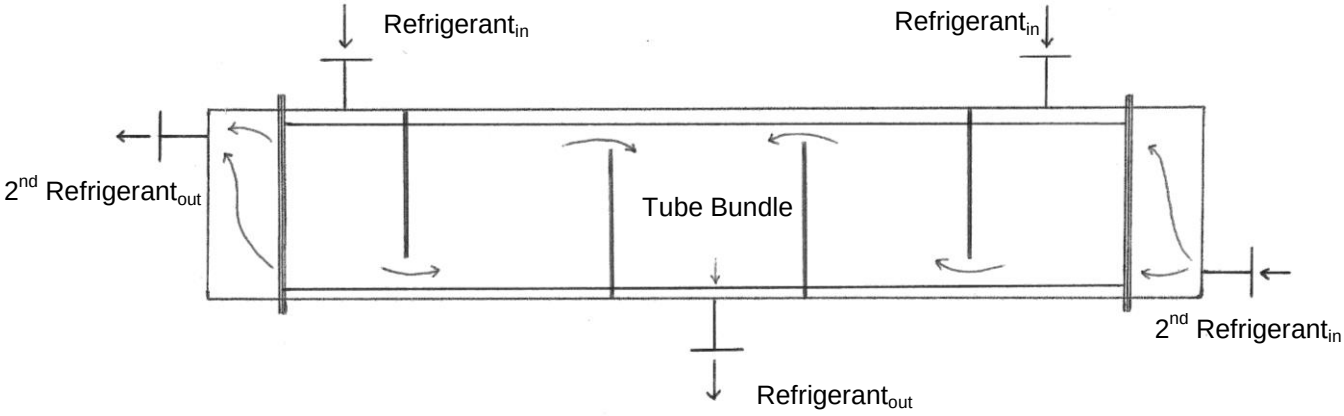

Figure C.14: DHC and PC – Concept 4

The final concept is depicted in Figure C.14, and is a permutation of shell type J and single segmented baffles. The aqueous ammonia refrigerant flows into the shell side via two inlets and exits via a central outlet. The flow of the shell side has both parallel and counter-flow, which might not be optimal for the heat transfer rating and heat transfer coefficient.

Each of the subsequent concept design evaluation tables will be ranked with a weighted importance scale and a 1 to 4 ranking of each criterion, which works as follows:

- 1 = Requirement not met.
- 2 = Requirement partially met.
- 3 = Requirement sufficiently met.
- 4 = Requirement excellently met.

Table C.4: De-superheating condenser and Pre-cool HTEX concept evaluation.

Criteria	Weighted Importance	Concepts			
Thermodynamic Requirements		**1**	**2**	**3**	**4**
Heat transfer rating	1	3	3	3	3
Heat transfer coefficient	1	3	4	3	3
Stream allocation	0.7	4	4	4	4
Coolant outlet temperatures	0.8	3	3	3	3
Number of tubes	0.7	3	3	3	3
Number of tube passes	0.7	4	4	4	4
Heat transfer surface length	0.8	3	3	3	3
Pressure drop	0.4	3	4	3	2
Total	6.1	4.925	5.275	4.925	4.825

Table C.4 continued:

Fluid Flow Requirements					
Fluid distribution	0.7	3	3	3	3
Blockage of fluids	0.7	3	3	3	2
Thermo siphoning flow	0.8	3	4	3	3
Total	2.2	1.65	1.85	1.65	1.475
Mechanical Module Requirements					
Size	0.5	3	3	3	3
Mass	0.5	4	4	4	4
Safety requirements	0.9	4	4	4	4
Cost effectiveness	0.8	2	1	4	3
Maintainability	0.6	3	3	4	3
Seal	1	4	4	4	4
Separate fluids	0.9	3	3	3	3
Piping and fittings	0.8	3	3	3	3
Manufacturability	0.7	2	1	4	4
Total	6.7	5.25	4.875	6.15	5.8
Grand Total	15	11.825	12	12.725	12.1
Percentage	100	78.833	80	84.833	80.667

In conclusion, Table C.4 suggests that concept 3 would be the best alternative to which the thermodynamic design sizing and mechanical design should represent. Though concept 3 might have a slightly larger pressure drop to that of concept 1 and 2, it does make economically more sense as it is cheaper to manufacture and to maintain.

2.5 Condenser Concept Designs

Concepts for the condenser module have been created using the knowledge obtained from the standardised shell types of which are specialised to condenser units. The concepts generated are permutations of shell type J and X, with variances of inlets, outlets and baffles. Though it is convention for the high pressure refrigerant to be allocated to tube side, for the condenser it is decided that the condensing aqueous-ammonia refrigerant be allocated to the shell side.

Figure C.15 illustrates the first concept of the condenser module, and it is simply a representation of shell type J. Saturated aqua-ammonia vapour enters the shell side via two inlets and exits the shell as saturated liquid at a central outlet, which creates a cross-flow heat exchanger. A distribution volume added to the top of the design facilitates the distributing of aqua-ammonia vapour over the entire length of the heat exchanger. Concept 1 has very low pressure drops, as it is specifically used for condenser applications.

Concept 1:

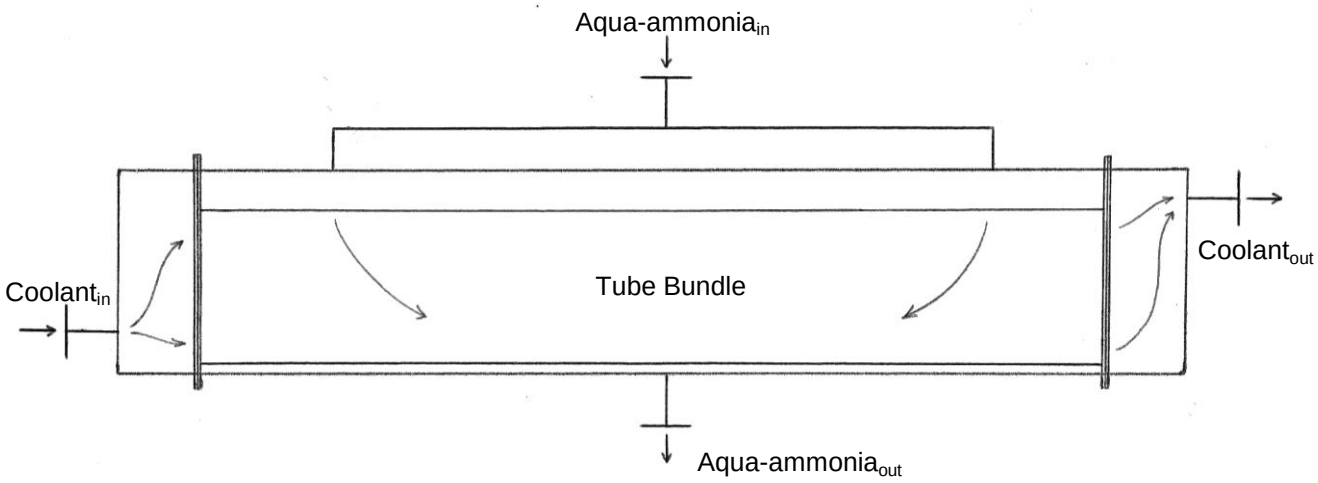

Figure C.15: Condenser – Concept 1

Concept 2:

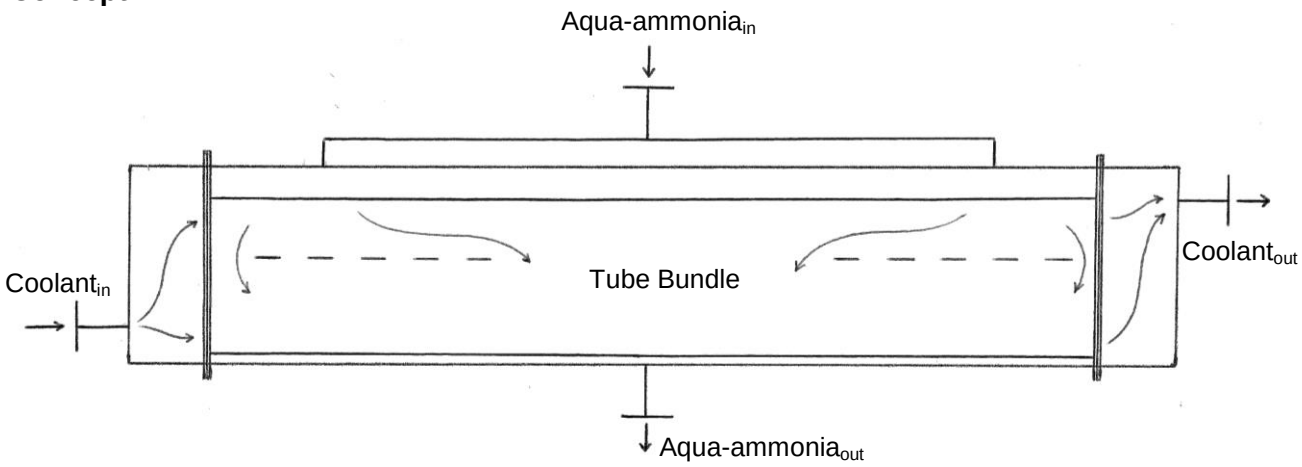

Figure C.16: Condenser – Concept 2

Concept 2 as illustrated in Figure C.16 is a permutation of shell types H and J, where the shell has two inlets, two horizontal baffles, and one central baffle. The horizontal baffles will split the flow, distributing the fluid over the entire length of the condenser, thus creating a cross-flow heat exchanger. The pressure drop of concept 2 might be higher than concept 1, and the horizontal baffles might accumulate saturated liquid droplets.

Concept 3:

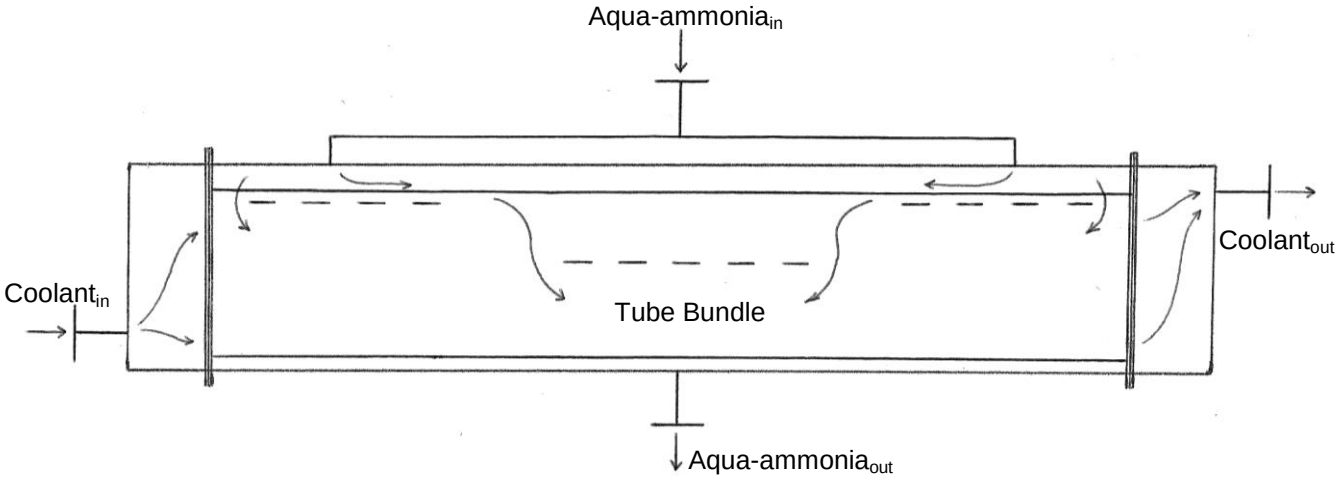

Figure C.17: Condenser – Concept 3

Figure C.17 illustrates concept 3, which is a permutation similar to concept 2, with the only difference being the placement and size of the horizontal baffle. Concept 3's horizontal baffles are closer to the inlets above the tube bundle, thus, changing the horizontal baffles to impingement plates. The impingement plates facilitate the distribution of the vapour entering the condenser concept. Concept 3 will have the largest pressure drop of the 4 concepts, but a similar heat transfer coefficient to concept 2.

Concept 4:

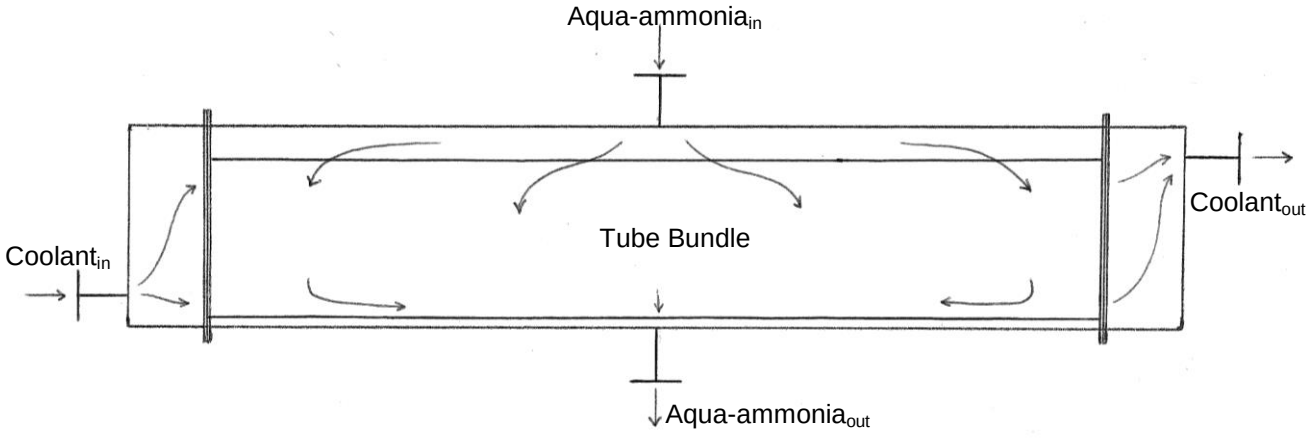

Figure C.18: Condenser – Concept 4

Concept 4 depicted by Figure C.18 is simply a representation of shell type X, where it is specifically used for most practical condensing applications. The saturated aqua-ammonia vapour enters the shell via a single central inlet and exits as saturated liquid via a concentric outlet. Concept 4 has similar pressure drop values and distribution volume to that of concept 1. Concept 4 would be the

cheapest to manufacture of the four concepts, but might be ranked lower on its shell side heat transfer coefficient. The concept designs generated for the condenser unit are evaluated in the following table as:

Table C.5: Condenser concept evaluation.

Criteria	Weighted Importance	Concepts			
Thermodynamic Requirements		**1**	**2**	**3**	**4**
Heat transfer rating	1	3	3	3	3
Heat transfer coefficient	0.9	3	3	4	3
Q ≤ 0.00	1	3	3	3	3
Stream allocation	1	3	3	3	3
Coolant outlet temperatures	0.8	3	3	4	3
Number of tubes	0.7	3	3	3	3
Number of tube passes	0.7	4	4	4	4
Heat transfer surface length	0.8	3	3	4	3
Pressure drop	0.4	4	3	1	4
Total	7.3	5.75	5.65	6.075	5.75
Fluid Flow Requirements					
Fluid distribution	0.7	4	3	4	2
Blockage of fluids	0.7	4	2	2	4
Thermo siphoning flow	0.8	4	3	3	4
Total	2.2	2.2	1.475	1.65	1.85
Mechanical Module Requirements					
Size	0.5	3	4	4	3
Mass	0.5	3	3	3	3
Safety requirements	0.9	4	4	4	4
Cost effectiveness	0.8	4	2	2	4
Maintainability	0.6	4	3	3	4
Seal	1	4	4	4	4
Separate fluids	0.9	4	4	4	4
Piping and fittings	0.8	3	3	3	4
Manufacturability	0.7	4	3	3	4
Total	6.7	6.25	5.65	5.65	6.45
Grand Total	16.2	14.2	12.775	13.375	14.05
Percentage	100	87.654	78.858	82.562	86.728

To conclude, Table C.5 indicated concept 1 has the reigning concept, though concept 4 is a narrow second. Concept 2 is cost effective, has good refrigerant distribution, and low pressure drop, which are telling factors when designing a condenser unit.

2.6 Evaporator Concept Designs

The concepts of the evaporator are permutations of type K shell, with variances in inlet and outlet placement. The concepts also take into consideration the tertiary gas of helium within the heat exchanger module, which creates partial pressure. Though it is convention for the high pressure refrigerant to be allocated to tube side, for the evaporator it is decided that the evaporating aqueous-ammonia refrigerant be allocated to the shell side and the ethylene glycol water mixture to tube side.

Concept 1:

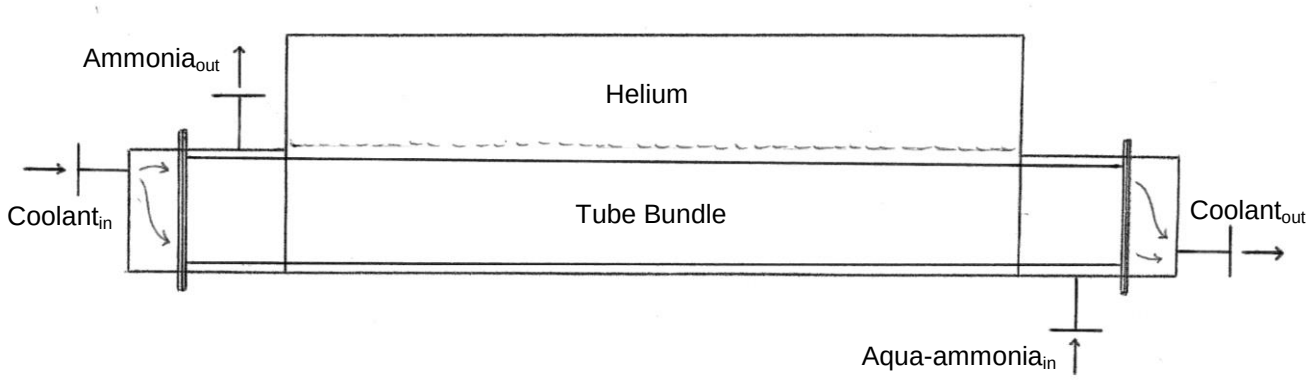

Figure C.19: Evaporator – Concept 1

Figure C.19 illustrates the first evaporator design concept, with is an adaptation of the shell type K, but as a single tube pass heat exchanger. The top vapour compartment will fill the much lower density helium that creates the partial pressure of the aqua-ammonia. The sub-cooled aqua-ammonia liquid enters the shell at the bottom right of the shell through the venturi nozzle and exits as saturated vapour ammonia at the top left of the shell, thus creating a counter-flow heat exchanger with no transverse baffles. The outlet of ammonia is below the helium line to prevent helium from exiting the evaporator. The shell would be difficult to manufacture and would require a lot of laser cut components.

Concept 2:

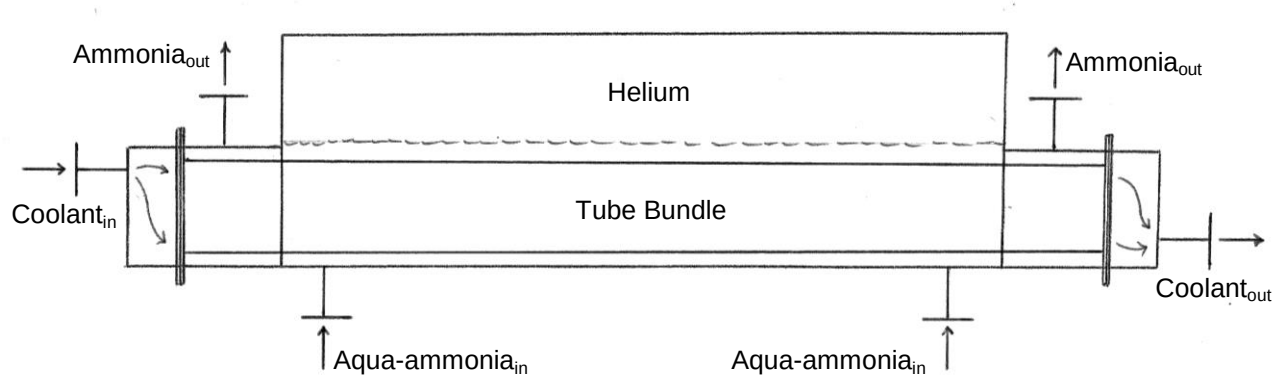

Figure C.20: Evaporator – Concept 2

Evaporator concept 2 is illustrated by Figure C.20 and is a permutation of the shell type K, but with a bit more manufacturability of the shell housing. The sub-cooled aqua-ammonia liquid enter the shell via two nozzles where only one is a venturi nozzle, with the saturated vapour ammonia exiting the shell at the top left. Concept 2 is a counter-flow heat exchanger with no transverse baffles, with single tube pass arrangement, and top kettle compartment for helium gas.

Concept 3:

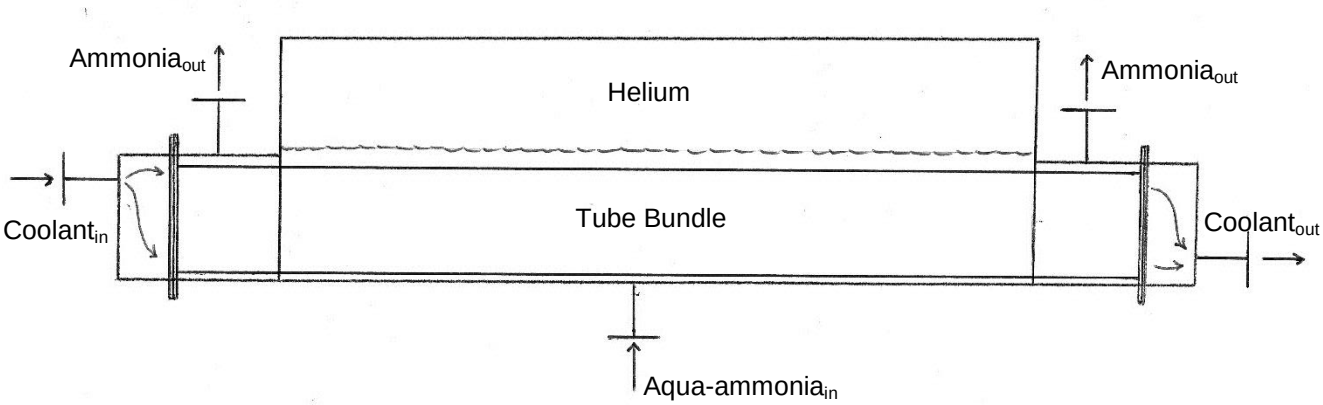

Figure C.21: Evaporator – Concept 3

Concept 3 is depicted in Figure C.21 and is a permutation of concept 2 and shell type J, where only now sub-cooled aqua-ammonia liquid enters through a single venturi nozzle at the bottom of the shell. The saturated ammonia vapour exits the shell opposite ends of the shell, but the outlets must remain lower than the helium gas line to prevent helium from exiting the evaporator. Concept 3 is simpler to manufacture than the previous two concepts and has a more symmetrical cross-flow pattern of refrigerant than the previously the mentioned concepts. Though, concept 3 might have short comings in terms of distribution of sub-cooled liquid over the entire tube length.

Concept 4:

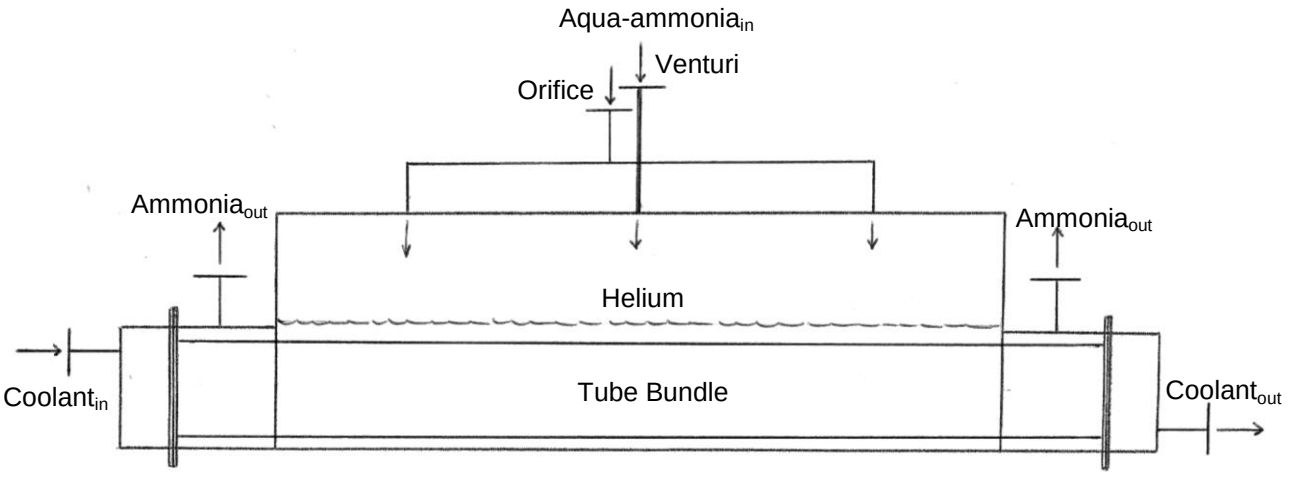

Figure C.22: Evaporator – Concept 4

Concept 3 is depicted in Figure C.22 and is an improved distribution concept of concept 3 and shell type J, where now the sub-cooled aqua-ammonia liquid enters the evaporator from the top of the shell via three inlets. The central inlet is the venturi nozzle, with adjacent normal nozzles to the left and right. The saturated ammonia vapour still exits at opposite ends of the shell, but the outlets must remain lower than the helium gas line to prevent helium from exiting the evaporator. Concept 4 has a symmetrical cross-flow to co-counter-flow pattern of refrigerant. Though, concept 4 has the best distribution of sub-cooled liquid over the entire tube length.

The evaporator's concept evaluation is illustrated in the following table as:

Table C.6: Evaporator concept evaluation.

Criteria	Weighted Importance	Concepts			
Thermodynamic Requirements		**1**	**2**	**3**	**4**
Heat transfer rating	1	3	3	3	3
Heat transfer coefficient	0.9	3	3	3	4
Q ≤ 1.00	1	3	3	3	3
Stream allocation	1	3	3	3	3
Coolant outlet temperatures	0.8	3	3	4	4
Number of tubes	0.7	2	2	3	3
Number of tube passes	0.7	4	4	4	4
Heat transfer surface length	0.8	2	3	2	4
Partial pressure across evaporator	0.7	1	2	1	3
Total	7.6	5.15	5.525	5.525	6.5

Table C.6 continued:

Fluid Flow Requirements					
Fluid distribution	0.7	1	3	2	3
Blockage of fluids	0.7	4	3	3	3
Thermo siphoning flow	0.8	4	2	3	3
Total	2.2	1.675	1.45	1.475	1.65
Mechanical Module Requirements					
Size	0.5	2	2	2	3
Mass	0.5	2	2	2	3
Safety requirements	0.9	4	4	4	4
Cost effectiveness	0.8	4	3	3	3
Maintainability	0.6	3	3	3	3
Seal	1	4	4	4	4
Separate refrigerant and coolant	0.9	4	4	4	4
Piping and fittings	0.8	4	3	4	3
Manufacturability	0.7	2	2	2	2
Total	6.7	5.7	5.3	5.5	5.55
Grand Total	16.5	12.525	12.275	12.5	13.7
Percentage	100	75.909	74.394	75.758	83.03

To conclude the evaporator concept designs, Table C.6 shows that concept 4 has the best concept out of the four concepts made. Concept 4 has the best distribution of sub-cooled aqua-ammonia liquid, which will benefit the creation of partial pressure. Concept 4 has symmetric outlets to benefit cross-flow fluid patterns and it situated at the top half of the shell assisting the low density expanding saturated vapour ammonia.

2.7 Regenerative Heat Exchanger Concept Designs

The regenerative heat exchanger design concepts are permutations of type E, G, J, and X shell types. The allocations of fluid streams remain open for the concept designs. Concept 1 is illustrated in Figure C.23 and is a simple shell type E with single segmented transverse baffles. The heat exchanger concept has counter-flow and the strong solution aqueous ammonia is allocated to tube side heat transfer. The outlet of the strong solution is placed at the top of the header as there is a possibility of vapour bubbles forming, which flows upwards due to its low density. Concept 1 has simplicity and is easy to manufacture, which is therefore cheap, but does compromise on shell side pressure drop and possible vapour entrapment.

Concept 1:

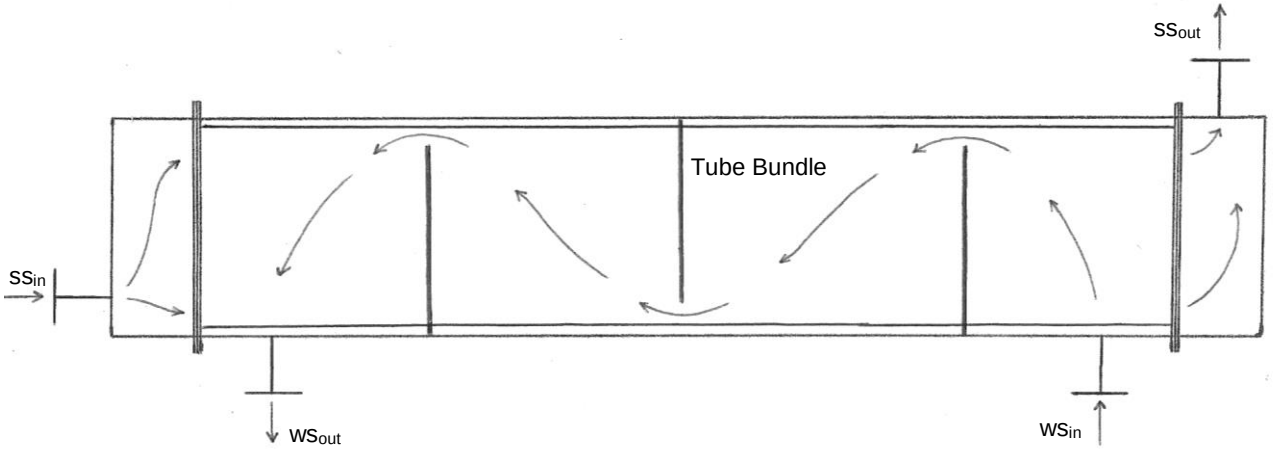

Figure C.23: Regenerative heat exchanger – Concept 1

Concept 2:

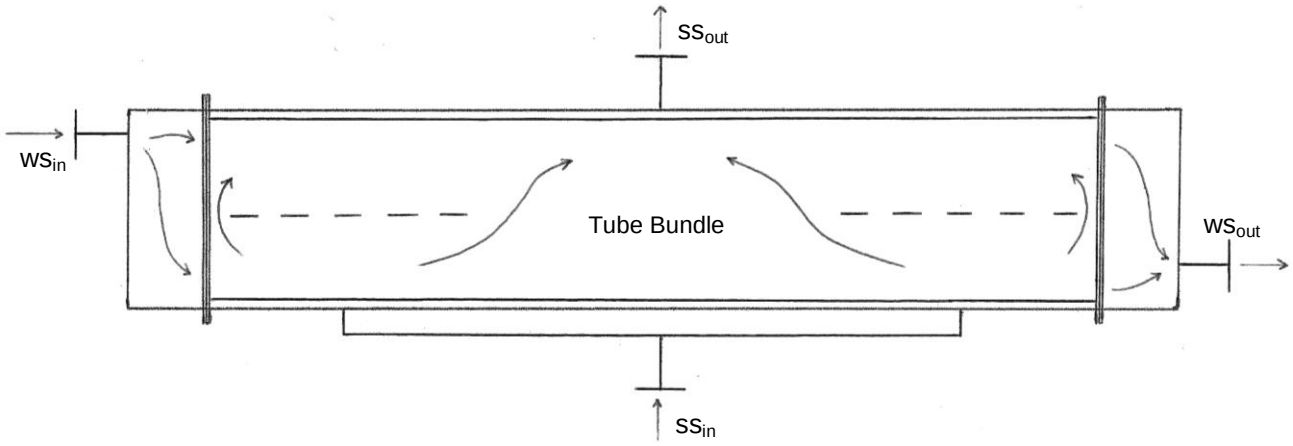

Figure C.24: Regenerative heat exchanger – Concept 2

The second concept is depicted by Figure C.24 and is a permutation of shell types J and H, where the shell has divided inlets, two horizontal baffles, but only one central outlet. The allocation of fluid streams for concept 2 is switch around from concept 1, where the strong solution aqua-ammonia now flows over the tubes at the shell side. Concept 2 has a cross-flow pattern upwards with horizontal baffle splitting the flow into four fluid streams. This would benefit the heat transfer coefficient of the shell side at the compromise of pressure loss.

Concept 3:

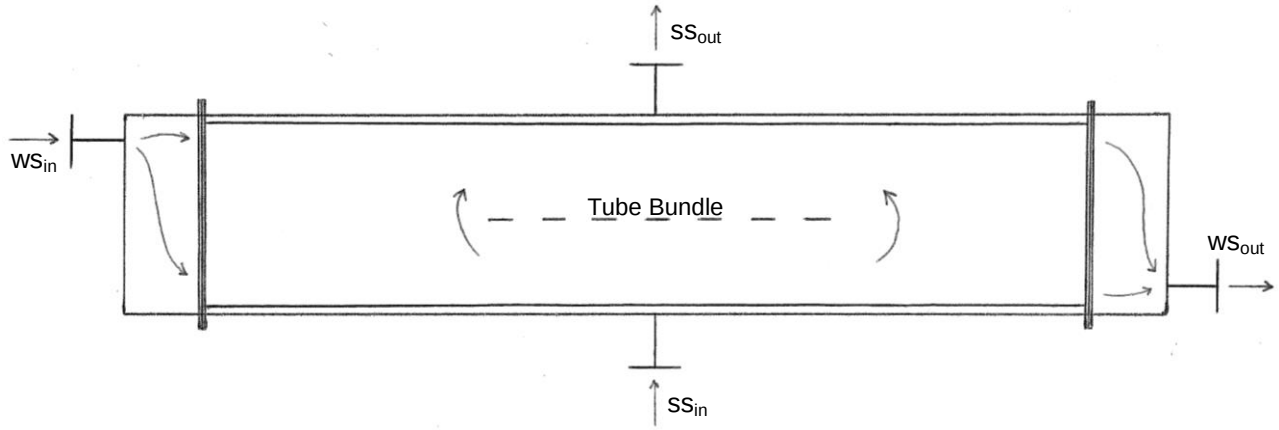

Figure C.25: Regenerative heat exchanger – Concept 3

Concept 3 is depicted by Figure C.25 and is a simple representation of shell type G, where the shell has a single inlet and outlet, concentrically placed in the middle of the shell creating a cross-flow pattern. The shell side has a horizontal baffle at approximately 75% of the tube length, which splits the flow of the strong solution aqua-ammonia. Similar to concept 2 the horizontal baffle would benefit the heat transfer coefficient of shell side, but this is at the cost of pressure loss. Concept 3 would be cheaper to manufacture than concept 1 and 2 as it has less parts to laser cut and weld.

Concept 4:

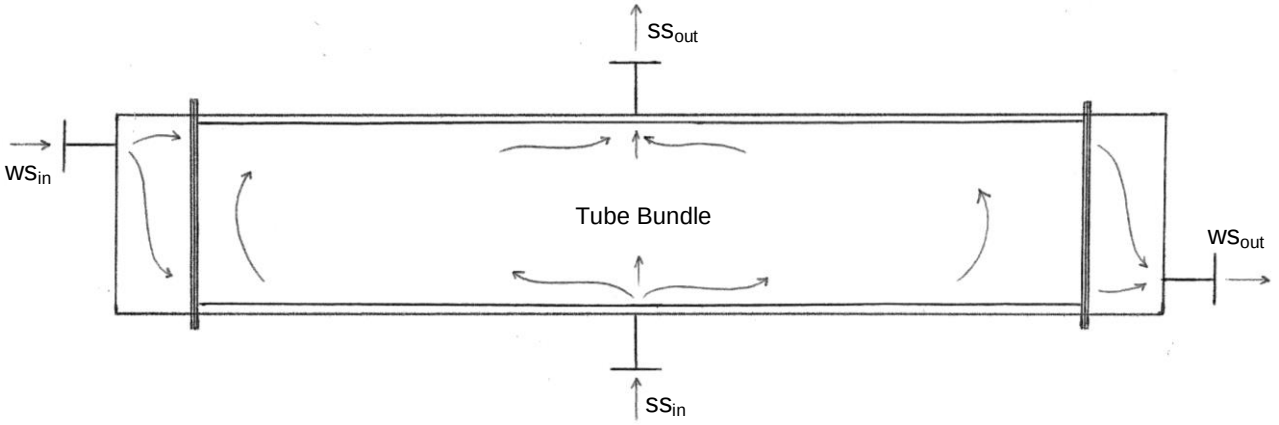

Figure C.26: Regenerative heat exchanger – Concept 4

Lastly, concept 4 is represented by Figure C.26 which is an adaptation of shell type X, with the strong solution aqua-ammonia allocated to shell side heat transfer. Concept 4 will produce the lowest pressure loss of the 4 concept designs, and would be the cheapest to manufacture as there are no baffles to be laser cut. Concept 4 will have a lower heat transfer coefficient to that of concept 2 and 3, which would result in a slightly longer heat transfer surface area.

The concept designs of the regenerative heat exchanger are evaluated in the following table as:

Table C.7: Regenerative heat exchanger concept evaluation.

Criteria	Weighted Importance	Concepts			
Thermodynamic Requirements		**1**	**2**	**3**	**4**
Heat transfer rating	1	3	3	3	3
Heat transfer coefficient	0.9	3	4	4	3
Stream allocation	1	4	3	3	3
Outlet temperatures	0.8	4	4	4	3
Number of tubes	0.7	3	3	3	3
Number of tube passes	0.7	4	4	4	4
Heat transfer surface length	0.8	4	3	3	3
Pressure drop	0.7	1	2	2	4
Total	6.6	5.425	5.375	5.375	5.525
Fluid Flow Requirements					
Fluid distribution	0.7	3	4	4	3
Blockage of fluids	0.7	2	3	3	4
Thermo siphoning flow	0.8	2	3	3	4
Total	2.2	1.275	1.825	1.825	2.025
Mechanical Module Requirements					
Size	0.5	3	3	3	2
Mass	0.5	3	3	3	3
Safety requirements	0.9	4	4	4	4
Cost effectiveness	0.8	2	3	3	4
Maintainability	0.6	3	3	3	3
Seal	1	4	4	4	4
Separate refrigerant and coolant	0.9	4	4	4	4
Piping and fittings	0.8	3	3	3	3
Manufacturability	0.7	4	4	4	4
Total	6.7	5.7	5.9	5.9	5.975
Grand Total	15.5	12.4	13.1	13.1	13.525
Percentage	100	80	84.516	84.516	85.806

In conclusion, Table C.7 indicates concept 4 as the reigning concept between the four concepts. Concept 4 is the cheapest to manufacture, but does compromise on heat transfer coefficient slightly. The lower heat transfer coefficient of concept 4 would translate in slightly longer tubes lengths, but won't cost as much as the horizontal baffles of concepts 1 and 2. Concept 4 has the lowest pressure drop, which benefits the slight boiling of strong solution allocated to shell side heat transfer.

2.8 Auxiliary Heat Exchanger Concept Designs

The auxiliary heat exchanger design concepts are representations of shell type E, with the only variance in the allocation of fluid lines. The concept designs are simple and effective, as the heat exchanger consists of liquid vs. liquid heat transfer.

Concept 1:

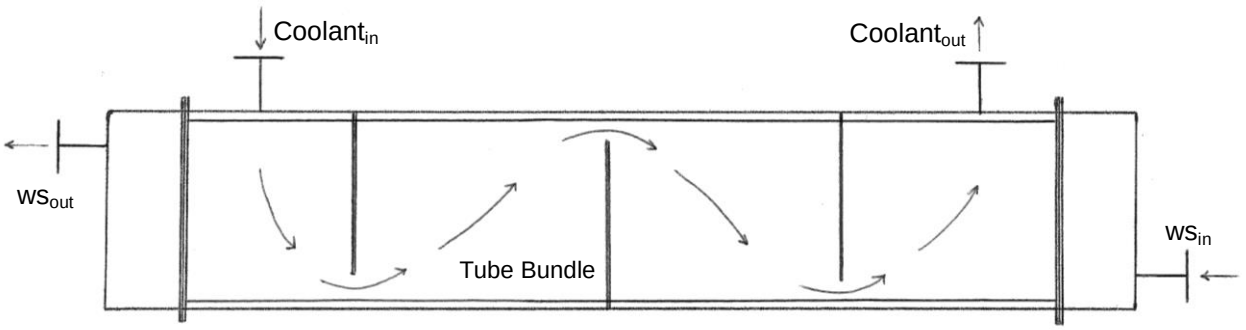

Figure C.27: Auxiliary heat exchanger – Concept 1

Concept 1 is represented by Figure C.27, with the weak aqua-ammonia solution allocated to tube side heat transfer. It is conventional to allocate the high pressure fluid to flow through the tubes.

Concept 2:

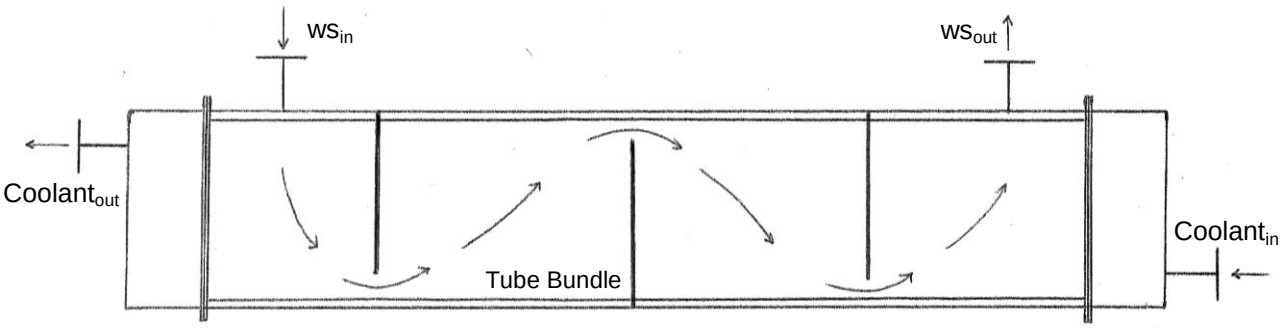

Figure C.28: Auxiliary heat exchanger – Concept 2

Concept 2 is depicted by Figure C.28, with the weak solution aqua-ammonia allocated to shell side heat transfer. This allocation is chosen as it would be easier to clean the tube side ethylene glycol water material build-up and the weak solution aqua-ammonia would have the lower heat transfer coefficient, therefore allocating it to flow over the tubes.

The concept designs generated for the auxiliary heat exchanger are evaluated in the following table as:

Table C.8: Auxiliary heat exchanger concept evaluation.

Criteria	Weighted Importance	Concepts	
Thermodynamic Requirements		**1**	**2**
Heat transfer rating	1	3	3
Heat transfer coefficient	0.9	4	3
Stream allocation	1	3	4
Outlet temperatures	0.8	4	4
Number of tubes	0.7	3	3
Number of tube passes	0.7	4	4
Heat transfer surface length	0.8	4	2
Pressure drop	0.7	1	4
Total	6.6	5.4	5.55
Fluid Flow Requirements			
Fluid distribution	0.7	3	3
Blockage of fluids	0.7	3	3
Thermo siphoning flow	0.8	1	4
Total	2.2	1.25	1.85
Mechanical Module Requirements			
Size	0.5	3	3
Mass	0.5	3	3
Safety requirements	0.9	4	4
Cost effectiveness	0.8	3	3
Maintainability	0.6	4	2
Seal	1	4	4
Separate refrigerant and coolant	0.9	4	4
Piping and fittings	0.8	3	3
Manufacturability	0.7	4	4
Total	6.7	6.05	5.75
Grand Total	15.5	12.7	13.15
Percentage	100	81.935	84.839

In conclusion of the auxiliary heat exchanger concept designs, Table C.8 illustrates the allocation of weak solution to tube side heat transfer be more beneficial than shell side heat transfer. Though, concept 2 might be more difficult to maintain, the benefit of low pressure drops within the tubes far out weight maintenance.

2.9 Auxiliary-Regenerative Heat Exchanger Concept Design

The decision to use concept 4 of the regenerative heat exchanger and concept 2 of the auxiliary heat exchangers gave the opportunity to be innovative by synthesizing the two concepts to form a single heat exchanger module. This is made possible by the weak solution aqua-ammonia flowing through the tubes for both concepts. The newly formed synthesized Aux-Regen HTEX is illustrated by Figure C.29 below.

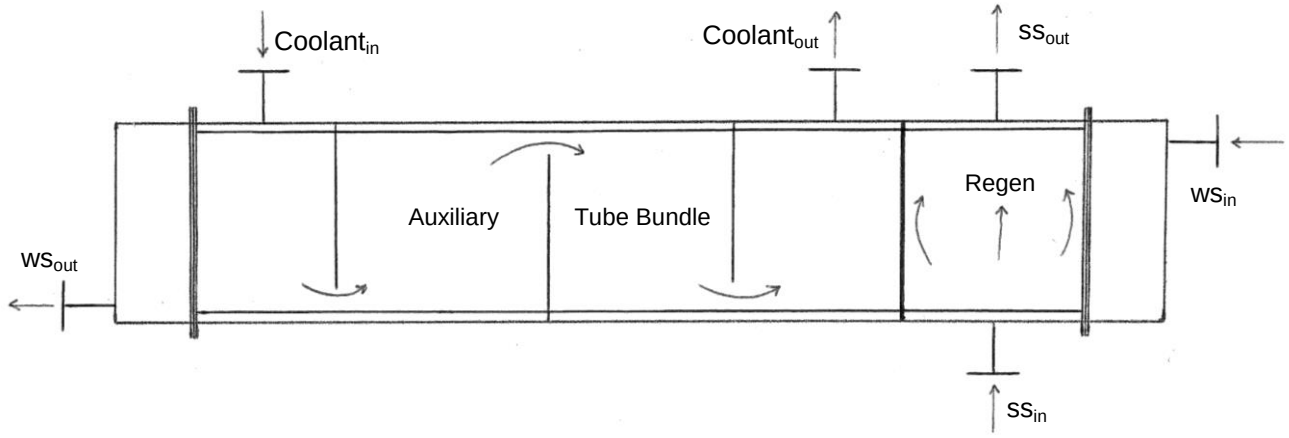

Figure C.29: Auxiliary-Regenerative heat exchanger concept design.

Appendix D 1

Extended Chapter 4 - Thermodynamic Design

Summary

Recorded in Appendix D 1 is an extension of the omitted temperature vs. unit surface area figures and an explanatory guide of further Appendix D documentation. The explanatory guide focuses on the layout of the rest of the appendix, in terms of folder to file references to guide the reader to each heat exchanger's MS Excel thermodynamic design model and the EES verification thereof.

Table of Contents

List of Tables

List of Figures

1 TEMPERATURE VS. UNIT SURFACE AREA

Presented in the tables below are the inlet and outlet temperatures of each heat exchanger for their respective design conditions.

Table D 1.1: Stage 1 condenser - Inlet and outlet temp for summer ambient conditions.

Parameter	Inlet Temp [°C]	Outlet Temp [°C]
Refrigerant	28 (State TP)	23 (State 5)
Coolant	18.404	22.653

Table D 1.2: Stage 2 condenser - Inlet and outlet temp for winter ambient conditions.

Parameter	Inlet Temp [°C]	Outlet Temp [°C]
Refrigerant	47.681 (State 4)	28 (State TP)
Coolant	4.133	46

Table D 1.3: De-superheating cond - Inlet and outlet temp for summer ambient conditions.

Parameter	Inlet Temp [°C]	Outlet Temp [°C]
Refrigerant	95.36 (State 3)	60.055 (State 4)
Coolant	56.5	82.712

Table D 1.4: Pre-Cool HTEX - Inlet and outlet temp for summer ambient conditions.

Parameter	Inlet Temp [°C]	Outlet Temp [°C]
‘Hot’ Refrigerant	23 (State 5)	8.353 (State 6)
‘Cold’ Refrigerant	-15 (State 9)	15.11 (State 10)

Table D 1.5: Evaporator - Inlet and outlet temp for summer ambient conditions.

Parameter	Inlet Temp [°C]	Outlet Temp [°C]
Refrigerant	-15 (State 8)	-15 (State 9)
Coolant	10	-14.5

Table D 1.6: Regenerative HTEX - Inlet and outlet temp for winter ambient conditions.

Parameter	Inlet Temp [°C]	Outlet Temp [°C]
Strong solution	33.223	49.55
Weak solution	61.72	44.94

Table D 1.7: Auxiliary HTEX - Inlet and outlet temp for winter ambient conditions.

Parameter	Inlet Temp [°C]	Outlet Temp [°C]
Weak Solution	44.94	5
Coolant	0.455	43

The following figures represent the temperature vs. unit surface area of each heat exchanger, where these graphical representations are approximated as linear but are logarithmic in nature. The linear approximation is made possible by the design assumption that the overall heat transfer coefficient is constant and uniform across the length of the heat exchanger surface area.

1.1 Stage 1 Condenser

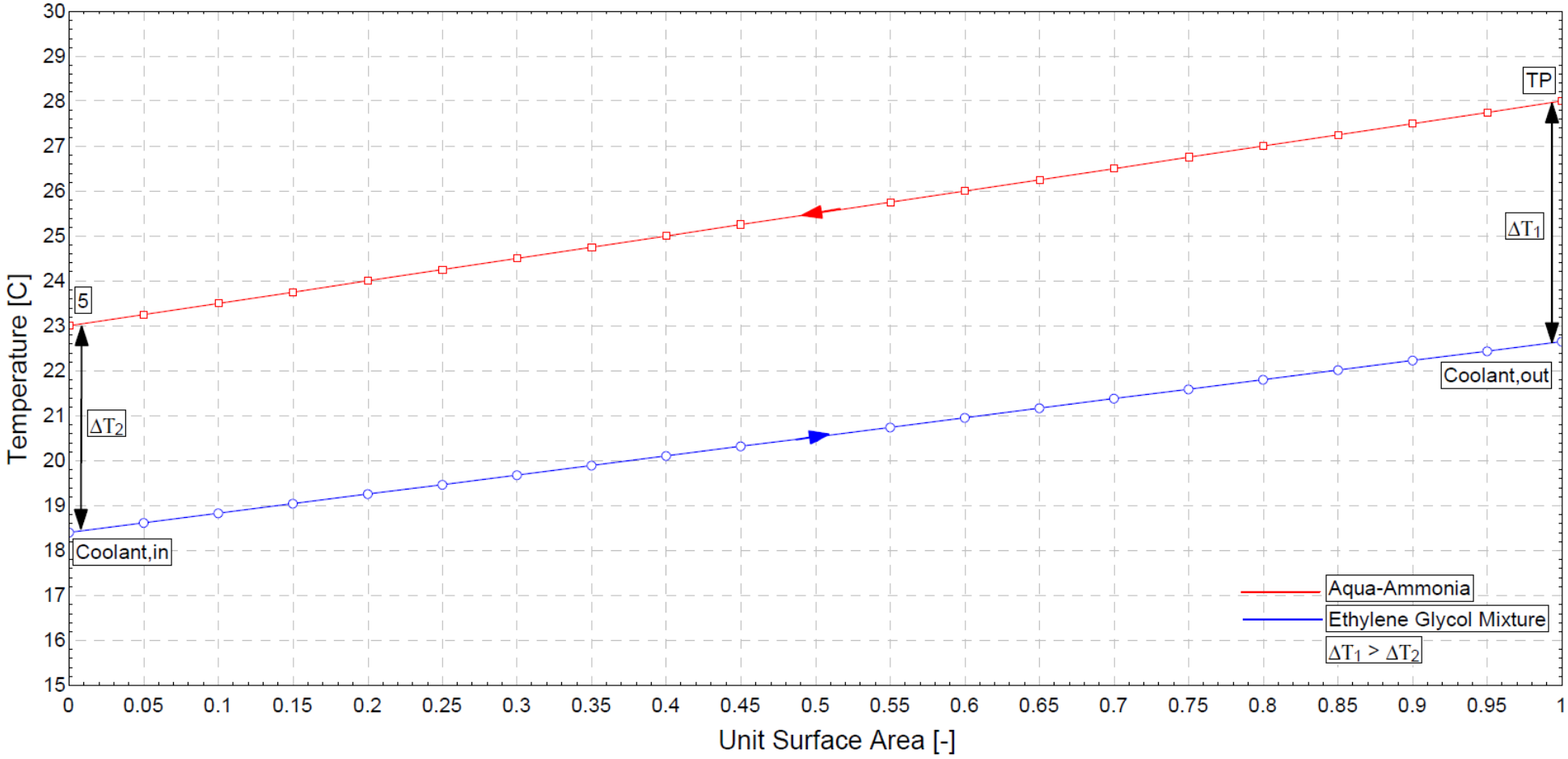

Figure D 1.1: Stage 1 Condenser – Temperature vs. unit surface area.

1.2 Stage 2 Condenser

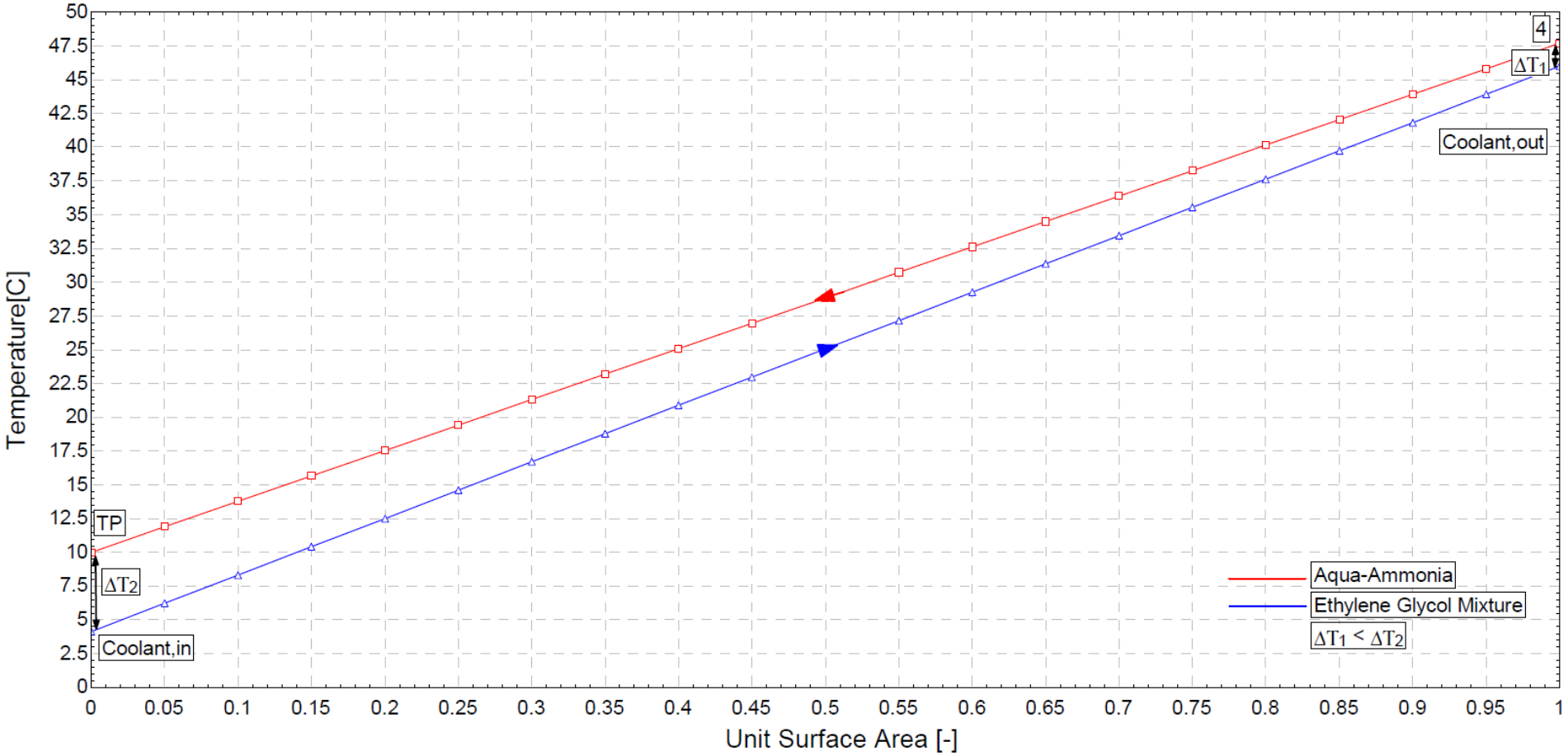

Figure D 1.2: Stage 2 Condenser – Temperature vs. unit surface area.

1.3 De-superheating Condenser

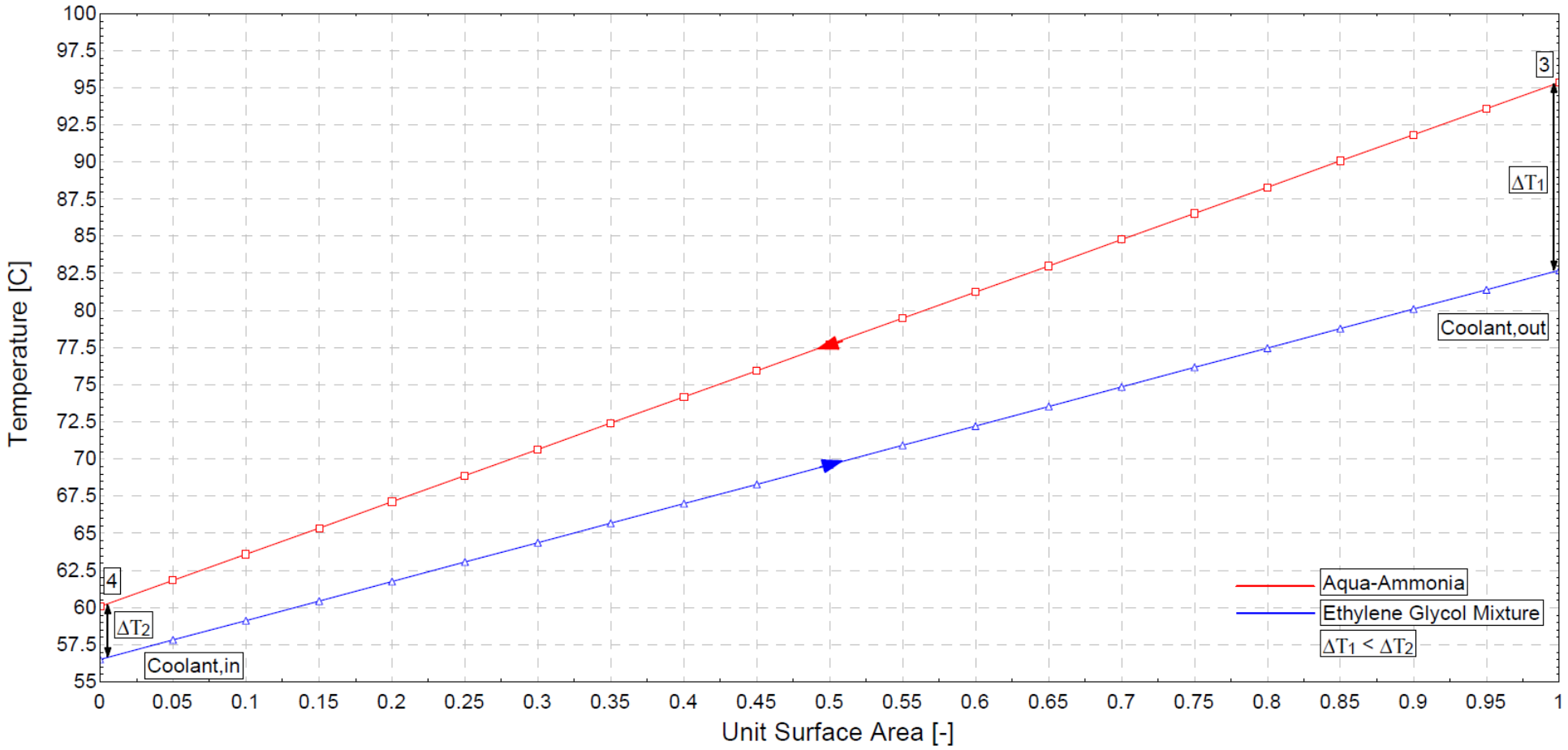

Figure D 1.3: De-superheating Condenser – Temperature vs. unit surface area.

1.4 Pre-Cool Heat Exchanger

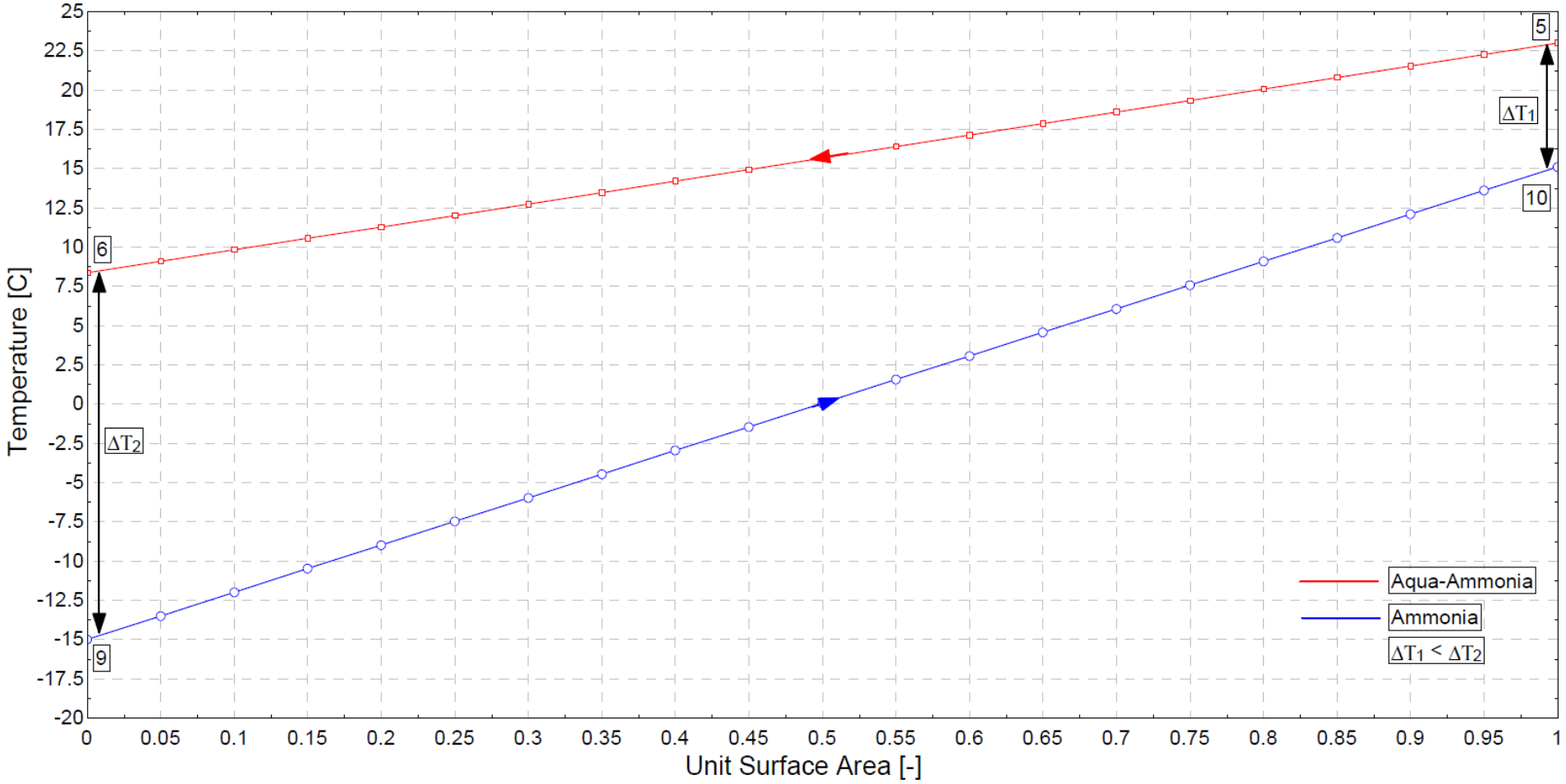

Figure D 1.4: Pre-Cool Heat Exchanger – Temperature vs. unit surface area.

1.5 Evaporator

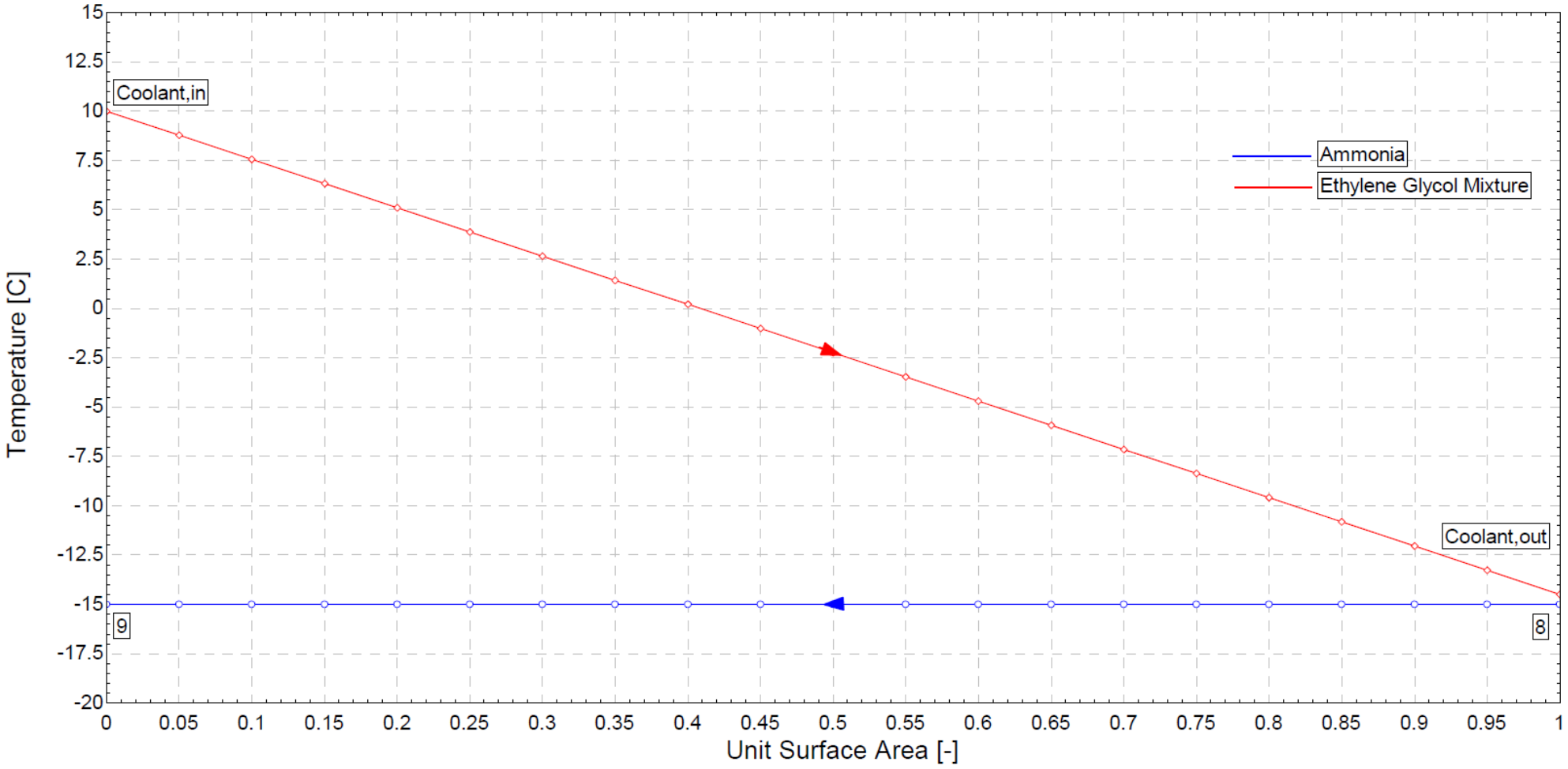

Figure D 1.5: Evaporator – Temperature vs. unit surface area.

1.6 Regenerative Heat Exchanger

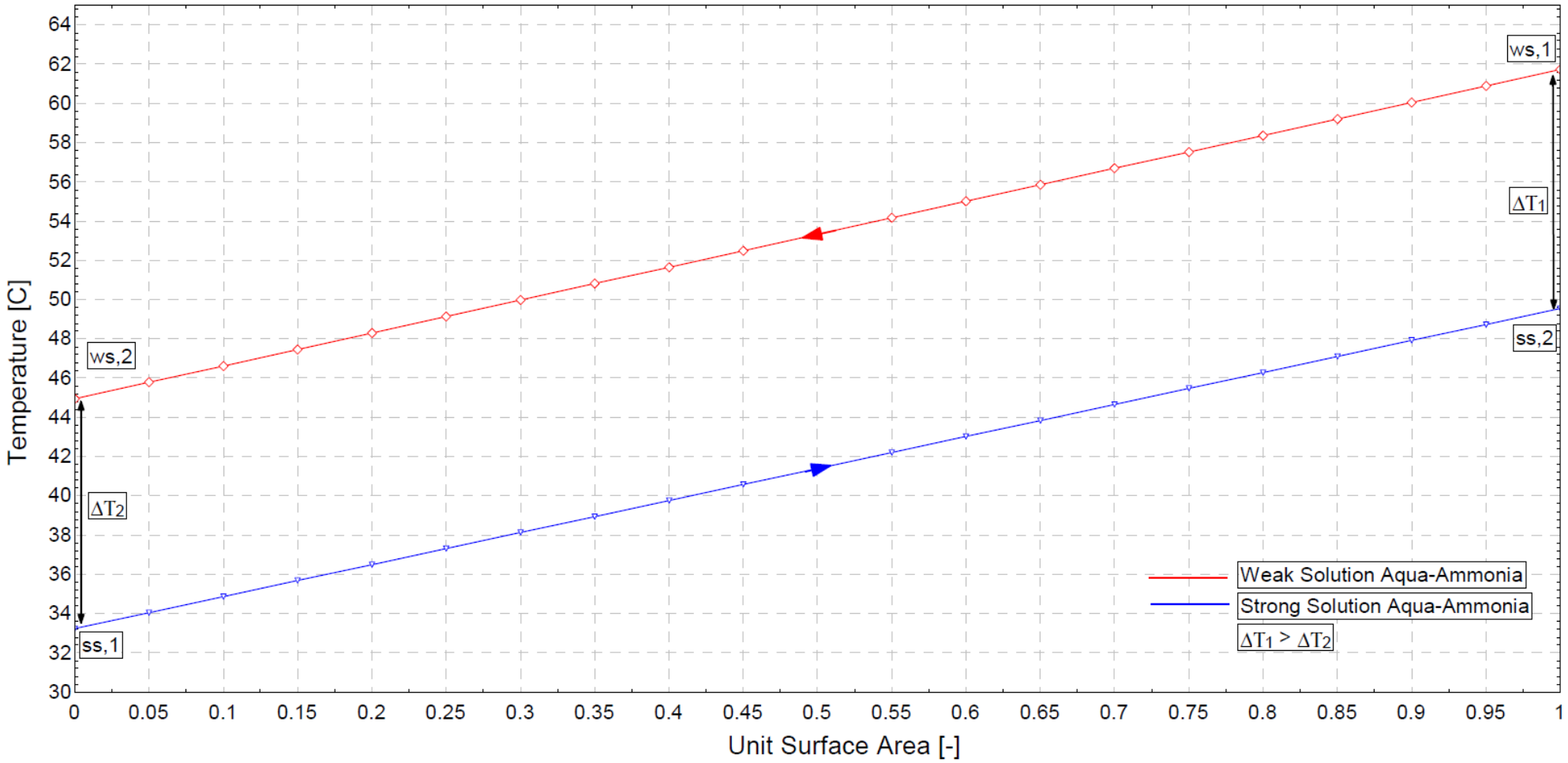

Figure D 1.6: Regenerative Heat Exchanger – Temperature vs. unit surface area.

1.7 Auxiliary Heat Exchanger

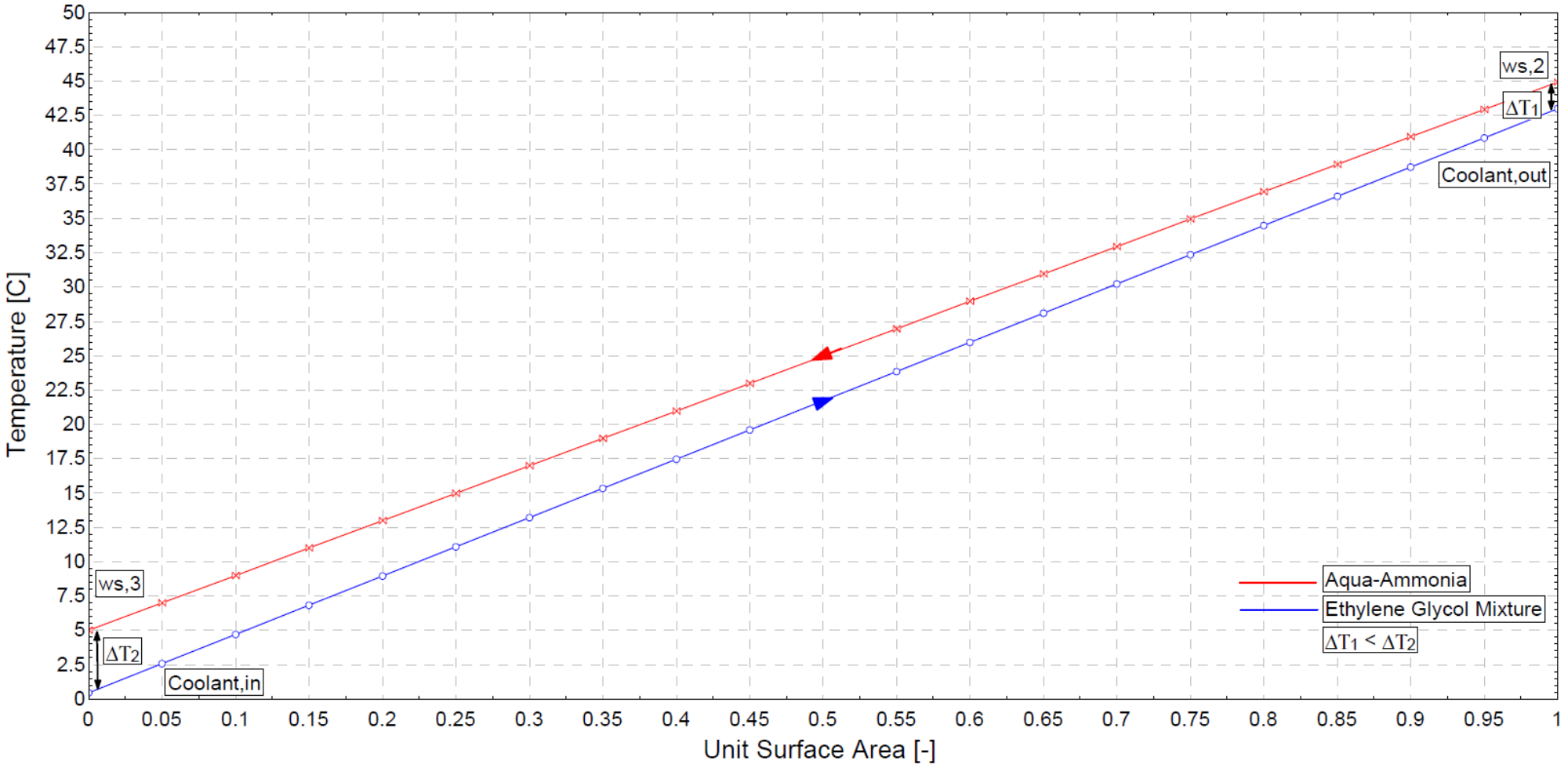

Figure D 1.7: Auxiliary Heat Exchanger – Temperature vs. unit surface area.

1.8 Appendix D Explanatory Guide

The following section focuses on the layout of the rest of the appendix, in terms of folder to file references to guide the reader to each heat exchanger's thermodynamic design sizing model and the verification thereof. For example Appendix D 2 contains two files of the stage 1 condenser, namely, the Excel Sizing model and the EES verification in pdf format.

1.8.1 Stage 1 Condenser – Thermodynamic Design Model

Stage 1 condenser has its folder to files directory illustrated by Figure D 1.8, where locked Excel Workbook illustrates the model used to determine the stage 1 condenser heat transfer surface area, and an EES model to depict the verification of the design sizing model in pdf format.

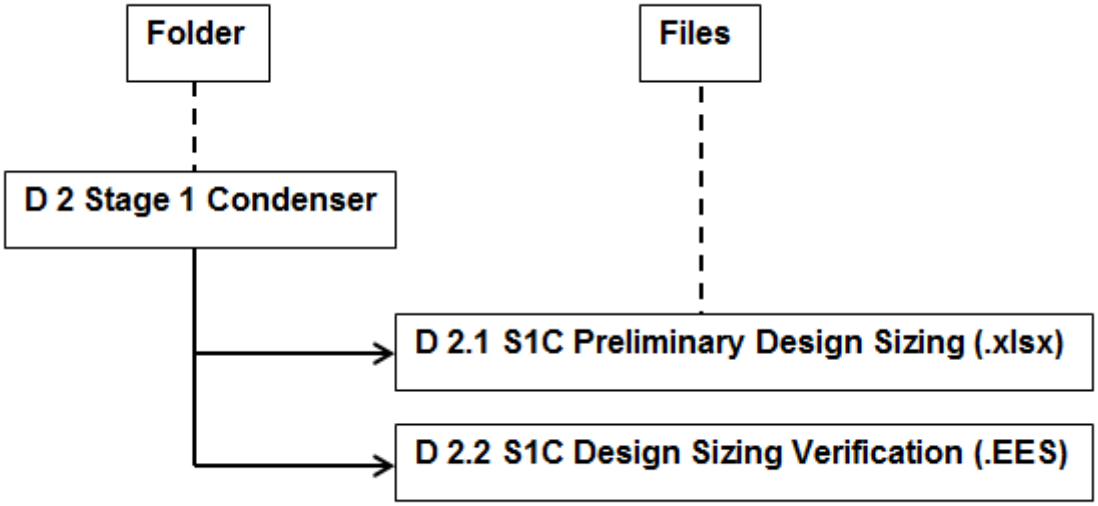

Figure D 1.8: Stage 1 Condenser – Thermodynamic design model directory.

1.8.2 Stage 2 Condenser – Thermodynamic Design Model

Stage 2 condenser has its folder to files directory illustrated by Figure D 1.9, where locked Excel Workbook illustrates the model used to determine the stage 2 condenser heat transfer surface area, and an EES model to depict the verification of the design sizing model in pdf format.

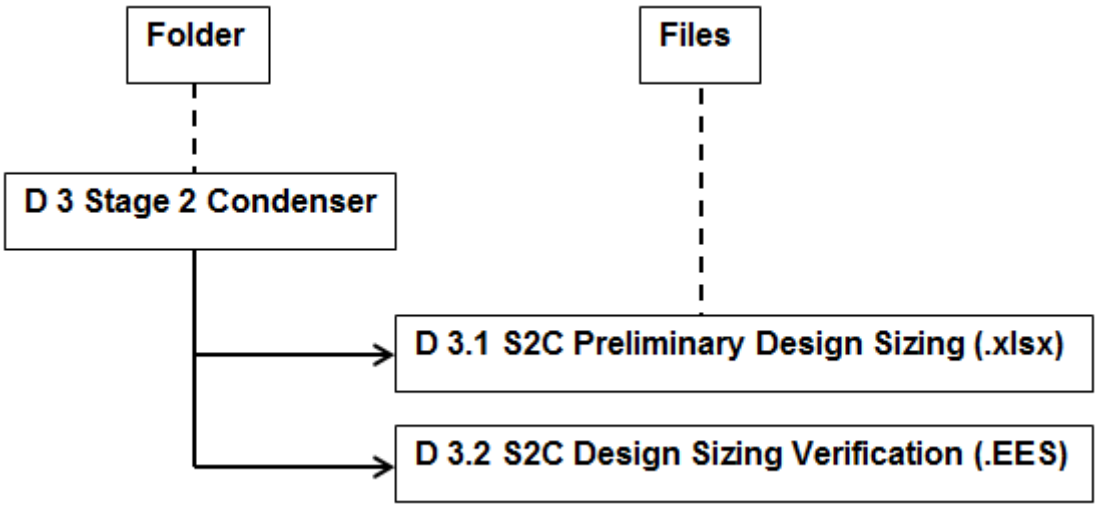

Figure D 1.9: Stage 2 Condenser – Thermodynamic design model directory.

1.8.3 De-superheating Condenser – Thermodynamic Design Model

The de-superheating condenser has its folder to files directory illustrated by Figure D 1.10, where locked Excel Workbook illustrates the model used to determine the de-superheating condenser heat transfer surface area, and an EES model to depict the verification of the design sizing model in pdf format.

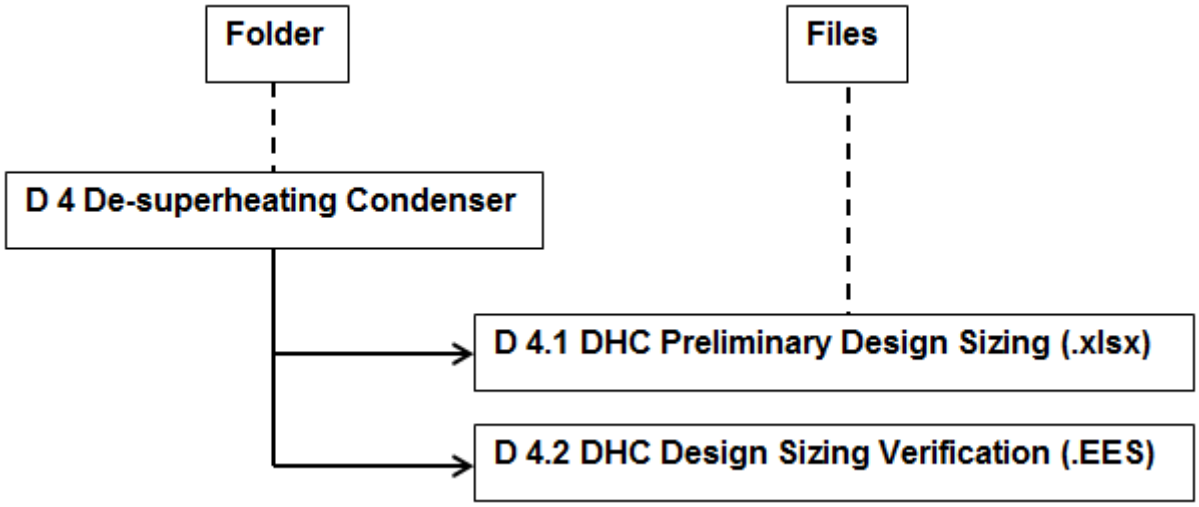

Figure D 1.10: De-superheating Condenser – Thermodynamic design model directory.

1.8.4 Pre-Cool Heat Exchanger – Thermodynamic Design Model

The pre-cool heat exchanger has its folder to files directory illustrated by Figure D 1.11, where locked Excel Workbook illustrates the model used to determine the pre-cool heat exchanger's heat transfer surface area, and an EES model to depict the verification of the design sizing model in pdf format.

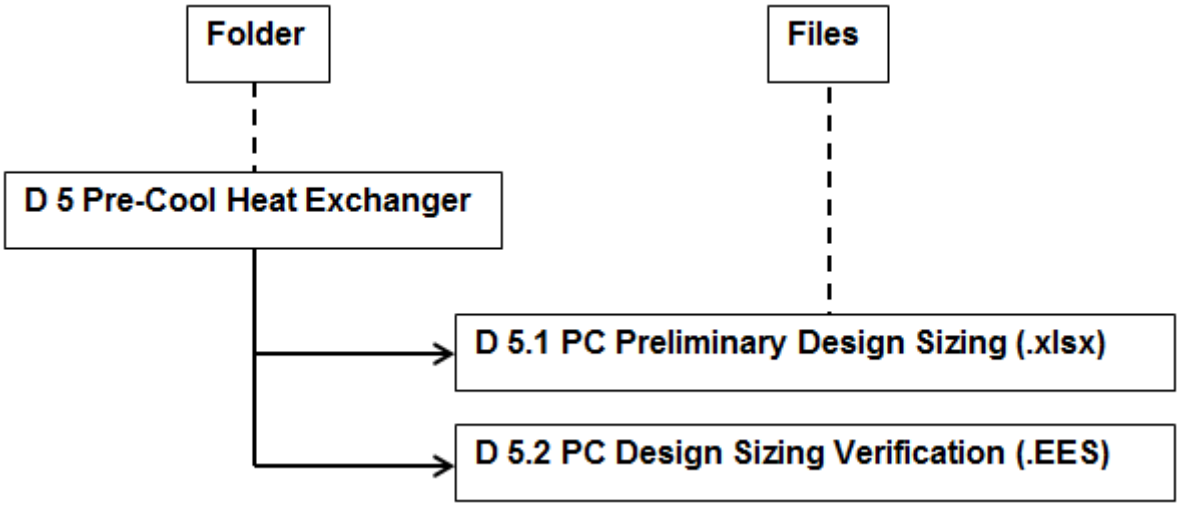

Figure D 1.11: Pre-Cool Heat Exchanger – Thermodynamic design model directory.

1.8.5 Venturi Nozzle and Orifice

Appendix D 6 contains the design, experimental setup, and proof of concept results of the venturi nozzle, where Figure 1.12 illustrates the folder to file directory of Appendix D 6.

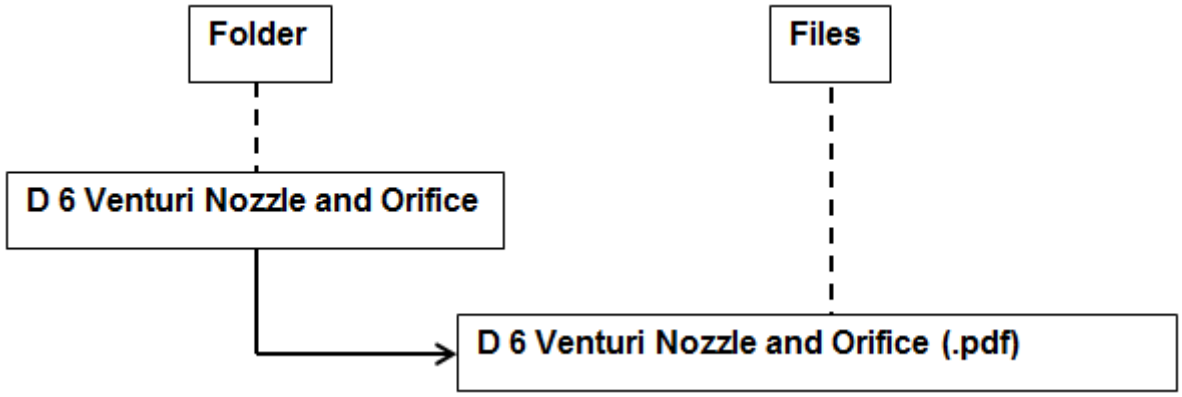

Figure D 1.12: Venturi Nozzle and Orifice – Design, experimental setup, and results.

1.8.6 Evaporator – Thermodynamic Design Model

The evaporator has its folder to files directory illustrated by Figure D 1.13, where locked Excel Workbook illustrates the model used to determine the evaporator's heat transfer surface area, and an EES model to depict the verification of the design sizing model in pdf format.

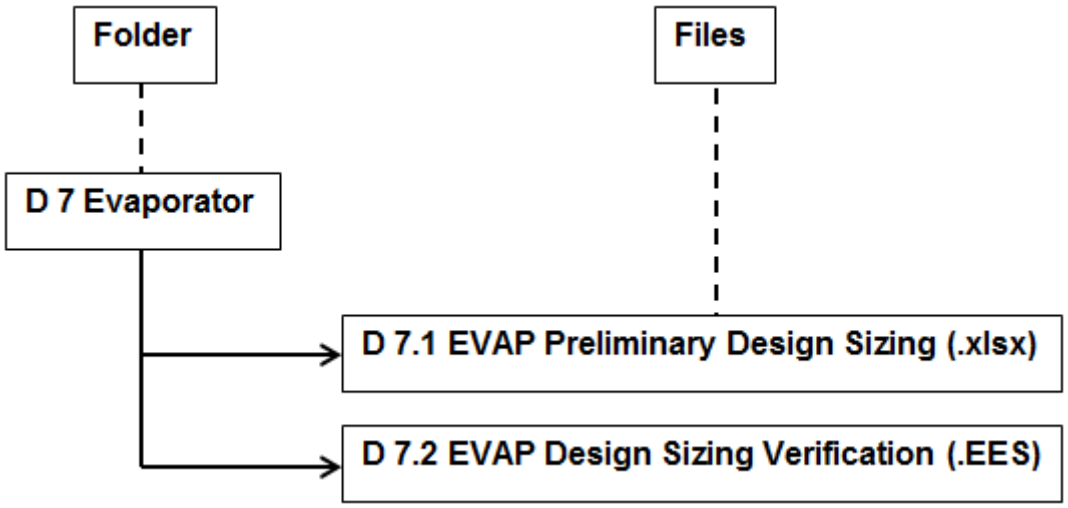

Figure D 1.13: Evaporator – Thermodynamic design sizing directory.

1.8.7 Auxiliary-Regenerative Heat Exchanger – Thermodynamic Design Model

The auxiliary-regenerative heat exchanger has its folder to files directory illustrated by Figure D 1.14, where locked Excel Workbook illustrates the model used to determine the aux-regen's heat transfer surface area, and an EES model to depict the verification of the design sizing model in pdf format.

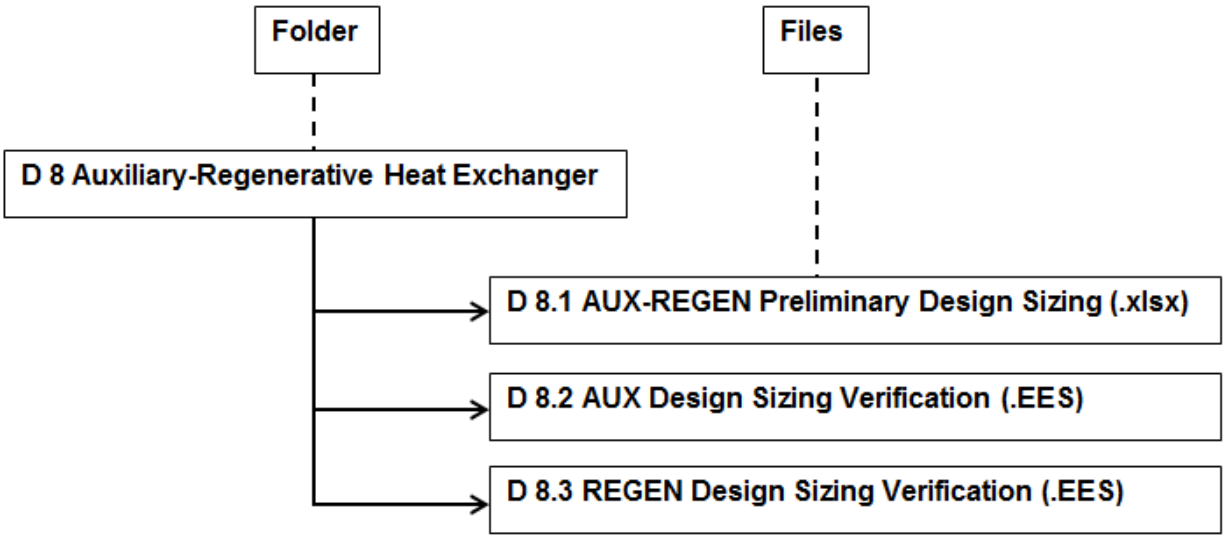

Figure D 1.14: Aux-Regen Heat Exchanger – Thermodynamic design model directory.

Appendix D 6

Extended Chapter 4 – Venturi Nozzle Design, Experimental Setup and Results

Summary

Appendix D 6 aims to explain the design and experimental setup behind the venturi nozzle, which is required for the thermodynamic design of the evaporator module. The venturi nozzle is designed using Bernoulli's equations set in Chapter 4. Compiled within this appendix are the manufacturing drawings of the venturi nozzle, the experimental setup and results. The experimental setup tries to emulate the conditions under which the venturi nozzle will operate within the aqua-ammonia absorption-desorption cycle, where the operating conditions are converted into a gravitational water flow system with the equivalent head pressure. The experiments are used as a proof of concept, not as a full venturi flow analysis.

Table of Contents

List of Tables

List of Figures

6 VENTURI NOZZLE EXPERIMENTAL SETUP AND RESULTS

6.1 Experimental Setup Calculations

The venturi nozzle is designed for winter ambient conditions, due to winter conditions having the lowest mass flow rate of the aqua-ammonia refrigerant. Therefore, the density properties of the fluid line entering the venturi nozzle are illustrated in Table D 6.1.

Table D 6.1: Density properties for experimental representation of the liquid column in the aqua-ammonia absorption-desorption cycle.

Density Properties		
ρ_3	3.351	kg/m^3
ρ_4	5.28899	kg/m^3
ρ_5	636.998	kg/m^3
ρ_6	648.048	kg/m^3
ρ_w	1000	kg/m^3

The schematic component diagram of the aqua-ammonia absorption-desorption H&R cycle is illustrated in Figure D 6.1, where the height of each segment of the fluid column leading towards the venturi is shown. The total height from the base of the evaporator to the top of the de-superheating condenser is 1.8 m, and the venturi nozzle is 0.4 m from the base of the evaporator. Thus, leaving a total of 1.4 m for the fluid line from the de-superheating condenser to the outlet of the venturi nozzle in the evaporator.

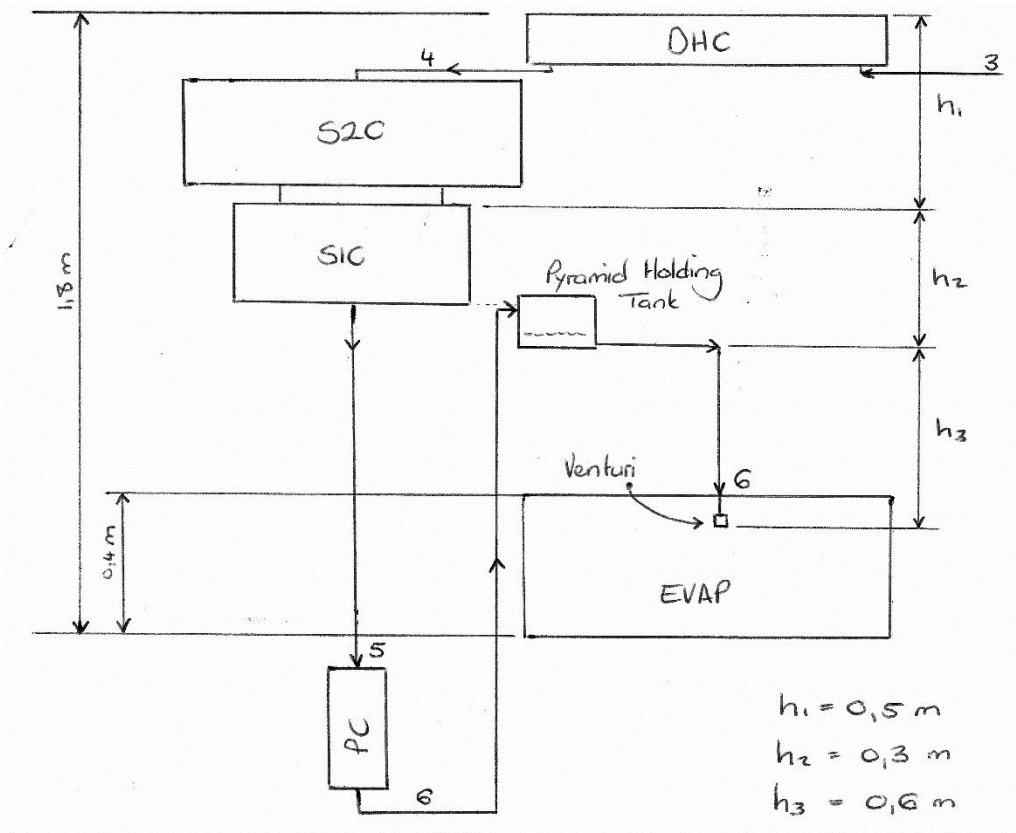

Figure D 6.1: Component schematic of the liquid column flowing towards the venturi nozzle.

Experimental Setup Height

As water will be used during the experiment, the experimental head needs to be determined to equal the head of the H&R cycle. Thus, it can be assumed that the head height of the H&R cycle is equal to the head height of the experimental setup. The experimental head height is calculated as:

$$\sum H_{cycle} = \sum H_{experiment}$$

$$\rho g h_1 + \rho g h_2 + \rho g h_3 = \rho g h_{experiment}$$

$$\left(\frac{\rho_3 + \rho_4}{2}\right) h_1 + \left(\frac{\rho_4 + \rho_5}{2}\right) h_2 + (\rho_6) h_3 = \rho_w h_{experiment}$$

$$\therefore h_{experiment} = \frac{\left(\frac{3.351+5.28899}{2}\right)(0.5) + \left(\frac{5.2889+636.998}{2}\right)(0.3) + (648.048)(0.6)}{1000}$$

$$\therefore h_{experiment} = 0.487332\ [m]$$

$$\therefore \cong 0.490\ [m]$$

Experimental Setup

The experimental setup that was used to complete the proof of venturi concept is illustrated in Figure D 6.2, with the design of the venturi nozzle illustrated in Figure D 6.3.

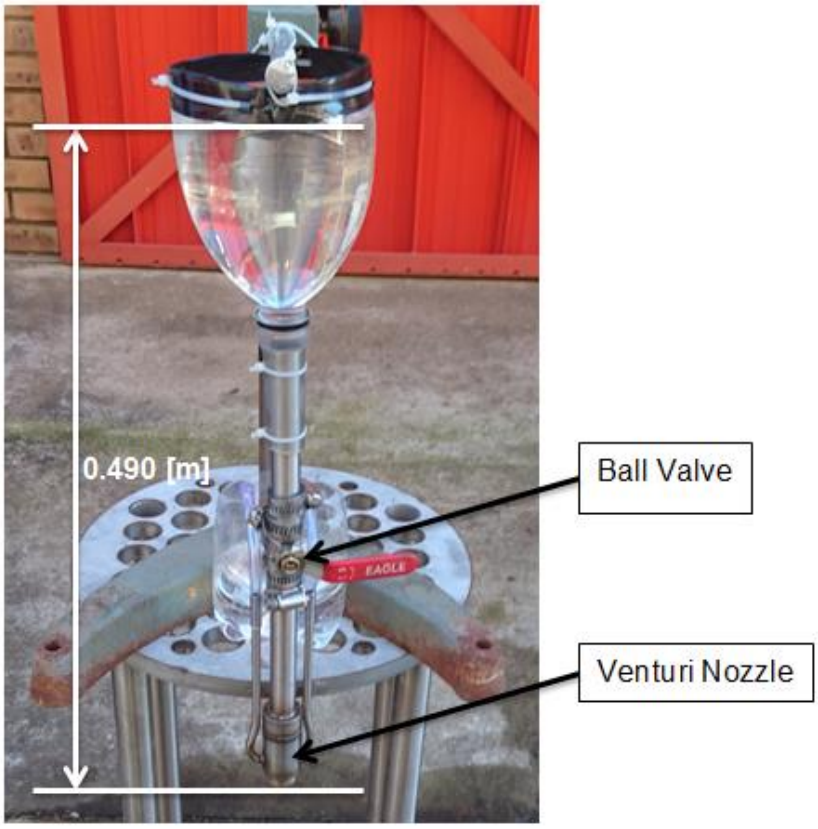

Figure D 6.2: Venturi proof of concept experimental setup.

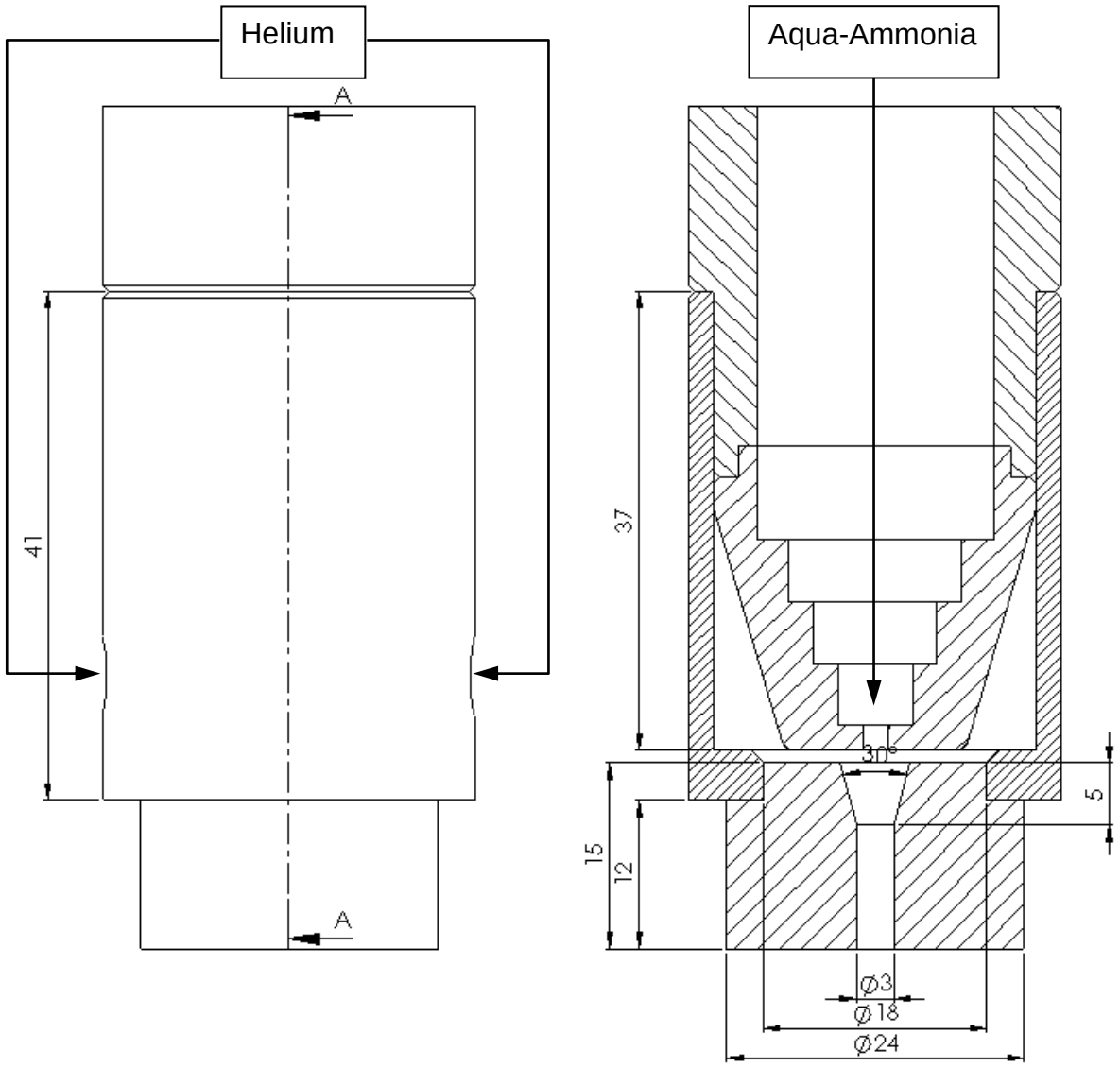

Figure D 6.3: Venturi nozzle – Manufacturing and assembly design.

6.2 Experimental Results

The experimental results of the venturi nozzle are available in Figure D 6.4, with supporting video documentation in Appendix D 6, namely, Appendix D 6.2 Experimental Results.mp4.

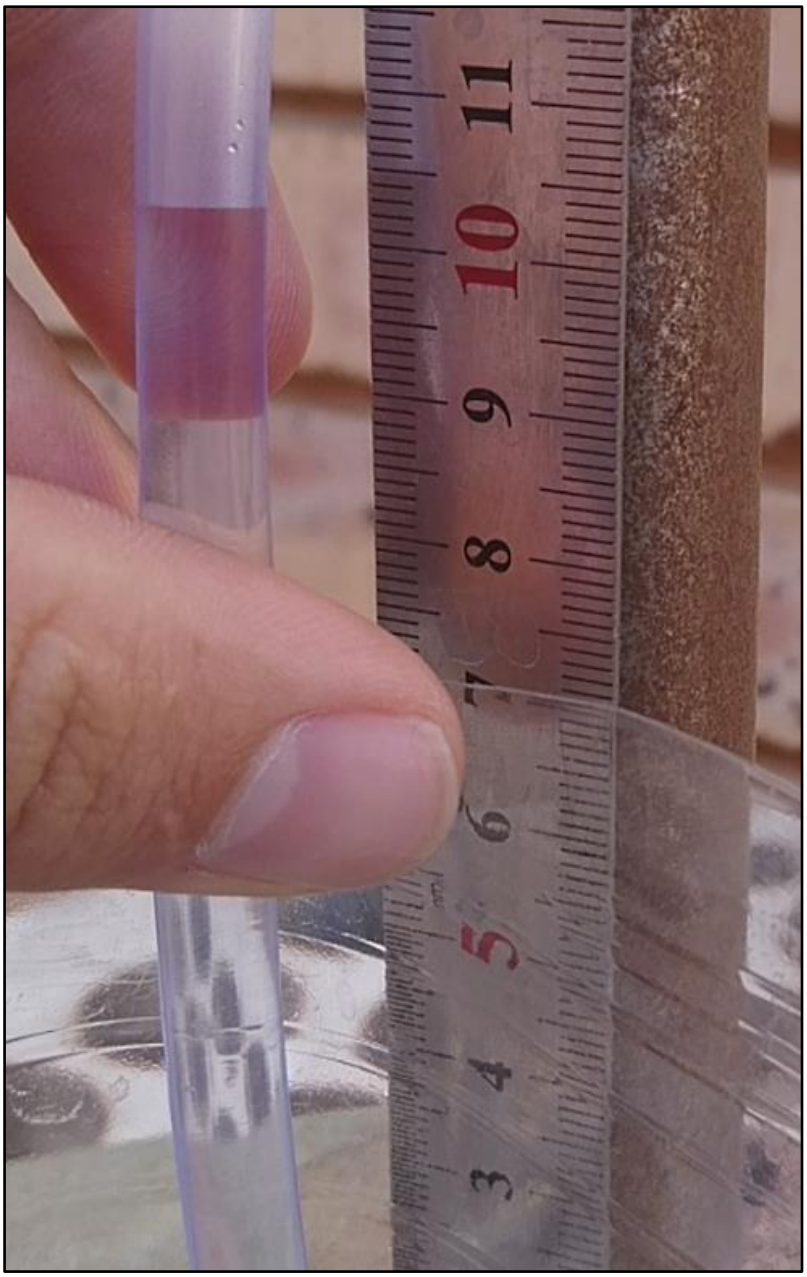

Figure D 6.4: Venturi nozzle suction height results.

As illustrated in Figure D 6.4, the venturi nozzle created a negative pressure strong enough to lift water to a total height of 101 mm. The starting point of the water meniscus is at 12 mm, with the water being sucked to a height of 113 mm, indicated. Taking the height of the water suction line and substituting it into a head calculation equation yields a suction pressure of:

$$\therefore P = \rho_w g h_{result}$$
$$\therefore \quad = 1000(9.81)(0.101)$$
$$\therefore \quad = 990.81\ [Pa]$$
$$\therefore \quad \cong 1\ [kPa] \quad Suction$$

The fact that the venturi was able to produce a negative pressure great enough to lift water up a tube 101 mm validates that the venturi nozzle has a feasible and functioning design to be implemented into the evaporator module.

Venturi Nozzle Drainage and Discharge Coefficient

The venturi nozzle was designed with an assumed discharge coefficient (in Chapter 4.4) of 0.9 [-], which is a typical value for smooth reducing nozzles, but the design of the venturi nozzle required a step reduction in diameter due to the small orifice diameter. Thus, after the experiment it is now possible to determine the practical value of the venturi nozzle. The venturi nozzle needed 138.4 seconds to drain 1 litre of water, with a discharge velocity of 2.30 [m/s]. The discharge velocity is slightly lower than what was calculated in Chapter 4.4, but was expected as the discharge coefficient was assumed to be 0.9 [-]. Now, by using the volumetric flow rate of 7.225 x 10^{-6} [m^3/s], and Eq. 4.4, the discharge coefficient is calculated as:

$$\dot{V} = C_D A \sqrt{2gh}$$

$$C_D = \frac{\dot{V}}{A\sqrt{2gh}}$$

$$\therefore \; = \frac{7.225 \text{ x } 10^{-6}}{\frac{\pi}{4}(0.002^2)\sqrt{2(9.81)(0.49)}}$$

$$\therefore \; = 0.7417$$

Standard discharge coefficients for various orifices are illustrated in Table D 6.2.

Table D 6.2: Standard discharge coefficients (Engineeringtoolbox, 2015).

Discharge Coefficient - C_D				
Diameter Ratio	**Reynolds Number - Re**			
$d = D_2/D_1$	10^4	10^5	10^6	10^7
0.2	0.968	0.988	0.994	0.995
0.4	0.957	0.984	0.993	0.995
0.6	0.95	0.981	0.992	0.995
0.8	0.94	0.978	0.991	0.995

Appendix D 9

Extended Chapter 4 – Effectiveness vs. NTU

Summary

Appendix D 9 deals with the effectiveness vs. number of transfer units of each of the rated heat exchangers. The effectiveness, NTU, and capacity ratios are used in the figures of Appendix D 9 to determine whether a heat exchanger lies within the practically excepted heat transfer efficiency. The effectiveness vs. NTU plots are good indicators to whether the correct coolant boundary conditions are implemented for each heat exchanger.

Table of Contents

List of Tables

List of Figures

9 EFFECTIVENESS VS. NTU CURVES

Illustrated in the tables below are the NTU, effectiveness, and capacity ratio of all ambient design conditions for all the sized heat exchangers.

Table D 9.1: S1C – NTU, Effectiveness, and Capacity Ratio output values.

Parameter	NTU	ε	c
Summer Ambient	50.0753	1	0.02252
Average Ambient	49.2701	1	0.02227
Winter Ambient	48.8386	1	0.02193

Table D 9.2: S2C – NTU, Effectiveness, and Capacity Ratio output values.

Parameter	NTU	ε	c
Summer Ambient	6.3260	0.82987	0.82056
Average Ambient	9.8643	0.81706	0.97111
Winter Ambient	16.005	0.90497	0.78114

Table D 9.3: DHC – NTU, Effectiveness, and Capacity Ratio output values.

Parameter	NTU	ε	c
Summer Ambient	4.8181	0.90093	0.75932
Average Ambient	3.9027	0.89167	0.65559
Winter Ambient	2.7280	0.81709	0.66395

Table D 9.4: PC – NTU, Effectiveness, and Capacity Ratio output values.

Parameter	NTU	ε	c
Summer Ambient	1.0399	0.57752	0.49601
Average Ambient	1.1109	0.59325	0.53021
Winter Ambient	1.1207	0.59514	0.53592

Table D 9.5: Evap – NTU, Effectiveness, and Capacity Ratio output values.

Parameter	NTU	ε	c
Summer Ambient	32.1550	1	0.05976
Average Ambient	32.5935	1	0.05896
Winter Ambient	33.1197	1	0.05802

Table D 9.6: Regen – NTU, Effectiveness, and Capacity Ratio output values.

Parameter	NTU	ε	c
Summer Ambient	0.62549	0.37879	0.82655
Average Ambient	1.20066	0.53473	0.85029
Winter Ambient	1.16130	0.59809	0.88102

Table D 9.7: Aux – NTU, Effectiveness, and Capacity Ratio output values.

Parameter	NTU	ε	c
Summer Ambient	13.8055	0.84448	0.95678
Average Ambient	16.0829	0.84236	0.99715
Winter Ambient	11.8119	0.86741	0.84953

Effectiveness vs. NTU Curve Legend

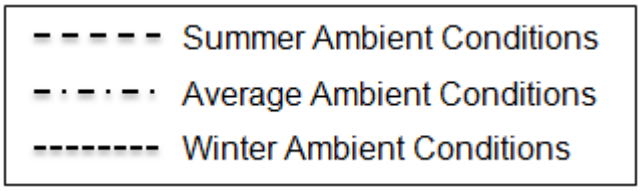

The standard effectiveness vs. NTU curve figures are obtained from (www.gcns.ac.uk, 2005)

9.1 Stage 1 Condenser

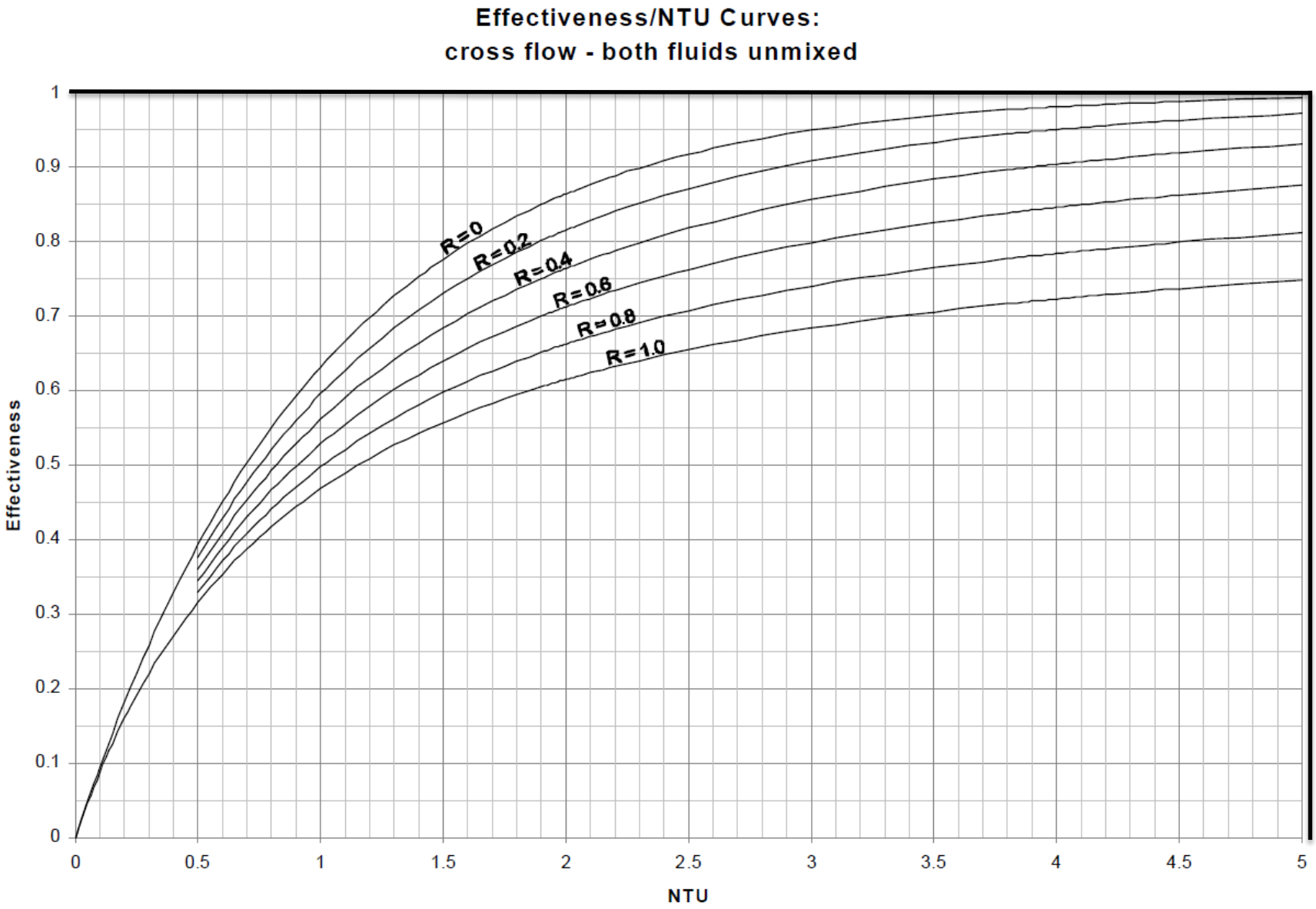

Figure D 9.1: Stage 1 condenser – Effectiveness vs. NTU rating.

9.2 Stage 2 Condenser

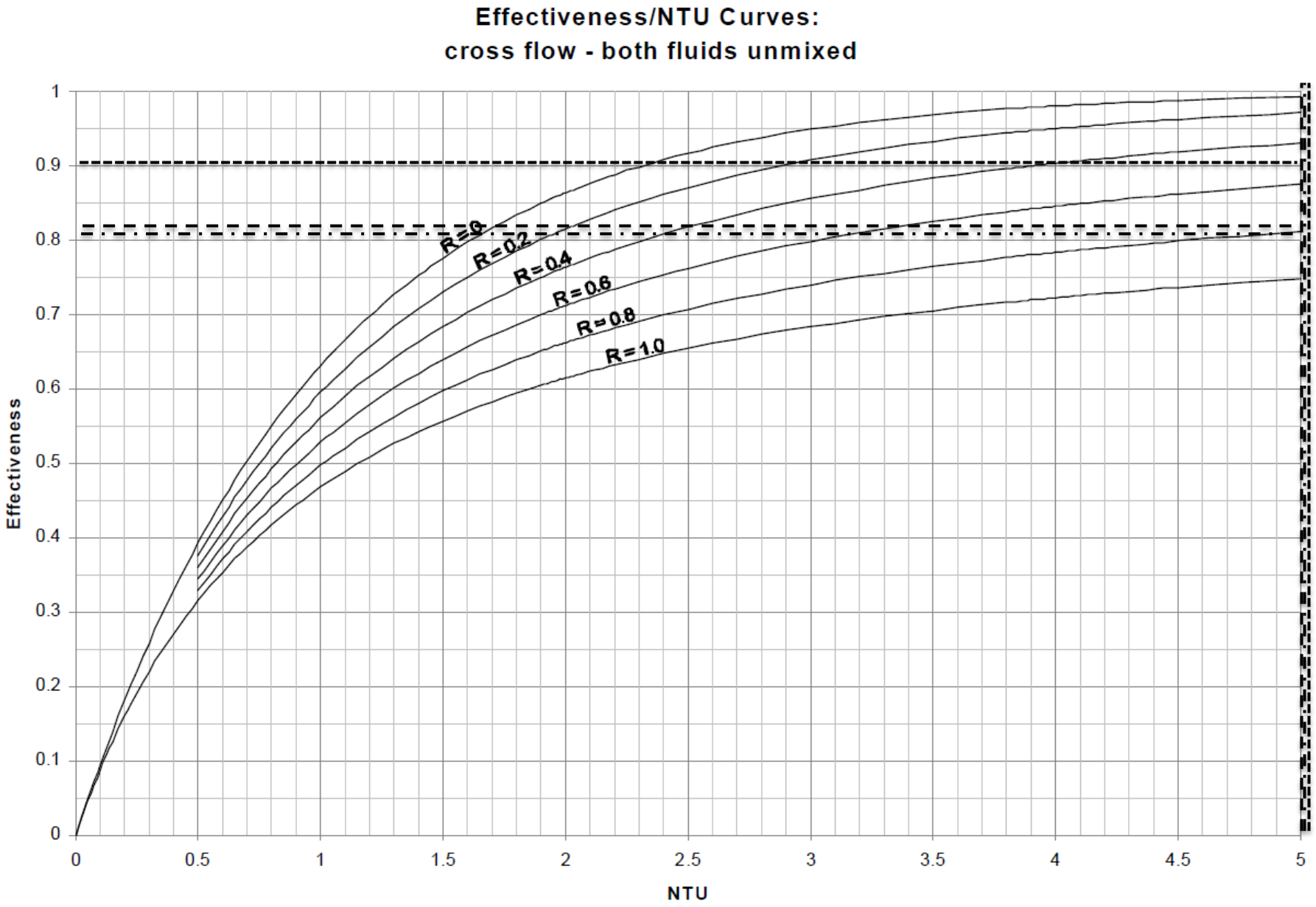

Figure D 9.2: Stage 2 condenser – Effectiveness vs. NTU rating.

9.3 De-superheating condenser

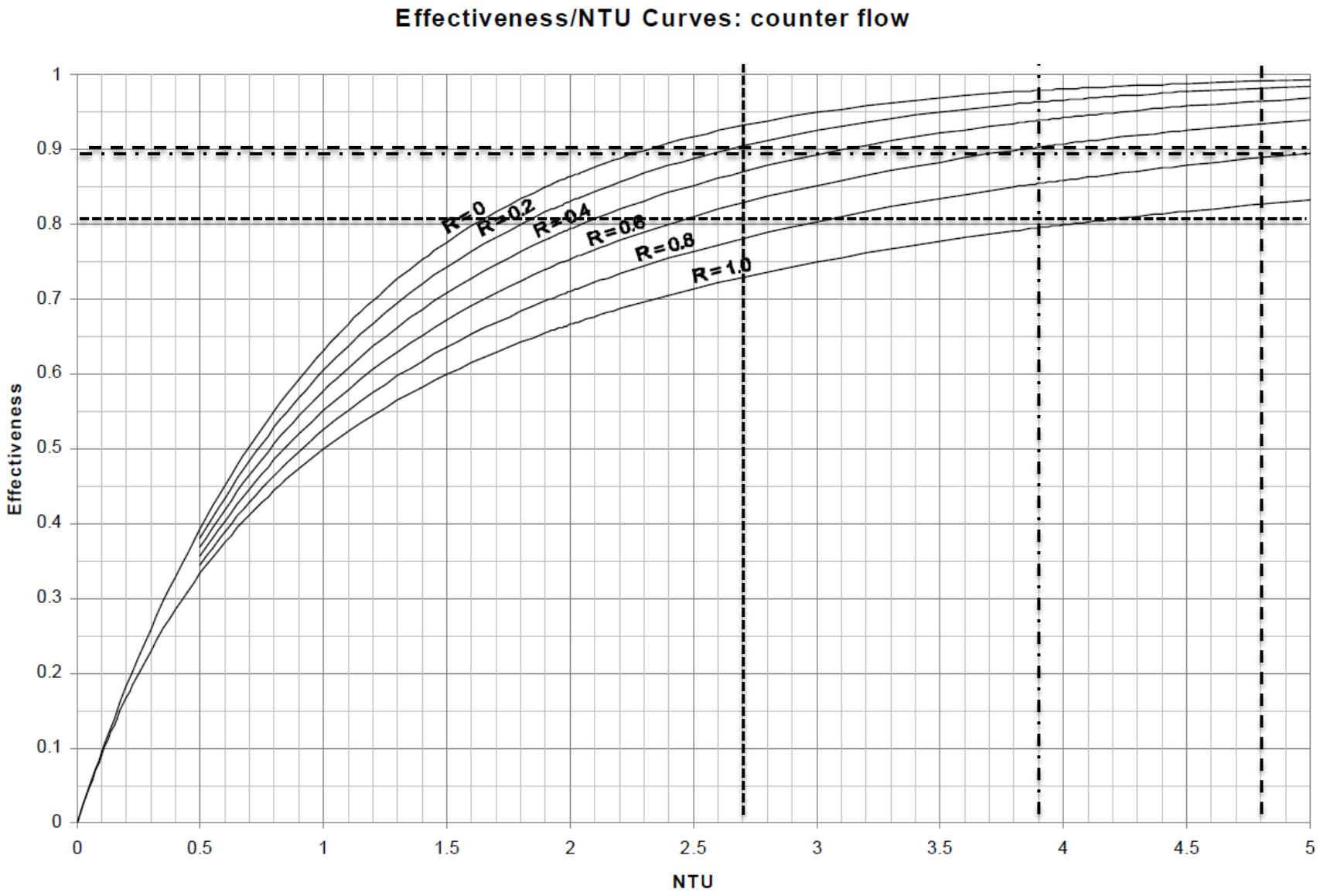

Figure D 9.3: De-superheating condenser – Effectiveness vs. NTU rating.

9.4 Pre-Cool Heat exchanger

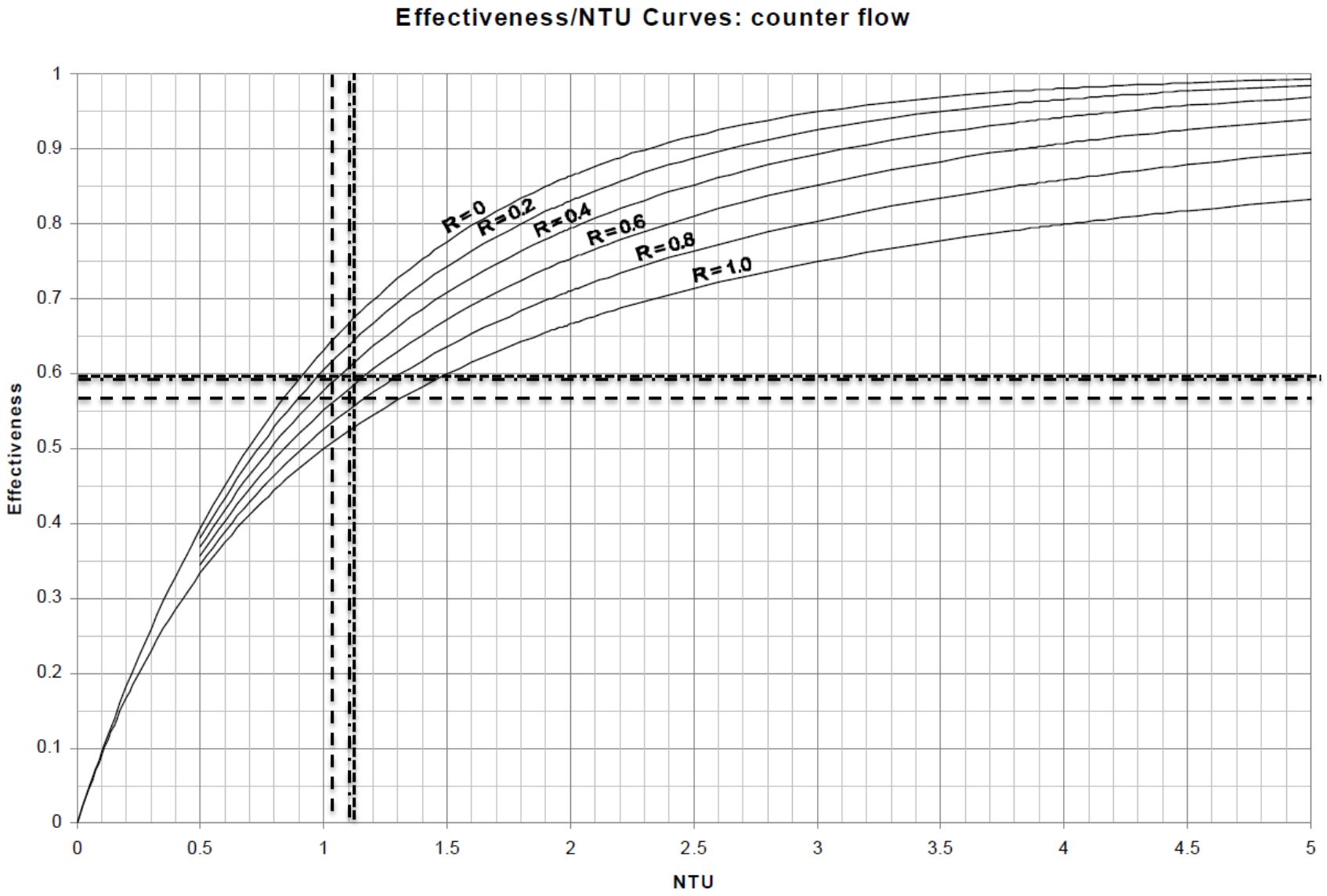

Figure D 9.4: Pre-cool heat exchanger – Effectiveness vs. NTU rating.

9.5 Evaporator

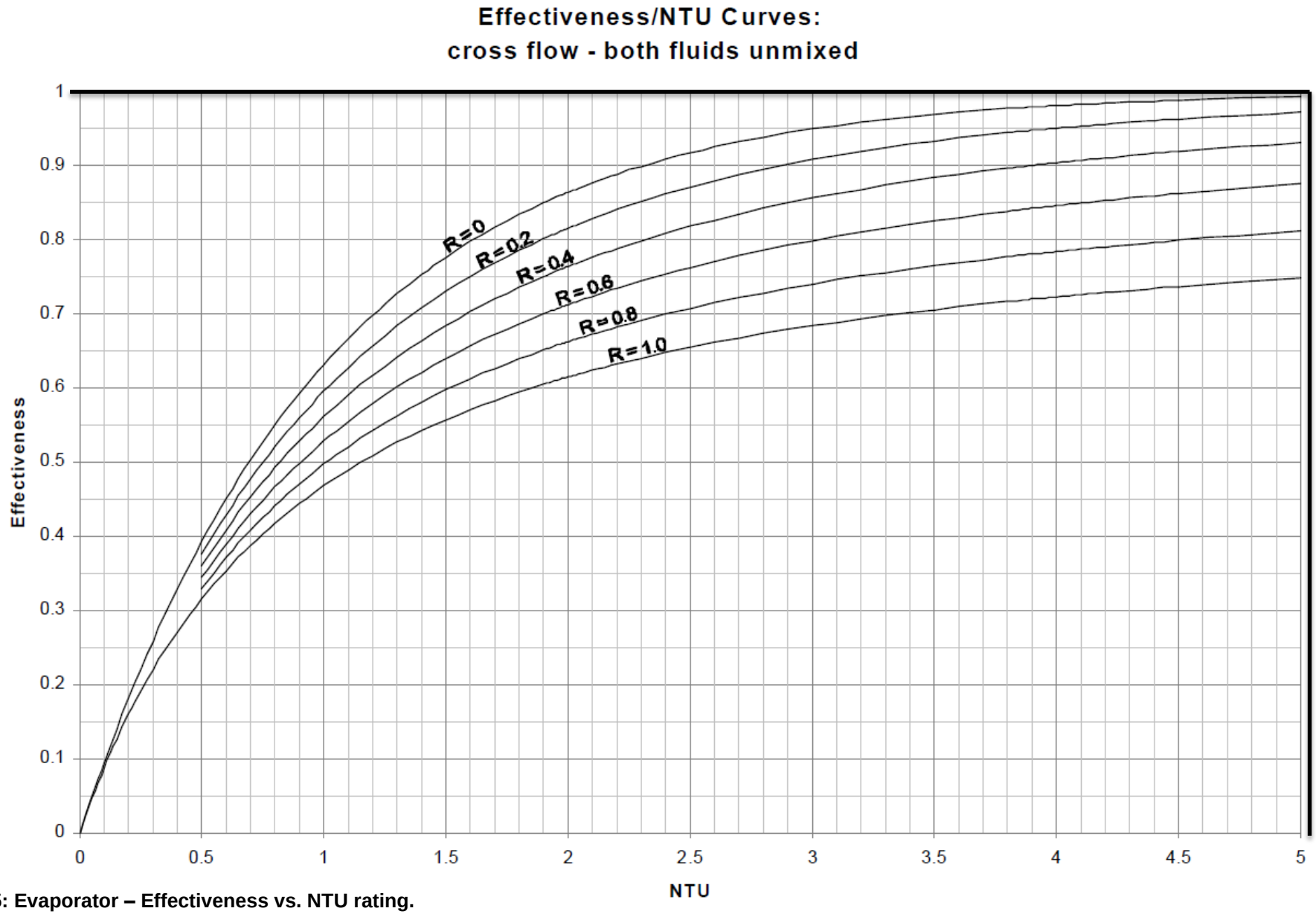

Figure D 9.5: Evaporator – Effectiveness vs. NTU rating.

9.6 Regenerative Heat exchanger

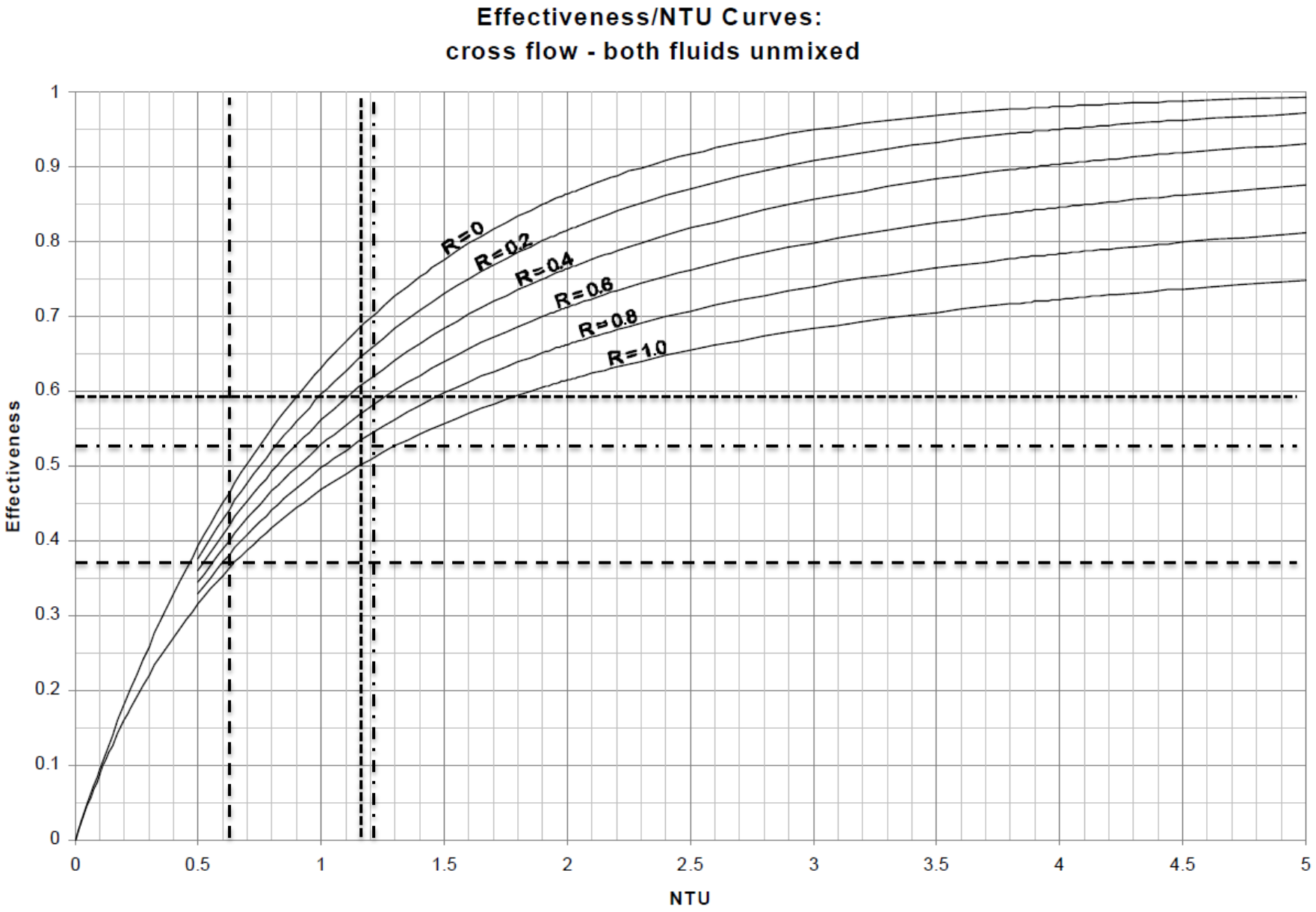

Figure D 9.6: Regenerative heat exchanger – Effectiveness vs. NTU rating.

9.7 Auxiliary Heat Exchanger

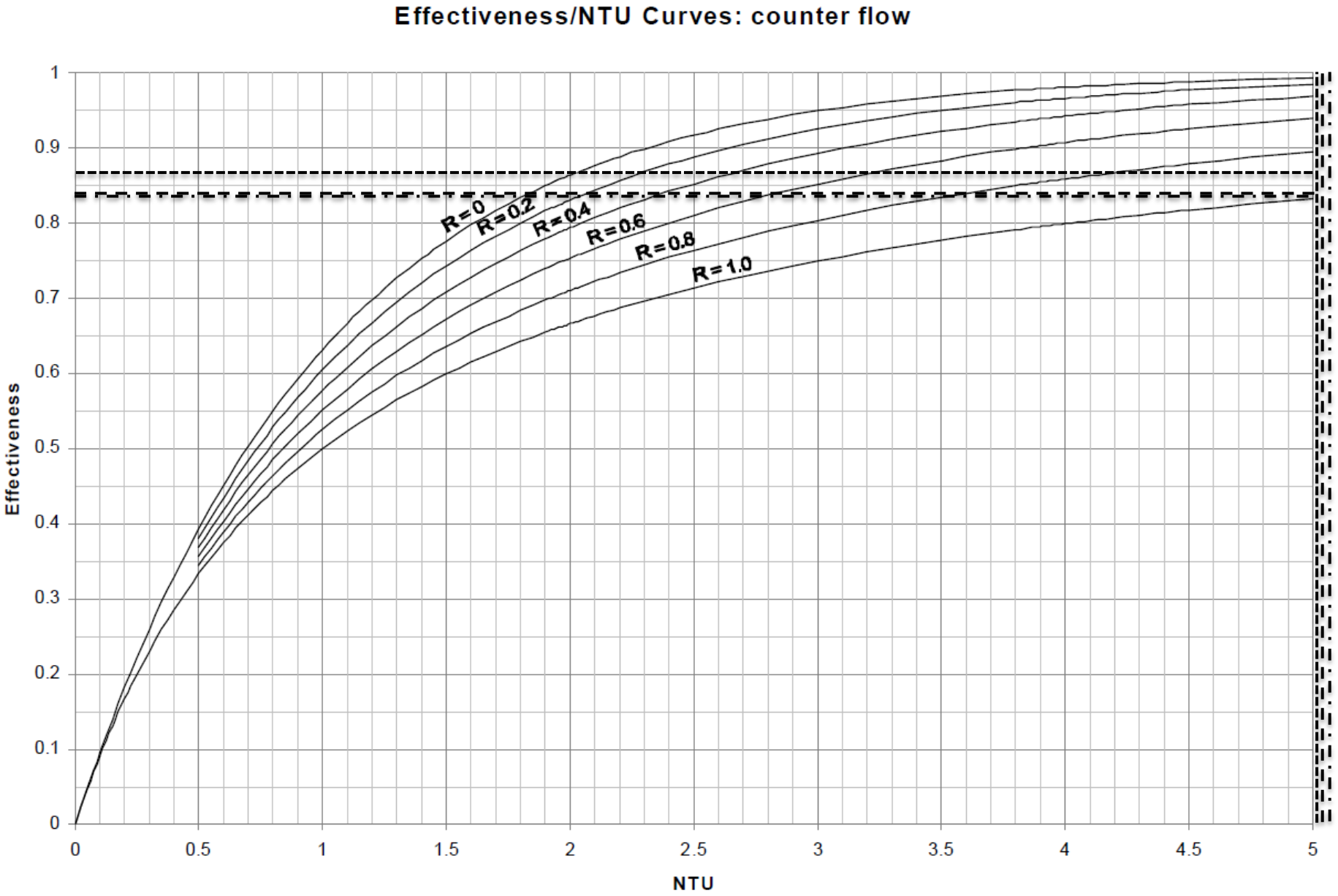

Figure D 9.7: Auxiliary heat exchanger – Effectiveness vs. NTU rating.

Appendix E

Mechanical Considerations and Design

Summary

This appendix focuses on the mechanical design of the sized heat exchanger models by using the necessary considerations that are required to complete the design of the heat exchangers for the solar-powered aqua-ammonia absorption-desorption H&R cycle. Appendix E also consists of the manufacturing and assembly drawings of each individual heat exchanger, together with component 'nesting' drawings of connecting pipes.

Table of Contents

List of Tables

List of Figures

1 MECHANICAL CONSIDERATIONS AND DESIGNS

1.1 Tube Sheet Thickness Calculations

The thickness of the tube sheet will be the same for the heat exchangers with the same design pressure and tube sheet diameters. According to the ASME Code the allowable stress for stainless steel 304L tube sheet is 205 [MPa]. Illustrated in Tables E.1, 2, and 3 are the thickness calculations for the 0.1345 [m], 0.26467 [m], and 0.34768 [m] tube sheet, respectively. The thicknesses are calculated using both first order and TEMA standards calculations.

Table E.1: Tube sheet thickness of D_s = 0.1345 [m].

	D_s [m]	P_D [kPa]	σ_{allow} [MPa]	η	t [mm]	Correlation
First Order	0.1345	1400	205	-	4.8129	Eq. A.28
TEMA	0.1345	1400	205	0.5	5.2397	Eq. A.29

Table E.2: Tube sheet thickness of D_s = 0.26467 [m].

	D_s [m]	P_D [kPa]	σ_{allow} [MPa]	η	t [mm]	Correlation
First Order	0.26467	1400	205	-	9.4709	Eq. A.28
TEMA	0.26467	1400	205	0.5	10.311	Eq. A.29

Table E.3: Tube sheet thickness of D_s = 0.34768 [m].

	D_s [m]	P_D [kPa]	σ_{allow} [MPa]	η	t [mm]	Correlation
First Order	0.34768	1400	205	-	12.441	Eq. A.28
TEMA	0.34768	1400	205	0.5	13.544	Eq. A.29

1.2 Shell Stress Calculations

The shell stress calculations consists of axial, hoop, and radial stress calculations, which are used to determine the safety factor of the shell housing. Recorded in the Tables E.4, 5, and 6 are the results of the abovementioned stresses acting on the three shell sizes, with their respective minimum shell thicknesses. Secondly, an ASME standards calculation of Appendix A 3.2, is used to prove that the wall thickness of the shell is sufficient.

Standard stainless steel 304L nominal bore welded pipe is used for the shells of the heat exchangers, with:

- D_s = 0.1345 [m]; t = 3.4 [mm];
- D_s = 0.26467 [m]; t = 4.19 [mm];
- D_s = 0.34768 [m]; t = 3.96 [mm].

The internal design pressure is equal to 1.4 [MPa] and the external pressure is equal to atmospheric pressure.

Where:

P_D = 1.4 [MPa];

D_o = the outer diameter of the shell;

S = 115 [MPa];

E = 0.85;

W = 1.0;

Y = 0.4,

for the calculation of the AMSE minimum thickness.

Table E.4: Output values of shell stress calculations of D_s = 0.1345 [m].

Parameter	Output [Units]	Correlation
Axial stress: σ_a	12.5153 [MPa]	Eq. A.29
Hoop stress: σ_c	25.7618 [MPa]	Eq. A.30
Radial stress: σ_r	-0.73114 [MPa]	Eq. A.31
Safety factor: SF	4.67 [-]	Eq. A.33
Minimum diameter: t_m	0.9577 [mm]	Eq. A.32

Table E.5: Output values of shell stress calculations of D_s = 0.26467 [m].

Parameter	Output [Units]	Correlation
Axial stress: σ_a	20.2322 [MPa]	Eq. A.29
Hoop stress: σ_c	41.2044 [MPa]	Eq. A.30
Radial stress: σ_r	-0.7400 [MPa]	Eq. A.31
Safety factor: SF	2.8 [-]	Eq. A.33
Minimum diameter: t_m	1.81 [mm]	Eq. A.32

Table E.6: Output values of shell stress calculations of D_s = 0.34768 [m].

Parameter	Output [Units]	Correlation
Axial stress: σ_a	28.2850 [MPa]	Eq. A.29
Hoop stress: σ_c	57.3142 [MPa]	Eq. A.30
Radial stress: σ_r	-0.74427 [MPa]	Eq. A.31
Safety factor: SF	2.01 [-]	Eq. A.33
Minimum diameter: t_m	2.48 [mm]	Eq. A.32

Therefore, it can be concluded that the design decision to use welded nominal bore pipe as the shell housing all of the heat exchanger designs is feasible and will have a safety factor in excess of 2 [-].

1.3 Tube Stress Calculations – Design Pressure Inside

With the design pressure being on the inside of the tubes, there is a risk of the tubes bursting. Therefore, it's vital to calculate whether the tubes wall thickness is sufficient to contain the high pressure aqua-ammonia refrigerant. To determine the maximum stress within the tube walls a thin walled analysis is required. The results of the analysis are tabulated in Table E.7 for the 19.1 [mm] tube and Table E.8 for the 31.8 [mm] tube as:

Table E.7: Output values of tube stress calculations (19.1 mm) – Pressure inside.

Parameter	Output [Units]	Correlation
Hoop stress: σ_h	6.95625 [MPa]	Eq. A.34
Longitudinal stress: σ_l	3.47813 [MPa]	Eq. A.35
Safety factor: SF	16.532	Eq. A.33

Table E.8: Output values of tube stress calculations (31.8 mm) – Pressure inside.

Parameter	Output [Units]	Correlation
Hoop stress: σ_h	12.5125 [MPa]	Eq. A.34
Longitudinal stress: σ_l	6.25625 [MPa]	Eq. A.35
Safety factor: SF	9.191	Eq. A.33

1.4 Tube Stress Calculations – Design Pressure Outside

The design pressure is now applied to the outside of the tube wall, Similar to the shell calculation the tube's axial, hoop, and radial stresses will be calculated to determine the maximum stress direction under design pressure on the outside of the tube. The results of the tube stress calculations with the pressure from the aqua-ammonia refrigerant on the outside of the tube are illustrated by Table E.9 for the 19.1 [mm] tube and Table E.10 for the 31.8 [mm] tube. With the pressure working in on the outside of the tube, the direction of the stresses will be inward and thus be negative.

Table E.9: Output values of tube stress calculations (19.1 mm) – Pressure outside.

Parameter	Output [Units]	Correlation
Axial stress: σ_a	-6.9447 [MPa]	Eq. A.29
Hoop stress: σ_c	-13.788 [MPa]	Eq. A.30
Radial stress: σ_r	-1.4093 [MPa]	Eq. A.31
Safety factor: SF	8.351 [-]	Eq. A.33

Table E.10: Output values of tube stress calculations (31.8 mm) – Pressure outside.

Parameter	Output [Units]	Correlation
Axial stress: σ_a	-4.3617 [MPa]	Eq. A.29
Hoop stress: σ_c	-8.6221 [MPa]	Eq. A.30
Radial stress: σ_r	-1.4093 [MPa]	Eq. A.31
Safety factor: SF	13.35 [-]	Eq. A.33

1.5 Header Bolt Calculations

The end cap headers are fastened to the heat exchangers via bolt and nut fasteners, which aid to the cleaning procedures required to maintain optimal heat transfer. Table E.11 illustrates the total force working in on the bolt and nut, which has been illustrated by Figure A.7.

Table E.11: Total design force working in on the bolts.

	D_s [m]	D_F [m]	P_i [kPa]	F_D [kN]	Correlation Used
S1C	0.26467	0.35	150	25.704	Eq. A.36 & A.38
S2C	0.26467	0.35	150	25.704	Eq. A.36 & A.38
DHC	0.1345	0.22	150	14.789	Eq. A.37 & A.38
PC	0.1345	0.22	1400	138.95	Eq. A.37 & A.38
EVAP	0.26467	0.35	150	25.704	Eq. A.36 & A.38
AUX-REGEN	0.34768	1400	1400	13.544	Eq. A.36 & A.38

The number of bolts can be calculated with Eq. A.39 and 4.8 grade fasteners, which are illustrated in Table E.12 as:

Table E.12: Number of bolts required per heat exchanger.

	Property Class	N_{bolts} (Calc)	N_{bolts} (Selected)	Correlation Used
S1C	4.8 – M10	0.963	4	Eq. A.39
S2C	4.8 – M10	0.963	4	Eq. A.39
DHC	4.8 – M10	0.554	4	Eq. A.39
PC	4.8 – M10	5.21	8	Eq. A.39
EVAP	4.8 – M10	3.273	8	Eq. A.39
AUX-REGEN	4.8 – M12	8.25	24	Eq. A.39

These calculations are simplified first order calculations, thus for the practical application of the heat exchangers, 8.8 grade bolts will be used to increase the safety factors of each heat exchanger's header. The bolted on headers have machined/milled O-ring grooves that house special order silicone O-rings, although these calculations are omitted for its trivial nature they form a vital role in the seal of each heat exchanger as per design requirements of Appendix C.

1.6 Appendix E explanatory guide

The following section deals with the layout of the rest of the appendix, in terms of folder to file references to guide the reader to each heat exchanger's manufacturing and assembly drawings. For example Appendix E 2 is a folder containing the stage 1 condenser's parts in E 2.1 (non-standard parts) and assembly drawings in E 2.2. The subsequent files within these folders contain the manufacturing and assembly drawings in pdf format.

1.6.1 Stage 1 Condenser Manufacturing & Assembly Drawings

Stage 1 condenser has a folder to folders to files directory as illustrated by Figure E.1, where detailed manufacturing drawings are found for the non-standard components and assembly drawings of the heat exchanger in the order of practical assembling.

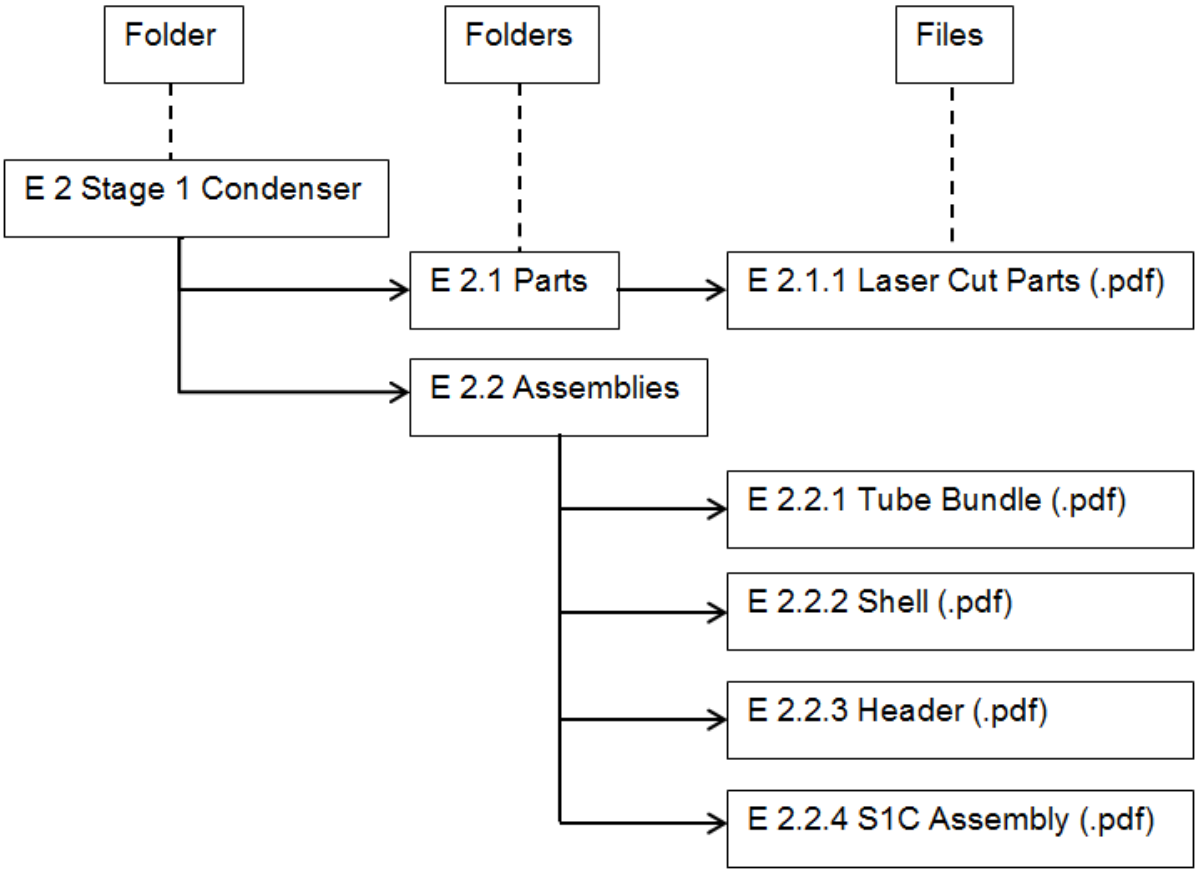

Figure E.1: Stage 1 Condenser – Drawings directory.

1.6.2 Stage 2 Condenser Manufacturing & Assembly Drawings

Figure E.2 shows the folder to folders to files directory of the stage 2 condenser as:

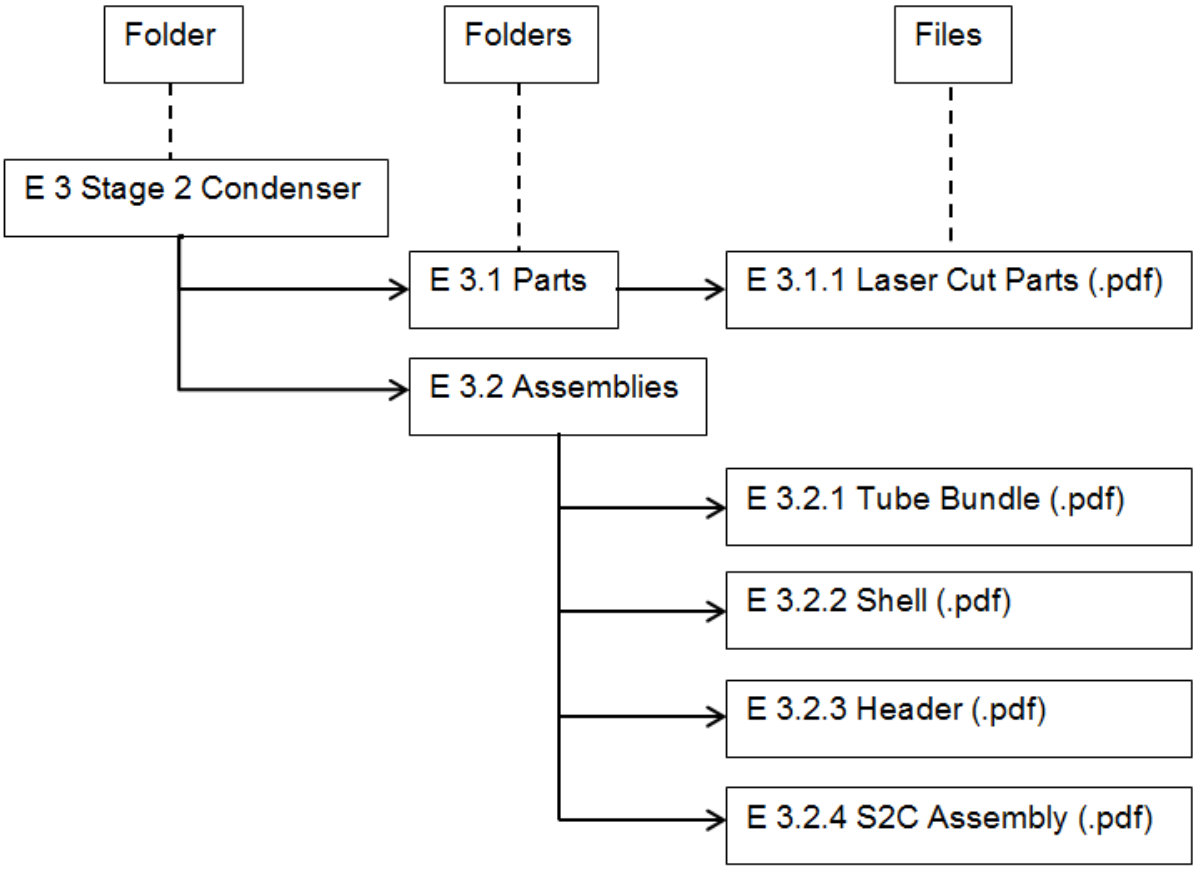

Figure E.2: Stage 2 condenser – Drawings directory.

1.6.3 De-superheating Condenser Manufacturing & Assembly Drawings

Figure E.3 shows the folder to folders to files directory of the de-superheating condenser as:

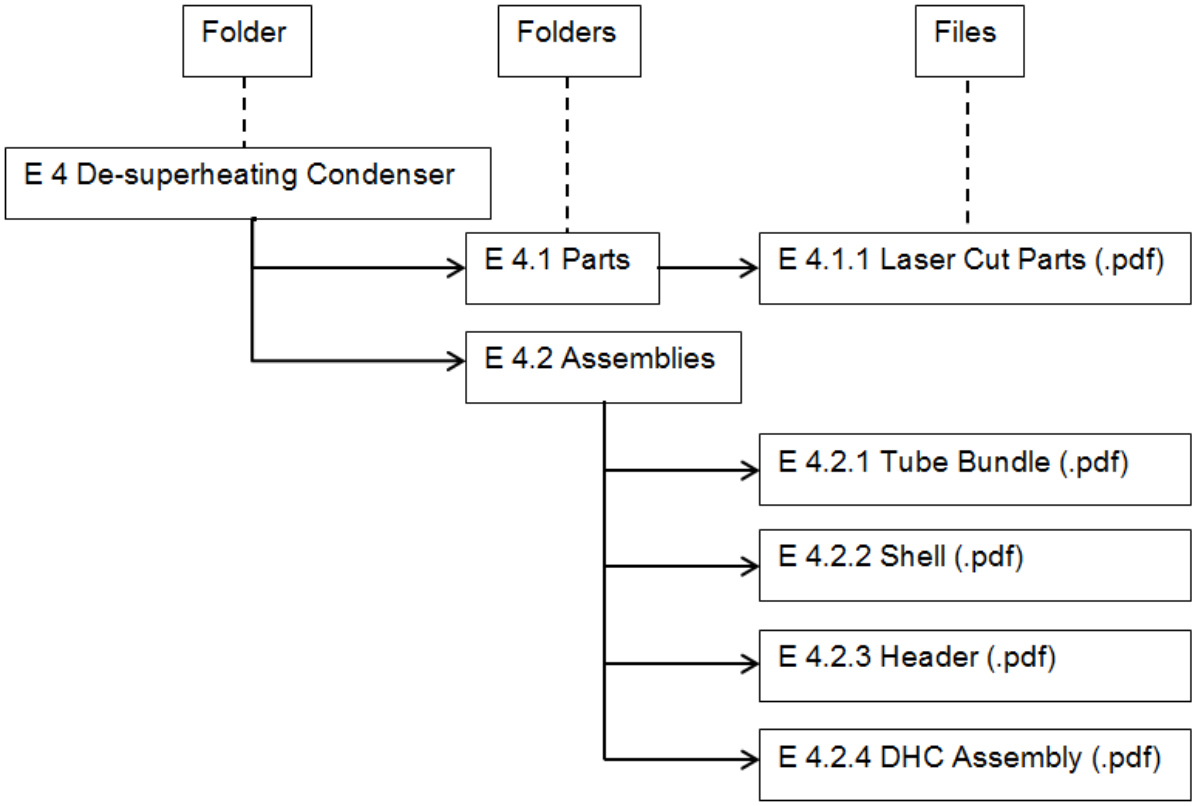

Figure E.3: De-superheating condenser – Drawings directory.

1.6.4 Pre-Cool Heat Exchanger Manufacturing & Assembly Drawings

Figure E.4 shows the folder to folders to files directory of the pre-cool heat exchanger as:

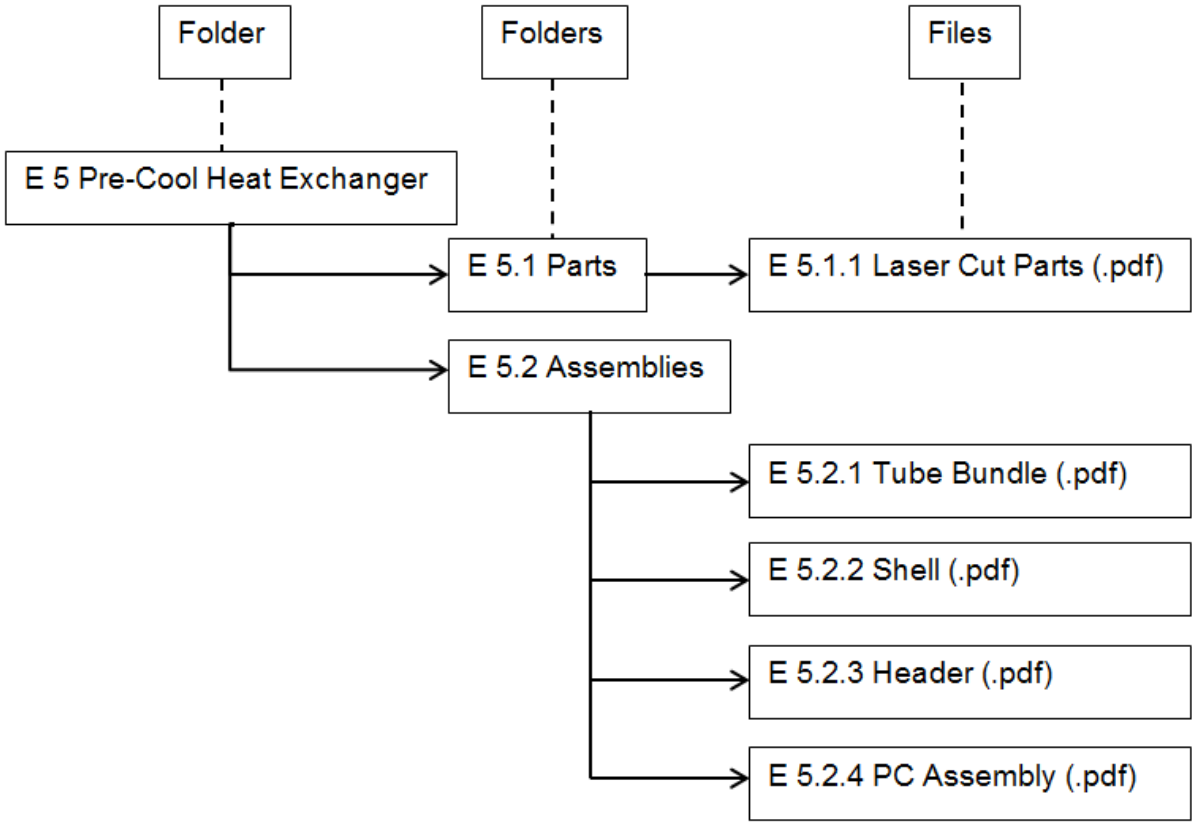

Figure E.4: Pre-Cool heat exchanger – Drawings directory.

1.6.5 Evaporator Manufacturing & Assembly Drawings

Figure E.5 shows the folder to folders to files directory of the evaporator as:

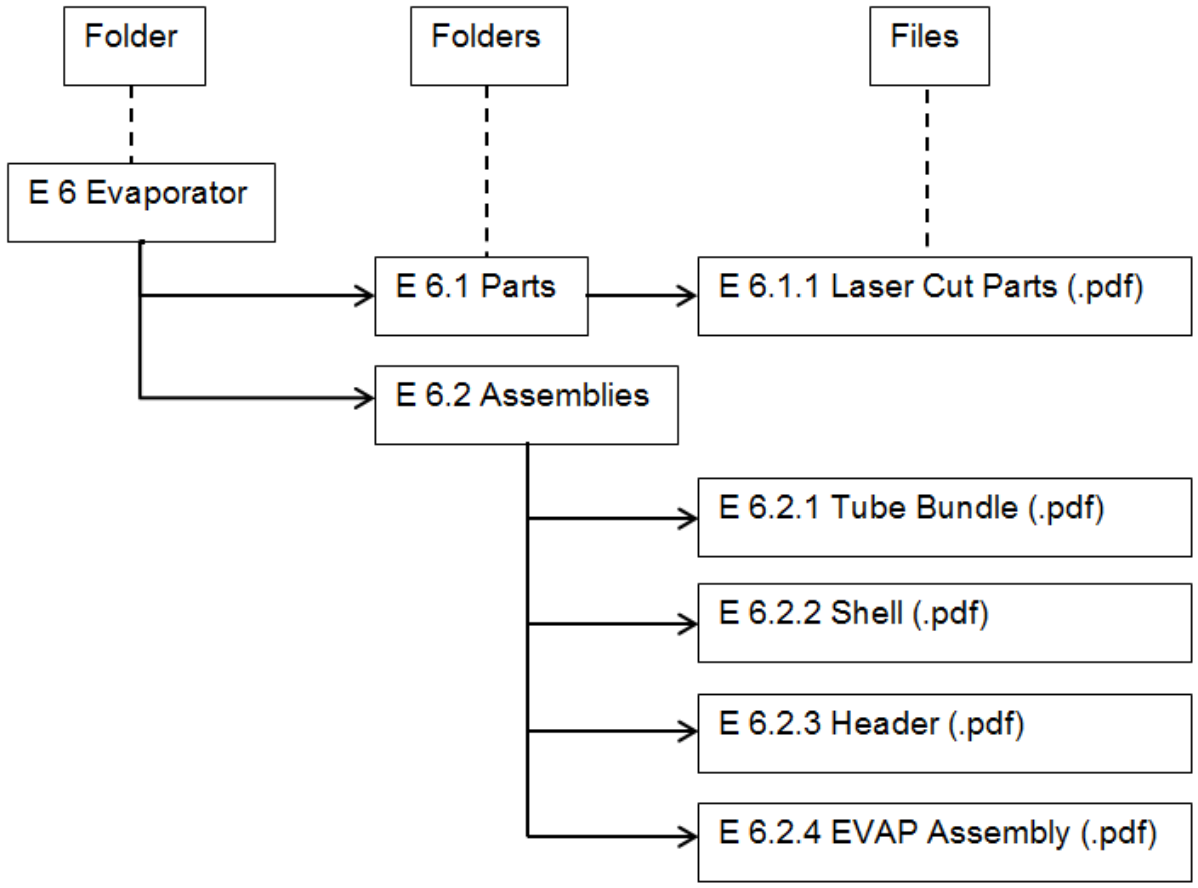

Figure E.5: Evaporator – Drawings directory.

1.6.6 Auxiliary-Regenerative Heat Exchanger Manufacturing & Assembly Drawings

Figure E.6 illustrates the folder to folders to files directory of the auxiliary-regenerative heat exchanger as:

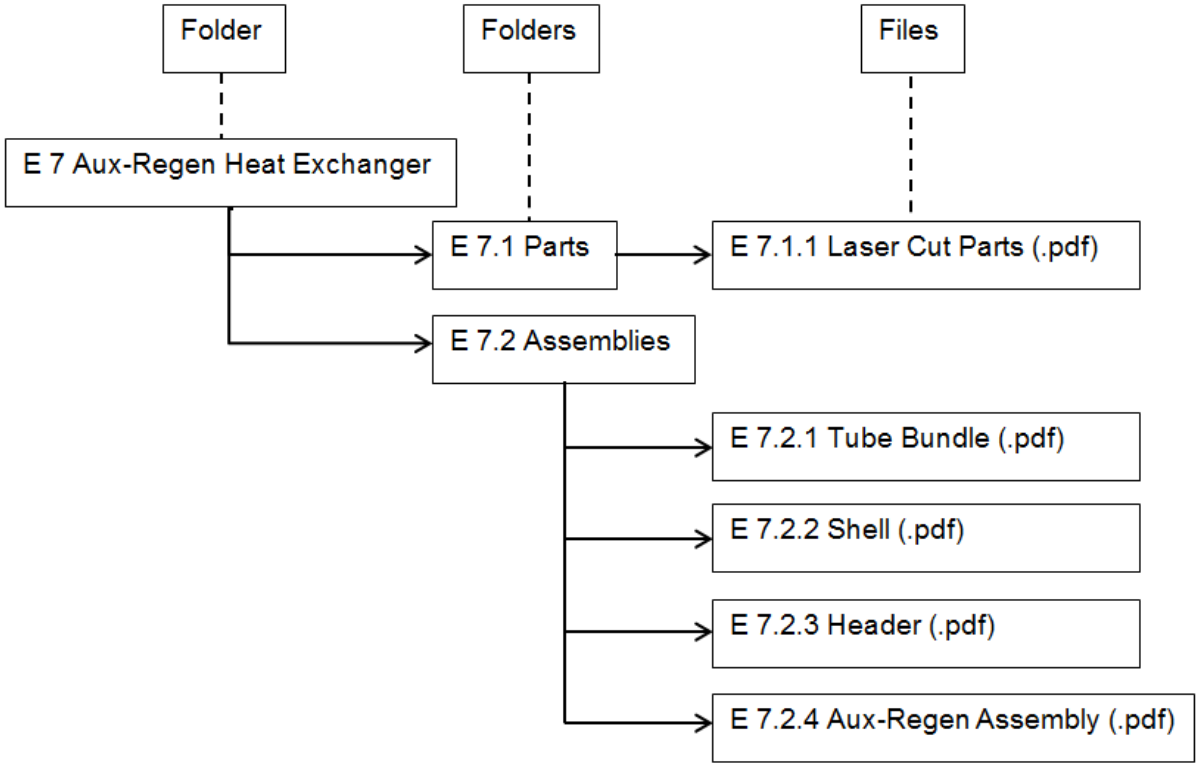

Figure E.6: Auxiliary-Regenerative heat exchanger – Drawings directory.

1.6.7 Aqua-Ammonia H&R Unit Manufacturing & Assembly Drawings

Figure E.7 illustrates the folder to files directory of the aqua-ammonia absorption-desorption heating & refrigeration unit as 4 main components, namely, condenser unit, pre-cool heat exchanger unit, evaporator unit, and auxiliary-regenerative heat exchanger unit.

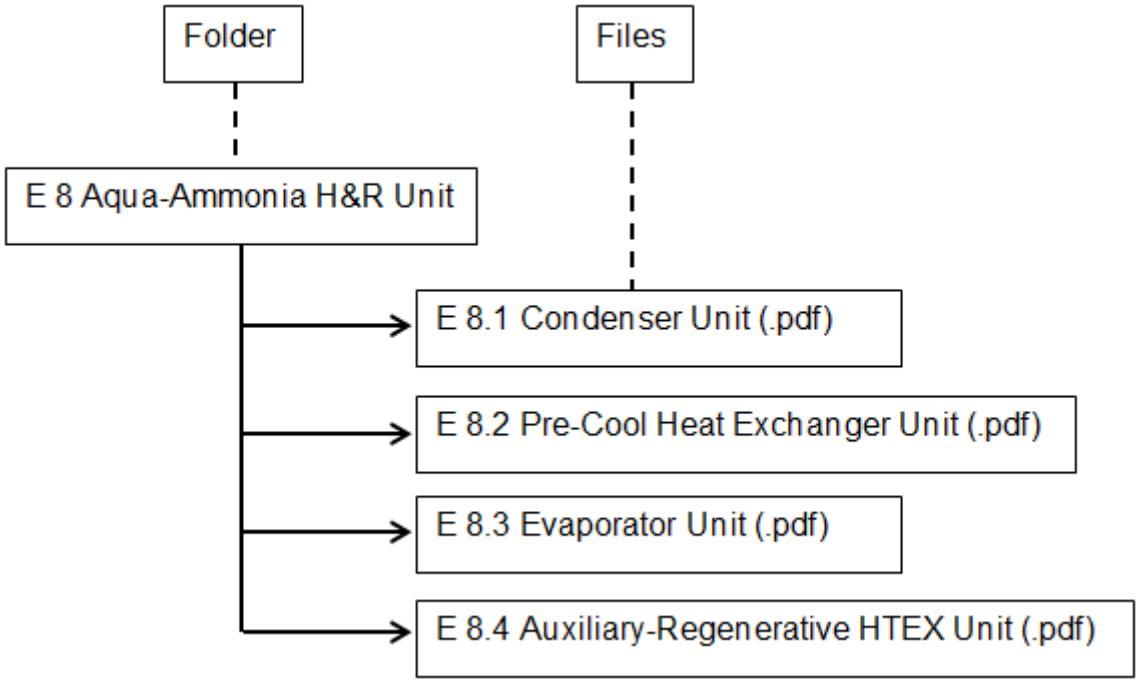

Figure E.7: Aqua-Ammonia H&R Unit Drawings Directory

The manufacturing drawings compiled in Appendix E 8 illustrates the necessary piping needed to connect the heat exchangers to one another, though the cycle can't be fully completed due to two absent components, namely, bubble pump generator and absorber module.

1.7 Manufacturing and assembly process

The following section focuses on the manufacturing and assembly process that was followed to construct each heat exchanger. This section will mostly consist of the visual documentation recorded during the manufacturing and assembly process. Figure E.8 illustrates the components that have been laser cut and ready for assembly.

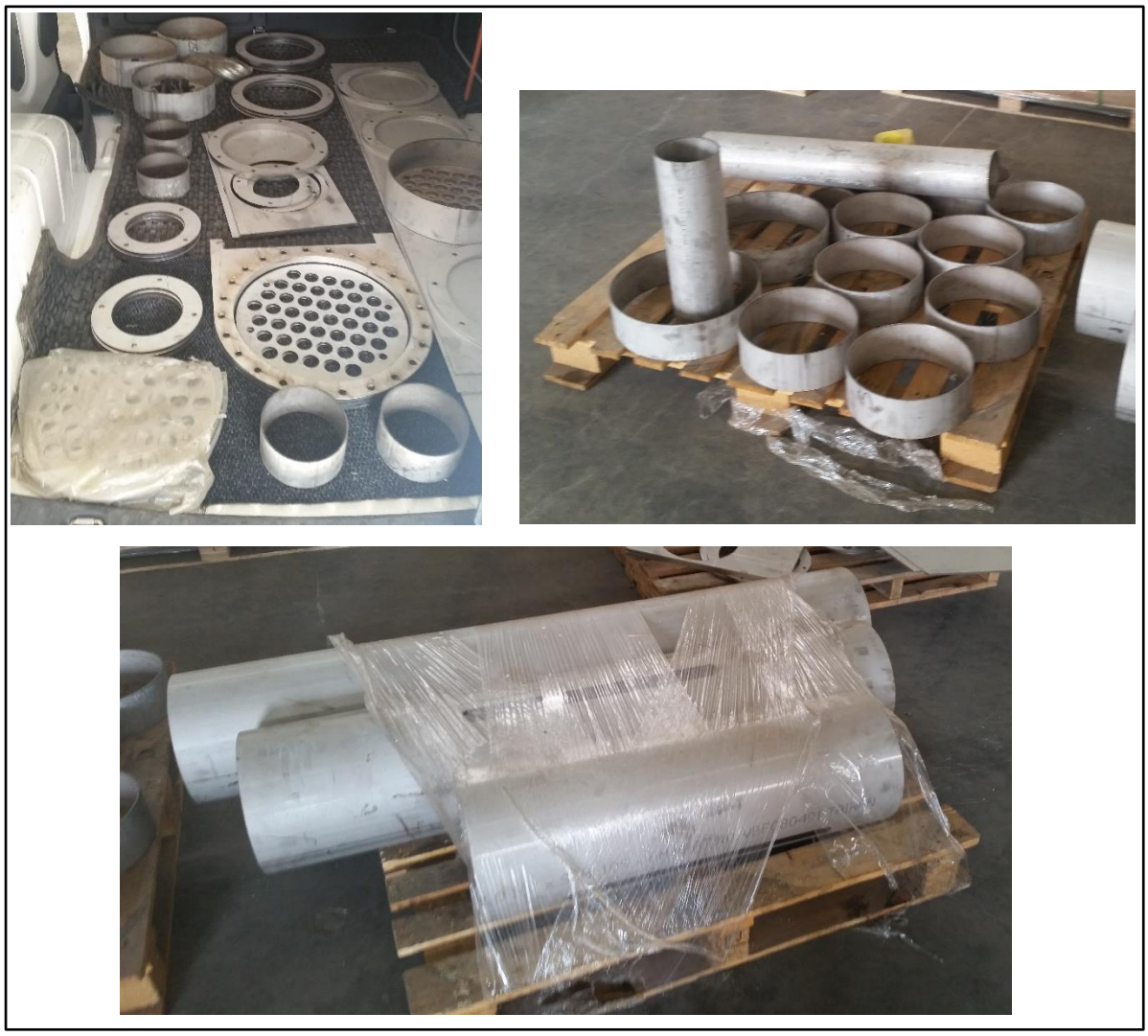

Figure E.8: Laser Cut Components

Illustrated in Figure E.9 is the assembly and welding processes of the heat exchanger's tube bundles.

Figure E.9: Tube Bundle Assembly Process

Illustrated in Figure E.10 are the tube bundles and respective heat exchanger shells, which underwent a cleaning process before the two assemblies were fitted into one another and welded shut. The tube bundles were treated with industrial strength general chemical soap to clean the tubes from any dust or metal debris.

Figure E.10: Tube Bundle Cleaning Process

Illustrated in Figure E.11 are the finished heat exchangers, ready for installation into the aqua-ammonia absorption-desorption H&R package unit.

Figure E.11: Completed Aqua-Ammonia Heat Exchangers